DROUGHT DETECTION AND QUANTIFICATION USING FIELD-BASED SPECTRAL MEASUREMENTS OF VEGETATION IN SEMI-ARID REGIONS

By

Geoffrey Stuart Marshall

Submitted in Partial Fulfillment of the Requirements for the

Masters of Science in Hydrology

New Mexico Institute of Mining and Technology
Department of Earth and Environmental Science

Socorro, New Mexico

May 2005

ACKNOWLEDGEMENTS

I would like to thank my advisor Xiaobing Zhou for his invaluable assistance, suggestions and guidance on every aspect of this thesis's research, from field data collection to data analysis to remote sensing and image processing and all points in-between. Without his input on all of these issues, this research would not have been possible. I would also like to thank my other committee members, Enrique Vivoni and Jan Hendrickx, for their guidance and input as well. Enrique helped me to expand my ideas of applications for this work, and Jan's experience and suggestions were very helpful in the statistical analysis of the data. Eric Small and Will Pockman are the primary investigators who perform research at the field site where I collected the data, and I appreciate them permitting me to use their research site. I also would like to recognize the USGS and Space Imaging INC. for their assistance in acquiring satellite data and explaining issues with some of the satellite images used in this thesis. Funding for this research was provided by EPSCOR, and was very much appreciated by me. I would also like to recognize all those who assisted me at various times in my field data collection, namely Renee Sandvig, Elizabeth Bryant, Hongjie Xie, Huade Guan and Kathy Fleming. Also, I would like to thank Pat Mills, Connie Apache and Mary Haenichen for their general support to all E&ES grad students. Finally, I would like to recognize my family back home in Jamaica, who I have not seen in a long time due to school requirements but who is always in my thoughts.

TABLE OF CONTENTS

Page

LIST OF FIGURES iv
LIST OF TABLES x
LIST OF ABBREVIATIONS xii
1. INTRODUCTION AND LITERATURE REVIEW 1
1.1 Definitions of Drought 1
1.2 Drought Indices 4
1.3 Palmer Drought Severity Index and Palmer Drought Index 7
1.3.1 Definition of PDSI 7
1.3.2 Use of PDSI 12
1.4 Standardized Precipitation Index 12
1.4.1 Definition of SPI 12
1.4.2 Use of SPI 16
1.5 Comparison of SPI and PDSI 17
1.6 Remote Sensing and Drought Stress Detection in Vegetation 19
1.7 Vegetation Indices 23
1.7.1 Normalized Difference Vegetation Index 24
1.7.2 Normalized Difference Water Index 25
1.7.3 Vegetation Index Number and Ratio Vegetation Index 25
1.7.4 Atmospherically Resistant Vegetation Index 26
1.7.5 Soil-Adjusted Vegetation Index 27
1.7.6 Modified Soil-Adjusted Vegetation Index 27
1.7.7 Normalized Difference Index 29
1.7.8 Normalized Difference Greenness Index 30
1.7.9 Normalized Difference Redness Index 30
1.7.10 Water Band Index 30
1.7.11 Red-Edge Vegetation Stress Index 31
1.8 Previous Work Relating Remote Sensing, Vegetation Indices, Environmental Parameters and Drought 32
1.9 Objectives 49
2. METHODS AND INSTRUMENTATION 50
2.1 Study Region and Vegetation 50
2.2 Remote Sensing Methods 52
2.2.1 Site Description 52
2.2.2 Instrument Description 53
2.2.3 Data Collection and Processing 55
2.3 Precipitation Methods 58
2.3.1 Data Collection and Processing 58
3. RESULTS AND ANALYSIS OF FIELD DATA 60

3.1 Correlation between SPI and PDI data 60
3.2 Comparison of Rain-sheltered Vegetation with Control Vegetation 69
3.2.1 Rain-sheltered Site Vegetation Indices 69
3.2.2 Irrigated Site Vegetation Indices 87
3.3 Correlation between Vegetation Indices and Drought Indices 96
3.3.1 Rain-sheltered Site Correlation Analysis with No Time Lag 97
3.3.2 Rain-sheltered Site Correlation Analysis with One Week Lag 101
3.3.3 Rain-sheltered Site Correlation Analysis with Two Weeks Lag 103
3.3.4 Rain-sheltered Site Regression Analysis with Three Weeks Lag 106
3.3.5 Rain-sheltered Site Regression Analysis with Four Weeks Lag 108
3.3.6 Rain-sheltered Site Regression Analysis with Five Weeks Lag 111
3.3.7 Irrigated Site Regression Analysis with no lag 113
3.3.8 Irrigated Site Regression Analysis with one week lag 114
3.3.9 Irrigated Site Regression Analysis with two week lag 116
3.3.10 Irrigated Site Regression Analysis with three week lag 118
3.3.11 Irrigated Site Regression Analysis with four weeks lag 119
3.3.12 Irrigated Site Regression Analysis with five week lag 119
4. SATELLITE IMAGE ANALYSIS OF DROUGHT STRESS 122
4.1 Application of Derived Algorithms 122
4.2 Land Cover Classification and Linear Spectral Un-mixing 125
4.2.1 Previous Land Cover Classifications and Vegetation Index Classifications 125
4.2.2 Linear Spectral Un-mixing 132
4.3 Drought Index Images 140
4.4 Validation 146
5. DISCUSSION 148
5.1 T-Test Discussion 148
5.2 Vegetation Index-Drought Index Correlation Discussion 152
5.3 Satellite Image Analysis Discussion 155
6. CONCLUSIONS AND FUTURE WORK 161
APPENDICES 166
Appendix A 167
Appendix B 170
Appendix C 174
REFERENCES 206

LIST OF FIGURES

Page

Figure 1-1: Representative spectral signatures of green vegetation, dry vegetation and soil 21
Figure 1-2: Electromagnetic radiation interacting with a plant leaf 22
Figure 2-1: Map of Sevilleta National Wildlife Refuge 51
Figure 2-2: Control Field Plot 53
Figure 2-3: Drought Field Plot 54
Figure 2-4: Irrigated Field Plot 54
Figure 2-5: Irrigated Shrub and Irrigation system 55
Figure 3-1: Graph of linear correlations coefficients for 1-week through 30-week SPI with weekly PDI, over no lag through to 12 weeks lag. 60
Figure 3-2: 30-Week SPI vs. PDI, with PDI lagged 5 weeks behind SPI. 63
Figure 3-3: 1-Week SPI values for 5-Points Weather Station from Jan 1999 to Sept 2004 64
Figure 3-4: 2-Week SPI values for 5-Points Weather Station from Jan 1999 to Sept 2004 65
Figure 3-5: 3-Week SPI values for 5-Points Weather Station from Jan 1999 to Sept 2004 65
Figure 3-6: 4-Week SPI values for 5-Points Weather Station from Jan 1999 to Sept 2004 66
Figure 3-7: 6-Week SPI for 5-Points Weather Station from Jan 1999 to Sept 2004 66
Figure 3-8: 12-Week SPI for 5-Points Weather Station from Feb 2002 to Sept 2004 67
Figure 3-9: 16-Week SPI for 5-Points Weather Station from Mar 1999 to Sept 2004..... 67
Figure 3-10: Weekly PDI for West-Central New Mexico from Feb 2002 to Sept 2004 .. 68
Figure 3-11: Rain-sheltered Site Shrub NDVI time series 69
Figure 3-12: Rain-sheltered Site Grass NDVI time series 70
Figure 3-13: Shrub NDWI time series 71
Figure 3-14: Grass NDWI time series. 72
Figure 3-15: Rain-sheltered Site Shrub VIN time series 73
Figure 3-16: Rain-sheltered Site Grass VIN time series 74
Figure 3-17: Rain-sheltered Site Shrub SAVI time series 75
Figure 3-18: Rain-sheltered Site Grass SAVI time series 75
Figure 3-19: Rain-sheltered Site Shrub ARVI time index 76
Figure 3-20: Rain-sheltered Site Grass ARVI time series data 77
Figure 3-21: Rain-sheltered Site Shrub RVSI Time Series 77
Figure 3-22: Rain-sheltered Site Grass RVSI 78
Figure 3-23: Rain-sheltered Site Shrub WBI values 79
Figure 3-24: Rain-sheltered Site Grass WBI time series 80

Figure 3-25: Rain-sheltered Site Shrub RVI time series 81
Figure 3-26: Rain-sheltered Site Grass RVI time series 82
Figure 3-27: Rain-sheltered Site Shrub NDGI time series 82
Figure 3-28: Rain-sheltered Site Grass NDGI time series 83
Figure 3-29: Rain-sheltered Site Shrub NDRI time series 84
Figure 3-30: Rain-sheltered Site Grass NDRI time series 84
Figure 3-31: Rain-sheltered Site Shrub NDI time series 85
Figure 3-32: Rain-sheltered Site Grass NDI time series 85
Figure 3-33: Rain-sheltered Site Shrub MSAVI time series 86
Figure 3-34: Rain-sheltered Site Grass MSAVI time series 87
Figure 3-35: Irrigated Site Shrub NDVI time series 88
Figure 3-36: Irrigated Site Shrub NDWI time series 88
Figure 3-37: Irrigated Site Shrub VIN time series 89
Figure 3-38: Irrigated Site Shrub SAVI time series 90
Figure 3-39: Irrigated Site Shrub ARVI time series 90
Figure 3-40: Irrigated Site Shrub RVSI time series 91
Figure 3-41: Irrigated Site Shrub WBI time series 92
Figure 3-42: Irrigated Site Shrub RVI time series 93
Figure 3-43: Irrigated Site Shrub NDGI time series 93
Figure 3-44: Irrigated Site Shrub NDRI time series 94
Figure 3-45: Irrigated Site Shrub NDI time series 95
Figure 3-46: Irrigated Site Shrub MSAVI time series 96
Figure 3-47: Linear correlations between SPI scales and measured NDVI, NDWI and VIN, no lag 98
Figure 3-48: Linear correlations between SPI scales and measured SAVI, ARVI and RSVI, no lag 99
Figure 3-49: Linear correlations between SPI scales and measured WBI, RVI and NDGI, no lag 99
Figure 3-50: Linear correlations between SPI scales and measured NDRI, NDI and MSAVI, no lag 100
Figure 3-51: Linear Correlations between SPI scales and NDVI, NDWI and VIN, one week lag. 101
Figure 3-52: Linear Correlations between SPI scales and SAVI, ARVI and RSVI, one week lag. 102
Figure 3-53: Linear Correlations between SPI scales and WBI, RVI and NDGI, one week lag 102
Figure 3-54: Linear Correlations between SPI scales and NDRI, NDI and MSAVI, one week lag 103
Figure 3-55: Linear Correlations between SPI scales and NDVI, NDWI and VIN, two weeks lag 104
Figure 3-56: Linear Correlations between SPI scales and SAVI, ARVI and RSVI, two weeks lag 104
Figure 3-57: Linear Correlations between SPI scales and WBI, RVI and NDGI, two weeks lag 105
Figure 3-58: Linear Correlations between SPI scales and NDRI, NDI and MSAVI, two weeks lag 105

Figure 3-59: Linear Correlation coefficients between various SPI scales and NDVI, NDWI and VIN, three weeks lag. 106
Figure 3-60: Linear correlation coefficients between various SPI scales and SAVI, ARVI and RSVI, three weeks lag. 107
Figure 3-61: Linear correlation coefficients between various SPI scales and WBI, RVI and NDGI, three weeks lag. 107
Figure 3-62: Linear correlation coefficients between various vegetation indices and NDRI, NDI and MSAVI, three weeks lag. 108
Figure 3-63: Linear correlation coefficients of SPI and NDVI, NDWI and VIN, four week lag. 109
Figure 3-64: Linear correlation coefficients of SPI and SAVI, ARVI and RSVI, four week lag. 109
Figure 3-65: Linear correlation coefficients between SPI and WBI, RVI and NDGI, four week lag. 110
Figure 3-66: Linear correlation coefficients between SPI and NDRI, NDI and MSAVI, four week lag 110
Figure 3-67: Linear correlation coefficients between SPI and NDVI, NDWI and VIN, five weeks lag. 111
Figure 3-68: Linear correlation coefficients between SPI and SAVI, ARVI and RSVI, five weeks lag 112
Figure 3-69: Linear correlation coefficients between SPI and WBI, RVI and NDGI, five weeks lag 112
Figure 3-70: Linear correlation between SPI and NDRI, NDI and MSAVI, five weeks lag 113
Figure 3-71: Linear Correlation graphs of various SPI scales vs. various vegetation index values for the irrigated Site, no lag. 114
Figure 3-72: Linear Correlation graph of SPI vs. vegetation indices for the irrigated Site, no lag 115
Figure 3-73: Linear Correlation coefficients between various SPI scales and vegetation indices, one week lag. 115
Figure 3-74: Linear Correlation coefficients between various SPI scales and vegetation indices, one week lag 116
Figure 3-75: Linear correlations between SPI and NDVI, NDWI, VIN, SAVI, ARVI and RSVI, two weeks lag 117
Figure 3-76: Linear correlations between SPI and WBI, RVI, NDGI, NDRI, NDI and MSAVI, two weeks lag. 117
Figure 3-77: Linear correlation coefficients between SPI and NDVI, NDWI, VIN, SAVI, ARVI and RSVI, watered Site, three weeks lag. 118
Figure 3-78: Linear correlation coefficients between SPI and WBI, RVI, NDGI, NDRI, NDI and MSAVI, watered Site, three weeks lag. 119
Figure 3-79: Linear correlation coefficients between SPI and NDVI, NDWI, VIN, SAVI, ARVI and RSVI, Irrigated Site, four weeks lag. 120
Figure 3-80: Linear correlation coefficients between SPI and WBI, RVI, NDGI, NDRI, NDI and MSAVI, Irrigated Site, four weeks lag. 120
Figure 3-81: Linear correlation coefficients between SPI and NDVI, NDWI, VIN, SAVI, ARVI and RSVI, 5 weeks lag. 121

Figure 3-82: Linear correlation coefficients between SPI and WBI, RVI, NDGI, NDRI, NDI and MSAVI, Irrigated Site, 5 weeks lag. 121
Figure 4-1: Linear Regression of Grass NDVI vs. 12 Week SPI, no lag 123
Figure 4-2: Linear Regression of Grass NDVI vs. 17 Week SPI, no lag 124
Figure 4-3: Linear Regression of Shrub NDVI vs. 12-Week SPI, no lag..... 125
Figure 4-4: Predicted Land cover map of the Sevilleta National Wildlife Refuge..... 127
Figure 4-5: Photos of various regions of the Sevilleta Wildlife Refuge as represented in Figure 4-4..... 128
Figure 4-6: Photo of the SNWR, in the shrub region. 128
Figure 4-7: ASTER Surface Reflectance (upper image) and NDVI (lower image) at the SNWR for April 20, 2002. 129
Figure 4-8: Comparison of measured NDGI values for shrub(1), grass(2) and soil(3) targets. 130
Figure 4-9: ASTER Surface Reflectance (upper image) and NDGI (lower image) at the SNWR for April 20, 2002. 131
Figure 4-10: Linear Spectral Un-mixing Results from grass targets. 136
Figure 4-11: Linear Spectral Un-mixing from Shrub Target..... 137
Figure 4-12: Linear Spectral Un-mixing Soil Classification results..... 138
Figure 4-13: Unsupervised Classification results from ASTER image. 139
Figure 4-14: Climatic divisions of New Mexico. 141
Figure 4-15: SPI Calculations for April 20, 2002..... 142
Figure 4-16: SPI Calculations for May 6, 2002..... 142
Figure 4-17: SPI Calculations, June 16, 2002..... 143
Figure 4-18: SPI classifications for September 30, 2003. 143
Figure 4-19: 3-Month SPI throughout the USA for April 2002. 144
Figure 4-20: 3-Month SPI throughout the USA for May 2002 144
Figure 4-21: 3-Month SPI throughout the USA for June 2002 145
Figure 4-22: 3-Month SPI throughout the USA for September 2003..... 145
Figure A-1: Linear Correlations between measured Soil ratios and SPI time scales, no lag..... 176
Figure A-2: Linear Correlations between measured Soil ratios and SPI time scales, no lag..... 176
Figure A-3: Linear Correlations between measured Soil ratios and SPI time scales, one week lag. 177
Figure A-4: Linear Correlations between measured Soil ratios and SPI time scales, one week lag. 177
Figure A-5: Linear Correlations between measured Soil ratios and SPI time scales, two week lag. 178
Figure A-6: Linear Correlations between measured Soil ratios and SPI time scales, two week lag. 178
Figure A-7: Linear Correlations between measured Soil ratios and SPI time scales, three week lag. 179
Figure A-8: Linear Correlations between measured Soil ratios and SPI time scales, three week lag. 179
Figure A-9: Linear Correlations between measured Soil ratios and SPI time scales, four week lag. 180

Figure A-10: Linear Correlations between measured Soil ratios and SPI time scales, four week lag. 180
Figure A-11: Linear Correlations between measured Soil ratios and SPI time scales, five week lag. 181
Figure A-12: Linear Correlations between measured Soil ratios and SPI time scales, five week lag. 181
Figure A-13: Linear Regression between Shrub VIN and 12-week SPI, no lag 182
Figure A-14: Linear Regression between Shrub ARVI and 12-Week SPI..... 182
Figure A-15: Linear Regression between Grass ARVI and 12-Week SPI, no lag 183
Figure A-16: Linear Regression between Shrub MSAVI and 12-Week SPI, no lag..... 183
Figure A-17: Linear Regression between Grass WBI and Palmer Drought Index, no lag 184
Figure A-18: Linear Regression of Shrub NDVI and 12-week SPI, one week lag 184
Figure A-19: Linear Regression of Grass NDVI and 12-Week SPI, one week lag..... 185
Figure A-20: Linear Regression of shrub VIN vs. 12-week SPI, one week lag..... 185
Figure A-21: Linear Regression of Grass VIN vs. 12-Week SPI, one week lag..... 186
Figure A-22: Linear Regression of Shrub SAVI vs. 12-Week SPI, one week lag 186
Figure A-23: Linear Regression of shrub ARVI vs. 12-Week SPI, one week lag 187
Figure A-24: Linear Regression of Grass ARVI vs. 12-Week SPI, one week lag 187
Figure A-25: Linear Regression of Shrub RVI vs. 12-Week SPI, no lag..... 188
Figure A-26: Linear Regression of Grass RVI vs. 12-Week SPI, no time lag 188
Figure A-27: Linear Regression of Shrub MSAVI vs. 12-Week SPI, one week lag..... 189
Figure A-28: Linear Regression of Shrub NDVI vs. 12-week SPI, two weeks time lag 189
Figure A-29: Linear Regression of Grass NDVI vs. 12-Week SPI, two weeks lag 190
Figure A-30: Linear Regression of Shrub VIN vs. 12-Week SPI, two weeks lag..... 190
Figure A-31: Linear Regression of Grass VIN vs. 12-Week SPI, two weeks lag 191
Figure A-32: Linear Regression of Shrub SAVI vs. 12-Week SPI, two weeks lag 191
Figure A-33: Linear Regression of Shrub ARVI vs. 12-Week SPI, two weeks lag..... 192
Figure A-34: Linear Regression of Grass ARVI vs. 12-Week SPI, two weeks lag 192
Figure A-35: Linear Regression of Grass WBI vs. PDI, two weeks lag 193
Figure A-36: Linear Regression of Shrub RVI vs. 12-week SPI, two weeks lag..... 193
Figure A-37: Linear Regression of Grass RVI vs. 12-Week SPI, two weeks lag 194
Figure A-38: Linear Regression of Shrub MSAVI vs. 12-Week SPI, two weeks lag.... 194
Figure A-39: Linear Regression of Shrub NDVI vs. 12-Week SPI, three weeks lag..... 195
Figure A-40: Linear Regression of Grass NDVI vs. 12-Week SPI, three weeks lag 195
Figure A-41: Linear Regression of Shrub VIN vs. 12-Week SPI, three weeks lag..... 196
Figure A-42: Linear Regression of Grass VIN vs. 12-Week SPI, three week lag..... 196
Figure A-43: Linear Regression of Shrub ARVI vs. 12-Week SPI, three weeks lag..... 197
Figure A-44: Linear Regression of Grass ARVI vs. 12-Week SPI, three week lag..... 197
Figure A-45: Linear Regression of Grass WBI vs. PDI, three week lag..... 198
Figure A-46: Linear Regression of Shrub RVI vs. 12-Week SPI, three weeks lag..... 198
Figure A-47: Linear Regression of Grass RVI vs. 12-Week SPI 199
Figure A-48: Linear Regression of Shrub NDVI vs. 6-Week SPI, four week lag..... 199
Figure A-49: Linear Regression of Grass NDVI vs. 12-Week SPI, four weeks lag..... 200
Figure A-50: Linear Correlation of 4-Week SPI and Shrub NDVI, no lag, Irrigated Site 200

Figure A-51: Linear Correlation of 4-Week SPI and Shrub VIN, no lag, Irrigated Site. 201
Figure A-52:Linear correlation plot between 4-Week SPI and Shrub ARVI, no lag, Irrigated Site..... 201
Figure A-53: Linear Regression of 4-Week SPI and Shrub NDGI, no lag, watered Site 202
Figure A-54: SNWR 4-Week SPI from all operational rain gauges/weather stations.... 202
Figure A-55: SNWR 8-Week SPI from all operational rain gauges/weather stations.... 203
Figure A-56: SNWR 12-Week SPI from all operational rain gauges/weather stations.. 203
Figure A-57: SNWR 16-Week SPI from all operational rain gauges/weather stations.. 204
Figure A-58: SNWR 20-Week SPI from all operational rain gauges/weather stations.. 204
Figure A-59: SNWR 24-Week SPI from all operational rain gauges/weather stations.. 205

LIST OF TABLES

Table 1: Dummy Variables in SPI analysis by Ji and Peters (2003) 44
Table 2: Correlation coefficients of weekly PDI values vs. SPI values derived for 5 Points weather station, from no lag to six weeks lag. 61
Table 3: Correlation coefficients of weekly PDI values vs. SPI values derived for 5 Points weather station, from seven weeks lag to twelve weeks lag. 62
Table 4: Percent Agreement of Derived SPI images with stated NDMC drought severity. 146
Table 5: T-Test results for Control Grass vs. Rain-Sheltered Grass, Rain-Sheltered site 151
Table 6: T-Test results for Control Shrubs vs. Rain-Sheltered Shrubs, Rain-Sheltered site 151
Table 7: T-Test results for Irrigated Shrub vs. Control Shrub, Irrigated Site 152
Table 8: Most Significant Correlations for Vegetation Indices at Drought Plot, No Lag 156
Table 9: Most Significant Correlations for Vegetation Indices at Drought Plot, one week lag 156
Table 10: Most Significant Correlations for Vegetation Indices at Drought Plot, two weeks lag 157
Table 11: Most Significant Correlations for Vegetation Indices at Drought Plot, three weeks lag 157
Table 12: Most Significant Correlations for Vegetation Indices at Drought Plot, four weeks lag 158
Table 13: Most Significant Correlations for Vegetation Indices at Drought Plot, five weeks lag 158
Table 14: Most Significant Correlations for Vegetation Indices at Irrigated Plot, no lag 159
Table 15: Most Significant Correlations for Vegetation Indices at Irrigated Plot, one-week lag 159
Table 16: Most Significant Correlations for Vegetation Indices at Irrigated Plot, two weeks lag 159
Table 17: Most Significant Correlations for Vegetation Indices at Irrigated Plot, three weeks lag 159
Table 18: Most Significant Correlations for Vegetation Indices at Irrigated Plot, four weeks lag 160
Table 19: Most Significant Correlations for Vegetation Indices at Irrigated Plot, five weeks lag 160
Table 20: Linear Correlation /between Rain-sheltered site control vegetation and various meteorological variables I 174

Table 21: Linear Correlation /between Rain-sheltered site control vegetation and various meteorological variables II 175

LIST OF ABBREVIATIONS

ARVI	Atmospherically Resistant Vegetation Index
ASTER	Advanced Spaceborne Thermal Emission and Reflection
ATI	Apparent Thermal Inertia
AVHRR	Advanced Very High Resolution Radiometer
AVIRIS	Airborne Visible/Infrared Imaging Spectrometer
CCC	Colorado Climatic Center
EOS	Earth Observation System
GIS	Geographical Information Systems
LWC	Leaf Water Content
MODIS	Moderate Resolution Imaging Spectroradiometer
MSAVI	Modified Soil Adjusted Vegetation Index
NCDC	National Climatic Data Center
NDGI	Normalized Difference Greeness Index
NDI	Normalized Difference Index
NDMC	National Drought Mitigation Center
NDVI	Normalized Difference Vegetation Index
NDSVI	Normalized Difference Senescent Vegetation Index
NDWI	Normalized Difference Water Index
NOAA	National Oceans and Atmospheric Administration
PDI	Palmer Drought Index
PDSI	Palmer Drought Severity Index
NDRI	Redness Index
RVI	Ratio Vegetation Index
RVSI	Red-Edge Vegetation Stress Index
SAVI	Soil-Adjusted Vegetation Index
SNWR	Sevilleta National Wildlife Refuge
SPI	Standardized Precipitation Index
SWSI	Surface Water Supply Index
VIN	Vegetation Index Number
VCI	Vegetation Condition Index
WBI	Water Band Index

1. INTRODUCTION AND LITERATURE REVIEW

1.1 Definitions of Drought

Drought is a serious and ubiquitous climatologically phenomenon in almost all of the world's climatic regions. It has played a significant role in many human affairs. Examples of this include the decline of the Mayan Civilization (Haug, *et al* 2003), the historical Dust Bowl of the 1930s in the USA, and the Sahel drought in sub-Saharan Africa today. The simple definition of drought is "an extended period of little or no rainfall", but the reality is more complex than this. For instance, precipitation levels which may be considered low in Seattle thus causing drought conditions there may be considered high in New Mexico and thus ending drought conditions at this location. Because of this, we need to take other hydrological parameters besides precipitation into account when defining drought conditions. These include parameters such as soil moisture, evapotranspiration (ET) rates and water balances. Thus, in defining drought, the long-term climate of a region needs to be considered as well, whether it is tropical, temperate or semi-arid. Generally, there are 4 different types of droughts as described by the National Drought Mitigation Center (NDMC):

1. **Hydrological:** Streamflow, groundwater and reservoir levels are all significantly lower than normal.
2. **Meteorological:** A change in the atmospheric circulation pattern which leads to a precipitation deficit compared to the average precipitation in a region.

3. **Agricultural:** Insufficient precipitation during critical agricultural growth periods, negatively affecting crop yield.
4. **Socioeconomic:** The effects of low precipitation and below-normal hydrological parameters affect everyday life, and curtail normal social and economic activity.

Semi-arid regions in particular are extremely affected by drought conditions because of the already low precipitation that is definitive of such regions. Any variation in precipitation levels and water balances can be extremely disruptive to the region's ecology and human activity, since there is already a limited supply of water available. For this reason, many drought monitoring programs have been established worldwide, and drought management and prediction has become an important area of research. According to Donald Wilhite (1990):

> Drought differs from other natural hazards in several ways. First, since the effects of drought often accumulate slowly over a considerable period of time and may linger for years after the termination of the event, the onset and end of drought is difficult to determine. Because of this, drought is often referred to as a creeping phenomenon. Climatologists continue to struggle with recognizing the onset of drought and scientists and policy makers continue to debate the basis (i.e. criteria) for declaring an end to a drought.

Since the effects of drought are cumulative over a period of time, it is considered to be a creeping phenomenon. Also, since there are multiple definitions of drought, it can be difficult to determine whether or not a drought has been broken. Drought quantification is made complicated by the differences that droughts take among themselves, both regionally and qualitatively. These differences usually involve three essential characteristics: intensity, duration and spatial coverage. Intensity refers to the degree of the precipitation shortfall and/or the severity of impacts associated with the

shortfall (Wilhite, 1990). I would amend this description to include hydrological parameters along with precipitation. Duration refers to the length of time that drought conditions are present. The longer a drought is in effect, the greater is its effect on human and ecological activities. Droughts may take a few months to take effect depending upon the region under stress, but once drought conditions are established they may last for several months or years. Repeated drought episodes and extended drought stresses will deplete water reserves and have a seriously adverse impact on agriculture, municipal water supplies, and vegetation/animal life.

Furthermore, the spatial aspect of drought is also significant. Drought may affect different regions at the same time, or affect one region while another recovers from drought, and regional intensity may shift from one region to the next over different time scales. For example, the Dust Bowl drought of 1934 affected approximately 65% of the USA, but it affected 95% of the Great Plains region of the USA. A recent drought analysis by the U.S. National Drought Mitigation Center for the 48 contiguous states demonstrated that severe drought affected more than 25% of the country in one out of four years (Wilhite, 2001).

Because of the potentially devastating effects of drought, it is advantageous to have a drought monitoring mechanism in effect. However, it is difficult to determine what parameters to measure as an indicator of drought because of the various definitions. For example, meteorological drought is principally defined as a deviation of precipitation from the average precipitation over a given region for a given time, while agricultural drought involves soil moisture deficiencies. Both of these variables depend upon human measurement. For precipitation, not only is a long-term dataset needed to calculate

"normal" precipitation, but a recent record of precipitation for the region under study is also needed for comparison to this "normal". For extremely remote regions, this record may not be available, and any available records are usually point data from a rain gauge or a network of rain gauges. This will cause issues if the spatial variability in precipitation is large and cannot be adequately represented by the number of rain gauges under review. Soil moisture is even more difficult to monitor than precipitation because of expense, time and spatial relevance. Thus, researchers have begun to focus on the response of vegetation to drought stress and remote sensing of vegetation as an indirect observation of drought stress.

1.2 Drought Indices

Because of the pervasive and varying degree of drought effects, it is important to develop methods for drought assessment. The intensity/severity of a drought is quantified by a **drought index** which measures the departure of some climatic index from normal, and is normally closely linked to duration in the determination of drought impact. The World Meteorological Organization defines a drought index as "an index which is related to some of the cumulative effects of a prolonged and abnormal moisture deficiency" (Heim, 2002). They are calculated from varying hydrological parameters dependent upon the purpose of each index. There are many different types of drought indices in existence. Heim (2002) did a review of drought indices and indicated that reliable precipitation observations became available about two centuries ago, and that practically all drought indices and definitions incorporated precipitation either solely or with other parameters. Most early drought indicators were defined by the length of precipitation deficit and the number of consecutive days of rainfall below a certain level. Such indicators were

regionally limited however, and only accounted for meteorological drought, not hydrological or agricultural. These inadequacies were realized early and scientists in the early 20th century focused on addressing these inadequacies. Munger (1916) developed a measure of annual and regional forest fire risk. For his drought index, he used the length of the period without a 24-hour rainfall of 0.05 inches. Mathematically, the severity was expressed as:

$$severity = \frac{L^2}{2} \tag{1}$$

where L is the length of drought in days. Kincer (1919) prepared charts showing seasonal distribution of precipitation across the USA, and defined drought as thirty or more consecutive days with less than 0.25 of an inch of precipitation in 24 hours. Marcovitch (1930) devised a drought index:

$$\frac{N^2(100/R)^2}{2} \tag{2}$$

where N is the total number of two or more consecutive days above 90 degrees Farenheight and R is the total summer rainfall for months.

One person whose work furthered the development of drought indices was Thornwaite (1931). He incorporated potential evapotranspiration and developed an index which used the ratio between monthly precipitation and monthly evaporation. As time progressed, drought identification evolved from simplistic approaches focusing on rainfall deficiency to more involved models of limited applicability. The apex of these involved models was the Palmer Drought Severity Index (PDSI), developed by Wayne Palmer in 1965 (Palmer, 1965). It was hailed as "the most satisfactory solution to the problem of combining precipitation and temperature as predictor variables." (Julian and

Fritts, 1968) and has been widely used in the USA in its modified form called the Palmer Drought Index (PDI), but has had mixed results in other areas of the world. Other indices were introduced later, and the most recognized of them has been the Standardized Precipitation Index or SPI (McKee, 1993) which will be examined later in this thesis. Other indices developed post-PDSI also includes the Surface Water Supply Index or SWSI (Shafer and Dezman, 1982) and Rainfall Deciles (Gibbs and Maher, 1967). The SWSI was designed to complement the PDSI by integrating snowpack, reservoir storage, streamflow and precipitation at high elevations, and has a similar scale to the PDSI (Heim, 2000). Rainfall Deciles use median levels of precipitation as a means of monitoring meteorological drought. It ranks observed precipitation totals for the preceding three months against climate records. If the sum falls below the lowest decile of the historic distribution of 3-month totals, then the region is considered to be in drought (Keyantash and Dracup, 2002). Other indices have been developed regionally in various locations around the world, and there are many references available with additional information. Drought index development is an evolving study, as Heim (2002) states:

> The monitoring and analysis of drought have long suffered from the lack of an adequate definition of the phenomenon. This has affected the development of drought indices, which have slowly evolved during the last two centuries from simplistic approaches based on some measure of rainfall deficiency to be more complex problem-specific models. These models continue to evolve as new data sources become available. The incorporation of evapotranspiration as a measure of water demand by Thornwaite led to the landmark development by Palmer of a water budget-based drought index, which is still widely used thirty years later.

1.3 Palmer Drought Severity Index and Palmer Drought Index

1.3.1 Definition of PDSI

Wayne Palmer published his model for a drought index in 1965 (Palmer, 1965). This index was designed to incorporate antecedent precipitation, moisture supply and moisture demand and was based upon the pioneering evapotranspiration work by Thornwaite (1931). In his landmark paper, Palmer stated that agriculture and hydrology are more concerned with the effects of a moisture shortage than with solely the meteorological aspects, this in response to the mainly precipitation-based indices previously developed. He went on to define a drought period as a period of time (duration in months or years) during which the actual moisture supply at a given location consistently falls short of the climatically expected or appropriate moisture supply. He also stated that the severity of drought may be considering as a function of both the duration and magnitude of the moisture deficiency. In developing his index, Palmer chose 2 climatically dissimilar sites in the Midwestern USA. The first site was the western third of Kansas, comprising of 31 counties with temperature and precipitation data available monthly and recorded from January 1887. He classified this region as a semi-arid/dry subhumid climate with cold winters and hot summers, and 70% of the precipitation occurs during the freeze-free months. The second site chosen consisted of the 12 counties of Iowa's central climatic division. Available data for this region extended from January 1931 through December 1957, and the region was classified as moist sub humid with colder winters and summers than the Kansas region. This region was chosen as a contrast to the Kansas site because weather that would be considered normal in Kansas would be

considered exceptionally dry in Iowa, and the idea was to develop a drought index that would provide relevant results for both sites.

Palmer used various techniques in developing the index. The first technique he derived incorporated evapotranspiration based on Thornwaite's work and determined availability of water in the soil. The soil was divided into two arbitrary layers. The upper layer was called surface soil and was assumed to contain 1 inch of available moisture at field capacity. This is the layer assumed to encounter precipitation and where evaporation takes place, and in accounting for moisture Palmer assumed that evapotranspiration occurs at the potential rate from this surface layer until all available moisture from this layer is removed. Only after this could moisture be removed from the underlying layer, and it was also assumed that there was no recharge to the lower layer until the upper layer had reached field capacity. It was also assumed that the water loss from the underlying area was dependent upon initial water content, the potential evapotranspiration and the available soil water capacity. Thus:

$$L_s = S_s' \text{ or } (PE - P) \tag{3}$$

whichever is smaller and

$$L_u = (PE - P - L_s)\frac{S_u'}{AWC}, \quad L_u \le S_u' \tag{4}$$

where L_s = moisture from surface layer, S_s' = available moisture stored in surface layer at beginning of month, PE= monthly potential evapotranspiration, P=precipitation for the month, L_u=water loss from underlying levels, S_u' =available moisture stored in underlying levels at start of month, and AWC=combined available water capacity of both levels. All units are in dimensions of length, (inches as described by Palmer).

Palmer then carried out a hydrological accounting procedure, calculating various potential values and coefficients. Specifically, he described potential recharge as $AWC-S_s^{'}$, and potential loss as PL_s+PL_u where PL_s=the smaller of PE or $S_s^{'}$ and $PL_u=(PE-PL_s)*\ S_u^{'}/AWC$. He also described coefficients of evapotranspiration, recharge, runoff and loss. The coefficient of evapotranspiration α is defined as:

$$\alpha = \frac{ET}{PE} \tag{5}$$

This can also be called the evaporative fraction, being the ration of actual evapotranspiration to potential evapotranspiration.

The coefficient of recharge β is defined as:

$$\beta = \frac{R}{PR} \tag{6}$$

where R is recharge and PR is potential recharge.

The coefficient of runoff γ is defined as:

$$\gamma = \frac{RO}{S^{'}} \tag{7}$$

where RO is runoff and $S^{'}$ is as defined in equation (4).

The coefficient of loss δ is defined as:

$$\delta = \frac{L}{PL} \tag{8}$$

where L = water loss and PL = potential water loss.

All of these coefficients are dimensionless. Using these coefficients, he defined the CAFEC precipitation, where CAFEC stands for "Climatically Appropriate for Existing Conditions"; an ideal precipitation. This precipitation is defined as:

$$\hat{P} = E\hat{T} + \hat{R} + \hat{R}\hat{O} - \hat{L} \quad (9)$$

where all the right hand side elements are the product of the potential equivalents and the corresponding coefficients described above.

Palmer then compared the CAFEC precipitation to the actual precipitation and recorded the numerical difference between them as:

$$d = P - \hat{P} \quad (10)$$

Using an empirical formula for the Iowa and Kansas regions he was studying, he defined a climate characteristic *K*, where:

$$\frac{K_{Iowa}}{K_{Kan}} = \frac{d_{Kan}}{d_{Iowa}} \quad (11)$$

According to Palmer, these *K* values represent averages for some as yet undefined characteristics of the two areas' climates during an observed 14-15 month dry period. He then developed an approximation of K, where:

$$k = \frac{PE + R}{P + L} \quad (12)$$

and *k* is the first approximation of K, calculated monthly. However, this equation did not work very well in other climates, and a different equation had to be developed. Since the work on the final K was dependent upon this approximation, Palmer described the development based on this and then retraced the final evaluation of K.

Next, Palmer used these monthly *k* values as weighting factors for the monthly moisture departures during the two dry periods being considered. He thus defined the "moisture anomaly index" as:

$$z = dk \quad (13)$$

These z values express on a monthly basis and from a moisture standpoint the departure of the weather of the month from the average moisture climate of the month. These values are the basic indicators of the PDSI. Drought severity is approximated by:

$$X_t = \sum_{t=1}^{i} \frac{z_t}{(0.309t + 2.691)} \tag{14}$$

where t represents the month number in the period and i is the total number of months in the period. This is a first approximation to the relationship sought, and further detail and refinement (especially concerning the approximation k) is available in Palmer's 1965 paper "Meteorological Drought". The Modified PDSI is called the PDI and is calculated for month t by:

$$PDI = 0.897 * PDI_{t-1} + 0.333 * z_t \tag{15}$$

This equation was empirically developed by arbitrarily defining an extreme drought as an index value of -4, and using the driest periods in the Kansas and Iowa regions described above as the benchmark to find a relationship between the maximum observed monthly rates at which the negative values of z accumulated during the observed dry intervals, and then determining the rate at which z must increase in order to maintain a constant value of the PDI. The coefficient values show that a current month's PDI is composed of only one-third of that month's precipitation deficit and almost nine-tenths of the previous month's PDI, exhibiting a long-term memory of previous moisture conditions. This is the index variation most widely used today. In practice, separate indices are calculated for wet and dry spell, and the final PDI is either the wet or dry index. The decision is based on whether or not spells are incipient, established, or ended. This shows the complexity of the PDI, and because of this complexity it is not uncommon for a PDI time series to exhibit large sudden changes (Guttman, 1998).

1.3.2 Use of PDSI

Since its inception, the PDSI has been extensively used as a drought indicator for the continental USA. PDSI maps are available for all climatic regions of the USA from the Climate Prediction Center at the National Weather Services website at the following url: www.nws.noaa.gov. The PSDI ranges from values -5 to +4, with -5.0 to 4.0 indicating extreme drought, -3.9 to -3.0 indicating severe drought, -2.9 to 2.0 indicating moderate drought, -1.9 to 1.9 indicating near-normal conditions, 2.0 to 2.9 indicating a moderate moist spell, and 3.0 to 3.9 indicating a very moist spell.

1.4 Standardized Precipitation Index

The SPI was developed in 1993 by Thomas McKee of the Colorado Drought Center, and is based on precipitation records (Mckee, 1993). It was designed to serve as a versatile tool in drought monitoring and analysis and would require only one input variable. Usually this variable is precipitation, but it could be applied in a similar way to snow pack, streamflow, reservoir storage, soil moisture and other hydrological parameters. The nature of the SPI allows drought determination at a particular time scale for any region of the world that has a precipitation record.

1.4.1 Definition of SPI

Thom (1966) found the gamma distribution to fit climatological precipitation well. The gamma distribution is defined by its frequency or probability density function:

$$g(x) = \frac{1}{\beta^{\alpha}\Gamma(\alpha)} x^{\alpha-1} e^{\frac{-x}{\beta}} \qquad (16)$$

where x, α and β > 0 and α is a shape parameter, β is a scale parameter, x is the amount of precipitation and Γ(α) is the gamma function defined as:

$$\Gamma(\alpha) = \int_0^\infty y^{\alpha-1} e^{-y} dy \tag{17}$$

Computation of the SPI involves fitting a gamma probability density function to a given frequency distribution of precipitation totals for a station. The alpha and beta parameters of the gamma probability density functions are estimated for each station and each time scale of interest (3 months, 12 months, 4 weeks, etc), and for each time period division. From Thom (1966), the maximum likelihood solutions are used to optimally estimate α and β:

$$\hat{\alpha} = \frac{1}{4\mathrm{A}}\left(1 + \sqrt{1 + \frac{4A}{3}}\right) \tag{18}$$

$$\hat{\beta} = \frac{\overline{x}}{\hat{\alpha}} \tag{19}$$

where:

$$A = \ln(\overline{x}) - \frac{\sum \ln(x)}{n} \tag{20}$$

n=number of precipitation observations.

The resulting parameters are then used to find the cumulative probability of an observed precipitation event for the given month and time scale for the station in question. The cumulative probability is given by:

$$G(x) = \int_0^x g(x)\partial x = \frac{1}{\hat{\beta}^{\hat{\alpha}}\Gamma(\hat{\alpha})} \int_0^x x^{\hat{\alpha}-1} e^{\frac{-x}{\hat{\beta}}} dx \tag{21}$$

Letting $t = x/\hat{\beta}$, this equation becomes the incomplete gamma function:

$$G(x) = \frac{1}{\Gamma(\hat{\alpha})} \int_0^x t^{\hat{\alpha}-1} e^{-t} dt \qquad (22)$$

The gamma function is undefined for x=0, but precipitation distributions may contain values of zero. Thus, the cumulative probability becomes:

$$H(x)=q+(1-q)G(x) \qquad (23)$$

where q is the probability of a zero. If m is the number of zeros in a precipitation time series, Thom (1966) states that q can be estimated by m/n.

The cumulative probability, $H(x)$ is then transformed to the standard normal random variable z with a mean of zero and a variance of one; this is the value of the SPI. This is an equiprobability transformation which Panofsky and Brier (1958) state has the essential feature of transforming a variate from one distribution (*i.e.* Gamma) to a variate with a distribution of prescribed form (*i.e.* standard normal) such that the probability of being less than a given value of the variate shall be the same as the probability of being less than the corresponding value of the transformed variate. In other words, it is transformed to a z-score where the z term is the SPI value. This z-score is more easily obtained computationally using an approximation provided by Stegun (1965) that converts cumulative probability to the standard normal random variable z:

$$Z = SPI = -\left(t - \frac{c_0 + c_1 t + c_2 t^2}{1 + d_1 t + d_2 t^2 + d_3 t^3} \right) \text{ for } 0<H(x)\leq 0.5 \qquad (24)$$

$$Z = SPI = +\left(t - \frac{c_0 + c_1 t + c_2 t^2}{1 + d_1 t + d_2 t^2 + d_3 t^3} \right) \text{ for } 0.5<H(x)<1.0 \qquad (25)$$

where:

$$t = \sqrt{\ln\left(\frac{1}{(H(x))^2} \right)} \quad \text{for } 0<H(x)\leq 0.5 \qquad (26)$$

$$t = \sqrt{\ln\left(\frac{1}{(1-H(x))^2}\right)} \text{ for for } 0.5<H(x)<1.0 \qquad (27)$$

and c_0=2.515517;c_1=0.802853;c_2=0.010328;d_1=1.43788;d_2=0.189269;d_3=0.001308.

Conceptually, the SPI represents a z-score, or the number of standard deviations above or below the mean, assuming normal distribution. This assumption is not valid for short time scales, since the distribution is skewed. The SPI also normalizes with respect to location and time, since it not only accounts for the frequency distribution and variation of precipitation at a station, it can also be computed at any number of time scales depending upon the impacts of interest to the analyst. Additionally, the SPI represents a cumulative probability in relation to the base period for which the gamma parameters were estimated for any location or timescale. Using the SPI as the indicator, a functional and quantitative definition of drought can be developed for each time scale. Usually, a drought event for time scale *i* is defined as a period in which the SPI is continuously negative and the SPI reaches a value of -1.0 or less. The drought begins when the SPI first falls below zero and ends with the positive value of SPI following a value of -1.0 or less. SPI values are usually classified in ranges, with values between -1.0 and 1.0 defined as near-normal conditions. Values between -1.0 and -1.50 are moderately dry, values from -1.50 to -2.0 are severely dry, and any value less than -2 is extremely dry. At the other end, values between 1.0 and 1.50 are moderately wet, 1.50 to 2.0 are very wet, and values greater than 2 are extremely wet conditions.

The SPI has several limitations to it. Firstly, it is only as good as the data used in calculating it, so extreme values may provide misleading results. Also, regional climatology knowledge is required, since at the smaller time scales (< 3 months), the SPI is very similar to the percentage of normal representation of precipitation, which can be

misleading in regions with low seasonal precipitation totals, leading to the issue stated above. Understanding the climatology improves the interpretation of these SPI values.

1.4.2 Use of SPI

The SPI was originally developed for use in Colorado, but interest in it has grown and propelled it to use at state, regional and national levels. The National Drought Mitigation Center (NDMC) and National Oceanic and Atmospheric Administration (NOAA) has monthly SPI maps for the continental USA available on the Internet (http://www.drought.unl.edu/monitor/spi.htm, http://www.wrcc.dri.edu/spi/spi.html), and the Colorado Climate Center (CCC) continues to present SPI maps of Colorado on various time scales, to cite a few examples. A specific example of the SPI's application was the drought of 1996. This drought affected most of the USA west of the Mississippi, and began in October 1995. From late 1995 to January 1996, very little precipitation fell in the southern plains and Southwest. February 1996 was a very dry month from southern Minnesota and South Dakota to the Texas-Mexico border. The 5-month SPI calculated for this period indicated that most climatic divisions from southern Nebraska to California had SPI values of less than -1.0, and the SPI was less than -2.0 in 8 of 9 climatic divisions in Kansas. By the end of February, the SPI clearly indicated that drought was occurring in the southern plains and Southwest, especially in Kansas, Oklahoma, New Mexico and northern Texas. Other indicators were also confirming the existence and severity of this drought, such as agricultural reports and wildfires. The SPI study of the drought was done after the fact, and the results demonstrated that it would have been a beneficial tool for detecting and monitoring the drought in the southern plains and southwestern United States. Although the drought was region wide, the

dynamics of the drought varied by location. Since awareness of this index has increased, it can be better used to monitor and predict future drought events.

1.5 Comparison of SPI and PDSI

Keyantash and Dracup (2002) performed an evaluation of drought indices classified by types of drought. Their evaluations were based on 6 criteria, listed below in decreasing order of significance:

1. **Robustness:** This refers to whether or not the index was useful and/or relevant over varying climatic condition, and whether it was consistently responsive or solely temperamental.
2. **Tractability:** This refers to whether or not the index is practical. In other words, this aspect examines if the index can be easily used due to simplicity, or is extremely complex either in calculation or in data/parameter collection or definition.
3. **Transparency:** This refers to the purpose of the index, examining whether the purpose for the index's existence is clear and reasonable, or extremely obfuscated and confusing.
4. **Sophistication:** This may seem to contradict the previous criterion, but is included to examine the validity of the index, and ensure that the index does not oversimplify reality.
5. **Extendibility:** This is the degree to which the index may be extended across time to other drought scenarios, either temporally or regionally.

6. **Dimensionality:** This refers to the connection of the index with the physical world, with indices comprising physical units or derived from a physical ratio having an advantage over dimensionless indices.

The drought indices under evaluation included the SPI and the PDSI along with Rainfall Deciles, the Surface Water Supply Index and a few other indices. The results of the evaluation placed the SPI as the second highest ranked drought index, with a total score of 115 (highest was Rainfall Deciles with a score of 116). The PDSI placed much lower with a total score of 61 (Keyantash and Dracup, 2002).

Also, Guttman (1998) compared the SPI and PDI using precipitation data from the National Electronic Drought Atlas to compute both the PDI and SPI (with timescales of 1-,2-,3-,6-,12-,24- and 36-month periods) for all the sites given in the Atlas. The sites with the longest record length were then selected for spectral analysis. This analysis technique is used to look for cyclical patters in a time series. The time series is decomposed into a sum of sine and cosine waves of different amplitudes and wavelengths. The amplitude of a given wave or cycle, when smoothed over the whole duration of the time series, is an estimate of the contribution or importance of the cycle to the observed time series. Spectral densities of the PDI time series and the 1-,2-,3-,6-,12-,24-, and 36-month SPI time series were computed. The higher the density, the more a given cycle contributes to the observed time series. Cross spectral analysis, which is similar to spectral analysis but looks at the interrelationships between two time series, was also performed. Cross spectral densities between the PDI time series and each of the SPI time series were computed. The aim of these analyses was to gain in understanding of the underlying structure of both the PDI and the SPI as well as to gain insight into the

spatial consistency of the indices. The results of the analyses showed that there were no spatially coherent patterns in the PDI spectra; i.e. the spectral patterns vary from site to site, while the SPI spectra exhibit the same pattern at all locations. High coherence between the PDI and SPI indicate that precipitation is the dominant factor in the PDI, and the phase relationship between the two indices show that for periods of less than a year, the PDI lags the SPI and for periods of about a year, the two indices are in phase.

1.6 Remote Sensing and Drought Stress Detection in Vegetation

Vegetation is significantly affected and impacted by drought conditions. Water comprises about 85-90% of the fresh weight of most herbaceous plants, and is usually absorbed by roots in the soil and translocated to the shoots as a result of pressure gradients developed from either root pressure or transpiration. Whenever the rates of water loss by transpiration exceeds the rates of water absorption by the roots, water in the conducting tissues is subject to a tension (negative pressure), that is, its potential is lowered and competition for water among the various tissues and organs of the plant takes place because the equilibra among the separate water potentials have been disturbed (Hale and Orcutt, 1987). Hale and Orcutt also state that drought stress occurs when available water in the soil is reduced and atmospheric conditions cause continued loss of water by transpiration and evaporation. Stress may occur on a daily basis or over a prolonged period, and the plant's leaves will wilt. At the permanent wilting point, the water potential of the leaves remains below the water potential of the soil, and at this point water cannot move to the roots rapidly enough to overcome the deficit in the plants. This stress affects the cell vacuoles and chlorophyll level (which give plant leaves their green color) in the leaves, which in turn has an effect on remote sensing of the plant.

Remote Sensing is sometimes defined as "the science of acquiring, processing and interpreting images and related data obtained from aircraft and satellites that record the interaction between matter and electromagnetic radiation" (Sabins, 2000). However, it can include ground-based sensing of remote data as well. Remote Sensing in its broadest sense is the observation from any distance of the reflection of electromagnetic waves of various wavelengths from various targets of interest, and determining the properties of the targets from the measurements of the emitted and/or reflected electromagnetic radiation. The spectral reflectance of a target is defined as the ratio of the reflected spectral radiance flux to the incident spectral radiance flux and can be measured in three ways: in the laboratory, in the field, or from an elevated platform such as an aircraft or satellite. The values of reflectance are unitless and range between 0 and 1. The reflectance of a particular target across a range of EM wavelengths is called its **spectral signature** and is a representative property of that target. To facilitate research of various regions of the spectrum, **bands** have been developed. These are selected wavelength intervals which may show variations in reflectance for various targets. Vegetation in particular has a signature that is easily recognizable in different bands. Plant leaf responses to various stresses usually dominate the spectral responses of the entire plant, with stems and branches providing a minor contribution. When a leaf intercepts incoming radiation, a portion of the radiation is absorbed, another portion is transmitted and the rest is reflected. The amount of absorption depends on the photon energy and also upon the concentration of leaf chlorophyll pigments and tissue water content (Gausman, 1985). Bowker (1985) summarized the features of vegetation reflectance. Figure 1-1 is an example of a reflectance curve for photosynthetically active vegetation, dry vegetation

with no chlorophyll and desiccated cells, and soil. The spectrum can be broken into three regions according to the major factor responsible for the curve behavior. Below 0.7 μm, absorption is dominated by carotenoid pigments (centered at 0.48 μm) and chlorophylls (centered at 0.68 μm).

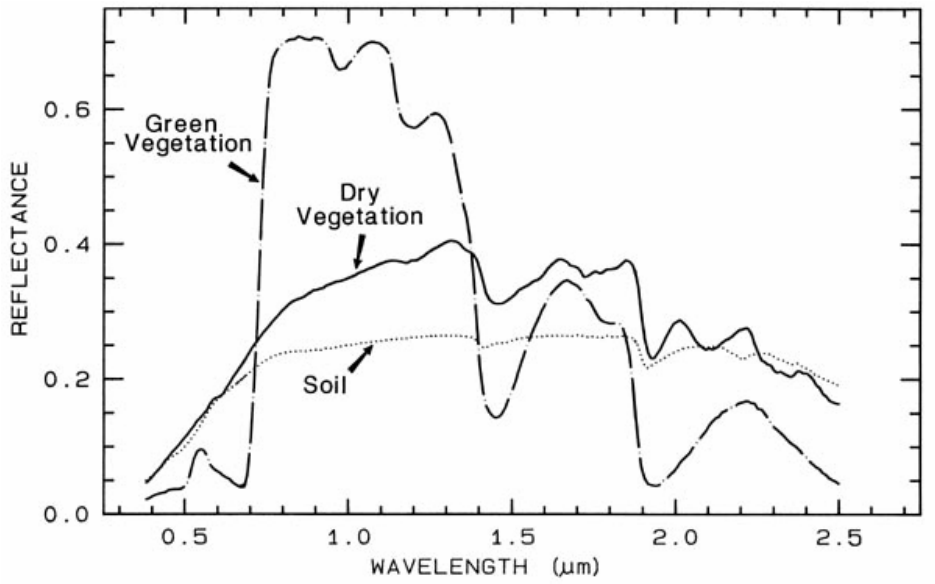

Figure 1-1: Representative spectral signatures of green vegetation, dry vegetation and soil (source http://www.iac.ethz.ch/staff/stockli/ndvimeasurement/ndvimeasurement.html)

The green peak (centered at approximately 0.56 μm) is the region of the visible spectrum corresponding to weak absorption. The sharp rise around 0.7 μm (called the red edge) marks the change from chlorophyll absorption to cellular reflectance. The near-infrared reflectance from 0.7 to 1.3 μm is dominated by the cell-wall/airspace interface and, to a lesser extent, by refractive index discontinuities of cellular constituents (Gausman 1985). Beyond 1.3 μm, reflectance is primarily controlled by leaf water content. Specular reflectance occurs at the leaf cuticle while diffuse reflectance originates from light scattering within the leaf mesophyll. Figure 2 is a diagram of reflectance of EM radiation interaction with a leaf. From the Figure, it is seen that while blue and red light are

strongly absorbed by the leaf chloroplasts, green light is reflected from it; and though infrared radiation is unaffected by chloroplasts, it is strongly reflected by the spongy mesophyll.

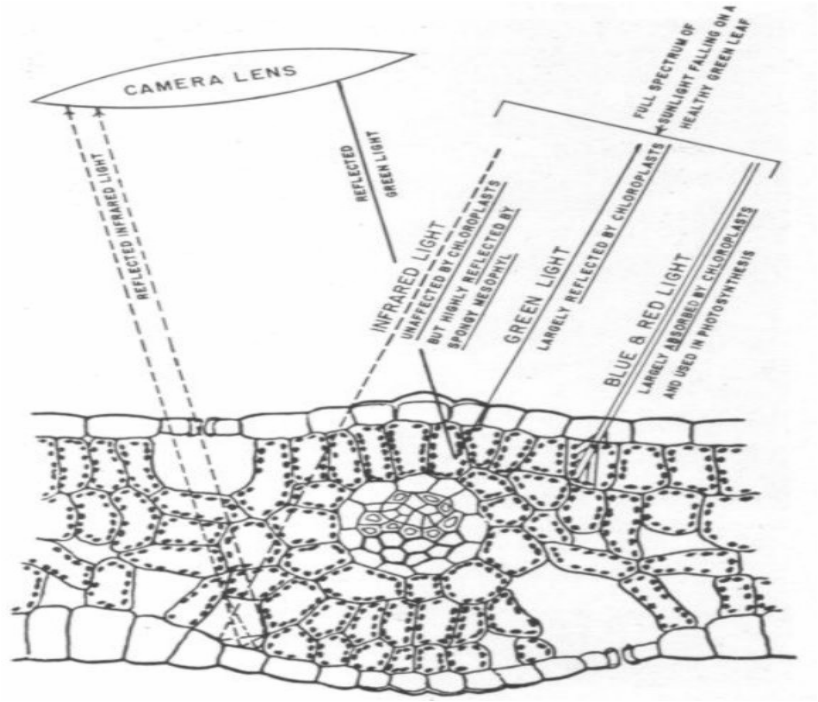

Figure 1-2: Electromagnetic radiation interacting with a plant leaf. (Source: http://www.geog.ucsb.edu/~jeff/115a/lectures/films_and_filters.html)

Carter (1993) described the responses of vegetation reflectances to various stresses to determine the wavelengths at which leaf reflectance is most responsive to stresses, looking at a variety of plant species. He discovered that visible reflectance, particularly in the green spectrum and red spectrum increased consistently in response to stress regardless of stress agent or species. Differences near 710 *nm* were greater than those near 550 *nm*, and with dehydration a peak difference occurred in the yellow spectrum at 584 *nm*. Differences in the visible spectrum generally were smallest at the violet and blue wavelengths. Infrared reflectance responded consistently only when stress had developed enough to cause severe leaf dehydration.

Although much research is available on leaf optical properties, there is still work to be done in this field and this should be kept in mind by those who use remote sensing of vegetation. Jacquemond and Ustin (2001) did a review of various methods used in remote sensing and made the following conclusion:

> Contrary to accepted dogma, much more work is required before we will completely understand leaf optical properties. This knowledge is nevertheless crucial to develop more accurate relationships between these properties and important leaf functional characteristics, or to improve models which are directly used to interpret remote sensing data when coupled with canopy reflectance models To give an example, the separation of leaf photosynthetic pigments (chlorophyll *a, b*, carotenoids and xanthophylls) is still at issue, and this information would greatly improve the cartography of plant photosynthetic activity from space. Additionally, other aspects of leaf optics like fluorescence have not been developed here [in this paper] but provide critical information about photosynthetic function. As mentioned earlier [in this paper] our understanding of leaf bidirectional properties is still in its infancy.

1.7 Vegetation Indices

A vegetation index is defined as the various combinations of reflectances of channels/bands of remote sensing sensors, and is an indicator of the target vegetation's inherent properties as examined by their reflectance in these different bands. In principle, these combinations are applied to the reflectances of whatever the target is, but most indices have been developed with respect to vegetation spectral reflectance properties.

Vegetation indices are quantitative measurements indicating the vigor of vegetation and are developed to enhance the sensitivity of individual spectral bands in the detection of biomass. They serve many different purposes in remote sensing; they can be used for classification (identifying various land cover regions and separating vegetation from open soil etc.) as well as for land use changes, vegetation density, crop discrimination and prediction, among others. The most obvious properties of vegetation reflectance that are used for vegetation index calculation are the high absorption of the

red spectrum (630-690 *nm*) by plant chlorophyll and the strong reflection of the infrared spectrum (760-900 *nm*) by leaf cellular structures. While the vast majority of indices were developed for specific sensors, the principles behind their development can be usually applied to other sensors monitoring the same band regions, and most indices can be applied to any satellite sensors that monitors in the ranges that define the vegetation index. The indices used in the research for this thesis are defined and explained in the following sections.

1.7.1 Normalized Difference Vegetation Index

By far, the most common vegetation index in use today is the Normalized Difference Vegetation Index, or NDVI (Rouse, 1972). It is defined as:

$$NDVI = \frac{\rho_{NIR} - \rho_{red}}{\rho_{NIR} + \rho_{red}} \tag{28}$$

where ρ_{NIR} stands for the reflectance in the near-infrared band and ρ_{red} stands for the reflectance in the red band. This index is based on healthy vegetation having a high reflectance in the infrared band and a low reflectance in the red band, while stressed vegetation will have a lower IR reflectance and progressively higher red band reflectance. The NDVI values range from 1 to -1, with values below 0 indicating poor vegetation conditions or non-vegetation targets such as soil. The index is sensitive to the presence of green vegetation (Sellers, 1987) and permits the prediction of agricultural crops (Tucker and Sellers, 1986). It has also been used to predict monthly evaporation (Szilagyi, et al, 1998) and used as the basis for drought detection using remote sensing (Wan *et al*, 2004). Kogan (1997) developed the Vegetation Condition Index (VCI) which is defined in terms of NDVI. This index compares the vegetation of a region to the maximum values thus:

$$VCI = \frac{NDVI - NDVI_{\min}}{NDVI_{\max} + NDVI_{\min}} * 100 \quad (29)$$

where $NDVI_{max}$ is the maximum *NDVI* recorded on record for the region during the study period, $NDVI_{min}$ is the minimum NDVI recorded for the region, and *NDVI* is the current NDVI measurement. This was developed using the AVHRR sensors, and requires a lengthy record of NDVI values. It is not used in this research for that reason. Further discussion of VCI applications is presented further along in this chapter.

1.7.2 Normalized Difference Water Index

The Normalized Difference Water Index (NDWI) was proposed by Bo-Cai Gao (1996) for remote sensing of vegetation liquid water from space. It uses two infra-red channels, one at 0.86 μm and the other at 1.24 μm. The index is defied as:

$$NDWI = \frac{\rho(0.86\ \mu m) - \rho(1.24\ \mu m)}{\rho(0.86\ \mu m) + \rho(1.24\ \mu m)} \quad (30)$$

where ρ is the reflectance at the given wavelength. These wavelengths were chosen because of their reflectance properties when considering absorption by water. Since the 1.24 μm channel has similar vegetation scattering properties as the 0.86 μm channel, and because the 1.24 μm channel is sensitive to liquid water content (Bo-Cai Gao, 1996), NDWI is expected to be sensitive to vegetation liquid water changes. In general, NDWI values are positive for green vegetation due to the weak liquid water absorption near 1.24 μm.

1.7.3 Vegetation Index Number and Ratio Vegetation Index

The Vegetation Index Number (VIN) is also referred to as the Simple Ratio.

It also relies on the contrasts in reflectance of plants in the infrared and red spectrums, and is defined as:

$$VIN = \frac{\rho_{NIR}}{\rho_{red}} \tag{31}$$

The VIN was one of two vegetation indices developed by Pearson and Miller in 1972. The other index was simply the inverse of the VIN, and was called the Ratio Vegetation Index (RVI). These indices enhance the contrast between the ground and vegetation; they are less affected by the effect of illumination conditions but are sensitive to ground optical properties (Baret and Guyot, 1991). The relationships between the reflectances of the two bands permit to eliminate disturbances from factors affecting in the same manner the radiances of each band. (Holben and Justice, 1981.) The RVI index is sensitive to atmospheric effects and its discriminating power is weak when the vegetation cover is less dense (less than 50%) while it is best when the vegetation cover is dense (Bannari, *et al,* 1995).

1.7.4 Atmospherically Resistant Vegetation Index

The Atmospherically Resistant Vegetation Index (ARVI) was developed for use with the Earth Observing System (EOS) Moderate Resolution Imaging Spectroradiometer MODIS sensor (Kaufman and Tanré, 1992). It utilizes the blue band for MODIS and Landsat satellites in addition to the red and infrared bands. The resistance of the ARVI to atmospheric effects when compared to the NDVI is accomplished by a self-correction process for the atmospheric effect on the red channel, using the difference in radiance between the blue and red channels to correct the radiance in the red channel. The ARVI has a similar dynamic range to the NDVI and is on average 4 times less sensitive to

atmospheric effects than the NDVI (Kaufman and Tanré, 1992). In reflectance terms, it is defined as:

$$ARVI = \frac{\rho_{NIR} - \rho_{rb}}{\rho_{NIR} + \rho_{rb}} \quad (32)$$

where

$$\rho_{rb} = \rho_{red} - \gamma(\rho_{blue} - \rho_{red}) \quad (33)$$

where γ is a constant which depends on aerosol type (particles present in the atmosphere). Research performed by Kaufman and Tanré (1992) showed that the best value for γ is 1.0 if information on the aerosol type is unavailable, and this was the value used in this research.

1.7.5 Soil-Adjusted Vegetation Index

The Soil-Adjusted Vegetation Index (Huete, 1988) is aimed at reducing the effect of soil brightness on the NDVI and is calculated by shifting the NIR and red channels towards a negative origin by adding a constant L to the NDVI formula. Thus:

$$SAVI = \left(\frac{\rho_{NIR} - \rho_{red}}{\rho_{NIR} + \rho_{red} + L} \right)(1 + L) \quad (34)$$

where (1+*L*) is the multiplication factor added so that the index can conform to the maximum and minimum NDVI range. For most purposes and in this thesis, the value of *L* was 0.5, corresponding to intermediate vegetation canopy cover.

1.7.6 Modified Soil-Adjusted Vegetation Index

Qi *et al.* (1994) have shown that the adjustment factor *L* in the SAVI definition is not a constant but a function which varies inversely with the amount of vegetation present. To minimize the effect of bare soil on the SAVI, they proposed a modification, the Modified Soil-Adjusted Vegetation Index (MSAVI). This modification was aimed at finding a self-adjustable *L* that would increase the SAVI vegetation sensitivity by increasing the dynamic range and further reduce the soil background effects. The result would be an improved, modified SAVI with a higher "vegetation signal" to "soil noise" ratio. An induction method was used to derive *L* or the MSAVI. Using any seed value, L_0 $(0,\pm\infty)$ would reduce the effect of soil to the MSAVI value:

$$MSAVI_0 = \left(\frac{\rho_{NIR} - \rho_{red}}{\rho_{NIR} + \rho_{red} + L_0} \right)(1 + L_0) \tag{35}$$

Now, since there is an initial $MSAVI_0$, another L function L_1 may be obtained:

$$L_1 = 1 - MSAVI_0 \tag{36}$$

which would result in an $MSAVI_1$ that further minimizes the soil effect:

$$MSAVI_1 = \left(\frac{\rho_{NIR} - \rho_{red}}{\rho_{NIR} + \rho_{red} + 1 - MSAVI_0} \right)(2 - MSAVI_0) \tag{37}$$

Continuing this process *n* times, we obtain

$$L_n = 1 - MSAVI_{n-1} \tag{38}$$

and

$$MSAVI_n = \left(\frac{\rho_{NIR} - \rho_{red}}{\rho_{NIR} + \rho_{red} + 1 + MSAVI_{n-1}} \right)(2 + MSAVI_{n-1}) \tag{39}$$

With this processing, there exists an iteration time *N* such that $MSAVI_N = MSAVI_{N-1}$, where soil effects cannot be minimized further. Then:

$$MSAVI_N = \left(\frac{\rho_{NIR} - \rho_{red}}{\rho_{NIR} + \rho_{red} + 1 + MSAVI_N} \right) \left(2 + MSAVI_N \right) \quad (40)$$

One of the two solutions for the above equation within the range of 0 and 1 is:

$$MSAVI_N = \frac{-b - \sqrt{b^2 - 4c}}{2} \quad (41)$$

where b = -(2ρ_{NIR}+1) and c=2(ρ_{NIR}-ρ_{red}). Therefore, with an inductive *L* function of

$$L = 1 - MSAVI_2 \quad (42)$$

the resultant MSAVI by induction, $MSAVI_2$, becomes:

$$MSAVI_2 = \frac{2\rho_{NIR} + 1 - \sqrt{\left(2\rho_{NIR} + 1\right)^2 - 8\left(\rho_{NIR} - \rho_{red}\right)}}{2} \quad (43)$$

This was the formula used in this research. Research by Qi *et al* (1994) indicated that the MSAVI showed itself to be a more sensitive indicator of vegetation amount than the SAVI, but this research was validated using ground and aircraft-based radiometric measurements only.

1.7.7 Normalized Difference Index

For establishing the relationship between spectral reflectance and the surface covered by corn crop residues and for developing a methodology for mapping these residues, McNairn and Protz (1993) examined various combinations of Landsat bands to form Normalized Difference Indices (NDI). The combination that produced the best results for their study used the middle shortwave infrared and the near infrared bands. It is insensitive to soil organic matter content but quite sensitive to corn residues and soil types. It is defined as:

$$NDI = \frac{\rho_{NIR} - \rho_{MIR}}{\rho_{NIR} + \rho_{MIR}} \quad (44)$$

where ρ_{NIR} is Band 4 of the Landsat TM sensor or a similar band in wavelength, and ρ_{MIR} can be Band 5 of the Landsat TM sensor, or a similar bandwidth.

1.7.8 Normalized Difference Greenness Index

The Normalized Difference Greenness Index (NDGI) is calculated using the red and green bands, and has revealed itself quite useful for identifying and mapping different active vegetation formations in inundated regions. It is defined as:

$$NDGI = \frac{\rho_{green} - \rho_{red}}{\rho_{green} + \rho_{red}} \quad (45)$$

and was defined by Chamard *et al* in 1991 (Chamard *et al*, 1991; Bannari *et al*, 1995).

1.7.9 Normalized Difference Redness Index

The Normalized Difference Redness Index is a coloration index which is a correction factor for soil color effect on vegetation indices (Bannari, *et al,* 1995). Variations caused by soil color greatly hinder the detection of low vegetative cover rates. This factor comes in second place after soil brightness, and the soil coloration index is thus a correction permitting to double the sensitivity of vegetation indices. By analogy with the NDVI, this index is defined as:

$$RI = \frac{\rho_{red} - \rho_{green}}{\rho_{red} + \rho_{green}} \quad (46)$$

It is the exact inverse of the NDGI.

1.7.10 Water Band Index

The Water Band Index (WBI) was developed by Penuelas *et al* (1997) for the estimation of plant water concentration by ground-based reflectance measurements. It takes advantage of the reflectance of plant leaves at wavelength 970 nm (a water absorption band) and 900 nm (no absorption of water but strong indicator of plant vigor). The ratio is defined as:

$$WBI = \frac{\rho_{900}}{\rho_{970}} \tag{47}$$

1.7.11 Red-Edge Vegetation Stress Index

The red-edge, centered at the largest change in reflectance per wavelength change, is located between the widely used red band and NIR band and may hold valuable information that may benefit aspects of ecological-based research. The wavelengths of the red-edge range from 670-760 nm, and high spectral resolution Airborne Visible/Infrared Imaging Spectrometer (AVIRIS) data encompassing this range has been used to describe community phenological response through time as a function of changes to red-edge symmetry. The RVSI was developed to identify inter- and intra-community vegetation stress trends based on spectral changes in upper red-edge geometry (Merton and Huntington, 2002). In simple terms, reflectance spectra with upper red-edge convexity calculate negative RVSI values indicating low vegetation stress, whereas upper red-edge spectra with near-linear or concave curves indicate an “apparent stress” response. It is defined as:

$$RVSI = \left(\frac{\rho_{714} + \rho_{752}}{2} \right) - \rho_{733} \tag{48}$$

1.8 Previous Work Relating Remote Sensing, Vegetation Indices, Environmental Parameters and Drought

Because of the effects of drought stress on vegetation and the detection of these effects through vegetation reflectance, remote sensing and satellite imagery have been often used to detect and/or predict drought conditions (Kogan, 1996). Traditional drought indicators like precipitation and soil moisture are locally measured and can be difficult to obtain on a regional scale, while a remotely sensed satellite image of a region's vegetation can be easily obtained for virtually any region on the earth and at a very large scale. Images have been acquired on many satellite platforms for drought analysis, such as the Advanced Very High Resolution Radiometer (AVHRR), Moderate Resolution Imaging Spectroradiometer (MODIS) and Landsat series.

The AVHRR in particular has been used extensively with the NDVI to investigate drought in many regions due to its high temporal frequency (images are acquired daily for any point on the earth). It has a very coarse spatial resolution of 1 km. The NDVI was originally developed for this sensor and most global drought remote sensing is done with this sensor. The VCI as previously described in this chapter has also been extensively used for global drought monitoring. Vogt (2000) examined the relationship between the 3-month SPI and the 3-month running mean for the decadal NDVI and VCI for weather stations in Andalusia, Spain. He looked at the simultaneous trends over time between the SPI and the vegetation indices, with varying results. However, he did not do a statistical correlation in that paper. The VCI has also been used in Argentina (Seiler *et al*. 1998) to monitor crop production as a proxy of drought stress. The reflectance at the Middle Infrared band of the AVHRR sensor has also been used to monitor drought stress on tropical vegetation canopies in Malaysia showing an inverse correlation to rainfall over a

15-day period and a 5-day lag (Boyd, *et al* 2002). Links between NDVI and precipitation have also been established, and an example of this can be seen in a study done by Nicholson *et al* (1990) based in the Sahel and Eastern Africa. This study showed that the spatial patters of annually integrated NDVI closely reflect mean annual rainfall, and there was a good relationship between rainfall variations and NDVI on seasonal and interannual time scales for areas where mean annual rainfall ranges from 200 to 1200 *mm*. However, the relationships varied with location, with NDVI being linearly related to mean annual rainfall in the Sahel, but log linear in East Africa and then only to a certain threshold, over which there was a minimal relationship.

Ghosh (1997) performed a study of drought in India using digital analysis of satellite data and Geographical Information Systems (GIS). He used Indian Remote Sensing Satellite-1A Series Linear Imaging Self-Scanning Sensors 2 (IRS-1A LISS 2) datasets over the dry season (April to June) and the growing period (November to January) of 1988, 1990 and 1991, and analyzed it with a GIS system along with a continuous set of rainfall data over a 70-year period at 22 weather stations. He also incorporated soil-moisture measurements from all 22 stations, and created a final result of composite images based on vegetation, slope, albedo, soil moisture and land cover image analyses, and then compared this image analysis to field results in drought-stricken areas. Ghosh concluded that a composite drought index derived from the combined analyses can provide a useful tool for investigation, monitoring and prediction of drought.

Bahrun *et al* (2003) examined water stress detection in maize using the RVI, defined as:

$$RVI = \frac{\frac{NI_c}{NI_i}}{\frac{PAR_c}{PAR_i}} \quad (49)$$

where NI_i=incoming near infrared radiance and NI_c=reflected near infrared radiance, and PAR_i=incoming photosynthetically active radiation (between 400 and 700 *nm*) and PAR_c=outgoing photosythetically active radiation. This differs from the RVI definition used in this thesis and described by Bannari *et al* (1995), in that equation (47) describes this thesis's VIN index, using the panchromatic visible reflectance instead of the red band reflectance. Bahrun *et al* derived values for this index from field-grown but closely monitored maize plants and compared the RVI values with various plant parameters. He concluded that an increase in xylem [ABA] increment coincided with a decrease in the RVI of drought-stressed plants, that changes in drought-stressed plant RVI as compared to control plant RVI occurred at early stages of drought stress, and that RVI measurements of field measurements when compared with fully irrigated references could be used as an early warning system for timing of irrigation.

Jacobberger-Jellison (1994) investigated the detection of post-drought condition in Sahelian West Africa using Landsat TM-derived NDVI and SAVI. He used six Landsat TM images from March 1986 to April 1988, applying corrections where needed. He found that NDVI and SAVI values exhibited a relationship that is inverse to seasonal vegetation trends, with the calculated vegetation indices being highest for dry season data, lower in the rainy season, and values for the dry 1988 season being lower than the less dry 1986 season. Jacobberger-Jellison stated that the usefulness of the NDVI was still limited in regions like this, where the soil brightness apparently overwhelms the

slight vegetation signature, while the SAVI's failure was due to uncertainty in scaling factors and constants.

Szilagyi *et al* (1998) investigated the relationship between NDVI and monthly evaporation using Landsat imagery over the Crescent Lake National Wildlife Refuge in the Sand Hills region, Nebraska. This region consists of undisturbed natural mixed-grass prairie over sandy soils. He calculated NDVI for thirty scenes of Landsat during the growing seasons between 1979 and 1983, and estimated monthly evaporation using the Thornwaite and Mather (1957) algorithm modified by Vorosmarty (1989) based on the monthly precipitation and potential evaporation estimated by the Jensen-Haise (1963) method. Szilagyi *et al* discovered that when no time lag was applied, the linear correlation between NDVI and both monthly precipitation and evaporation was very poor to moderate, with r=0.39 for precipitation and r=0.56 for evaporation. However, when a lag of one month was applied, the correlations improved significantly, with r=0.75 for precipitation and r=0.80 for evaporation. Szilagyi *et al* concluded that the NDVI vs. evaporation relationship can be strong for a water-restricted natural environment with an apparent time-lag between the two variables.

Di *et al* (1994) investigated modeling relationships between NDVI and precipitation during vegetative growth cycles. He conceptualized the NDVI as a function of climate, terrain, vegetation/ecosystem and soils/hydrological variables, with a governing equation of:

$$NDVI = f\left(C, V, P, S\right) + E \tag{50}$$

where C is the climate submodel, V the vegetation/ecosystem submodel, P the physiography submodel, S the soil/hydrology submodel and E is modeling error caused

by unaccounted-for environmental variables and potential inaccurate measurement. The submodels in turn may be represented as functions of their major respective components, with *C* being a function of precipitation, temperature and insolation; *V* a function of ecosystem and vegetation class; *P* a function of elevation, slope and aspect; and *S* being a function of soil moisture retention, nutrients, permeability, surface water availability and ground water supply. All of these functions have similar *E* terms incorporated. This is still a huge simplification since the function components themselves are also dependent variables with time and space and with each other. Thus, it should be possible to partially or totally describe one environmental variable by other environmental variables, thus limiting the total number of variables. Di *et al* stated that the major climate variables which have a cumulative effect on NDVI were precipitation, temperature and insolation, thus giving an approximation of NDVI as:

$$NDVI(t) = f\left(precipitation(T_t), temperature(T_t), insolation(T_t)\right) + E \qquad (51)$$

where (T_t) refers to cumulative effect of a component for a period of time prior to the specific time *t*. Di further simplified the model by stating that in semi-arid to arid regions, insolation and temperature can often be partially described by precipitation as well as being highly correlated with a particular season of the year. Thus, a designated variable such as Julian day *j* could be used to represent climatic seasons. The model would then be simplified to:

$$NDVI(t) = f\left(precipitation(T_t), j\right) + E \qquad (52)$$

If the temporal resolution is daily, then *t* becomes *j.* Since equation (52) states that NDVI at Julian day *j* is a function of precipitation and Julian day, Di *et al* separated the function into three parts: those with only *j,* those with only precipitation (T_t) and those with both.

The first part is the seasonal effect described by Julian day, the second part describes the precipitation effects on NDVI, and the third part describes the combined effect of precipitation and season (e.g. the precipitation in May may have a greater effect on vegetation growth than in September). Thus, the model can be rewritten as:

$$NDVI(j) = S(j) + P\left(precipitation\left(T_j\right)\right) + R\left(precipitation\left(T_j\right), j\right) + E \qquad (53)$$

where j is the Julian day, S(j) is the background value due to soil and $\left(T_j\right)$ is a period of time prior to Julian day j. $P\left(precipitation\left(T_j\right)\right)$ describes the precipitation variables, and $R\left(precipitation\left(T_j\right), j\right)$ describes the combined effect of the two variables. Di *et al* assumed that both P and R would be positive, and if the precipitation within $\left(T_j\right)$ was zero, then the soil would be too dry to support vegetation and both P and R would become zero, making the NDVI equal to the soil background value. Di *et al* further assumed that the soil background value has little change and could be approximated by a constant C that is the NDVI value for the area without vegetative activity, such as during winter. Combining functions P and R using the precipitation $\left(T_j\right)$ term, Di *et al* created a new function called U. Thus:

$$NDVI(j) = C + U\left(precipitation\left(T_j\right), j\right) + E \qquad (54)$$

Di *et al* then went on to add weight functions to account for seasonal variation. He tested his model using a time-series of NDVI images from the Crescent Hills National Wildlife Refuge in Nebraska. The results were positive, and demonstrated that the model may be useful in understanding NDVI-precipitation relationships. From the case study, Di *et al*

found that the duration of NDVI response to precipitation varies within a growing season, and thus it may be possible to estimate precipitation from NDVI.

Peters *et al* (1991) investigated the 1988 Nebraska drought using AVHRR NDVI data, PDSI data and Crop Moisture Index (CMI) data. They used NDVI data from April to September of 1987 (a normal year) and 1988 (a drought year), and incorporated precipitation data via the PDSI and CMI values for the study regions during those times. Their results showed that while the PDSI showed a distinct separation between years, it did not respond quickly to soil moisture components. The CMI was more responsive to short-term soil moisture variability and the NDVI appeared to reflect the related response of vegetation to soil moisture variability. They concluded that the AVHRR data could accurately locate the geographic core of the drought, and that a relationship existed between the NDVI and short-term variations in soil moisture.

Peters *et al* also investigated drought impact on semi-arid vegetation (1993) in New Mexico using AVHRR NDVI data, PDSI and CMI data, and monthly departure from precipitation for a wet year (1988) and a drought year (1989) in the region. The study area was an east-west transect of approximately 75 by 340 km extending from the Rio Grande between Las Cruces and Truth or Consequences, New Mexico to the Texas border. Peters *et al* classified the region into land cover classes using a two-step unsupervised classification procedure on nine images selected from the 1989 dataset by firstly separated them into two broad categories: woodland and non-woodland. Next, they ran the same unsupervised classification within those distinct groups. Their final result included classifications of desert basins, arid shrublands, arid grasslands, temperate grasslands, mixed forests and coniferous forests. Peters *et al* assessed the spectral

response of native plant communities to moisture stress by evaluating between-year changes in the mean and variance of NDVI values for each plant community type, and compared drought indices to vegetation indices by qualitative analyses of the shapes and trends of CMI, PDSI, monthly precipitation mean departures and NDVI. The results showed that grassland regions were more spectrally responsive to moisture stress than shrublands or forests, and shrublands did not respond as strongly as grasses to short-term changes in moisture availability. Peters *et al* stated that creosote (*Larrea tridentata*) is relatively insensitive to late summer precipitation and coniferous forest showd the least spectral variability of any plant community type during the 1989 growing season. Peters *et al* also concluded that the precipitation departure from monthly normal was the indicator most closely related to spectral NDVI response, and the CMI was more indicative of NDVI trends than the PDSI was, especially in grassland regions.

Wang, Price and Rich (2001) investigated the spatial patterns of NDVI in response to precipitation and temperature in the central Great Plains, focusing on the entire state of Kansas. For this investigation, they derived bi-weekly NDVI images of Kansas for the growing seasons (March to October) from AVHRR satellite images between the years 1989 – 1997. They also derived biweekly and month precipitation maps for each entire year from daily precipitation data from 410 weather stations in and around Kansas. Biweekly temperature maps comprising of maximum, minimum, average and accumulated growing degree day (AGDD) were constructed using daily maximum and minimum temperature data derived from 17 weather stations. AGDD is defined as:

$$AGDD = \sum \frac{T_{\max} + T_{\min}}{2 - T_{base}} \qquad (55)$$

where T_{max} is the daily maximum temperature, T_{min} is the daily minimum temperature and T_{base} is set at 10^{o}C. They also stratified their analyses according to the categories of cropland, grassland and forest as defined in the land cover map for Kansas prepared by the U.S.G.S. Wang *et al* examined spatial relations between NDVI and each of the climate factors- precipitation, temperature (maximum, minimum, average and degree days) stratified according to the three land cover categories (cropland, grassland and forest). Correlation coefficients between NDVI and each climate factor were calculated for the state of Kansas by directly comparing corresponding spatial locations for pairs of NDVI and climate maps. The primary goal of the analyses was to evaluate the correspondence between NDVI spatial patterns and climate variation, and the analyses examined relationships both within growing seasons (within-season) and between seasons (seasonal). Within-season analysis compared different biweekly periods within the same growing season, while seasonal analyses compared NDVI and precipitation values between different years. For each year, the NDVI was averaged through growing season, and precipitation was accumulated for the entire growing season plus 14 preceding months. The results indicated that the spatial correlation coefficients between NDVI and precipitation were quite different for NDVI according to of the growing season, time interval and lag over which precipitation was summed, and land cover type. Higher correlation coefficients were observed for longer time intervals over which precipitation was summed, and time lags only had a weak influence on correlation coefficients. However, when average growing season NDVI deviation was compared with precipitation deviation as a function of time interval over which precipitation was summed, the results were quite different and complicated in different years. For 1989, a

very dry year, correlation coefficients remained high for all precipitation time intervals, but for 1993, an extremely wet year, there was no significant correlation. When compared with temperature, the growing season average NDVI showed strong correlations with minimum temperature, moderate correlations with average temperature, weak or no correlations with maximum temperature and weak or no correlations with AGDD. Wang *et al* stated that NDVI spatial patterns in the central Great Plains are primarily related to precipitation spatial patterns, and temporal variation of NDVI spatial pattern was largely explained by precipitation deviation from the average. They also stated that the NDVI at any given time is influenced by precipitation during an interval that includes both the current growing season and part or all of the previous growing season. Furthermore, NDVI spatial pattern for a given biweekly period is generally more strongly correlated with the average precipitation than with recent precipitation and short-term variations in precipitation patterns does not change the underlying spatial patterns of NDVI because the underlying gradients are controlled by long-term climate conditions. Their conclusion was that the general spatial distribution of NDVI in the central Great Plains corresponds directly with the spatial pattern of average annual precipitation, while year-to-year variation of NDVI depends largely on the variation of precipitation. Temperature influence on the NDVI was only seen during the early and late growing season.

Wang *et al* also investigated the temporal responses of NDVI to precipitation and temperature (2003) over the same study region, stratifying the raster maps of biweekly NDVI, precipitation and temperature according to land cover categories, and calculating correlation coefficients between each of the factors and NDVI for the entire pixels for each land cover category. He discovered that the nine-year average biweekly NDVI

values from 1989-1997 increased rapidly during the spring, peaked in the summer months and decreased rapidly during the fall. Correlation coefficients between NDVI and precipitation in grassland, cropland and forest were high in specific combinations of time duration and lag. In terms of time duration within season, NDVI was more strongly related to the sum of precipitation in four or five biweekly periods than in one-to three periods. In terms of time lag within season, NDVI was more strongly influenced by the second preceding biweekly period (four-week lag) though differences existed among different land cover types. The correlation coefficients were also different for the different land cover types. For grassland, correlation coefficients were mostly positive and maximum values for each year were between 0.7-0.96. For forest, correlation coefficients were also mostly positive and maximum values for each year were between 0.66-1.0. For cropland, correlation coefficients were positive for some years but negative for other years. Wang *et al* concluded that NDVI values are most strongly correlated with the precipitation that has been integrated over three to four recent biweekly periods. The strength of the relationship varied depending on the land cover type under evaluation.

Washington-Allen *et al* (2004) investigated the spatiotemporal mapping of dry season sagebush steppe vegetation response using Landsat TM images and derived SAVI images. The study site for this research was a private ranch in the Utah Panhandle called Deseret Land and Livestock Company Ranch. Washington-Allen *et al* acquired 22 dry-season Landsat images from 1972 through 1997, with the dry season from late June to September and derived the SAVI from them. He then clustered the SAVI time series to identify spatial and temporal signatures, based on the hypothesis that there are four coarse time series trends possible: increasing, decreasing, stable, or combinations of these.

Washington-Allen *et al* also acquired PDSI data from the Utah Climate Center to correlate with the SAVI. The results indicated that only the increasing trend of one-year lagged first order difference of SAVI was positively correlated with the first order difference of PSDSI with r=0.38 and p=0.07, suggesting that the PDSI is not very well correlated with the SAVI.

Ji and Peters (2003) investigated drought using the SPI, studying the northern and central Great Plains. The precipitation record of the region was from 1885-2000, and based on the 50-year normal period (1951-2000) annual precipitation ranged from 400 *mm* in the northwest to 980 *mm* in the southeast region of the study area. The NDVI images used were biweekly 1-km resolution Maximum Value Composites (MVC) produced by the U.S. Geological Survey's Earth Resources Observation System (EROS) Data Center. The MVC technique retains the highest NDVI value for each pixel during a 14-day period producing images that are spatially continuous and relatively cloud free, with temporal resolution sufficient for evaluating vegetation dynamics (Ji and Peters, 2003). The vegetation in the study regions were mostly croplands (wheat, corn) and grasslands (sagebrush, gramma). Ji and Peters used monthly NDVI data from the growing season (May-October) for the analysis, and performed correlation analyses for the NDVI vs. 1-, 2- through to 12-month SPIs. They analyzed each month separately, implemented linear regression on the NDVI time series and 3-month SPI, and employed seasonal dummy variables for analysis because the linear relationships between the NDVI and SPI were different for varying seasonal periods. Dummy variables are categorical variables used as predictors in regression models. These are a set of levels assigned to the categorical variables and used to account for the effect of the variables on the response

variable (Ji and Peters, 2003). In this study, the dummy variables were a set of six levels assigned to the six months of the growing season and used to account for the effect of the "month" on the NDVI. The regression model containing seasonal dummy variables is expressed as:

$$\begin{aligned} NDVI = {} & \beta_0 + \beta_1(SPI) + \beta_2 D_1 + \beta_3 D_2 + \beta_4 D_3 \\ & + \beta_5 D_4 + \beta_6 D_5 + \beta_7 D_1(SPI) + \beta_8 D_2(SPI) \\ & + \beta_9 D_3(SPI) + \beta_{10} D_4(SPI) + \beta_{11} D_5(SPI) + \varepsilon \end{aligned} \tag{56}$$

where NDVI is the average NDVI of grassland or cropland in a climate division, SPI is the 3-month SPI in a climate division, D_1-D_5 are the dummy variables, $\beta_1 - \beta_{11}$ are the regression coefficients and ε is random error. Dummy variables were assigned binary values depending on the month as seen in Table 1.

Table 1: Dummy Variables in SPI analysis by Ji and Peters (2003)

D1	D2	D3	D4	D5	
0	0	0	0	0	if observation is for May
1	0	0	0	0	if observation is for June
0	1	0	0	0	if observation is for July
0	0	1	0	0	if observation is for August
0	0	0	1	0	if observation is for September
0	0	0	0	1	if observation is for October

Consequently, the regression models corresponding to the 6 months were:

$$\begin{aligned} &\text{May} && NDVI = \beta_0 + \beta_1(SPI) + \varepsilon \\ &\text{June} && NDVI = (\beta_0 + \beta_2) + (\beta_1 + \beta_7)(SPI) + \varepsilon \\ &\text{July} && NDVI = (\beta_0 + \beta_3) + (\beta_1 + \beta_8)(SPI) + \varepsilon \\ &\text{August} && NDVI = (\beta_0 + \beta_4) + (\beta_1 + \beta_9)(SPI) + \varepsilon \\ &\text{September} && NDVI = (\beta_0 + \beta_5) + (\beta_1 + \beta_{10})(SPI) + \varepsilon \\ &\text{October} && NDVI = (\beta_0 + \beta_6) + (\beta_1 + \beta_{11})(SPI) + \varepsilon \end{aligned} \tag{57}$$

For comparison, a simple regression model that did not use dummy variables was used, where each month followed the equation for May in equation 48, and where all slopes

and intercepts were assumed equal to those values. The results from this exercise showed varying responses for various months and various locations. For the grasslands in climate division 2, Nebraska in May, there were no significant correlations between NDVI and SPI. In June, there were significant correlations with the 2-, 3-, 6- and 9-month SPI. Very high positive correlations between all scales of SPI were noted in July. The correlation was still strong in August, but the 1-month SPI and NDVI correlation was not significant. Only the 3-month SPI was significant in September, and there were no significant correlations in October. The correlation between NDVI and SPI varied depending on the time-scale, with the 3-month SPI being the highest correlation overall for all the months. Li interpreted this to mean that the impact of precipitation on vegetation does not occur instantaneously, but is a cumulative effect. The regression fit was tested to compare the predicted results of equations 47 and 48, and the dummy fit model was shown to be very accurate as compared to the simple regression. Li concluded that the relationships between vegetation condition and moisture availability for the grassland and cropland in the northern Great Plains are significant in all climate divisions, and that the 3-month SPI had the most significant correlation to the NDVI. He also concluded that seasonality has a very significant effect on the relationship between the NDVI and SPI, due to the sensitivity of plants to water availability during the reproductive growth stage, and that seasonal effects must be taken into account.

Although it is not examined in this thesis, remote sensing of temperature has also been used to investigate drought. Wan (2004) investigated using Land Surface Temperature (LST) and NDVI to create an index called the Vegetation Temperature Condition Index (VTCI) which is defined as:

$$VTCI = \frac{LST_{NDVI_{i.\max}} - LST_{NDVI_i}}{LST_{NDVI_{i.\max}} - LST_{NDVI_{i.\min}}} \tag{58}$$

where:

$$\begin{aligned} LST_{NDVI_{i.\max}} &= a + bNDVI_i \\ LST_{NDVI_{i.\min}} &= a' + b'NDVI_i \end{aligned} \tag{59}$$

where $LST_{NDVI_{i.\max}}$ and $LST_{NDVI_{i.\min}}$ are maximum and minimum LSTs of pixels which have the same $NDVI_i$ value in a study region, respectively, and LST_{NDVI_i} denotes LST of one pixel whose NDVI value is $NDVI_i$. Coefficients *a, b, a'* and *b'* were estimated from an area large enough where soil moisture at the surface area spanned from wilting point to field capacity at the pixel level. Wan *et al* performed a linear regression analysis between precipitation and NDVI, LST, LST/NDVI ration and VTCI in the Great Plains region of the USA, incorporating all land-cover types, croplands and grasslands therein. The precipitation data was obtained from the National Climatic Data Center, and included total monthly precipitation (TPCP) and departure from normal monthly normal precipitation (DPNP). Their results indicate a high correlation between the NDVI and TPCP on cropland regions for longer time periods, but a low correlation for shorter time periods. For the LST, he found a moderately high negative correlation between it and the total monthly precipitation for some shorter time periods. With the VTCI, there was a significant correlation with precipitation for 3- and 6-month intervals, and also a significant correlation with the DPNP. These results suggest that the VTCI is not only closely related to recent rainfall events but also related to past rainfall amounts, and indicate that the VTCI might be a better index for drought monitoring. Wan *et al*

concluded that the VTCI is a near-real time drought monitoring approach that is time-dependent and usually region specific.

Another technique called Soil Thermal Inertia has also been used to investigate drought (Lianmeng and Deren, 2001). It is based on the remote sensing of the thermal capacity of soil according to the Apparent Thermal Inertia (ATI) theory, based on NOAA AVHRR data. The distribution of soil temperature rests with thermal capacity and thermal conductivity. The thermal capacity is the quantity of heat that raises one unit soil temperature by 1 ^{o}C which is calculated by equation (59):

$$C = \frac{\left(C_s V_s + C_w V_w + C_a V_a\right)}{V} \tag{60}$$

where C_s, C_w and C_a are the soil's solid, water, and air thermal capacity per unit volume respectively, V_s, V_w and V_a are the soil's solid, water and air volume, and V is the sum of these three volumes, or the total volume of soil. Since C_a is very small, and the water thermal capacity is twice that of the soil particles, C varies primarily with the change of volumetric water content (θ), thus:

$$C = \frac{C_s V_s}{V} + C_w \theta = C_s \left(1 - \Phi\right) + C_w \theta \tag{61}$$

where Φ=soil porosity.

According to Fourier's law:

$$Q_s = \lambda \frac{\delta T}{\delta z} \tag{62}$$

where Q_s is the thermal flux, λ is the soil thermal conductivity, and $\frac{\delta T}{\delta z}$ is the change in temperature with the change in depth. According to Fourier's law and the law of conservation of energy, the soil thermal conduction equation can be defined as:

$$C\frac{\delta T}{\delta t} = \nabla \bullet \left(\lambda \nabla T\right) \tag{63}$$

where the left-hand side of equation (63) shows the energy change rate of the unit soil and the right-hand side shows the net import energy of the unit soil. For the isotropic homogeneous soil, if its water quantity is not changed by its depth and the effects of water volume change can be ignored for C and λ, then C and λ can be considered as constants. If the energy exchange is only in the vertical direction, then equation (63) can be simplified to:

$$\frac{\partial \mathrm{T}}{\partial \mathrm{t}} = \alpha \frac{\partial^2 T}{\partial z^2} \tag{64}$$

where $\alpha = \lambda / C$=the thermal diffusivity. Under a certain boundary condition (Liangmeng and Deren, 2001), the ATI equation can be defined as:

$$ATI = \frac{k(1-A)}{\Delta T_0} \tag{65}$$

where ΔT_0 is the daily temperature difference, A is the albedo and k is a constant. (Lianming and Deren, 2001). The soil temperature distribution depends on the soil thermal characteristic, which in turn depends on the soil water content. The daily albedo and temperature difference can be derived from soil reflectivity and brightness temperature, which can be obtained from the AVHRR sensor. Thus, one can monitor the soil water content. Lianming and Deren (2001) investigated drought conditions in Hubei province (People's Republic of China) using this method and discovered that severe and moderate drought conditions were evenly distributed in elevations between 50-500 m in elevation, affecting 80% and 73% of the total area respectively.

1.9 Objectives

The purpose of this thesis is two-fold. Firstly, it will examine whether differences between drought-stressed, natural, and regularly irrigated vegetation can be detected by the statistical analysis of reflectance data. Through this, it may then be possible to determine solely from reflectance images whether or not a region of a certain vegetation cover is drought stressed or not, and it may also indicate whether the vegetation under review is sensitive or not to precipitation levels and how sensitive it is. Secondly, it will examine the relationship between various vegetation indices and drought indices (Standardized Precipitation Index and Palmer Drought Index) to see which indices have a good correlation and can be used to indicate drought conditions. Through this, we can process satellite images for vegetation indices and then use those images to indicate drought severity. This can be in real-time or using various time lags and this thesis will also examine the correlation over various time lags.

2. METHODS AND INSTRUMENTATION

2.1 Study Region and Vegetation

The study region is located in the Sevilleta National Wildlife Refuge (SNWR), site of the Sevilleta Long-Term Ecological Research site in Central New Mexico. This region is about 35 km northeast of Socorro, New Mexico and about 80 kilometers south of Albuquerque, New Mexico. The Refuge, which is managed by the US Department of the Interior, Fish and Wildlife Service, is positioned at the intersection of several major biotic zones: Chihuahuan Desert grassland and shrub land to the south, Great Plains grassland to the north, Piñon-Juniper woodland in the upper elevations of the neighboring mountains, Colorado Plateau shrub-steppe to the west, and riparian vegetation along the middle Rio Grande Valley. The study region for this thesis is at the intersection of the Chihuahuan and Great Plains biotic zone. Figure 4-1 shows a map of the study region. The dominant vegetation types present in the study site are creosote shrubs (*Larrea tridentata*) and black gramma grass (*Bouteloua eriopoda*). Other vegetation such as sagebush and yucca are present on the plains regions, while piñon juniper appears in more elevated regions. Creosote shrubs are ubiquitous in Chihuahuan deserts and much research has been done on this species, especially on its drought tolerance and propensity for invasion/encroachment. While it is assumed that high precipitation limits (>150 mm total annual) limits the distribution of creosote, such limits are most likely an indirect effect (Smith *et al*, 1997). Creosote has been classified as a true drought-resisting species that remains metabolically active during dry seasons and exhibits growth at any time of

the year (Oechel *et al*, 1972), even when exposed to very low soil water potentials. Relative to other xerophytes, creosote has been described as having poor stomatal control of water loss (Odening *et al*, 1974). However, as in most other desert perennials, creosote exhibits pronounced declines in stomatal conductance during times of high evaporation demand (Oechel *et al*, 1972; Franco *et al* 1994). Such reductions in conductance are correlated with changes in plant water potential (Franco *et al*. 1994). Creosote has a relatively high photosynthetic capacity and is able to reach photosynthetic compensation at water potentials of -8 MPa, much more resistant than gramma grasses.

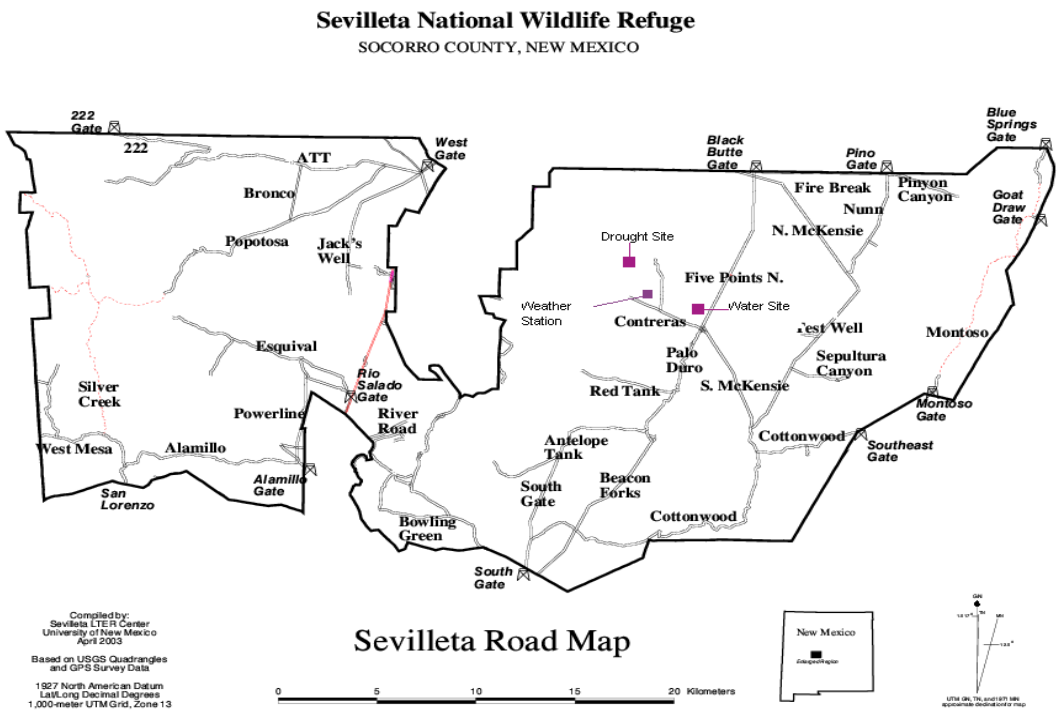

Figure 2-1: Map of Sevilleta National Wildlife Refuge (http://sev.lternet.edu)

2.2 Remote Sensing Methods

2.2.1 Site Description

There are two sites under study for this research. One site was established by Eric Small (Small and Kurc, 2003)for investigating differences between rain-sheltered and control desert vegetation ,specifically black gramma (*Bouteloua eriopoda*) and creosote shrubs (*Larrea tridentata*). The second site was established by Geoffrey Marshall and Xiaobing Zhou to investigate any detectable differences between normal creosote shrubs and regularly-irrigated creosote shrubs.

The first site is located at latitude 34.338^{o} N and 106.733^{o}W, and consists of 6 control plots and 3 rain-sheltered plots. Each plot is about 8 meters by 12 meters, rectangular, and has a vegetation cover of about 70%. The predominant vegetation in each plot is black gramma grass and between 4-6 creosote shrubs, along with various other small grasses and shrubs not under review in this report. The physically largest vegetation in each plot is the creosote shrub. Measurements were taken from one control plot and one drought plot. The measurements from the control plot came from two creosote shrubs, two black gramma grass patches, and two soil exposures. The rain-sheltered plot measurements came from two creosote shrubs, four black gramma grass patches and two soil exposures. The second site is located at latitude 34.329^{o} N and longitude 106.764. It consists of three creosote shrubs out in the open. One shrub is watered every 2 weeks or more frequently with the equivalent of a 2-hour intense precipitation event, while the other two shrubs are control shrubs. Both control shrubs are about 10 meters from the watered shrub and 60 meters from each other. Photos of both sites are seen in Figures 2-2 through 2-5.

2.2.2 Instrument Description

Radiance data was collected from all the plants and soil targets by an Analytical Spectral Devices spectroradiometer. This instrument has two target sensors that record reflected electromagnetic radiation over a 15-degree angle of view and for wavelengths from 350 *nm* to 2500 *nm*. Appendix A has more information on the instrument operation theory and specifics.

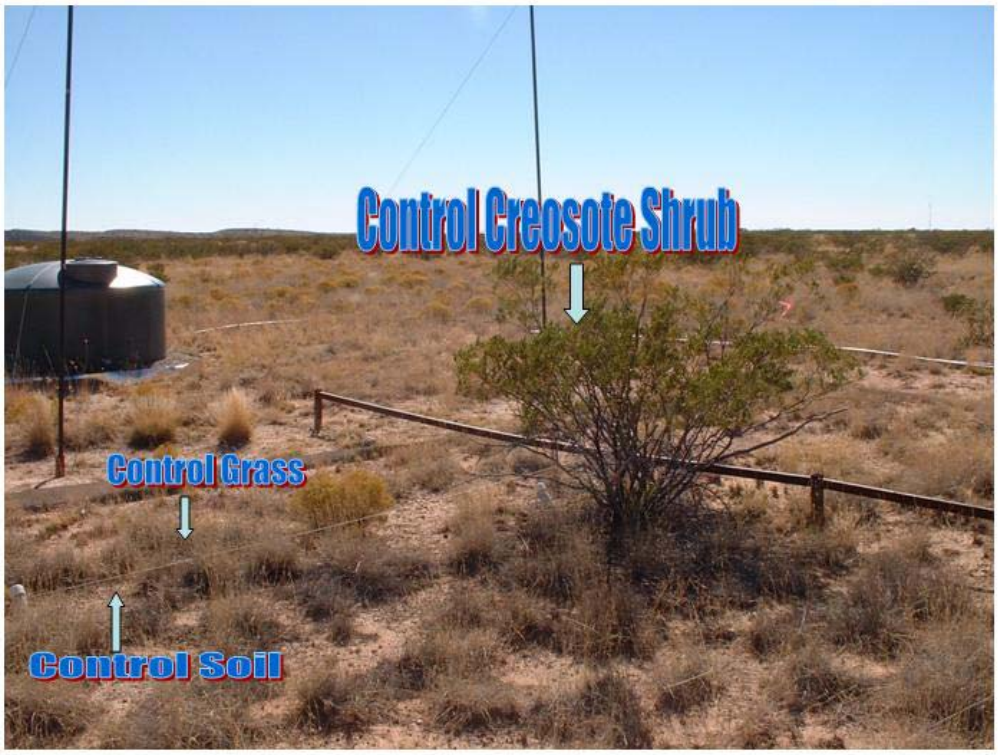

Figure 2-2: Control Field Plot

Figure 2-3: Drought Field Plot

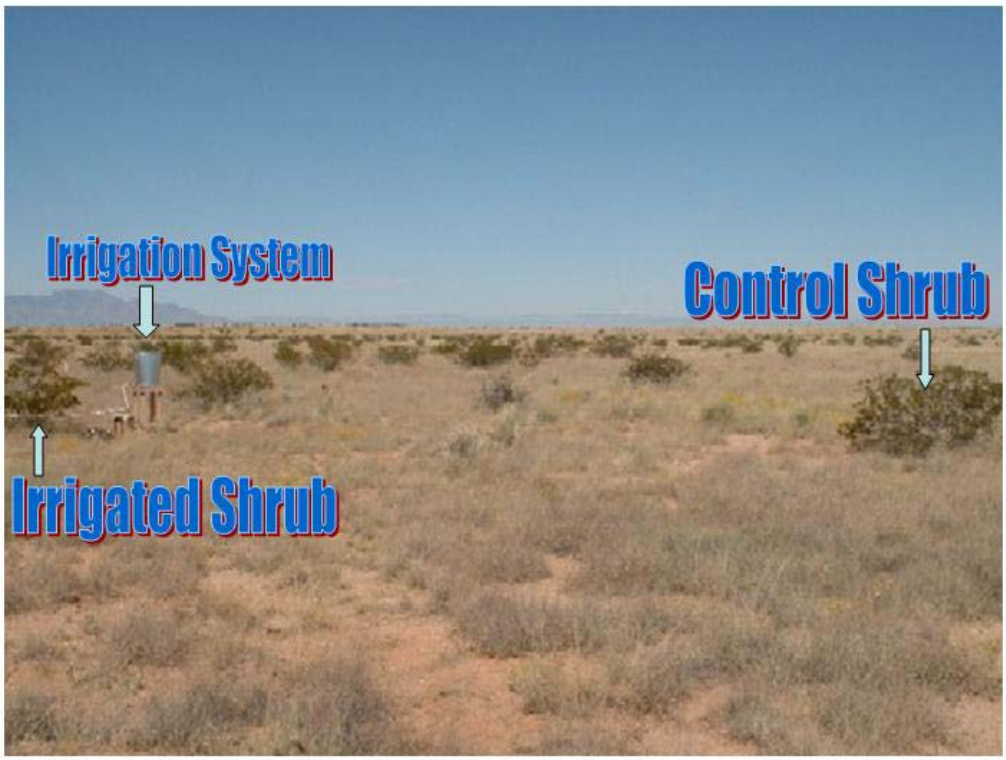

Figure 2-4: Irrigated Field Plot

Figure 2-5: Irrigated Shrub and Irrigation system. The spectroradiometer is visible in foreground

2.2.3 Data Collection and Processing

The radiance and reflectance data collection for the Rain-sheltered Site extends from January 2003 until October 2004. Data was collected over fortnightly periods, but was hampered by weather conditions and machine/human error such as the laptop battery dying, so there were periods of more than two weeks without measurement. Each measurement consisted of radiance data collections at both the watered shrub Site and the Rain-sheltered Site on one day, weather-permitting. At least 20 discrete radiance spectra were recorded on each shrub per measurement, while three spectra were taken for grass, soil and white reference targets per measurement. Each spectra consisted of 2150 values representing target radiance for every wavelength between 350 *nm* and 2500 *nm*. This radiance data was then processed for each target over the wavelength range to get a single average radiance value per period per target for each wavelength in the spectroradiometer

range, corrected for solar angle, collection time, Julian day, and location (latitude and longitude). Because of the large amounts of data, the process was automated using a Perl script which performed all necessary corrections on the raw radiance data. The code for this script is presented in Appendix B, and includes step-by-step information on what corrections were made and how they were made. The corrected data was then converted to reflectance data by dividing the target radiance average data by the white reference radiance average data per wavelength for each measurement period. After all of this processing, the result was a single reflectance spectral signature for every shrub, grass and soil target measured during that measurement period. A single spectral signature for the Rain-sheltered Site control shrub plot was then obtained by calculating the mean of all control shrub spectral signatures, and the same process was repeated for the control grass and soil, and the rain-sheltered shrub, grass and soil. The Irrigated Site had only one irrigated and one control shrub, so all that was needed from both targets was the single reflectance spectral signature. The data was then processed to calculate Landsat band reflectances and vegetation indices for all measurement periods. There are seven bands on the Landsat ETM sensor, 6 of which were calculated in the data processing. Bands 1 through 3 represent the blue, green and red spectrum respectively. The blue band wavelengths are from 450 *nm* to 520 *nm*. The green band wavelengths are from 520 *nm* to 600 *nm*, and the red band wavelengths are from 630 *nm* to 690 *nm*. Band 4 represents the near-infrared spectrum and ranges from 760 *nm* to 900 *nm*. Bands 5 and 7 are in the middle infrared region, and while they were calculated for the sake of completion and thoroughness, they were not utilized much in this research. Band 6 uses wavelengths in the thermal infrared region that are longer than the maximum 2500 *nm* range of the

spectroradiometer, and was therefore not calculated. The field-based reflectance of the Landsat bands was determined by calculating the mean reflectance of all the wavelengths between the upper and lower defining wavelengths of each band. Processing of these data was a very labor-intensive task, since each measurement period had 2150 discrete data values for each target, 6 targets in the control plot, 8 targets in the rain-sheltered plot and 2 targets for the Irrigated Site. Thus, even after processing and correcting the raw field data to get a single spectral signature for each target, there was a total of 34400 data values for each measurement period, not including White Reference radiance. When the mean spectral signature data for control and rain-sheltered shrub, soil and grass data are included, this Figure increases to 47300 data values. In addition, we must calculate 6 Landsat reflectance bands from all of the mean target spectral signature values, and then calculate vegetation index values from specific band and wavelength reflectance for 12 different indices for all 8 targets (Rain-sheltered Site control and rain-sheltered shrub, grass, and soil, Irrigated Site irrigated shrub and control shrub). Furthermore, all of the data described above is from just one measurement period; this entire process had to be performed and repeated for 34 measurement periods at the Rain-sheltered Site, and 26 measurement periods at the Irrigated Site. To aid in processing and calculating all of this data, several Microsoft Excel macros were created to calculate and manipulate the data in spreadsheets. Each macro was created for a specific purpose, from calculating the mean spectral signatures for all targets to creating spreadsheets of vegetation index data sorted by measurement date to creating a final spreadsheet ("archive") of all reflectance data and vegetation index data for each measurement site. All macros were updated regularly to include new measurement data and processing. All of the data, both raw and

processed, are archived on a series of three compact discs which are attachments to this thesis. They are not reproduced in table form here as it would be too cumbersome.

2.3 Precipitation Methods

2.3.1 Data Collection and Processing

The precipitation data was taken from the Five-Points weather station (station 49) located in the Sevilleta as shown in Figure 4-1. The weather station collects meteorological data on a daily basis and summarized data is available on the SNWR's website (http://sev.lternet.edu). The data dates from January 1999 to October 2004, and SPI values were calculated from the daily precipitation data from this weather station, using a program downloaded from the National Drought Mitigation Center website at http://drought.unl.edu , based at the University of Nebraska-Lincoln. For two weeks in November 2003 there was no precipitation data from this weather station, so precipitation data from the next closest weather station (named Deep Well) was used for this time period. Since the data processing program took monthly integer values, the weather-station precipitation was multiplied by a factor of 10 and then arranged in dummy months and years in order to calculate the SPI values for varying weekly intervals. The intervals selected were 1 through 30-week intervals. PDI values were taken from the NOAA's daily derivation taken for the entire Central New Mexico region from 2003-2004, as we did not have enough data for the various parameters to calculate the index locally.

Precipitation values for the Irrigated Site were calculated by dividing the volume of water added for irrigation by the area of the irrigation plot, and adding this to the precipitation from the 5-Points weather station for every day that irrigation was carried out. The volume of water added per event was 10 U.S. gallons, or 0.0378541 cubic

meters, while the irrigation outlet area was 0.25 square meters. Thus, the simulated precipitation in meters is 0.1514 meters, or 151.4 mm. This Figure was based from the highest recorded single day precipitation event for the Socorro precipitation records. This Figure was added to the daily precipitation recorded for the irrigation days, and then the SPI was calculated from this amended record. This irrigation Figure may seem to be quite high, but it is debatable as to whether all of the water was used by the plant or infiltrated to depth and remained *in situ*. Potential evapotranspiration is quite high in the region, and various grass and sundry vegetation could be seen at the base of the irrigated shrub. This vegetation also used the irrigation water along with the shrub. The presence of vigorous stands of creosote on mesic dunes in the southwest suggests that they can survive occasional high soil moisture (Smith, 1997). This site is taken as a reference site with excessive irrigation, to ensure that the plant is not subject to drought stress throughout the study period, even though the exact amount of water actually used by the plant is not known.

3. RESULTS AND ANALYSIS OF FIELD DATA

3.1 Correlation between SPI and PDI data

For this section of the research, weekly PDI measurements provided by the National Oceans and Atmosphere Administration (NOAA) from March 2002-March 2004 were correlated with the SPI measurements calculated from the weather station precipitation data at time lags from 0 weeks to 12 weeks (3 months). These are presented in tables 2 and 3. SPI measurements were calculated from the 5 Points weather station precipitation data for one through thirty week periods, while PDI measurements were calculated by the NOAA for the New Mexico Central Valley region. There were 104 weekly observations in each measurement set. The results show that correlations between the PDI and all SPI values became more significant both as the time lags increased and as the SPI period increased. A graphical representation of the correlation data is shown in Figure 3-1. Each cluster represents correlations from 1-week SPI through 30-week SPI.

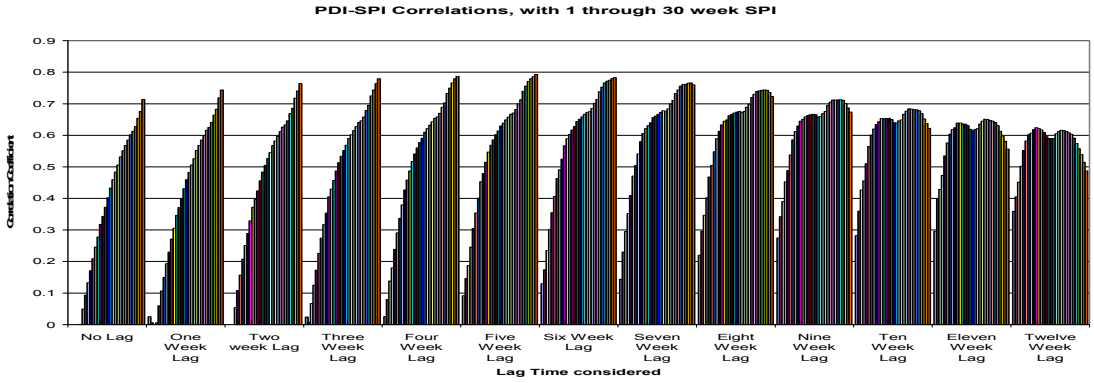

Figure 3-1: Graph of linear correlations coefficients for 1-week through 30-week SPI with weekly PDI, over no lag through to 12 weeks lag.

Table 2: Correlation coefficients of weekly PDI values vs. SPI values derived for 5 Points weather station, from no lag to six weeks lag.

	No Lag	One Week Lag	Two Week Lag	Three Week Lag	Four Week Lag	Five Week Lag	Six Week Lag
1-Week SPI	-0.014**	0.025**	-0.006**	0.024**	0.025**	0.092**	0.13**
2-Week SPI	-0.006**	0.006**	-0.013**	0.008**	0.08**	0.146**	0.174**
3-Week SPI	-0.015**	0**	-0.004**	0.067**	0.138**	0.187**	0.235*
4-Week SPI	-0.016**	0.006**	0.054**	0.125**	0.18**	0.246*	0.301
5-Week SPI	0.001**	0.06**	0.108**	0.173**	0.239*	0.305	0.355
6-Week SPI	0.05**	0.107**	0.157**	0.226*	0.291	0.354	0.406
7-Week SPI	0.094**	0.15**	0.208*	0.274	0.337	0.401	0.463
8-Week SPI	0.133**	0.193*	0.251**	0.317	0.38	0.453	0.491
9-Week SPI	0.171**	0.23*	0.289	0.354	0.427	0.479	0.525
10-Week SPI	0.209*	0.271	0.329	0.405	0.458	0.515	0.567
11-Week SPI	0.246*	0.306	0.372	0.43	0.487	0.547	0.589
12-Week SPI	0.278	0.346	0.397	0.457	0.517	0.569	0.603
13-Week SPI	0.318	0.371	0.424	0.487	0.541	0.586	0.617
14-Week SPI	0.343	0.399	0.456	0.513	0.56	0.602	0.628
15-Week SPI	0.372	0.431	0.484	0.534	0.577	0.614	0.644
16-Week SPI	0.402	0.459	0.505	0.552	0.591	0.63	0.651
17-Week SPI	0.433	0.483	0.527	0.569	0.61	0.639	0.659
18-Week SPI	0.459	0.506	0.545	0.59	0.621	0.649	0.667
19-Week SPI	0.484	0.526	0.568	0.602	0.632	0.658	0.673
20-Week SPI	0.506	0.552	0.582	0.615	0.643	0.667	0.675
21-Week SPI	0.532	0.568	0.597	0.628	0.654	0.671	0.685
22-Week SPI	0.551	0.585	0.612	0.641	0.659	0.682	0.702
23-Week SPI	0.568	0.6	0.626	0.646	0.67	0.7	0.714
24-Week SPI	0.585	0.616	0.633	0.658	0.689	0.713	0.738
25-Week SPI	0.602	0.625	0.646	0.679	0.703	0.74	0.753
26-Week SPI	0.613	0.641	0.669	0.695	0.733	0.756	0.766
27-Week SPI	0.628	0.664	0.686	0.725	0.75	0.771	0.772
28-Week SPI	0.654	0.683	0.718	0.744	0.766	0.779	0.775
29-Week SPI	0.676	0.719	0.741	0.764	0.779	0.786	0.78
30-Week SPI	0.714	0.744	0.764	0.779	0.787	0.793	0.783

** = Correlation has p-value significant between 5% and 1%*

***= Correlation p-value greater than 5% (no statistical significance)*

All other correlations have p-values less than 1% and are significant.

Table 3: Correlation coefficients of weekly PDI values vs. SPI values derived for 5 Points weather station, from seven weeks lag to twelve weeks lag.

	Seven Week Lag	Eight Week Lag	Nine Week Lag	Ten Week Lag	Eleven Week Lag	Twelve Week Lag
1-Week SPI	0.144**	0.22*	0.275	0.282	0.296	0.359
2-Week SPI	0.23*	0.296	0.342	0.36	0.399	0.405
3-Week SPI	0.295	0.347	0.39	0.427	0.429	0.452
4-Week SPI	0.352	0.402	0.453	0.456	0.473	0.502
5-Week SPI	0.409	0.468	0.488	0.51	0.535	0.552
6-Week SPI	0.471	0.505	0.538	0.565	0.576	0.582
7-Week SPI	0.504	0.548	0.586	0.601	0.604	0.602
8-Week SPI	0.541	0.589	0.612	0.62	0.618	0.607
9-Week SPI	0.58	0.613	0.63	0.634	0.624	0.618
10-Week SPI	0.606	0.633	0.645	0.643	0.639	0.624
11-Week SPI	0.621	0.645	0.651	0.653	0.639	0.621
12-Week SPI	0.631	0.649	0.659	0.652	0.636	0.617
13-Week SPI	0.64	0.662	0.663	0.653	0.635	0.609
14-Week SPI	0.656	0.667	0.665	0.654	0.631	0.596
15-Week SPI	0.661	0.671	0.667	0.65	0.619	0.59
16-Week SPI	0.667	0.674	0.665	0.64	0.614	0.59
17-Week SPI	0.673	0.676	0.658	0.639	0.618	0.59
18-Week SPI	0.678	0.672	0.66	0.646	0.621	0.605
19-Week SPI	0.675	0.676	0.669	0.649	0.636	0.612
20-Week SPI	0.684	0.689	0.676	0.667	0.645	0.616
21-Week SPI	0.7	0.699	0.695	0.677	0.651	0.615
22-Week SPI	0.711	0.72	0.705	0.684	0.65	0.612
23-Week SPI	0.733	0.73	0.712	0.683	0.647	0.608
24-Week SPI	0.744	0.739	0.712	0.681	0.645	0.603
25-Week SPI	0.756	0.741	0.712	0.681	0.641	0.591
26-Week SPI	0.761	0.743	0.713	0.678	0.631	0.574
27-Week SPI	0.762	0.744	0.711	0.669	0.613	0.558
28-Week SPI	0.765	0.743	0.701	0.652	0.598	0.539
29-Week SPI	0.766	0.736	0.687	0.638	0.581	0.515
30-Week SPI	0.76	0.723	0.674	0.622	0.557	0.487

** = Correlation has p-value significant between 5% and 1%*

***= Correlation p-value greater than 5% (no statistical significance)*

All other correlations have p-values less than 1% and are significant.

In Figure 3-1, there is a general increase of correlation coefficients up to the 5-week lag, and then a gradual decline afterwards. The double peaks apparent in the later lag periods should also be noted. This graph suggests that the weekly PDI value at any given instant is dependent upon the cumulative precipitation for up to 30 weeks previously in this region. However, the weekly PDI value may be affected more strongly by the amount of precipitation accumulated, rather than the length of time over which the precipitation accumulated. A representative linear fit of the highest correlation is shown in Figure 3.2.

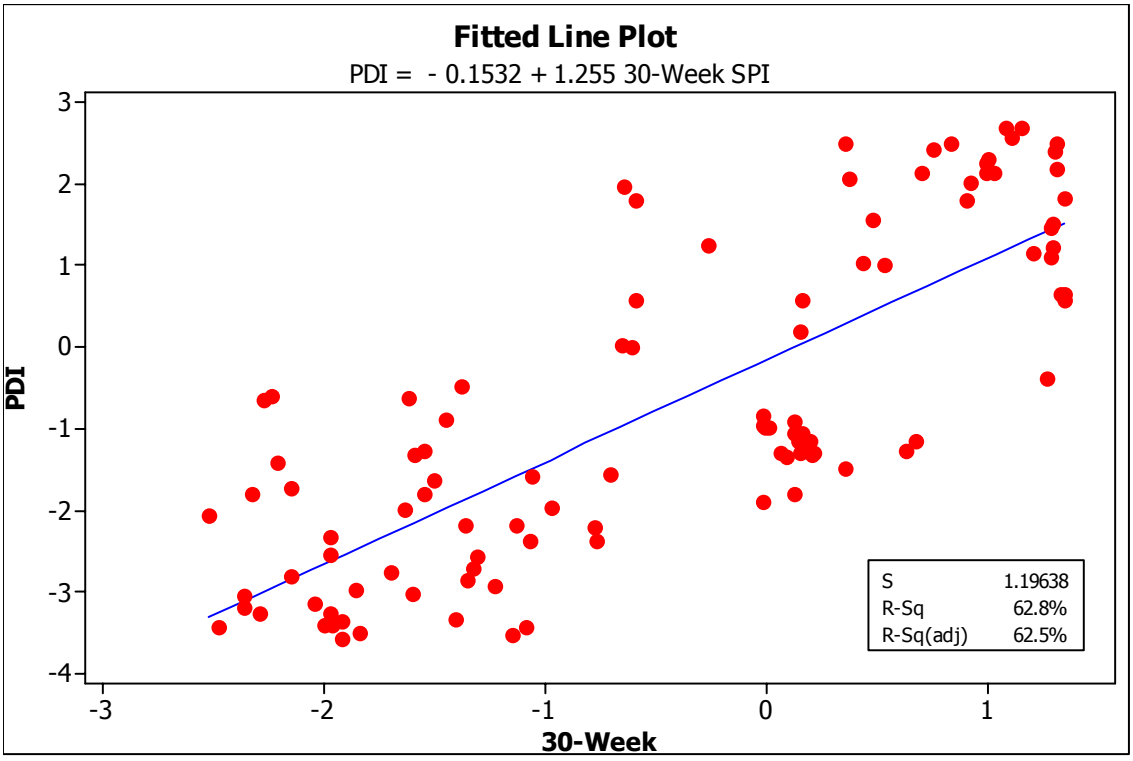

Figure 3-2: 30-Week SPI vs. PDI, with PDI lagged 5 weeks behind SPI.

These results not only show the significance of precipitation to the PDI values, but also show the slow response of the PDI to real-time conditions. Since the greatest correlation was with a lag of 5 weeks and an SPI scale of 30 weeks, we can say that the weekly PDI is dependent upon precipitation up to 36 weeks before the week under consideration in

this region. These results agree with Guttman (1998) whose research on phase relationships between the PDI and SPI indicated that precipitation is the dominant factor in the PDI, and that for periods less than a year (52 weeks) the PDI lags behind the SPI.

Timescale graphs for some of the drought index data are reproduced in Figures 3-3 through 3.10.

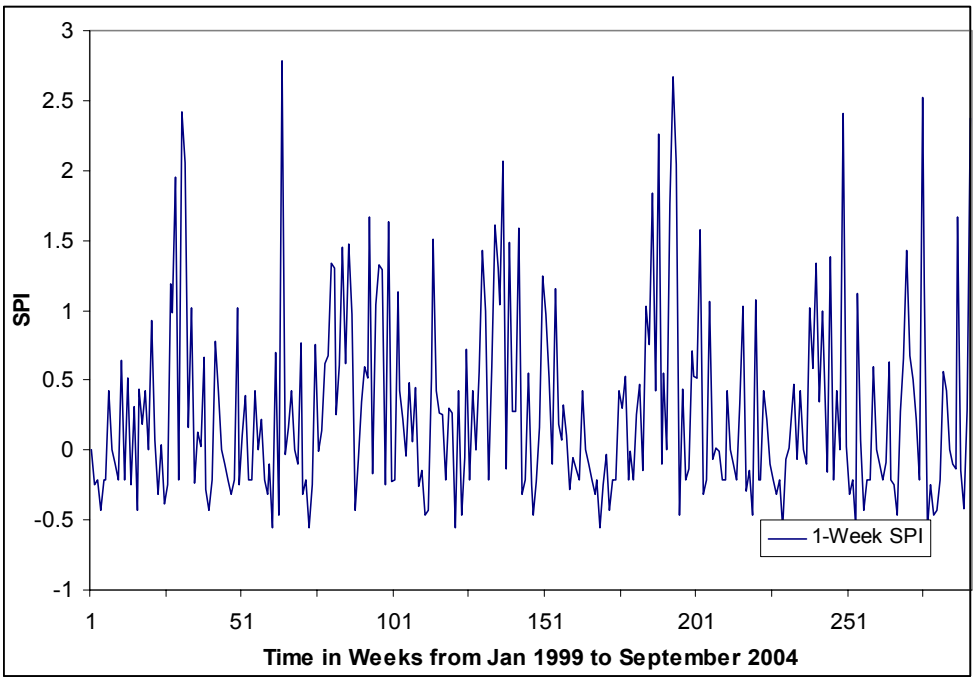

Figure 3-3: 1-Week SPI values for 5-Points Weather Station from Jan 1999 to Sept 2004

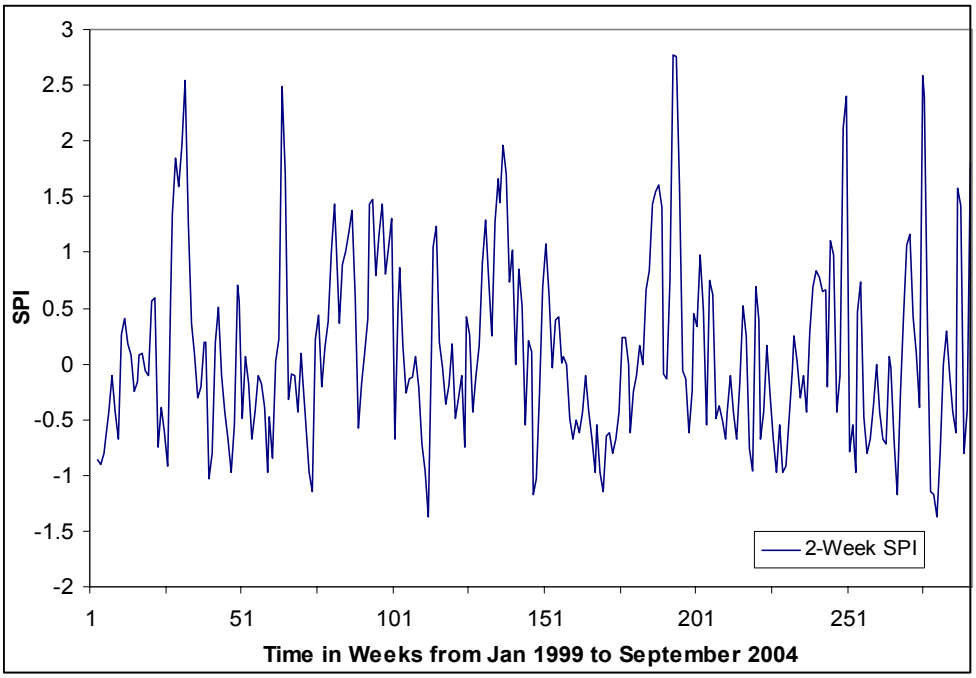

Figure 3-4: 2-Week SPI values for 5-Points Weather Station from Jan 1999 to Sept 2004

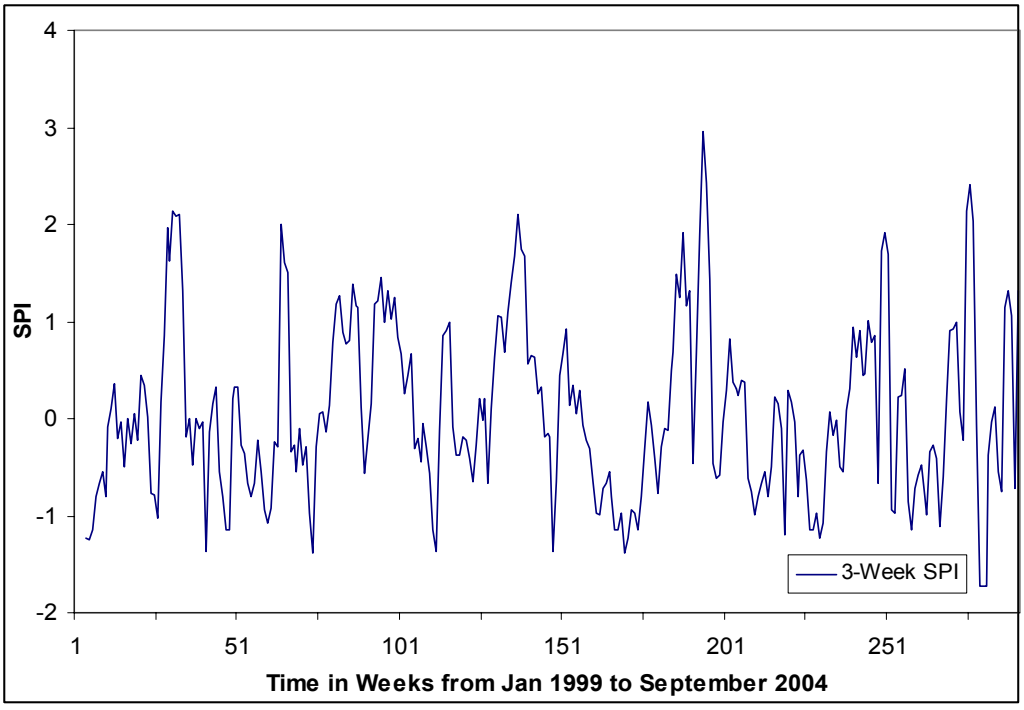

Figure 3-5: 3-Week SPI values for 5-Points Weather Station from Jan 1999 to Sept 2004

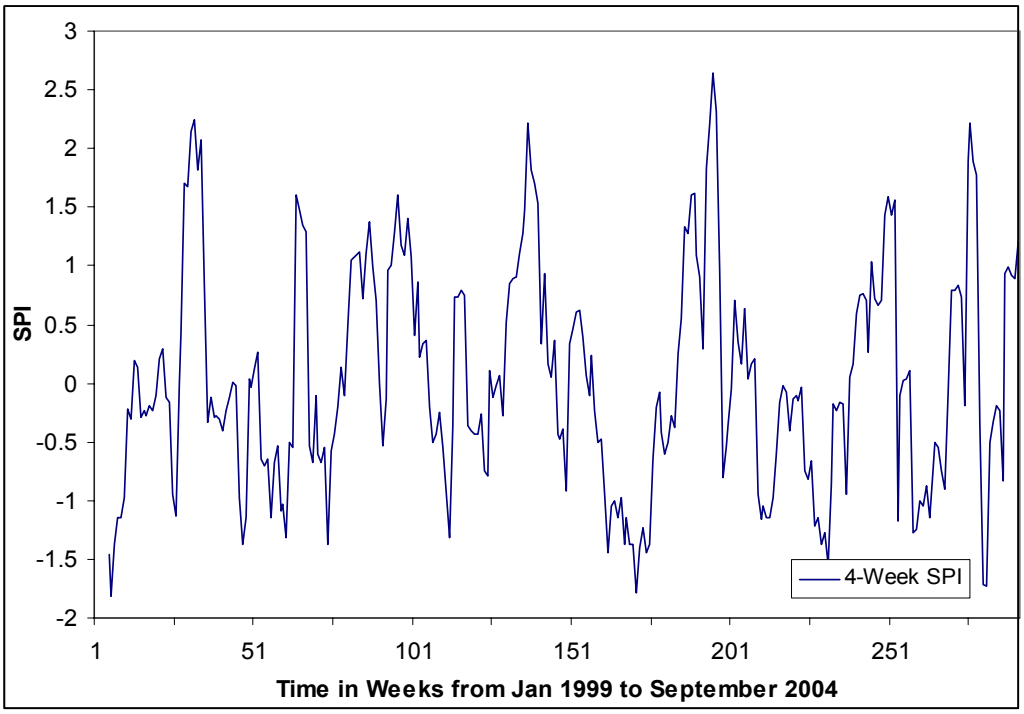

Figure 3-6: 4-Week SPI values for 5-Points Weather Station from Jan 1999 to Sept 2004

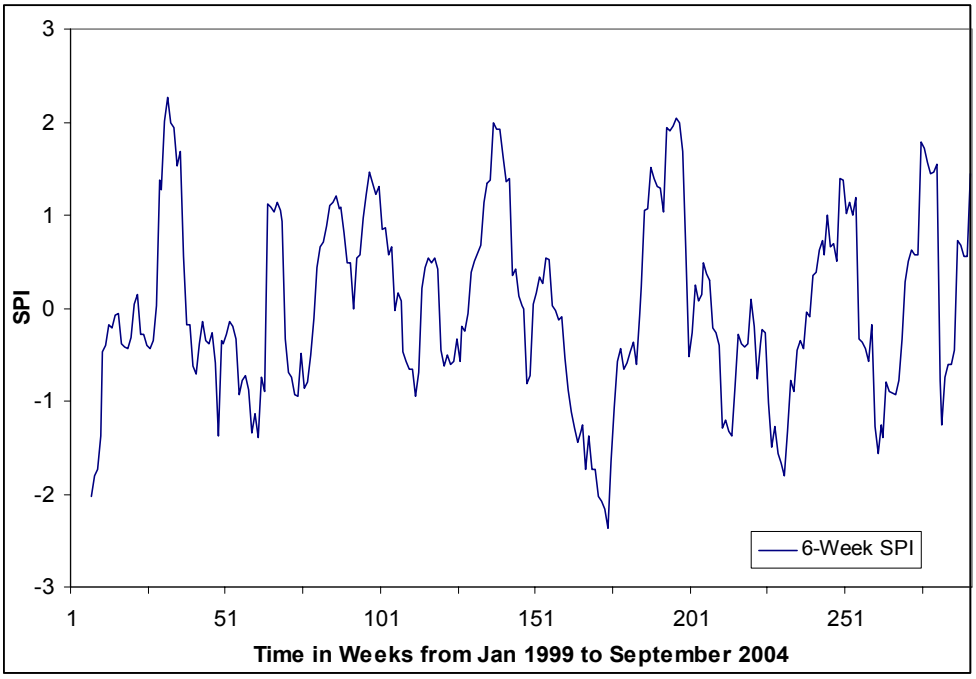

Figure 3-7: 6-Week SPI for 5-Points Weather Station from Jan 1999 to Sept 2004

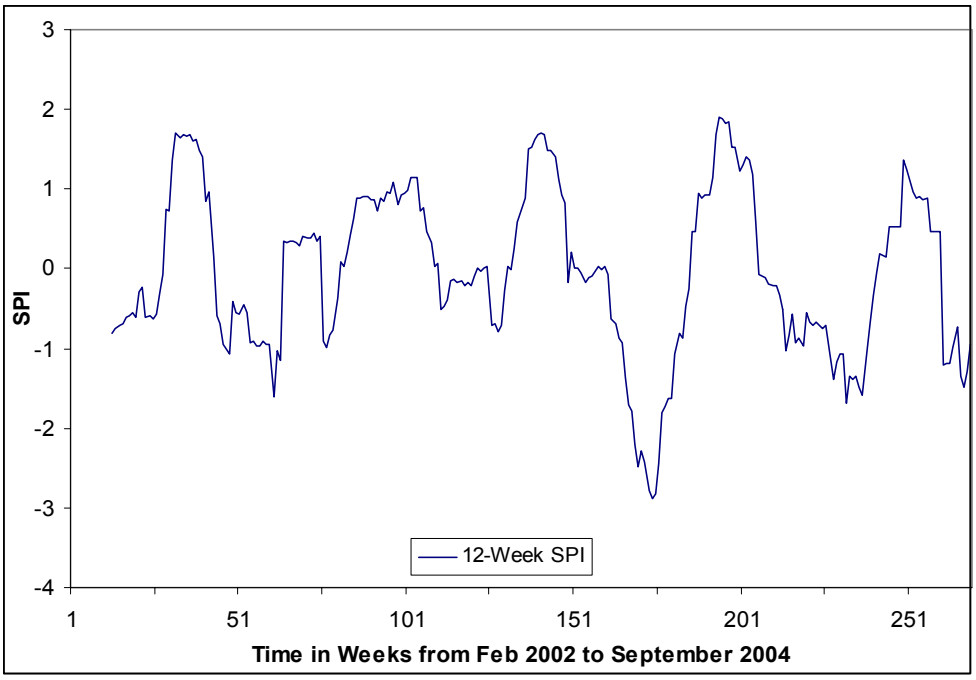

Figure 3-8: 12-Week SPI for 5-Points Weather Station from Feb 2002 to Sept 2004

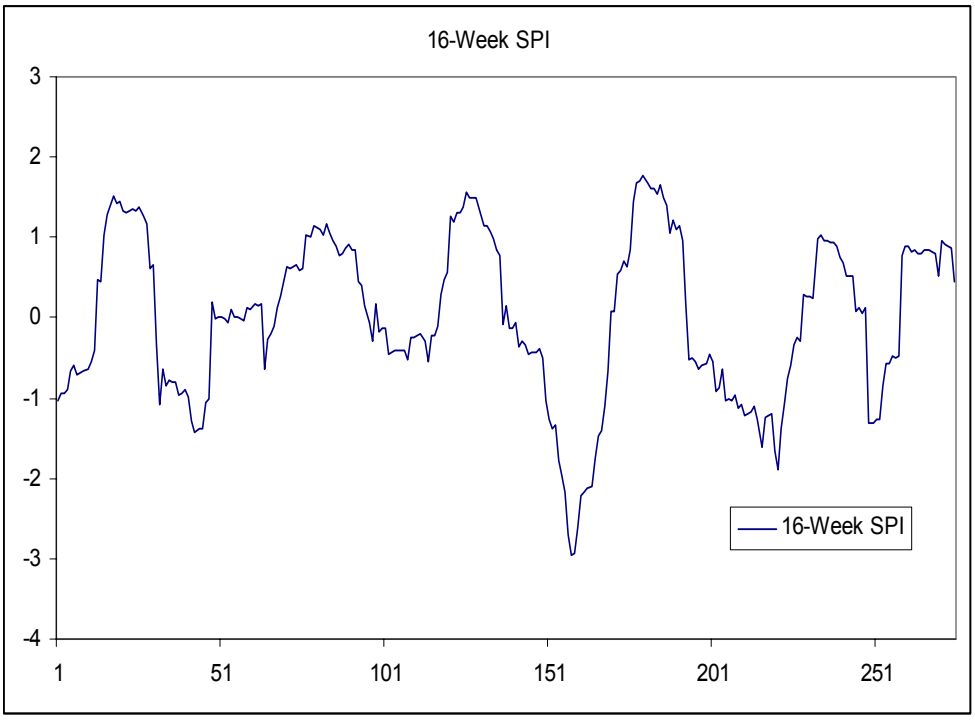

Figure 3-9: 16-Week SPI for 5-Points Weather Station from Mar 1999 to Sept 2004.

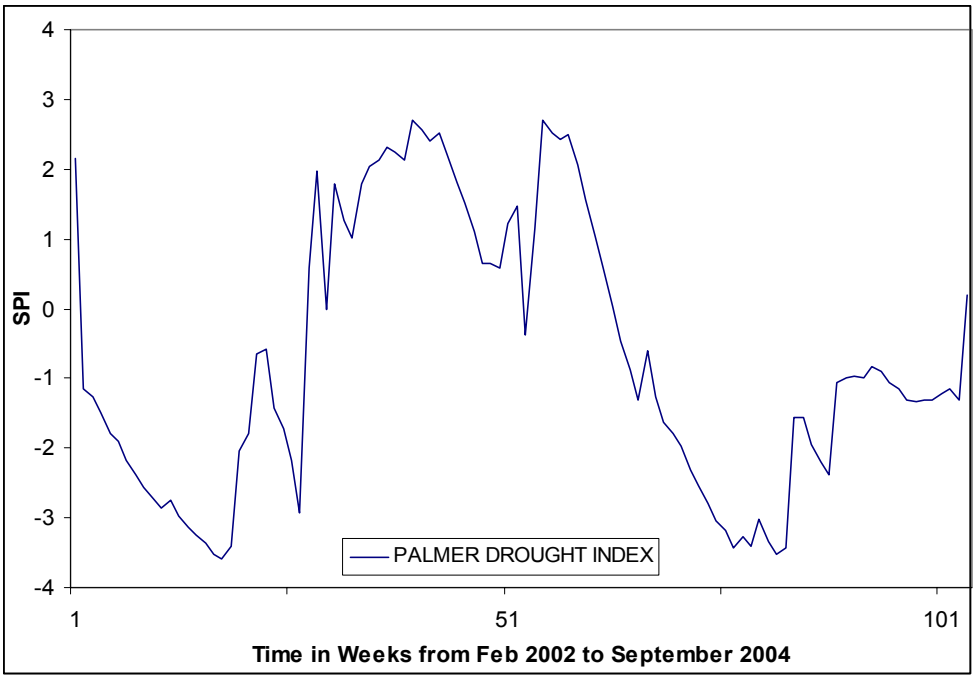

Figure 3-10: Weekly PDI for West-Central New Mexico from Feb 2002 to Sept 2004

In Figures 3-3 through 3-10, we see that the shorter SPI timescales have a lot of variance and do not show much of a pattern. However, as the timescale increases, a clearer pattern begins to emerge and smoother trends can be seen which better identify drought conditions. The SPI graphs from the 6-Week SPI onwards show more clearly when drought periods begin and end, beginning when the values fall below 0 and ending when they go above 0. The PDI follows the same rule. The graphs show that for most of the period under consideration, the region has been in moderate to severe drought stress, with more negative values than positive values. However, different timescales show varying degrees of drought conditions; the 16-week SPI in Figures 3-9 shows that the last days of the period are in near-normal conditions, but the 12-week SPI in Figure 3-8 shows a moderately-to-very dry condition.

3.2 Comparison of Rain-sheltered Vegetation with Control Vegetation

The vegetation indices trend with time is indicated below for both the mixed and Irrigated Site. Outliers and faulty data were removed where present. T-Tests of mean difference being equal to 0 vs. not 0 were done with the null hypothesis being no difference between the drought and natural data sets, while the alternative hypothesis was that there was a difference between the drought and natural data sets. The T-value limit showing a statistical difference was 2.00 with a p-value ≤0.05 (95% certainty). Positive T-values greater than 2 indicated that the control data set mean value was greater than the drought data set mean, while negative T-values less than -2 indicated that the drought data set mean was greater than the control data set mean. Graphs presented were created in Microsoft Excel or Minitab 14, and statistical analysis was done using Minitab 14 software.

3.2.1 Rain-sheltered Site Vegetation Indices

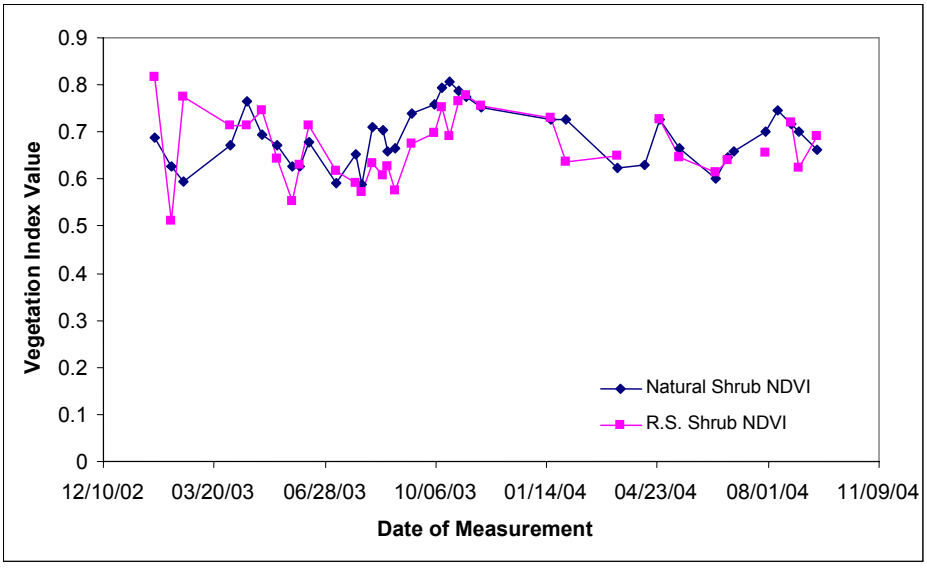

Figure 3-11: Rain-sheltered Site Shrub NDVI time series

Figure 3-11 shows the calculated NDVI for the creosote shrubs at the Rain-sheltered Site, both normal and rain-sheltered. The values are generally similar to each other, and follow similar trends. The extreme jumps at the beginning are possibly outliers. Both sets of values trend upwards throughout the summer and fall of 2003 as a result of the monsoon rainfall, although 2003 was overall a dry year and the control creosote shrubs were also under drought conditions for the most part. The mean NDVI for the normal shrubs was 0.688676 with a standard deviation of 0.062883, while the mean NDVI for the rain-sheltered shrubs was 0.671884 with a standard deviation of 0.073738. Paired T-Tests of mean difference being equal to 0 vs. not 0 on the control and rain-sheltered NDVI measurements differences gave a T-value of 1.43. Thus, we cannot statistically show a difference between both sets of measurements.

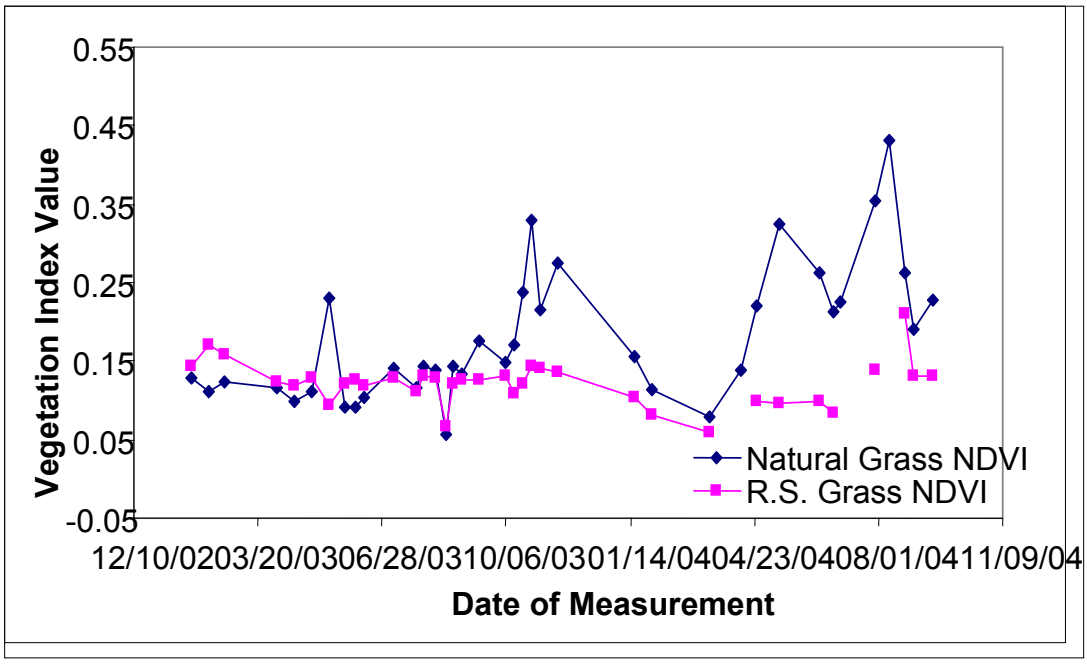

Figure 3-12: Rain-sheltered Site Grass NDVI time series

The grass indices showed more differences between the rain-sheltered and natural grass, as seen in Figure 3-12. Statistical analysis of the grass NDVI data gave the natural

grass mean NDVI as 0.17218 with a standard deviation of 0.076233, and the rain-sheltered grass mean NDVI as 0.121607 with a standard deviation of 0.028051. Paired T-test results gave a T-value of 3.97, which indicates a virtual certainty that the rain-sheltered and natural grass NDVI are statistically different. The spikes in NDVI value are a possible response to monsoon rainfall, as well as seasonal variation. Similar spikes are seen in the other datasets, and suggest that the grass responds more quickly to water availability than the shrubs do.

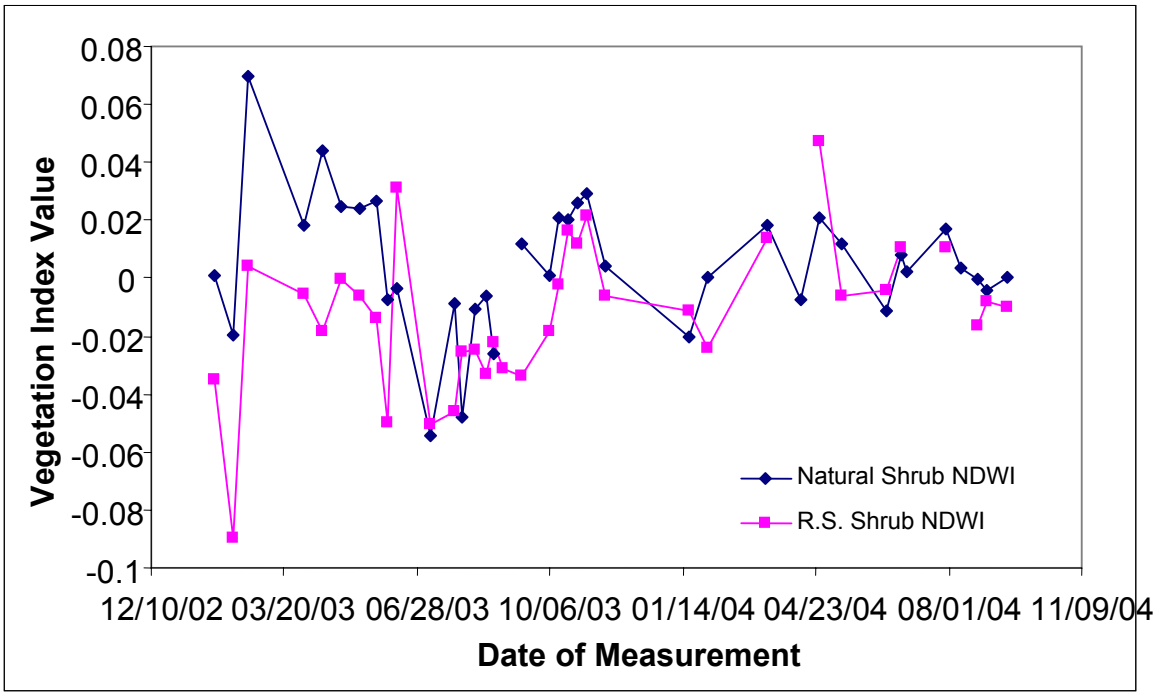

Figure 3-13: Shrub NDWI time series

The shrub NDWI time series data seen in Figure 3-13 is very erratic at the beginning, with large differences between the control and rain-sheltered measurements. The values become more similar towards the end of the time series. However, the field instrument measurements towards the higher end of the spectrum may not be as valid in the latter times of measurement. The mean control shrub NDWI was 0.014545 with a

standard deviation of 0.054896, while the rain-sheltered shrub mean NDWI was -0.011957 with a standard deviation of 0.02758. Paired T-tests gave a T-value of 2.57, and the confidence interval was between 0.00543 and 0.047552. Thus, we conclude that there is a statistical difference between both data sets. This is expected, as the water-stress absorption is expected to be less for the rain-sheltered shrub as compared to the control shrub.

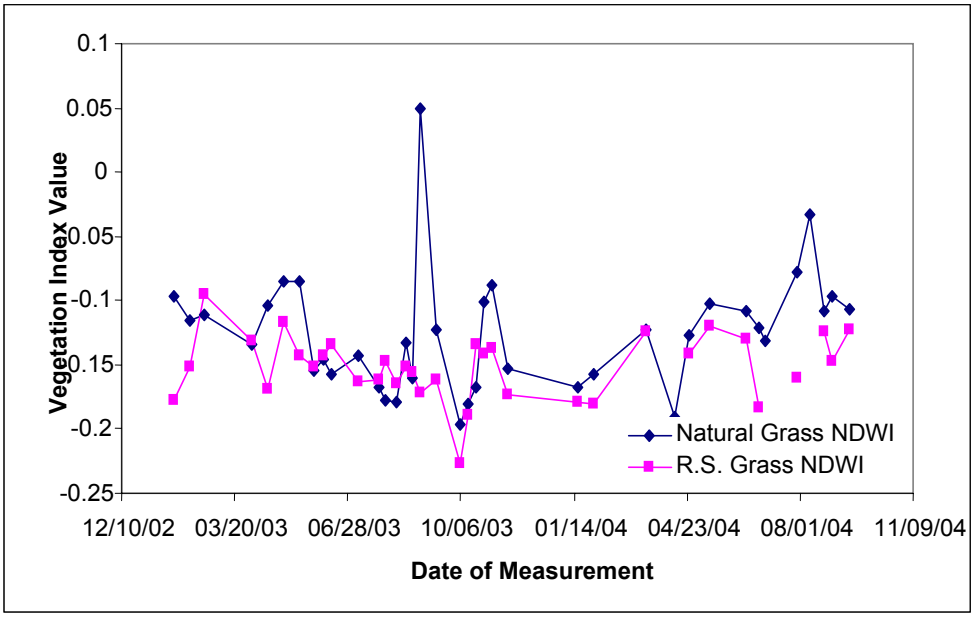

Figure 3-14: Grass NDWI time series.

As seen in Figure 3-14, the grass NDWI follows similar trends through time for both shrubs, although there is an apparent outlier on August 31 2003 for the natural grass measurement. When this outlier and its companion rain-sheltered grass measurement were removed, the mean control grass NDWI was -0.131 with a standard deviation of 0.032657, while the rain-sheltered grass NDWI was -0.151144 with a standard deviation of 0.0256. The T-test value was 3.97, so we conclude that these datasets are statistically different. Here also, we continue to see a lower water-absorption in the rain-sheltered vegetation which causes a lower mean value for this index.

Figure 3-15 represents the VIN time series, and shows that the VIN trends similarly to the NDVI data. The mean VIN for the natural shrubs was 5.69521 with a standard deviation of 1.431 and the mean VIN for the rain-sheltered shrubs was 5.38550 with a standard deviation of 1.512. T-test analysis gave a T-value of 1.21, indicating that there was no statistical difference between both sets of data.

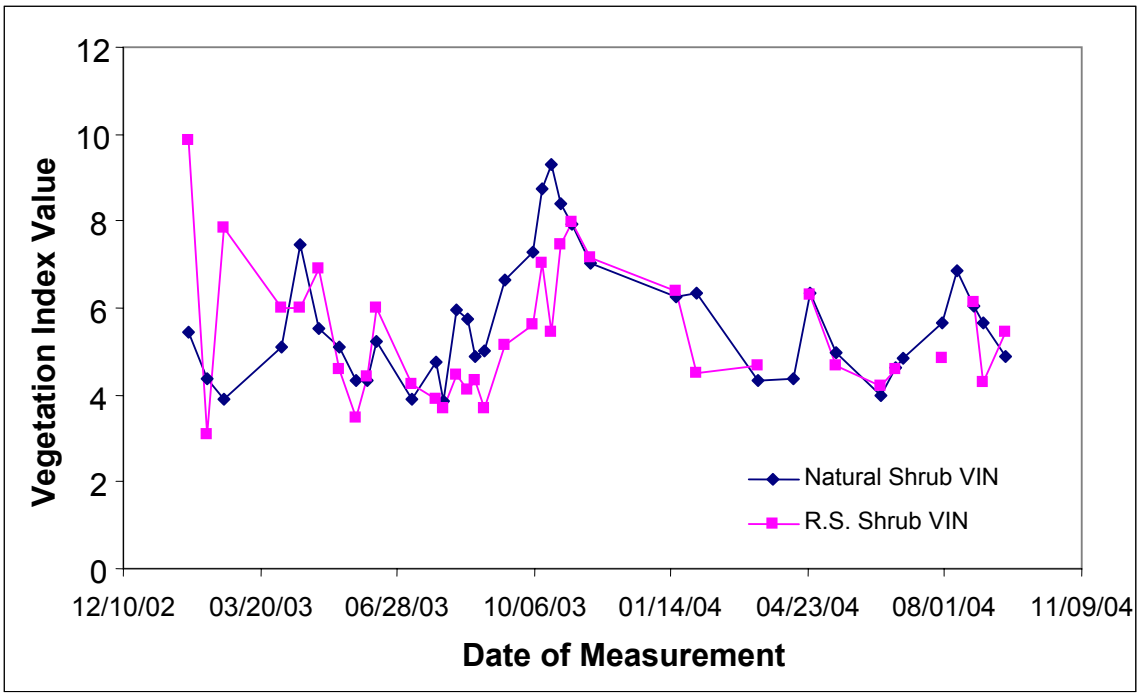

Figure 3-15: Rain-sheltered Site Shrub VIN time series

The rain-sheltered grass VIN values seen in Figure 3-16 were mostly constant throughout the measurement period, while the Natural Grass VIN values varied a lot more. The mean Natural Grass VIN was 1.43779 with a standard deviation of 0.245, while the mean Rain-sheltered grass VIN was 1.279 with a standard deviation of 0.0743. Paired T-Tests of mean difference being equal to 0 vs. not 0 gave a T-value of 3.89, which shows that there is a significant statistical difference between both data sets.

Figure 3-17 represents the Rain-sheltered Site shrub SAVI which also follows the trends of the shrub NDVI and VIN. The mean Natural Shrub SAVI was 0.466792 with a standard deviation of 0.0659, while the mean Rain-sheltered shrub SAVI was 0.456564 with a standard deviation of 0.0712. Paired T-Tests of mean difference being equal to 0 vs. not 0 gave a T-value of 1.49, so we cannot reject the null hypothesis.

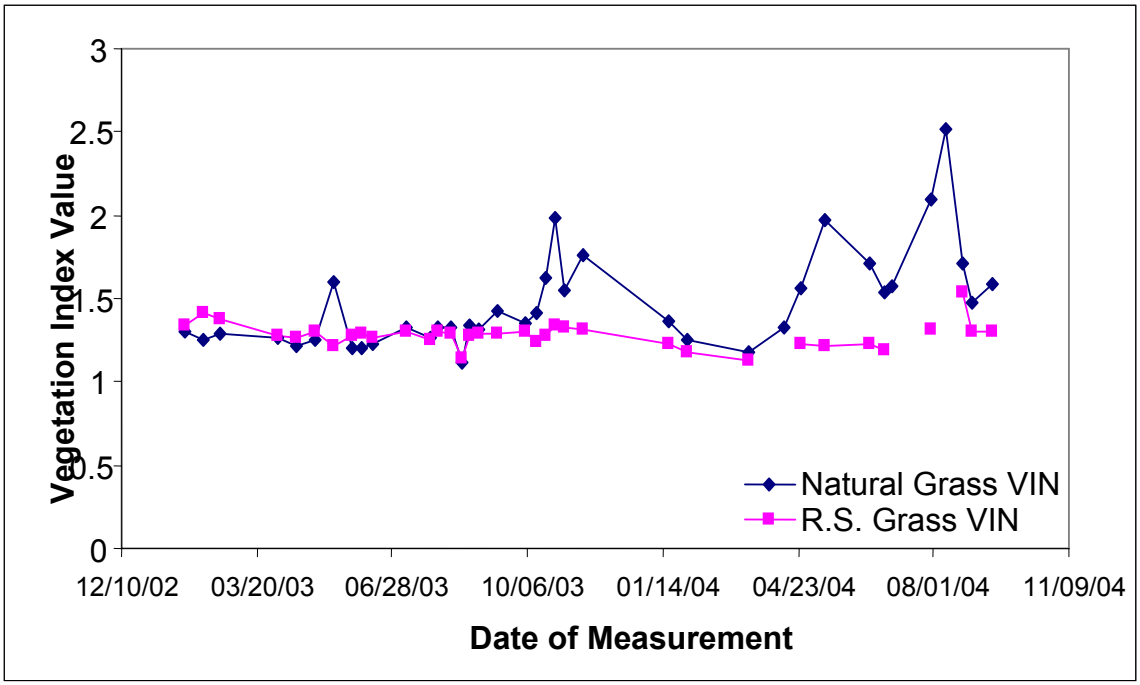

Figure 3-16: Rain-sheltered Site Grass VIN time series

Figure 3-18 shows the grass SAVI time series. The mean Natural Grass SAVI was 0.0858 with a standard deviation of 0.0403, while the mean Rain-sheltered grass SAVI was 0.059293 with a standard deviation of 0.017. The calculated T-value was 3.76, so we accepted the alternate hypothesis in this case.

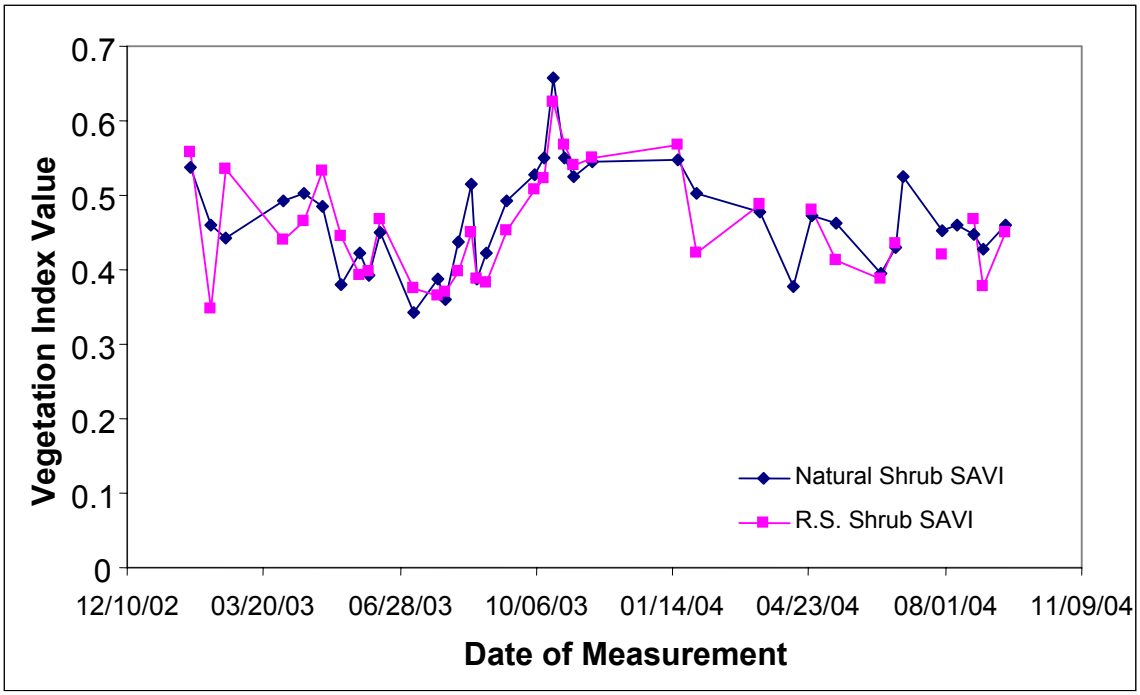

Figure 3-17: Rain-sheltered Site Shrub SAVI time series

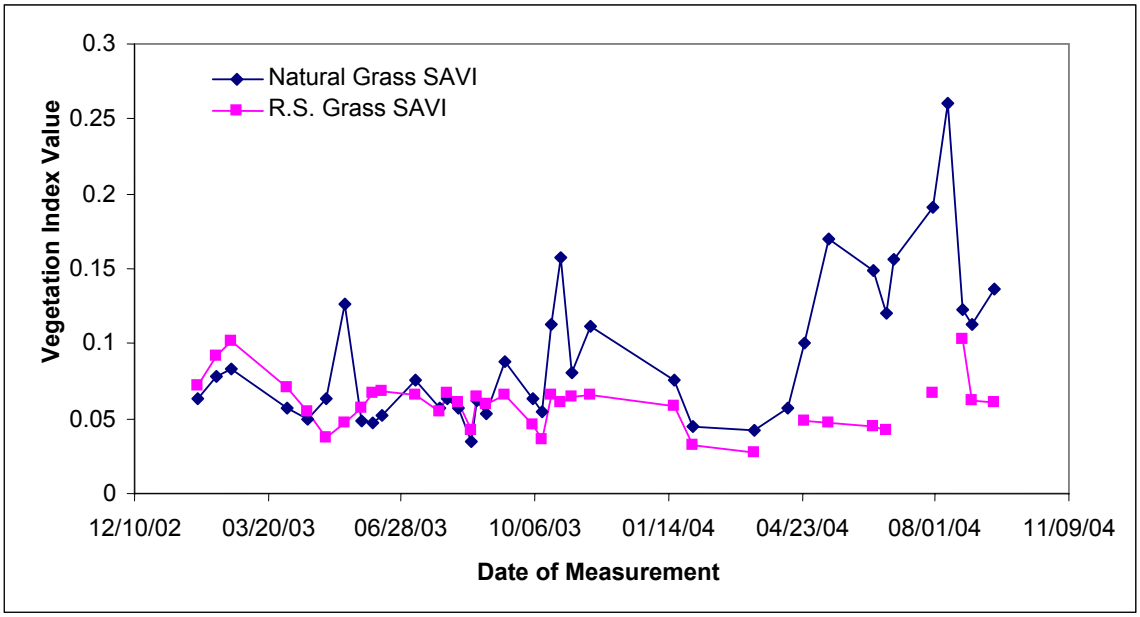

Figure 3-18: Rain-sheltered Site Grass SAVI time series

Figure 3-19 shows the mixed shrub ARVI data. The shrub ARVI measurements for both control and rain-sheltered vegetation also followed the general trends of the

NDVI and similar indices over time. The mean for the Natural Shrub ARVI was 0.5786 with a standard deviation of 0.07125, while the mean for the Rain-sheltered shrub ARVI was 0.0529 with a standard deviation of 0.08763. The calculated T-value was 2.05 with p of 0.049, which is just over the threshold of accepting the alternate hypothesis and concluding that there is a significant difference between both sets of measurements.

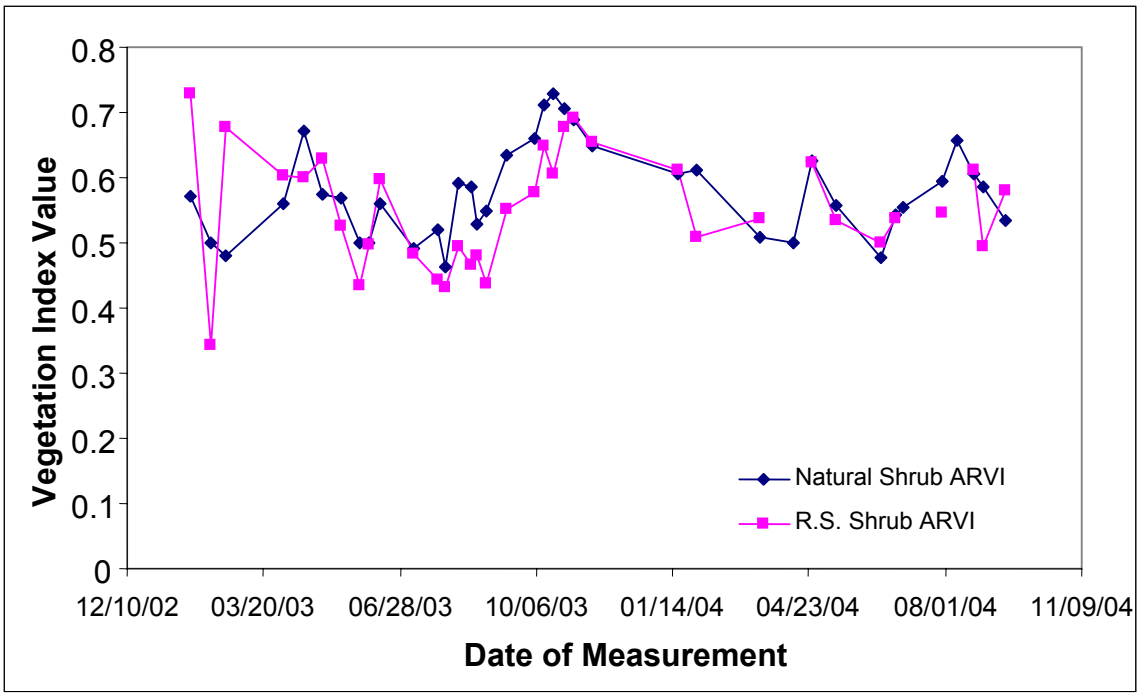

Figure 3-19: Rain-sheltered Site Shrub ARVI time index

Figure 3-20 shows the grass ARVI values. The rain-sheltered grass data clearly tends towards a value of 0, and is relatively constant just like the previous indices. The mean Natural Grass ARVI was 0.045 with a standard deviation of 0.08236, while the mean Rain-sheltered grass ARVI was -0.0079 with a standard deviation of 0.03048. The calculated T-value was 4.36 with a virtual certainty that both data sets were different from each other.

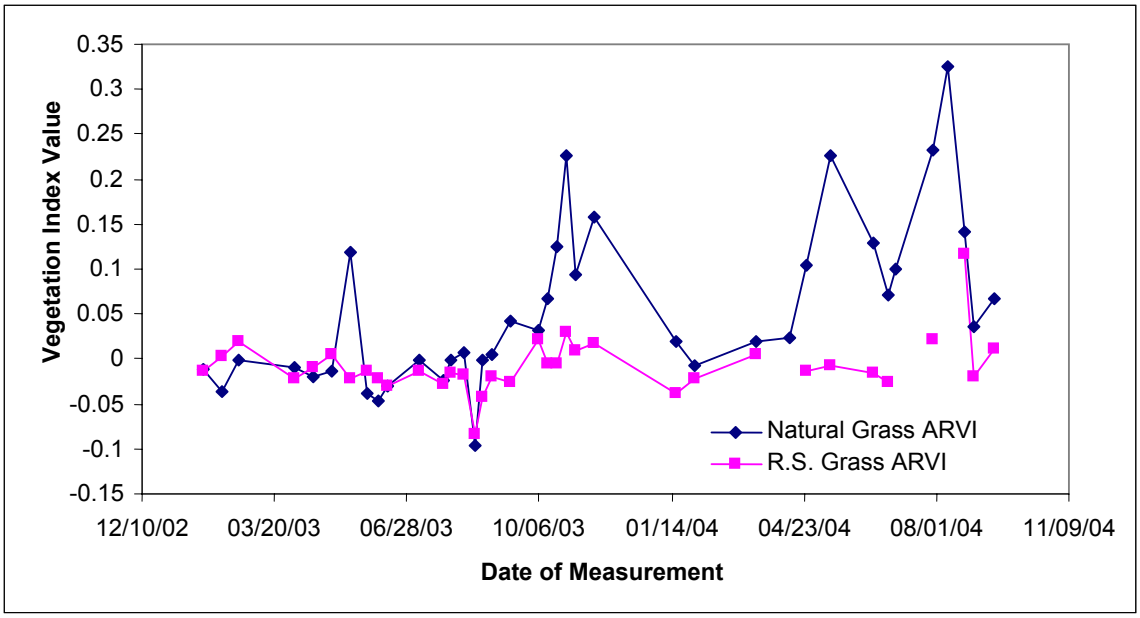

Figure 3-20: Rain-sheltered Site Grass ARVI time series data

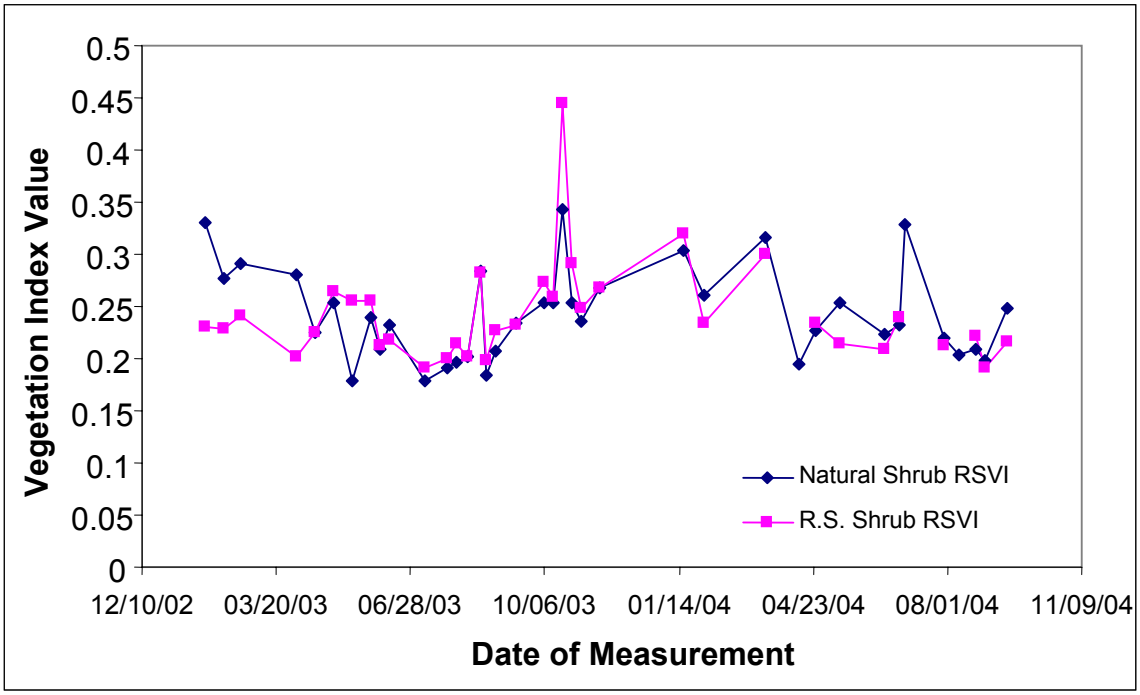

Figure 3-21: Rain-sheltered Site Shrub RVSI Time Series

Figure 3-21 shows the Rain-sheltered Site shrub RVSI values. Here, the values follow the same trend as each other, and there does not seem to be a large difference

between both sets of data. This is borne out in the T-test results, as the mean Natural Shrub RVSI is 0.2425 with a standard deviation of 0.0422, while the mean Rain-sheltered shrub RVSI is 0.2413 with a standard deviation of 0.0475. The calculated T-value was 0.19, so we accept the null hypothesis that there is no difference in this set of data.

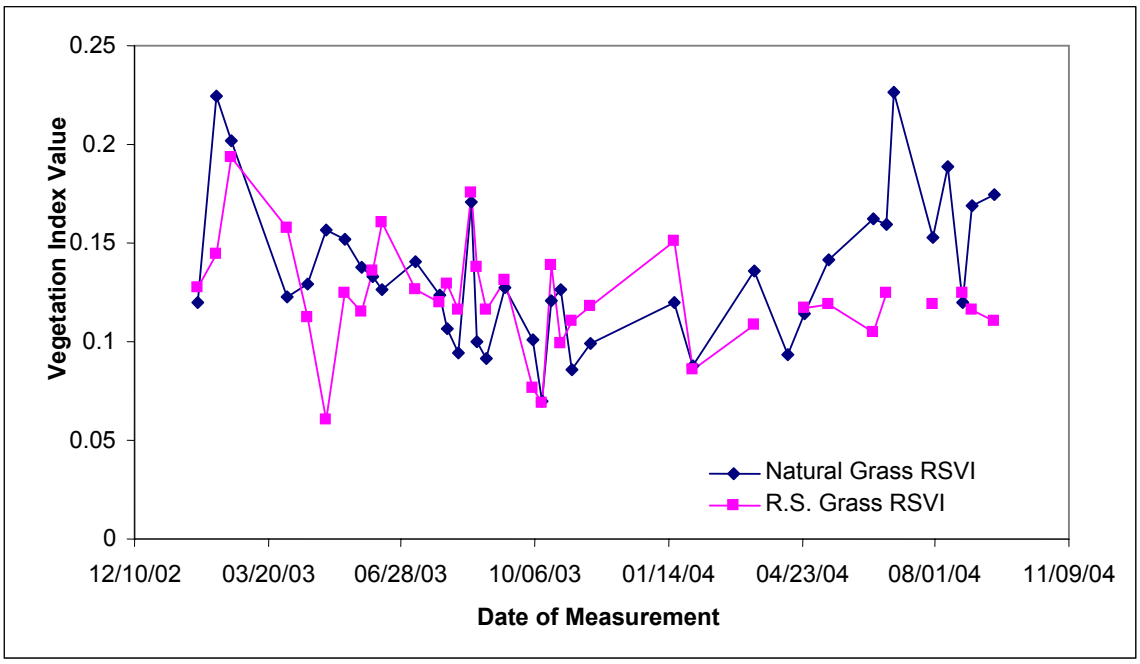

Figure 3-22: Rain-sheltered Site Grass RVSI

In Figure 3-22, which represents the Rain-sheltered Site grass RVSI, the trends over time for the grasses were similar to each other for the most part. The mean Natural Grass RVSI was 0.13135 with a standard deviation of 0.0331, while the mean Rain-sheltered grass RVSI was 0.12218 with a standard deviation of 0.0268. The calculated T-value was 1.63, so we concluded that the null hypothesis is valid and there is no difference between the datasets.

As seen in Figure 3-23, the range of the WBI values was very small when compared with other index ranges, between 0.96 and 1.04 for a range of 0.08. The mean control shrub WBI was 1.01234 with a standard deviation of 0.012, while the mean rain-

sheltered shrub WBI was 0.99319 with a standard deviation of 0.012. The calculated T-value was 10.87, making it a certainty that the alternate hypothesis was valid and there is a difference between both data sets.

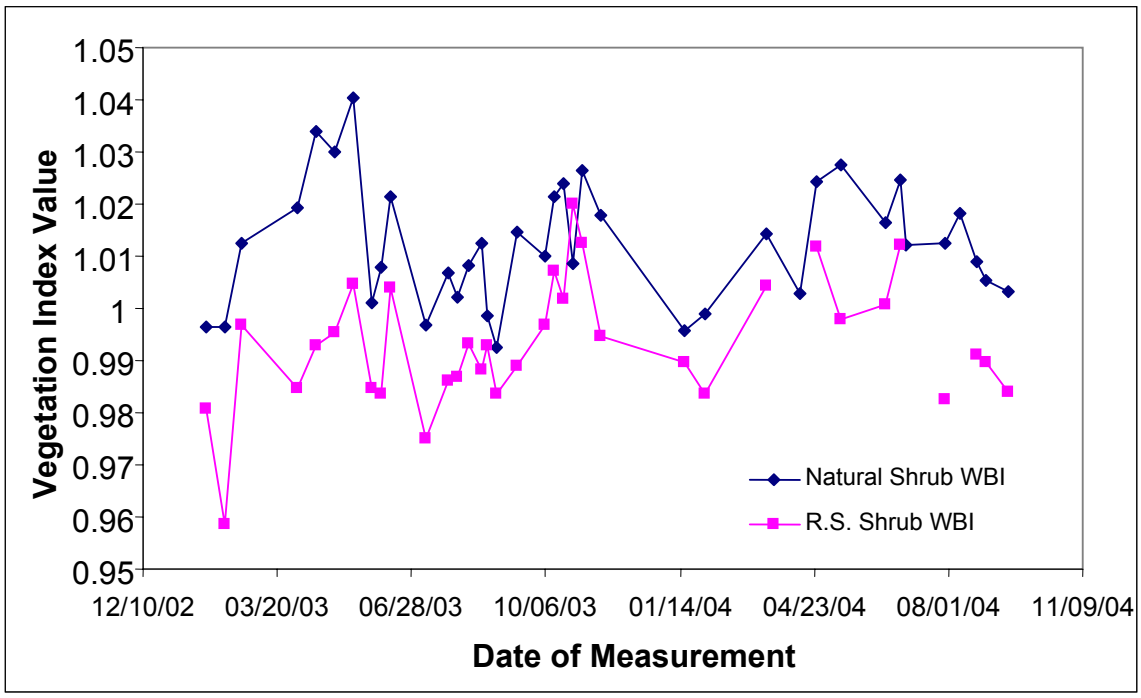

Figure 3-23: Rain-sheltered Site Shrub WBI values

Figure 3-24 shows the Rain-sheltered Site grass WBI data. The data values are all less than 1, which indicates low water content. The mean control grass WBI was 0.9555 with a standard deviation of 0.0123, while the mean rain-sheltered grass WBI was 0.9374 with a standard deviation of 0.009478. With such small standard deviations, the T-test value for the mean difference was 8.86, so we accepted the alternate hypothesis that there was a difference between the data sets.

Figure 3-25 shows the Rain-sheltered Site shrub RVI values. The RVI time series for both shrub plots follows similar trends, increasing in value through the monsoon

season and decreasing in the fall. The mean control shrub RVI was 0.1856 with a standard deviation of 0.04234, while the mean rain-sheltered shrub RVI was 0.1991 with a standard deviation of 0.051576. The calculated T-value was -1.77 with a p-value of 0.085, which is close but not enough to reject the null hypothesis.

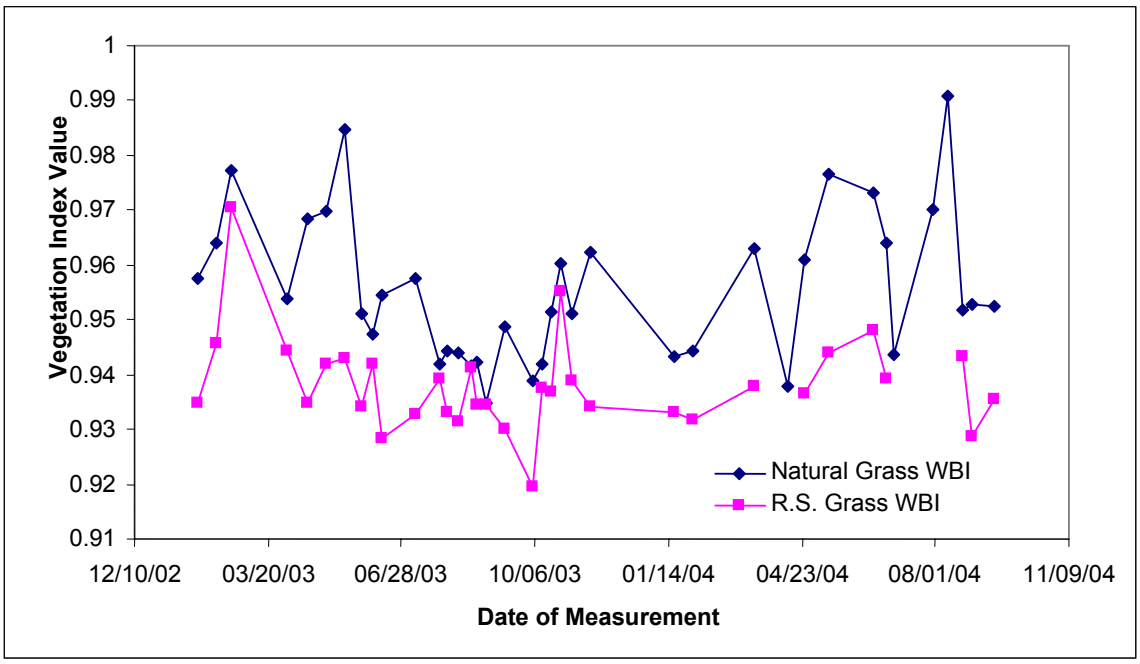

Figure 3-24: Rain-sheltered Site Grass WBI time series

Figure 3-26 represents the Rain-sheltered Site grass RVI values. The rain-sheltered grass data appears to be rather constant throughout the time series, while the control grass RVI data has more variation but still seems to be lower than the rain-sheltered grass data. The mean control grass RVI is 0.712962 with a standard deviation of 0.10689, while the mean rain-sheltered grass RVI was 0.78423 with a standard deviation of 0.044255. The calculated T-value was -3.99, so we accepted the alternate hypothesis that there is a difference between both data sets, and we note that the drought mean is actually greater than the control mean.

Figure 3-27 represents the Rain-sheltered Site shrub NDGI data. The mean control shrub NDGI was 0.080245 with a standard deviation of 0.0478, while the mean rain-sheltered shrub NDGI was 0.056576 with a standard deviation of 0.048931. The T-test on mean difference gave a value of 4.33, so we accepted the alternate hypothesis.

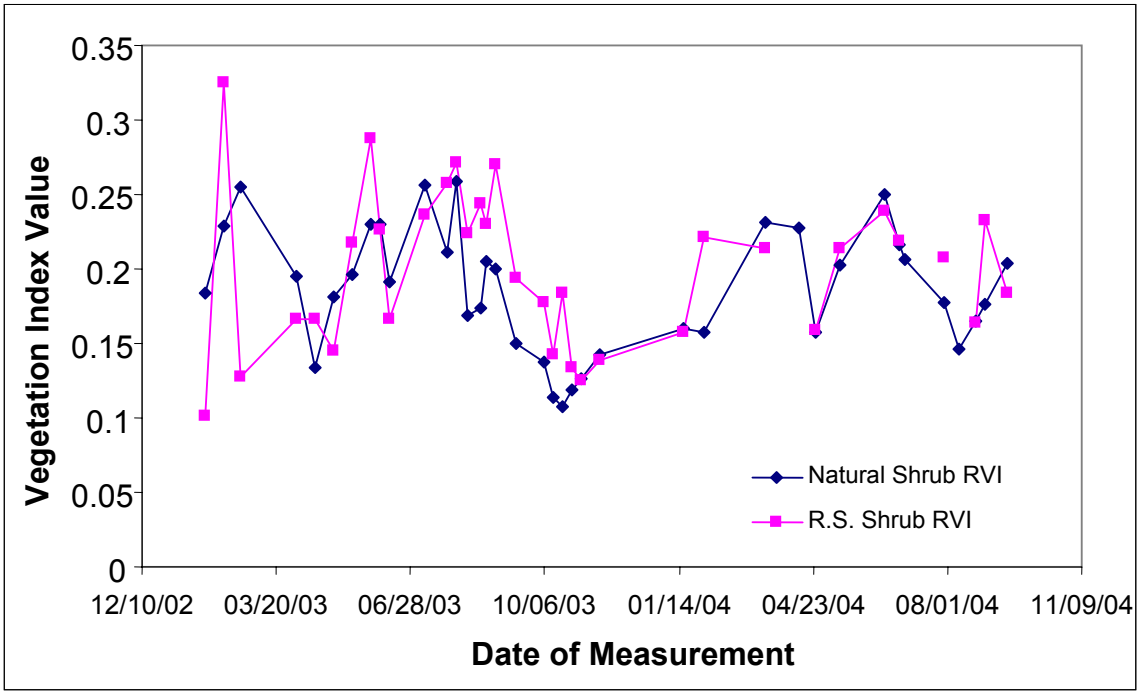

Figure 3-25: Rain-sheltered Site Shrub RVI time series

Figure 3-28 represents the Rain-sheltered Site grass NDGI time series. The mean control grass NDGI was –0.07233 with a standard deviation of 0.0244, while the rain-sheltered grass NDGI was -0.08439 with a standard deviation of 0.021768. T-Tests of mean difference being equal to 0 vs. not 0 gave a value of 3.87, so we reject the null hypothesis and accept the alternate hypothesis that there is a difference between both data sets.

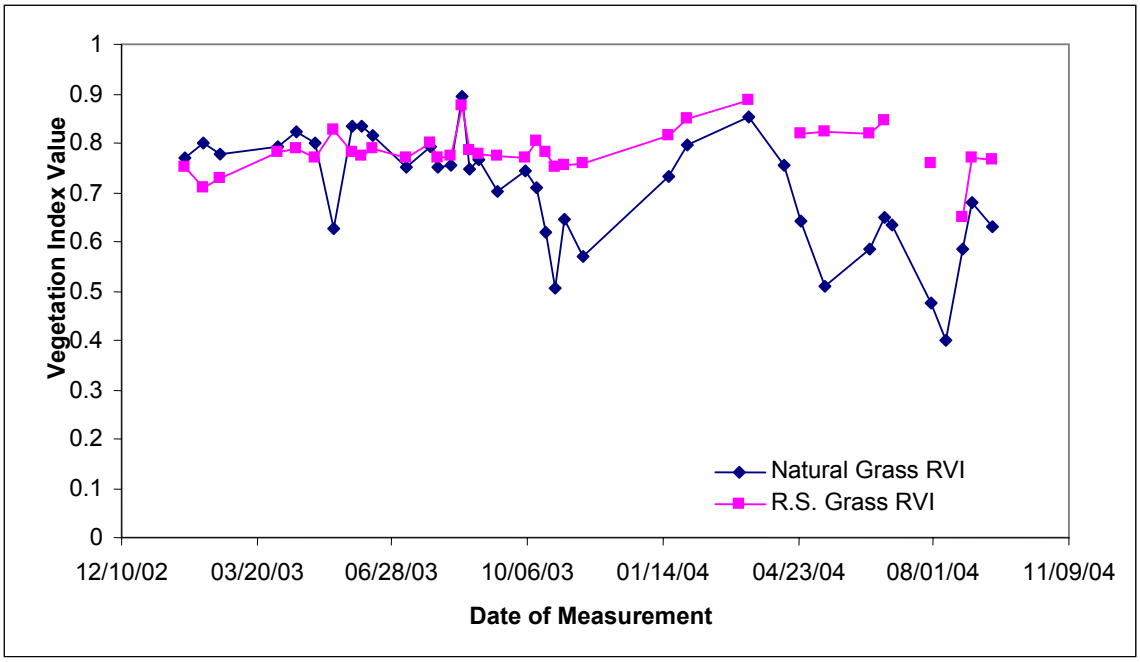

Figure 3-26: Rain-sheltered Site Grass RVI time series

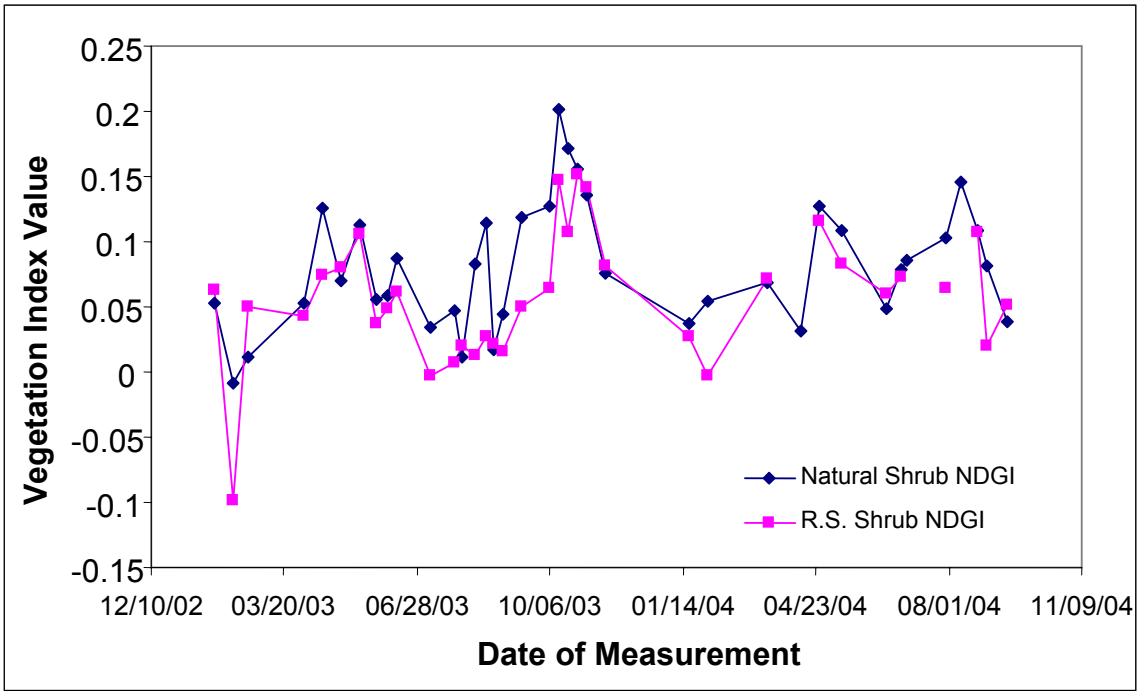

Figure 3-27: Rain-sheltered Site Shrub NDGI time series

Figure 3-29 represents the Rain-sheltered Site shrub NDRI datasets. The mean control shrub NDRI was -0.080245 with a standard deviation of 0.0478, while the mean rain-sheltered shrub NDRI was -0.056576 with a standard deviation of 0.0489. The T-test of mean difference value was -4.33, so we reject the null hypothesis and conclude that the drought data set is greater than the control data.

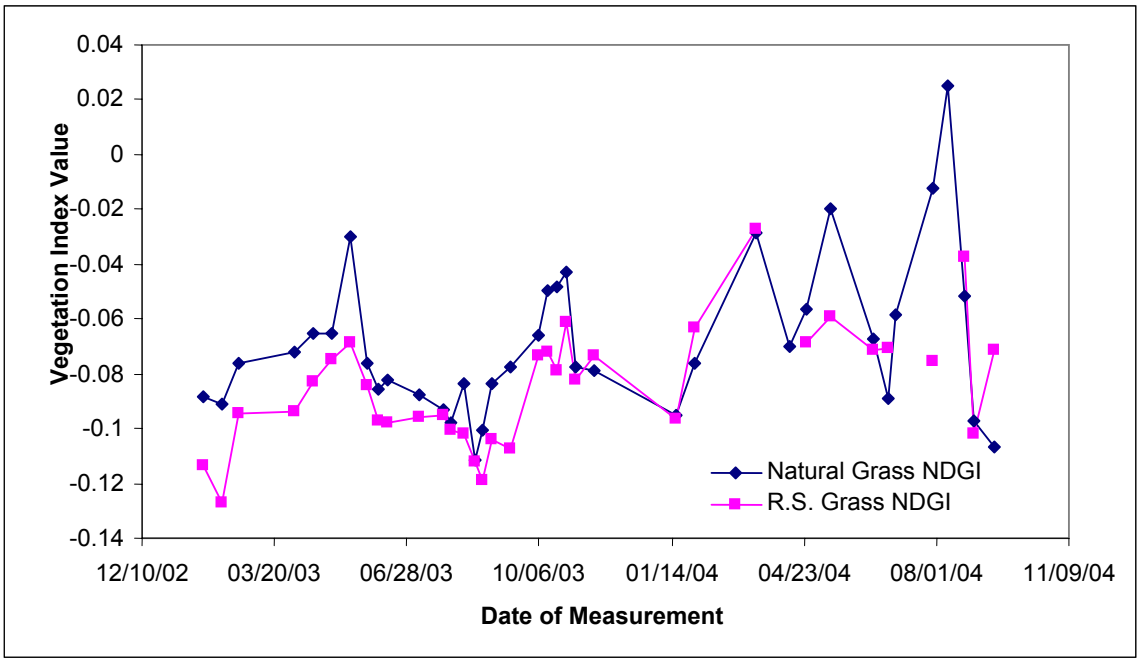

Figure 3-28: Rain-sheltered Site Grass NDGI time series

Figure 3-31 represents the Rain-sheltered Site shrub NDI. The mean natural shrub NDI is 0.287733 with a standard deviation of 0.06259, while the mean rain-sheltered shrub NDI is 0.255925 with a standard deviation of 0.063861. The T-test value of the mean difference was 2.88, so we accepted the null hypothesis that there was a difference between both shrubs with this data.

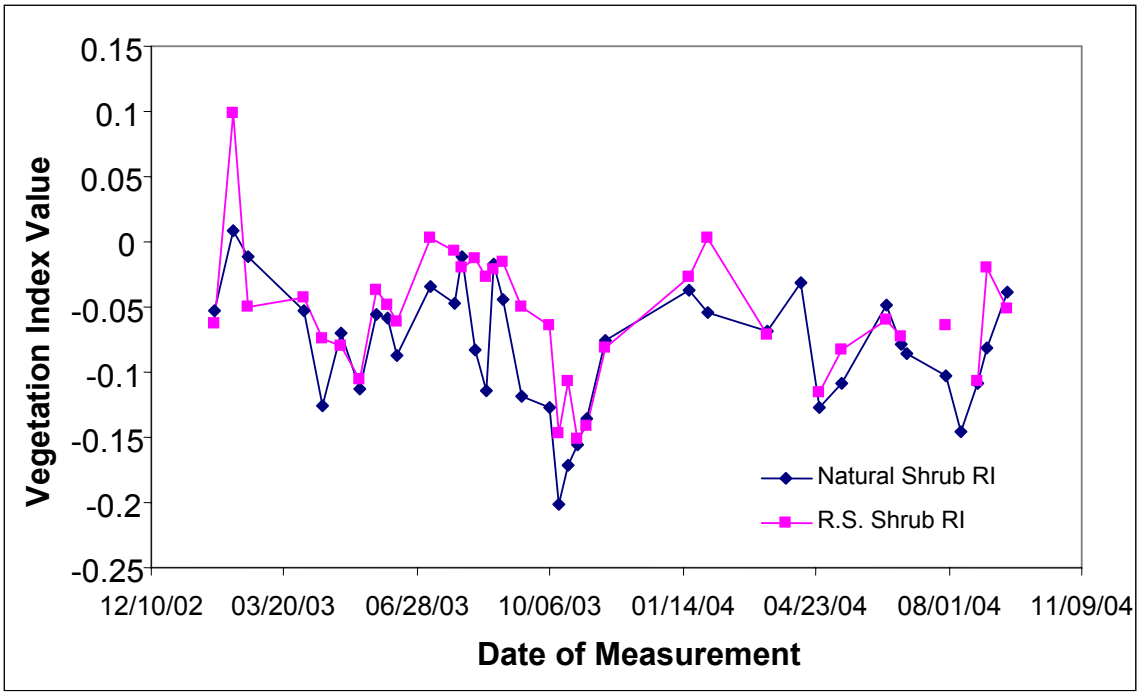

Figure 3-29: Rain-sheltered Site Shrub NDRI time series

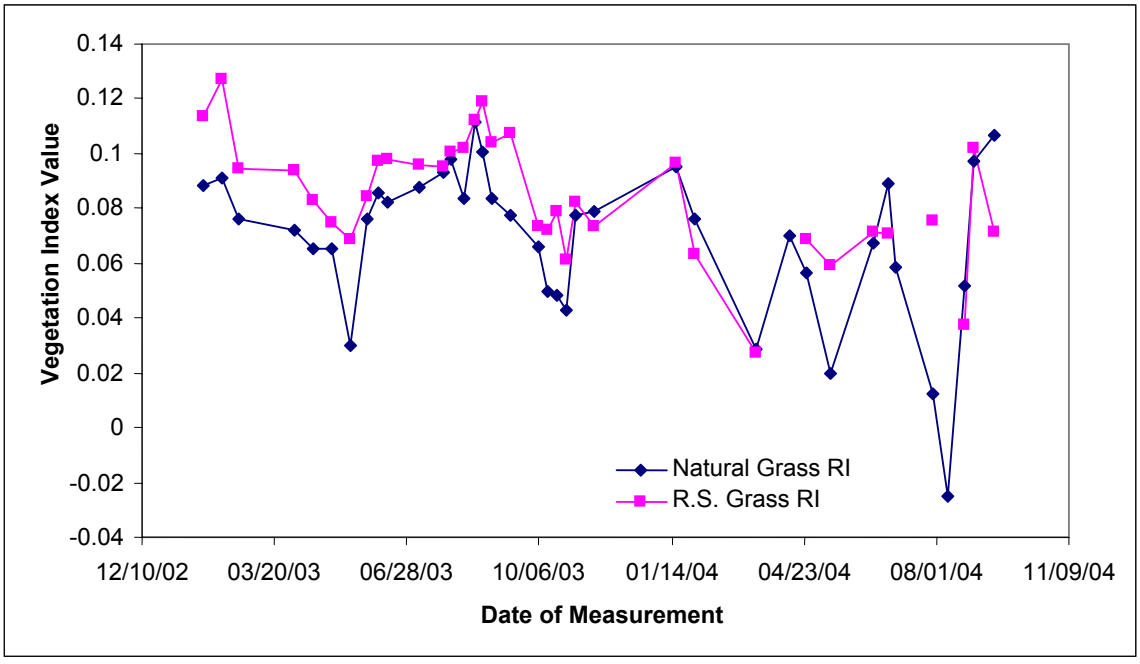

Figure 3-30: Rain-sheltered Site Grass NDRI time series

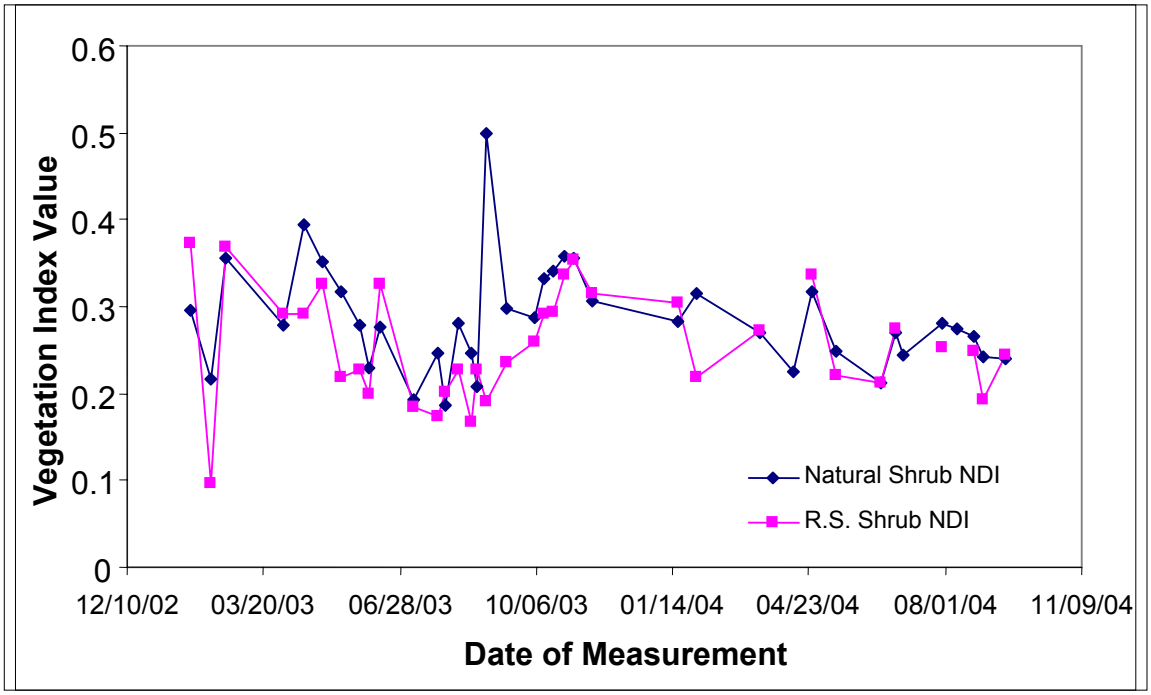

Figure 3-31: Rain-sheltered Site Shrub NDI time series

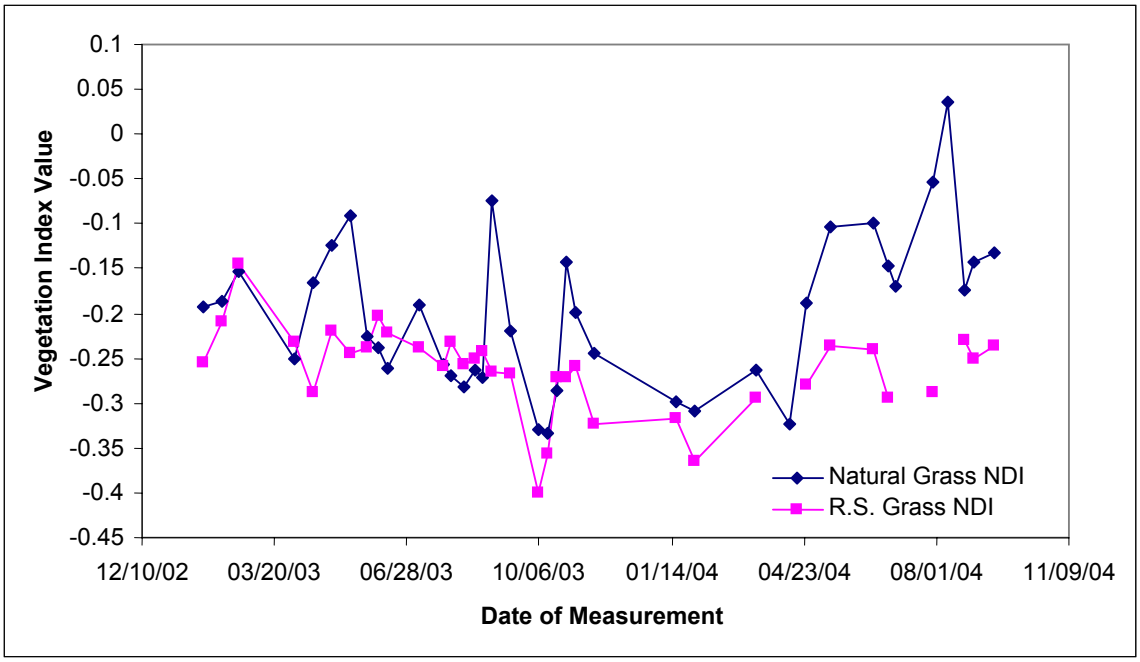

Figure 3-32: Rain-sheltered Site Grass NDI time series

Figure 3-32 shows the Rain-sheltered Site grass NDI data. The mean control grass NDI was -0.204745 with a standard deviation of 0.075612, while the mean drought NDI was -0.262386 with a standard deviation of 0.048273. T-Tests of mean difference being equal to 0 vs. not 0 gave a T-value of 4.87, so we accept the alternate hypothesis that there is a difference between both datasets. This is probably due to a higher water absorption in the control shrub vegetation in the middle infrared region for both the shrub and grass NDI data.

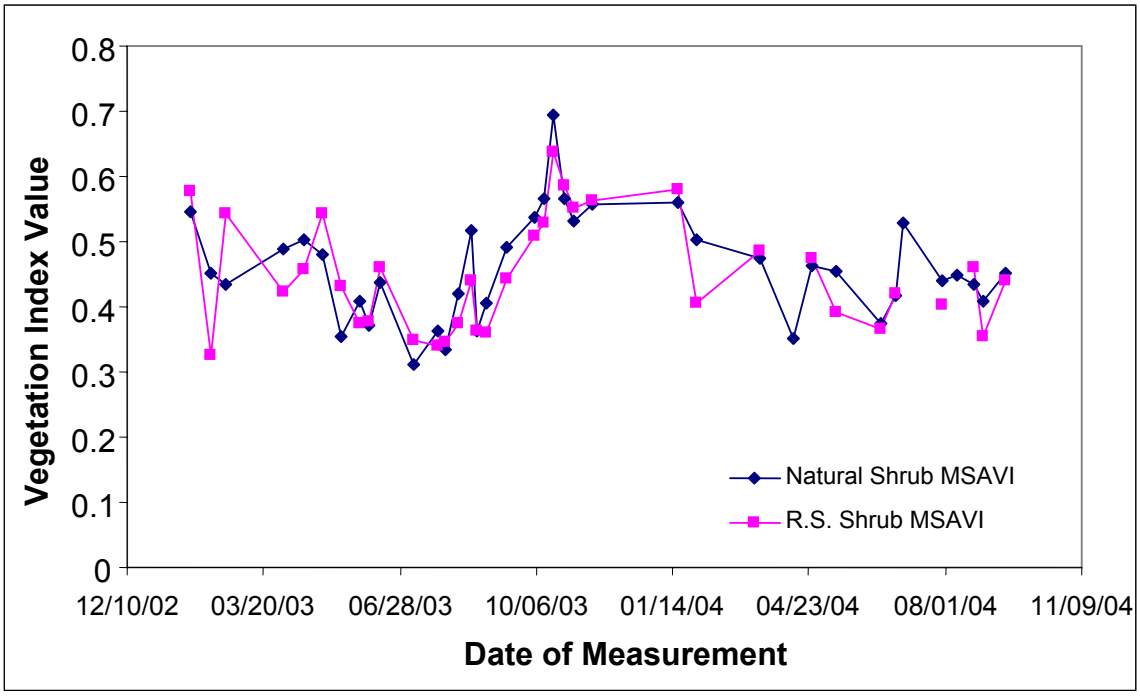

Figure 3-33: Rain-sheltered Site Shrub MSAVI time series

Figure 3-33 shows the Rain-sheltered Site shrub MSAVI data. The shrub MSAVI values trend similarly to the NDVI and similar indices. The mean control shrub MSAVI is 0.460365 with a standard deviation of 0.08075, while the mean rain-sheltered shrub

MSAVI is 0.44844 with a standard deviation of 0.095113. The T-test for mean difference was 1.44, so we accept the null hypothesis in this case that there is no difference.

Figure 3-34 shows the Rain-sheltered Site grass MSAVI data. The rain-sheltered grass MSAVI is close to a constant trend, while the control grass varies a lot. The mean control grass MSAVI is 0.070874 while the mean rain-sheltered grass MSAVI is 0.0482. The T-test for mean difference was calculated as 3.69, so we reject the null hypothesis.

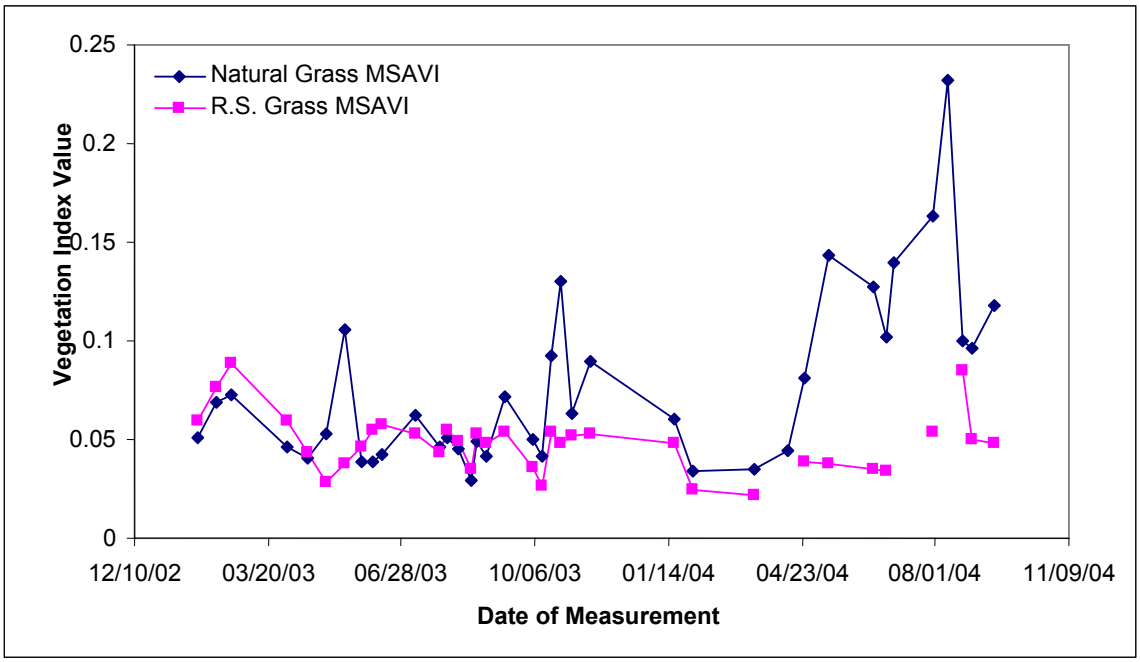

Figure 3-34: Rain-sheltered Site Grass MSAVI time series

3.2.2 Irrigated Site Vegetation Indices

Figure 3-36 presents the Irrigated Site shrub NDWI data. The NDWI trend for both shrubs is quite similar, except for one measurement on August 17 2003. There is also an obvious outlier for October 12 2003 in both measurements. Even if one includes this possible outlier, the statistical analysis was the same result as not including it. The mean NDWI for the watered shrub was 0.057 with a standard deviation of 0.172, while the mean for the control shrub was 0.023 with a standard deviation of 0.153. The T-value

was 0.74 with a p-value of 0.461, so we cannot statistically show a difference between both data sets.

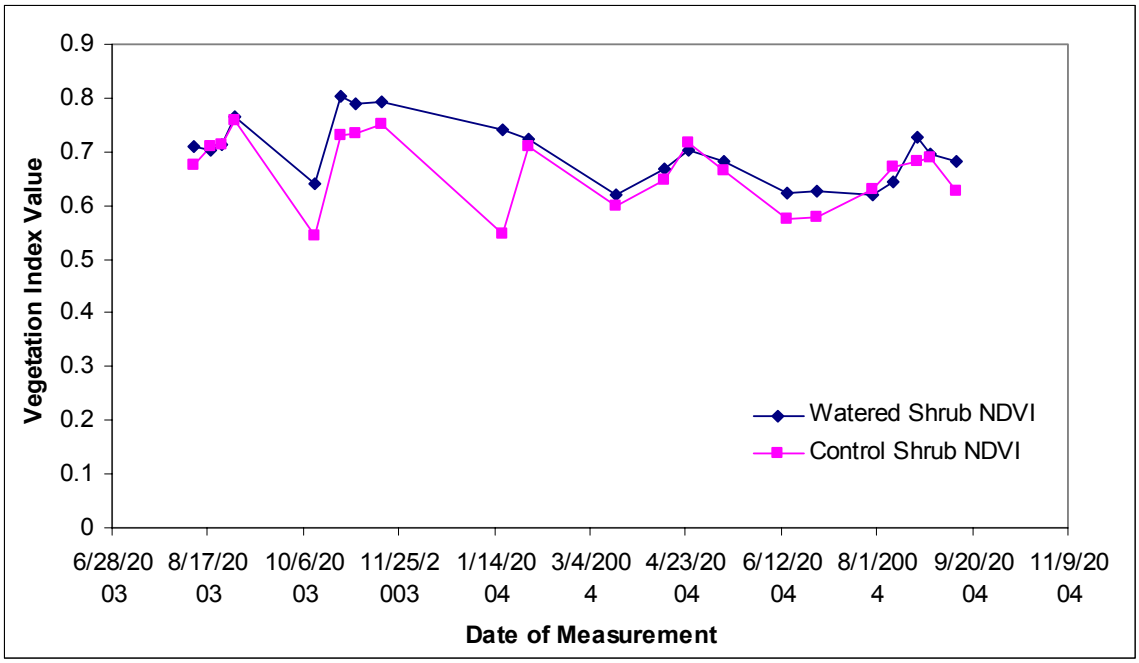

Figure 3-35: Irrigated Site Shrub NDVI time series

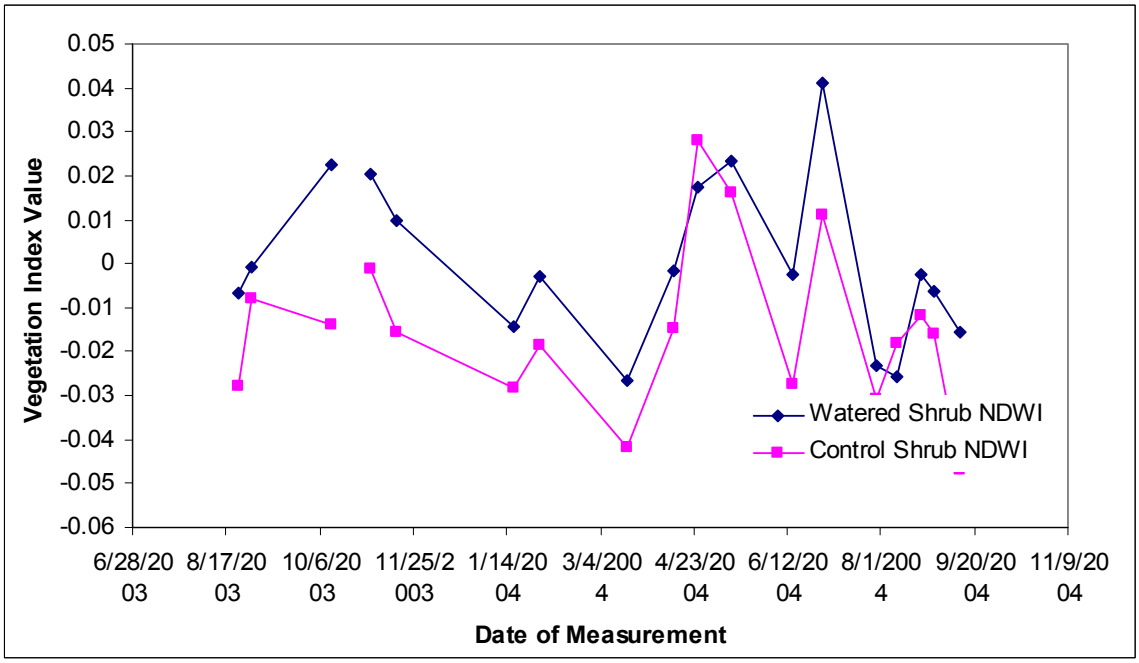

Figure 3-36: Irrigated Site Shrub NDWI time series

Figure 3-37 presents the Irrigated Site VIN data. The VIN time series follows a similar trend to the NDVI time series. The mean watered shrub VIN was 5.98551 with a standard deviation of 1.539, while the mean control shrub VIN was 5.09543 with a standard deviation of 1.167. T-Tests of mean difference being equal to 0 vs. not 0 gave a T-value of 3.78, so we accept the alternate hypothesis.

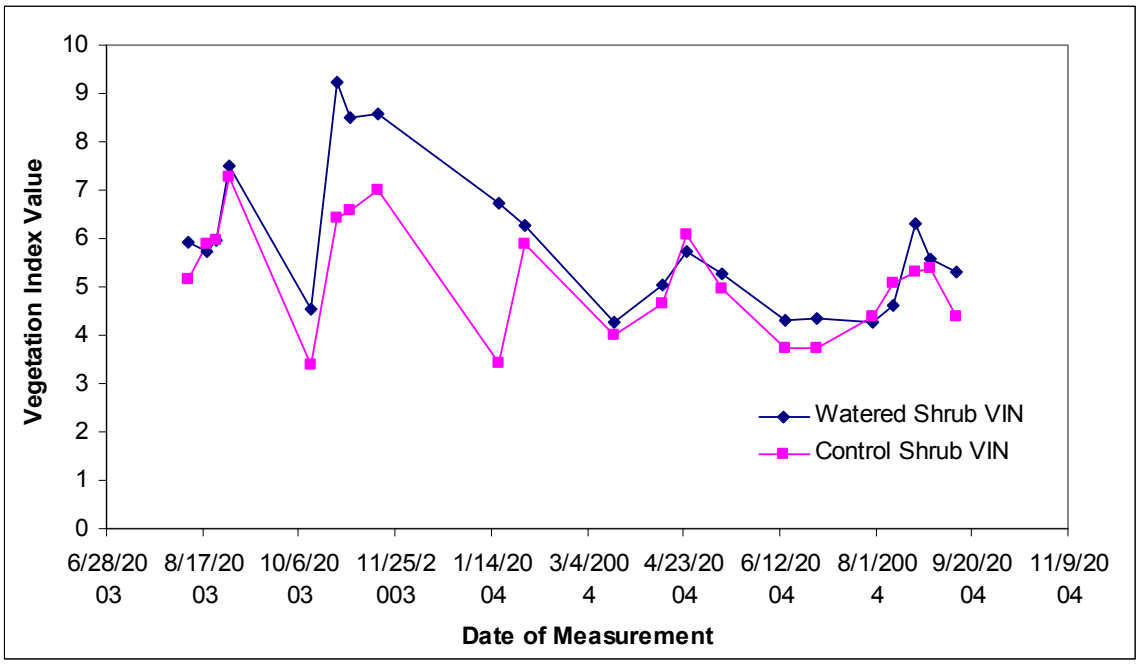

Figure 3-37: Irrigated Site Shrub VIN time series

Figure 3-38 presents the Irrigated Site Shrub SAVI data. The SAVI time series data seems to have a steady trend, and has an apparent outlier for the first measurement. When the first measurements were removed from analysis, the mean watered shrub SAVI was calculated as 0.487946 with a standard deviation of 0.05522, while the mean control shrub SAVI was 0.44692 with a standard deviation of 0.047847. The T-Tests of mean difference being equal to 0 vs. not 0 gave a T-value of 5.95, so we rejected the null hypothesis and accepted the alternate hypothesis.

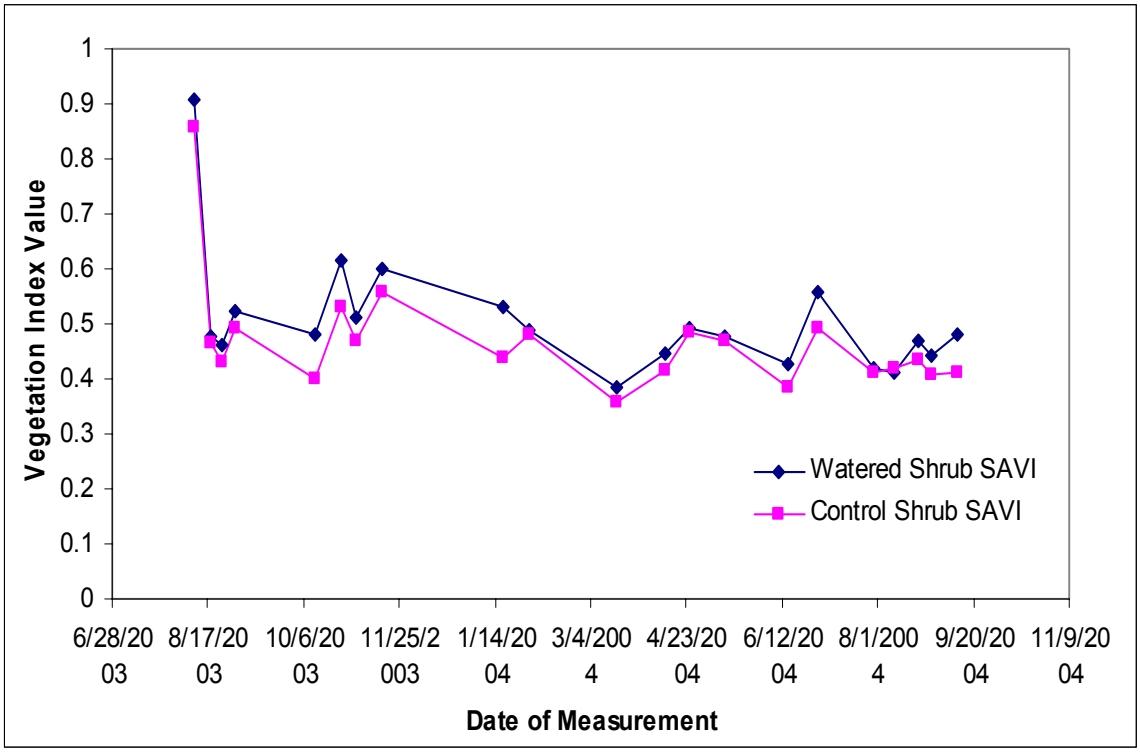

Figure 3-38: Irrigated Site Shrub SAVI time series

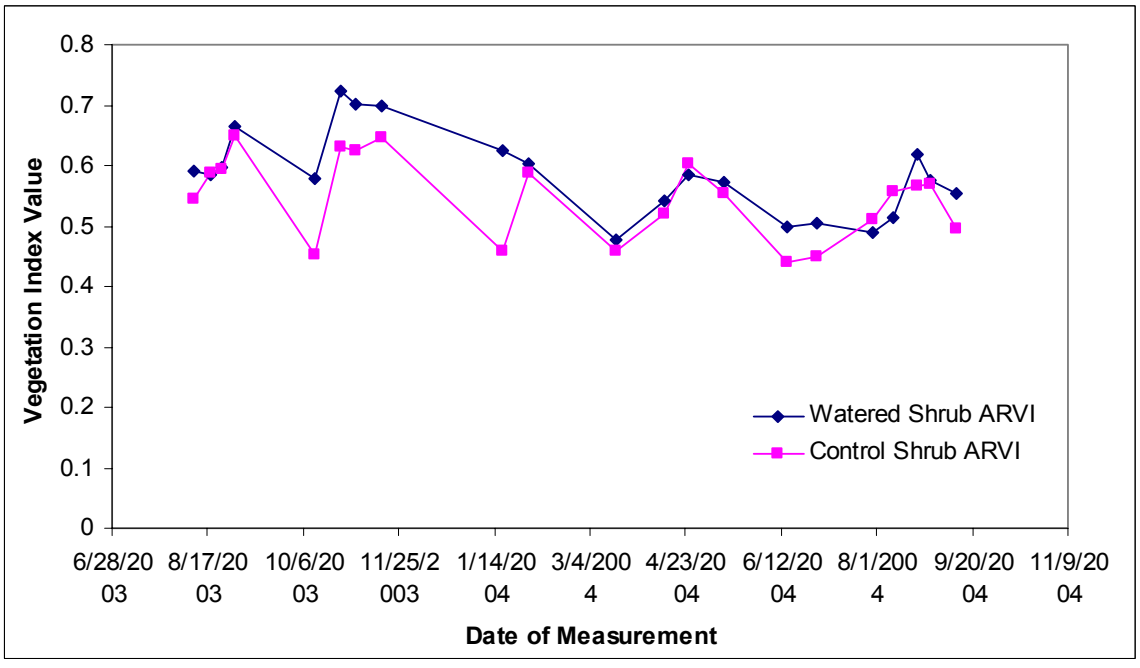

Figure 3-39: Irrigated Site Shrub ARVI time series

Figure 3-39 presents the Irrigated Site shrub ARVI data. The trend here is similar to the other infrared/red band indices. The mean watered shrub ARVI was 0.588456 with a standard deviation of 0.071676, while the mean control shrub ARVI was 0.543671 with a standard deviation of 0.070231. T-Tests of mean difference being equal to 0 vs. not 0 gave a T-value of 4.01, so we reject the null hypothesis and accept the alternate hypothesis.

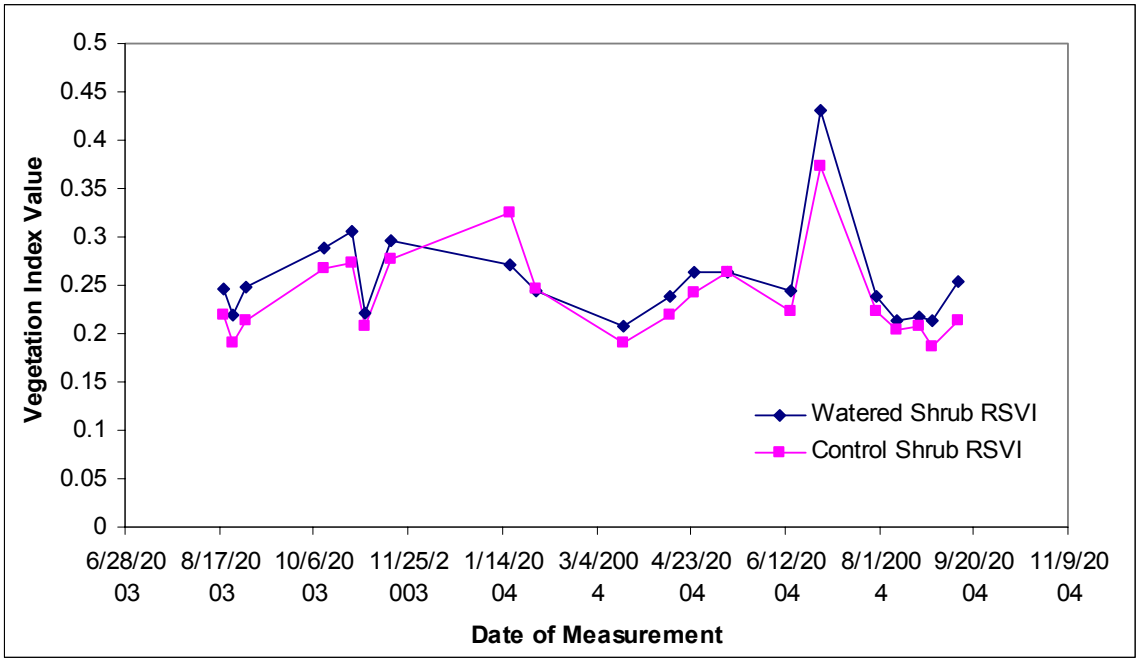

Figure 3-40: Irrigated Site Shrub RVSI time series

Figure 3-40 presents the Irrigated Site shrub RVSI date. The RVSI indices follow a mostly constant trend. The first data measurements were outliers and were removed. When the outliers were removed, the mean watered shrub RVSI was 0.257172 with a standard deviation of 0.046424, while the mean control shrub RVSI was 0.239774 with a standard deviation of 0.043068. T-Tests of mean difference being equal to 0 vs. not 0 gave a T-value of 4.23, so we accepted the alternate hypothesis that there is a difference between both datasets.

Figure 3-41 shows the Irrigated Site shrub WBI data. The WBI series has a much smaller numerical range than the other indices but still shows a statistical difference. The watered shrub WBI mean was 1.00905 with a standard deviation of 0.00888, while the control shrub WBI was 0.99467 with a standard deviation of 0.00987. T-Tests of mean difference being equal to 0 vs. not 0 gave a T-value of 8.76, so we reject the null hypothesis and accept the alternate hypothesis.

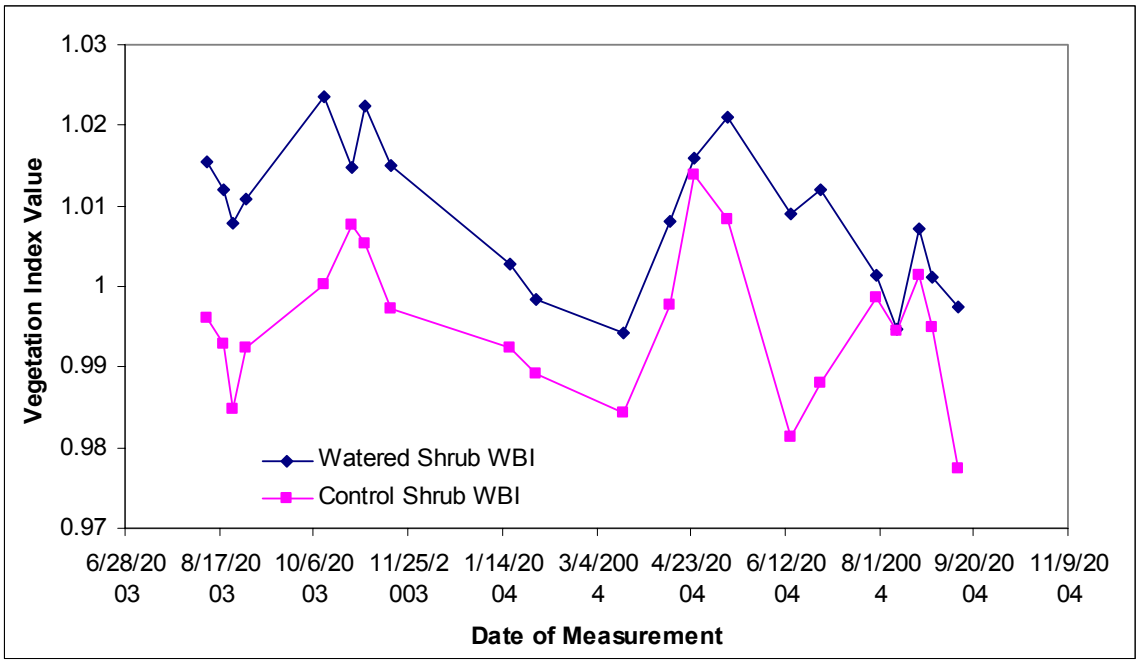

Figure 3-41: Irrigated Site Shrub WBI time series

Figure 3-42 shows the Irrigated Site shrub RVI data. The mean watered shrub RVI was 0.176765 with a standard deviation of 0.040198, while the mean control shrub RVI was 0.206863 with a standard deviation of 0.049. T-tests done on the mean difference gave a T-value of -3.67, so we accept the alternate hypothesis and note that the control data is larger than the Irrigated Site data.

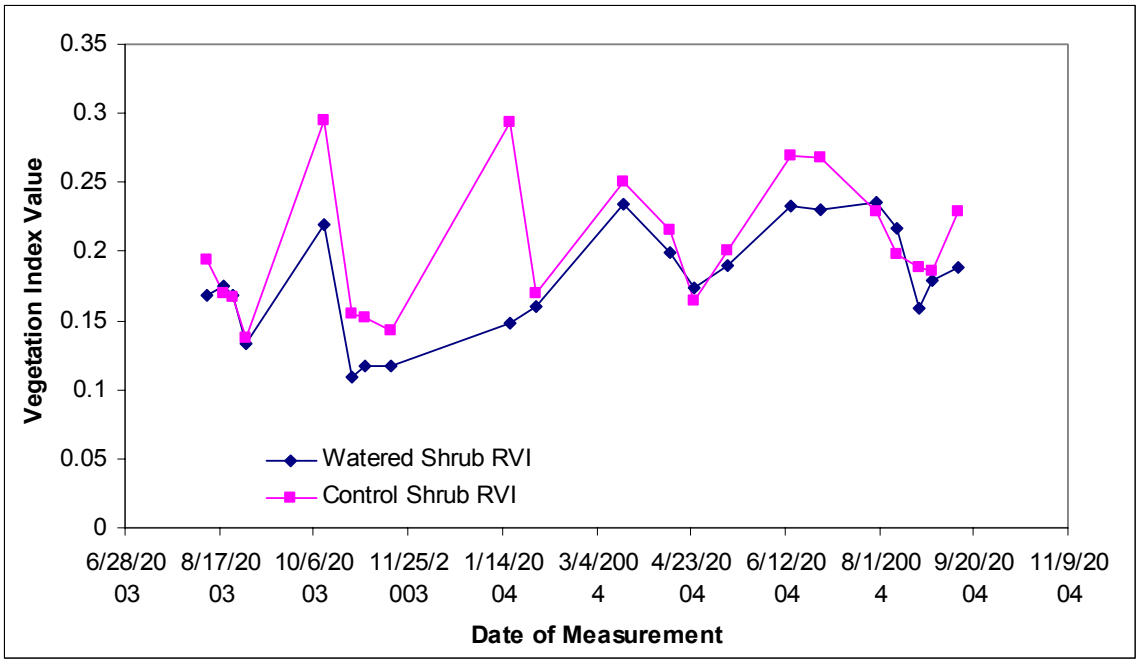

Figure 3-42: Irrigated Site Shrub RVI time series

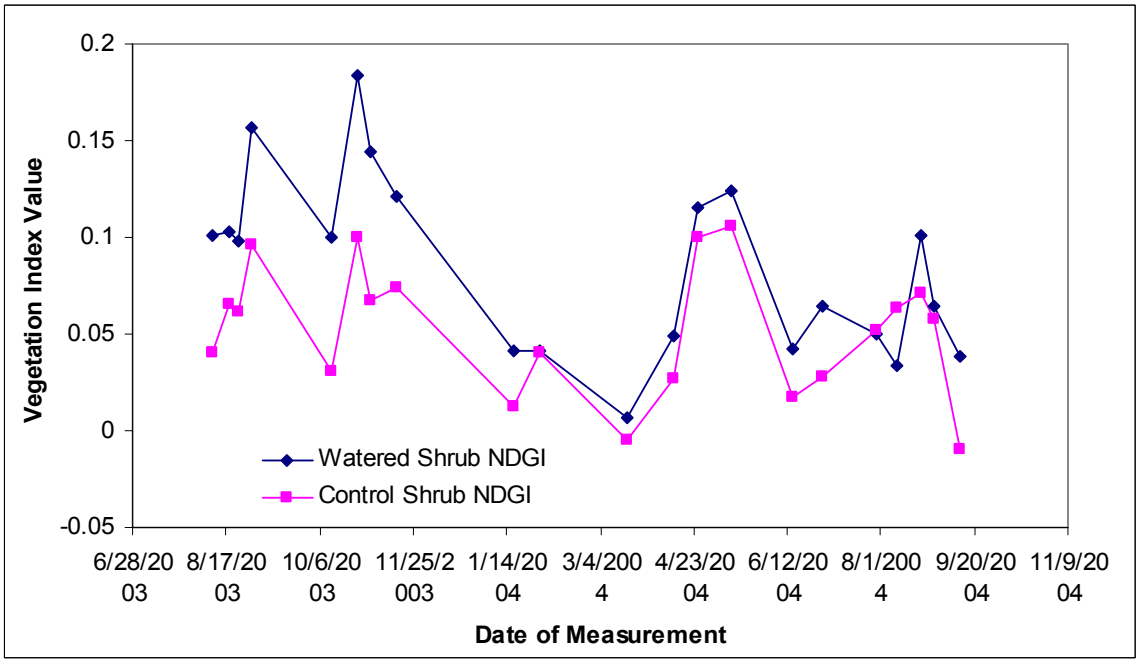

Figure 3-43: Irrigated Site Shrub NDGI time series

Figure 3-43 shows the Irrigated Site shrub NDGI data. The time series is highly variable, but both datasets follow similar trends in increasing and decreasing (until the

final few measurements). The mean watered shrub NDGI is 0.087942 with a standard deviation of 0.0561, while the mean control shrub NDGI is 0.05144 with a standard deviation of 0.0387. T-Tests of mean difference being equal to 0 vs. not 0 gave a T-value of 5.42, so we accept the alternate hypothesis.

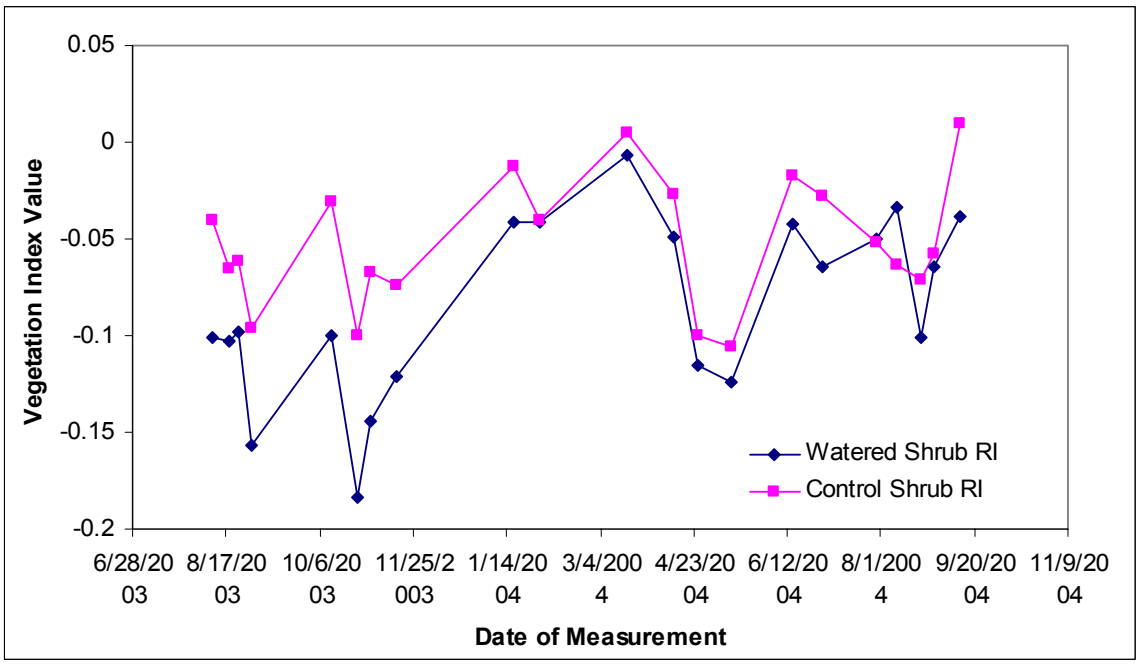

Figure 3-44: Irrigated Site Shrub NDRI time series

Figure 3-44 shows the Irrigated Site shrub NDRI data. The NDRI is the inverse of the NDGI, so its values are just the negative of the NDGI values. The mean watered shrub NDRI is -0.087942 with a standard deviation of 0.0561 while the mean control shrub NDRI is -0.05144 with a standard deviation of 0.0387. T-Tests of mean difference being equal to 0 vs. not 0 gave a T-value of -5.42, so we accept the alternate hypothesis and note that the control shrub has a higher value than the rain-sheltered shrub.

Figure 3-45 shows the Irrigated Site shrub NDI data. The NDI time series has an outlier measurement on Oct 12, which was deleted from the statistical analysis. The mean watered shrub NDI was 0.316796 with a standard deviation of 0.098367, while the mean

control shrub NDI was 0.263625 with a standard deviation of 0.076207. The T-test of mean difference = 0 vs. not 0 gave a T-value of 3.54, so we accept the alternate hypothesis.

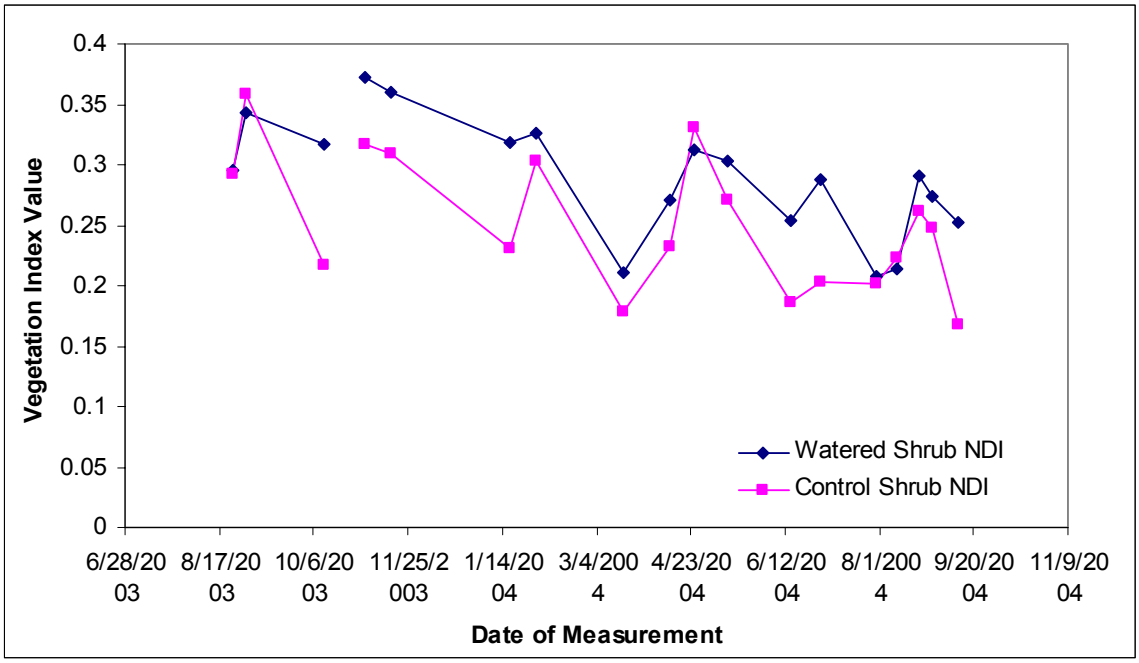

Figure 3-45: Irrigated Site Shrub NDI time series

Figure 3-46 shows the watered Site shrub MSAVI data. The MSAVI does not vary as much as the SAVI and similar indices. The mean watered shrub MSAVI was 0.498018 with a standard deviation of 0.090793, while the mean control shrub MSAVI was 0.449215 with a standard deviation of 0.085908. T-Tests of mean difference being equal to 0 vs. not 0 gave a T-value of 6.17, so we accepted the alternate hypothesis that the difference between both data sets was not 0.

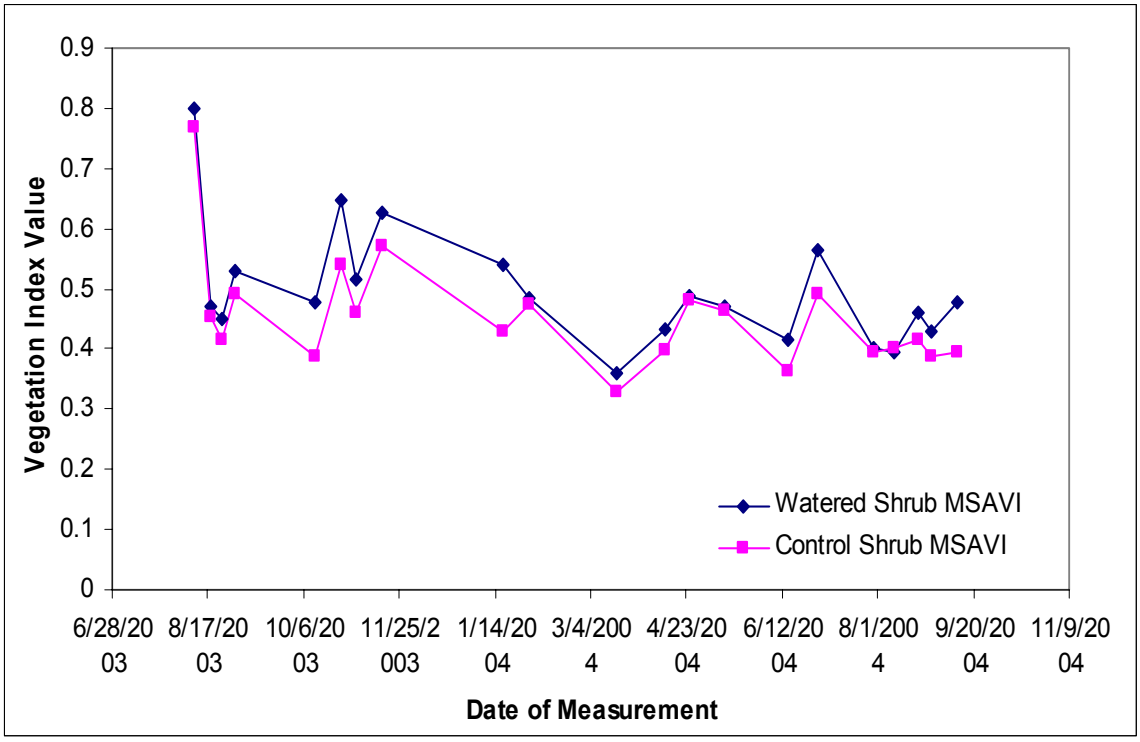

Figure 3-46: Irrigated Site Shrub MSAVI time series

3.3 Correlation between Vegetation Indices and Drought Indices

The major hypothesis of this thesis is that there is some correlation between drought conditions and vegetation index values. It is also possible that other factors such as temperature, relative humidity and vapor pressure may have had an effect on the vegetation and thus on the vegetation indices calculated. Also, the effect of drought and precipitation may be visible for a time-lag period, so time-lags from no lag to 5 weeks lag were considered in the analysis. Using Minitab 14, correlation coefficients were calculated for all indices and SPI values, along with correlation between mean temperature, mean relative humidity and mean vapor pressure to examine which vegetation index may have been affected by these meteorological variables and thus would provide a useful multi-regression analysis. The values for these meteorological variables come from the 5-Points weather station daily record. It was found that the mean

temperature had a moderately significant correlation with the rain-sheltered Site shrub SAVI and MSAVI, while the mean RH had a moderately significant correlation with the shrub and grass WBI. The vapor pressure only had a slight correlation with the grass WBI. For the watered shrub, the mean RH had a slight correlation with the NDVI and ARVI, but there were no other correlations. The correlation data used was for 2002-2003. Linear regression graphs and meteorological correlation coefficients are presented in Appendix C.

3.3.1 Rain-sheltered Site Correlation Analysis with No Time Lag

Figures 3-47 to 3-50 show the correlation coefficient of SPI vs. all 12 vegetation indices assuming no time lag between SPI and the rain-sheltered Site vegetation indices. For most of the indices, the correlation strength increases with increasing SPI timescale up to the 14-week mark and then decrease afterwards to give a bell-curved shape. This is clearly seen with the NDVI, VIN, SAVI, ARVI and MSAVI for both the grass and shrub data. The shrub RVSI followed a different trend, with a small decrease from the 1-week to 4-week SPI, and then increasing relatively steadily until the 30-week SPI. The shrub and grass RVI had a negative bell curve shape. The NDWI and WBI results for both the shrub and grass did not have any apparent significance to the SPI data, while the NDGI and NDI correlations were not significant enough to warrant further analysis. For some of the analyses, it was seen that the grass indices had a strong quadratic correlation with the SPI index. For the PDI, only the grass WBI had a significant correlation. The maximum correlations for the shrub NDVI in Figure 3-47 was with the 14-week SPI, with a coefficient of 0.818. For the grass NDVI, it was with the 17-week SPI with a coefficient of 0.726. The VIN values also had maximum correlations with the 14 and 17-week SPIs

for shrub and grass data respectively, with values of 0.848 for shrub and 0.715 for grass. The shrub SAVI had a maximum correlation at the 19-week SPI, with a value of 0.796, while the ARVI followed the NDVI and VIN in having maximum correlations with the 14-week SPI for the shrub and 17-week SPI for the grass. The values were 0.826 for the shrub and 0.734 for the grass.

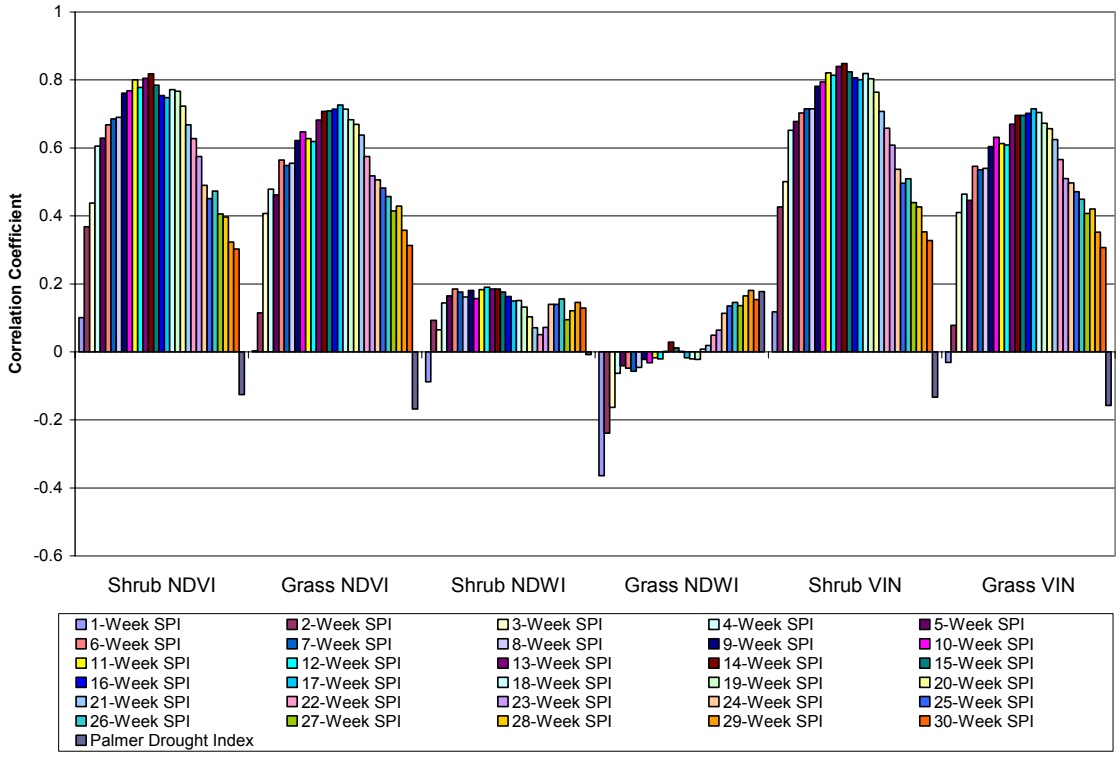

Figure 3-47: Linear correlations between SPI scales and measured NDVI, NDWI and VIN, no lag.

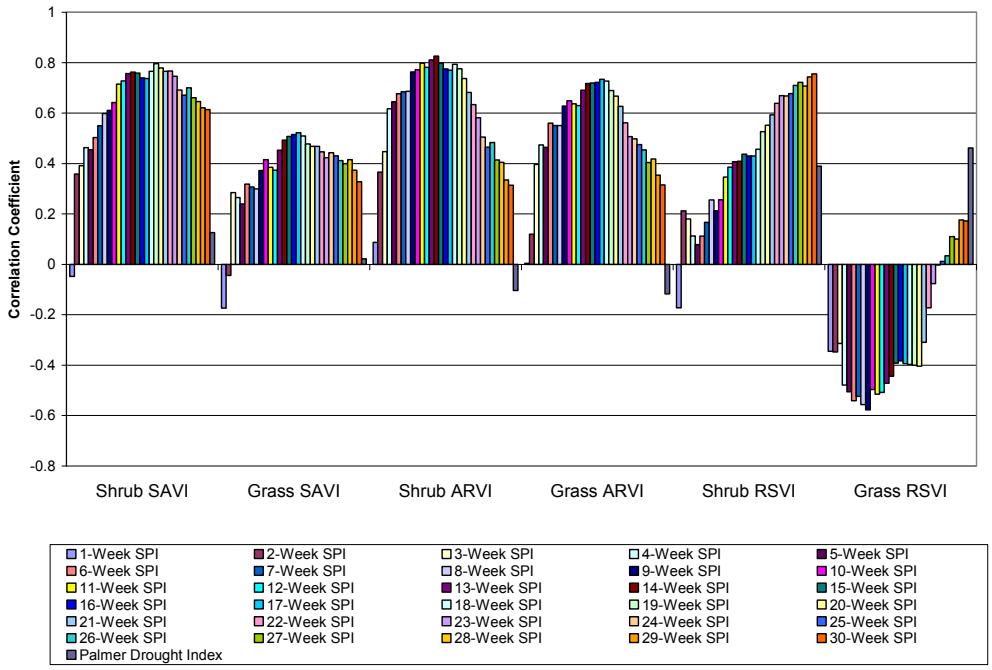

Figure 3-48: Linear correlations between SPI scales and measured SAVI, ARVI and RSVI, no lag.

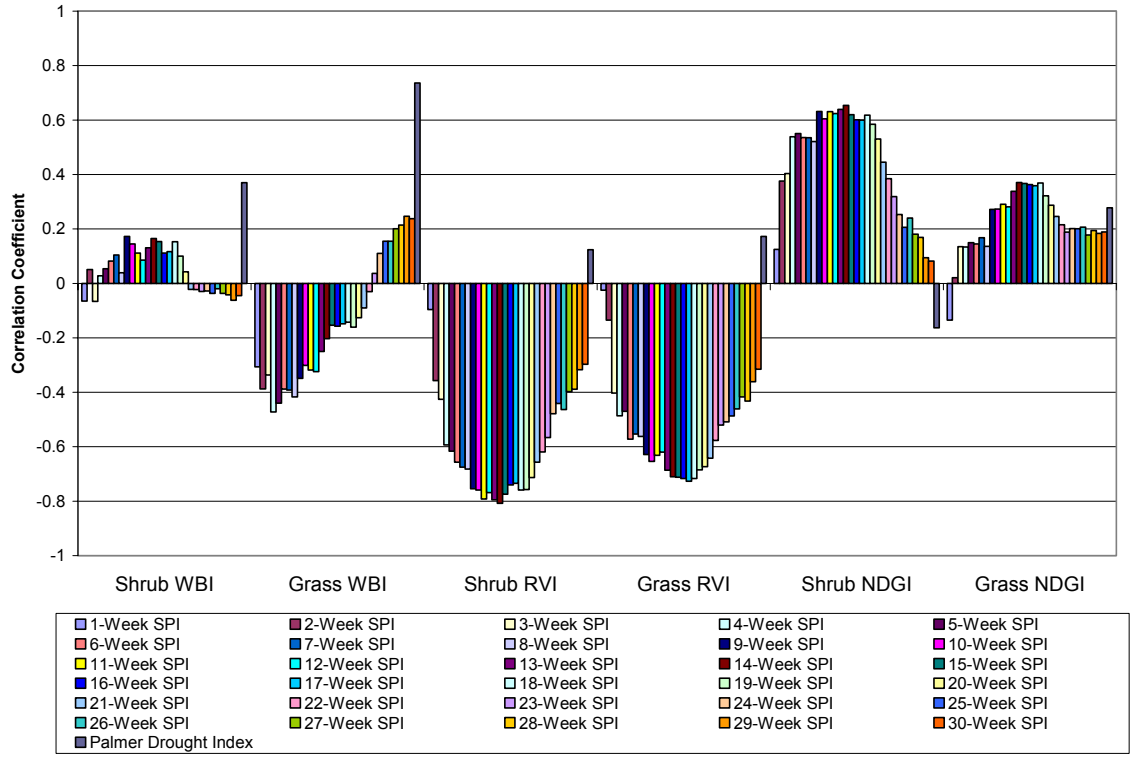

Figure 3-49: Linear correlations between SPI scales and measured WBI, RVI and NDGI, no lag.

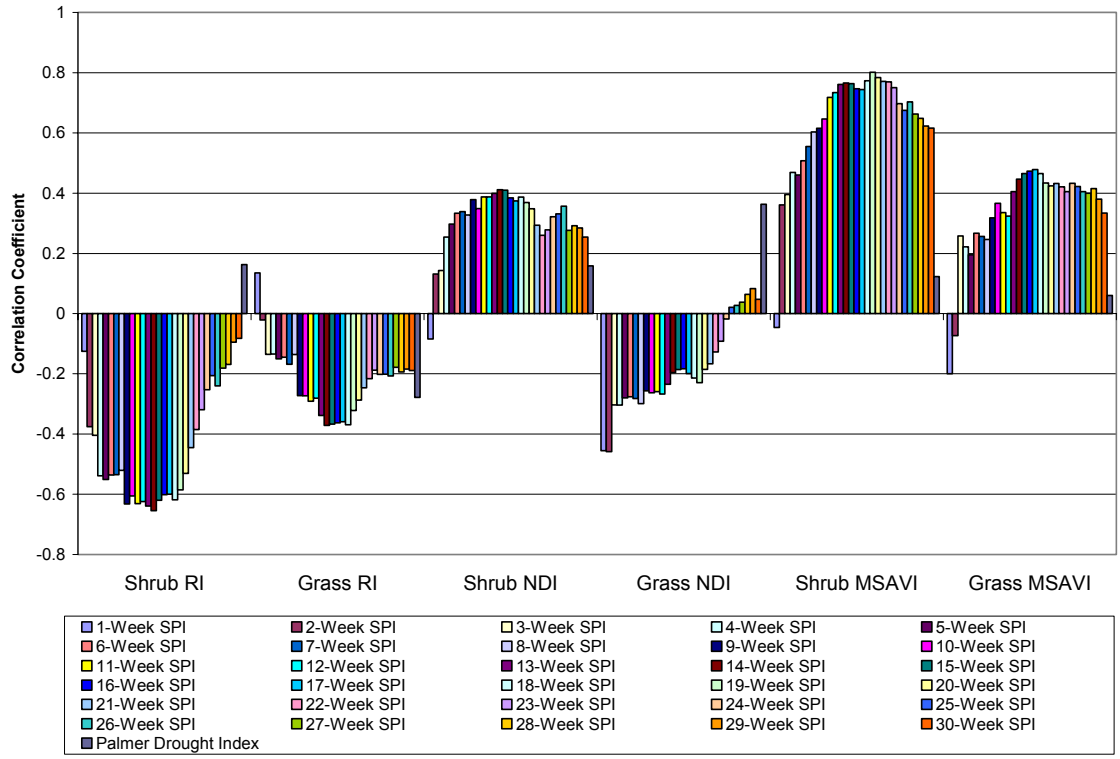

Figure 3-50: Linear correlations between SPI scales and measured NDRI, NDI and MSAVI, no lag.

From these correlation results, it is seen that the plant vegetation indices for the most part reflect the effect of precipitation up to 17 weeks preceding the current measurement, since the best correlations occur within those SPI timescales with no lag considered. Since most of the SPI data calculated by other agencies (for example, the Colorado Drought Center) is calculated on a monthly scale, the 12-week (3-month) SPI was chosen as a reference SPI for use in satellite image analysis as shown in chapter 4. The 12-week SPI was significant for most of the correlations with NDVI measurements, with a correlation coefficient of 0.778 with the shrub NDVI and a correlation coefficient of 0.609 with the grass NDVI. The better correlations with other SPI timescales and shrub vegetation index data are probably due to higher temporal resolution.

3.3.2 Rain-sheltered Site Correlation Analysis with One Week Lag

Figures 3-51 to 3-54 show the correlation coefficient of SPI vs. all 12 vegetation indices assuming a one-week time lag between SPI and the rain-sheltered Site vegetation indices. If we examine the maximum correlation coefficients for most of the vegetation indices with one week's lag, we see that they occur with the SPI timescale that is one week less than the maximum correlation value with no time lag. For example, the maximum NDVI correlation occurs with the 13-week SPI, instead of the 14-week SPI. The trends are similar to the no-lag correlation trends.

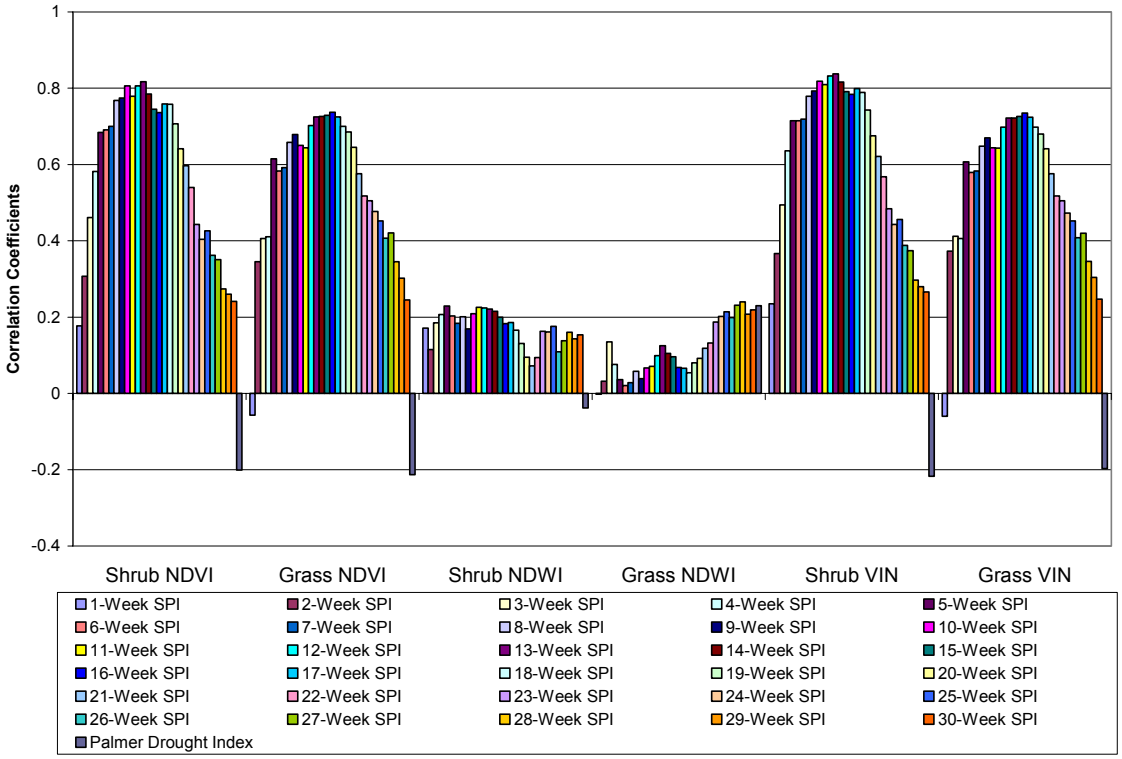

Figure 3-51: Linear Correlations between SPI scales and NDVI, NDWI and VIN, one week lag.

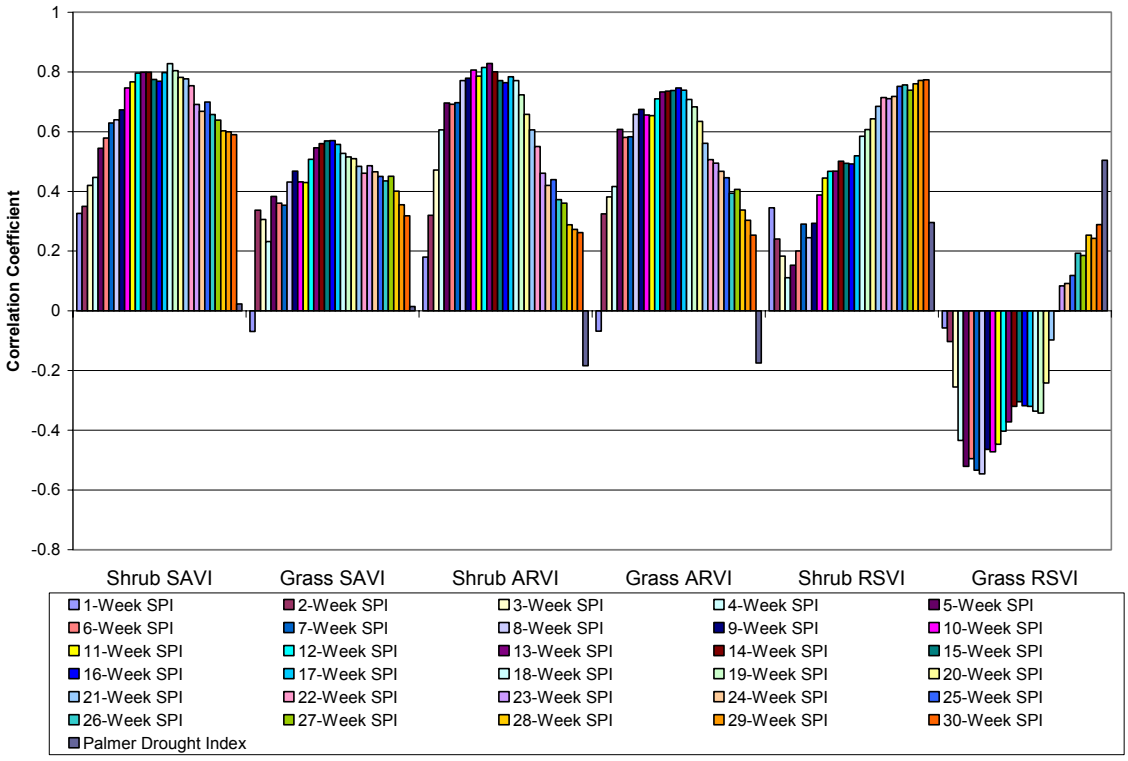

Figure 3-52: Linear Correlations between SPI scales and SAVI, ARVI and RSVI, one week lag.

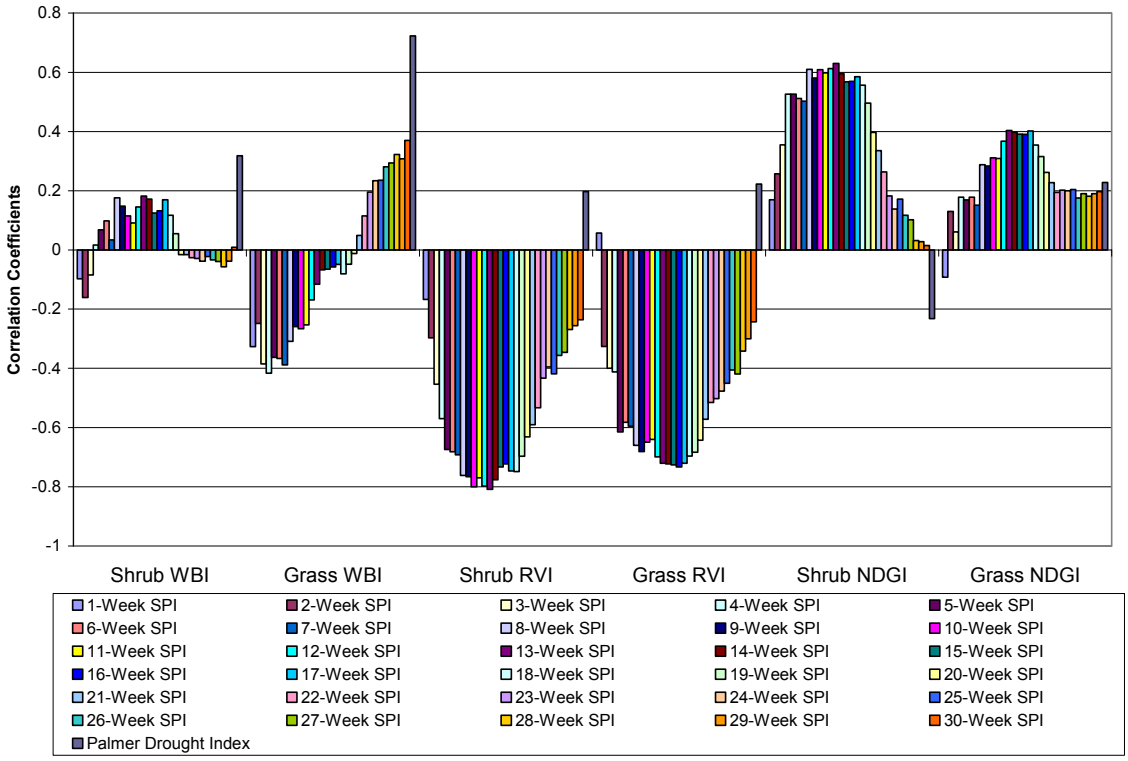

Figure 3-53: Linear Correlations between SPI scales and WBI, RVI and NDGI, one week lag.

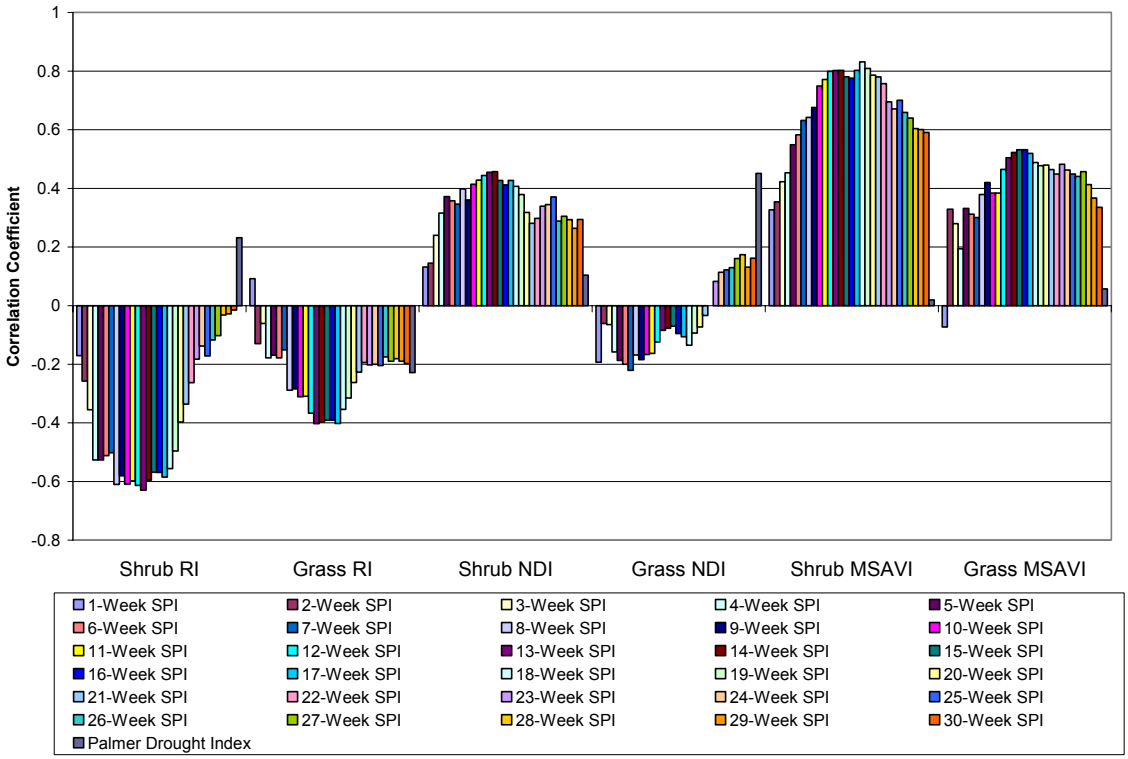

Figure 3-54: Linear Correlations between SPI scales and NDRI, NDI and MSAVI, one week lag

3.3.3 Rain-sheltered Site Correlation Analysis with Two Weeks Lag

Figures 3-55 to 3-58 show the correlation coefficient of SPI vs. all 12 vegetation indices assuming a two-week time lag between SPI and the rain-sheltered Site vegetation indices. The shift in maximum correlation timescales continues with the two week lag as seen in Figures 3-72 through 3-75. While the best correlations for the NDVI-based indices is with the 9-week SPI for the shrub, the 13-week SPI and similar scales are almost as high. The grass NDVI still has its highest correlation at the 15-week SPI scale, just two weeks less than the 17-week SPI of the no-lag measurements.

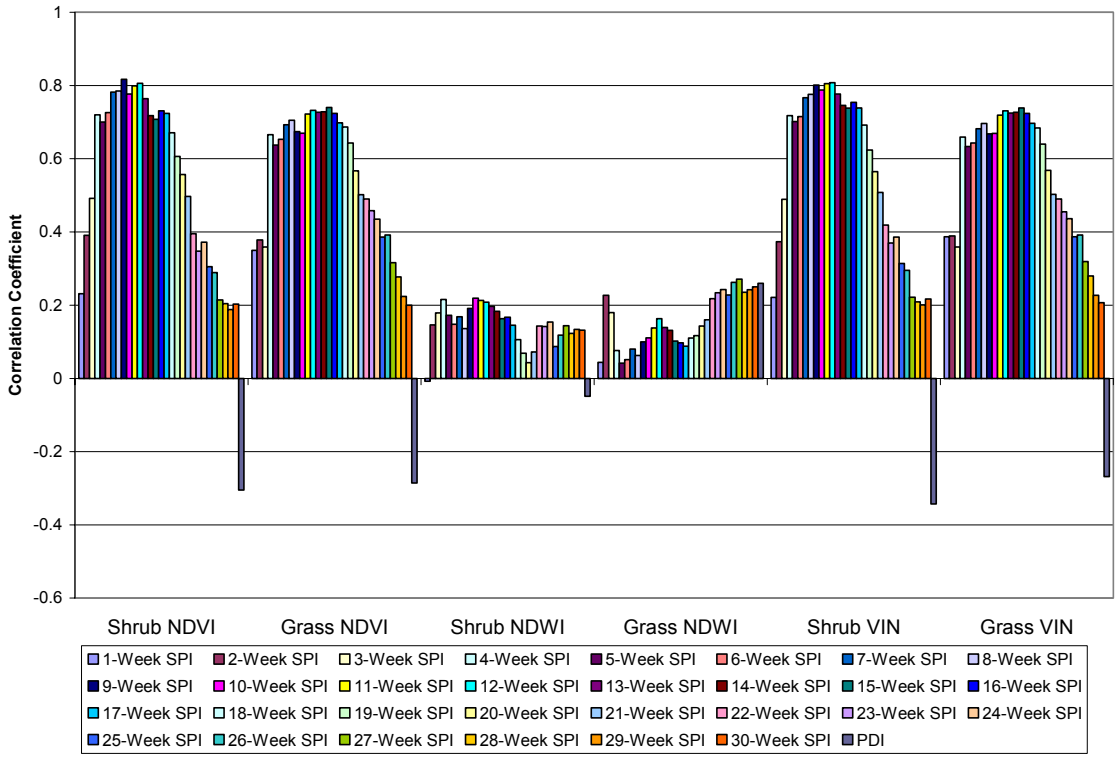

Figure 3-55: Linear Correlations between SPI scales and NDVI, NDWI and VIN, two weeks lag.

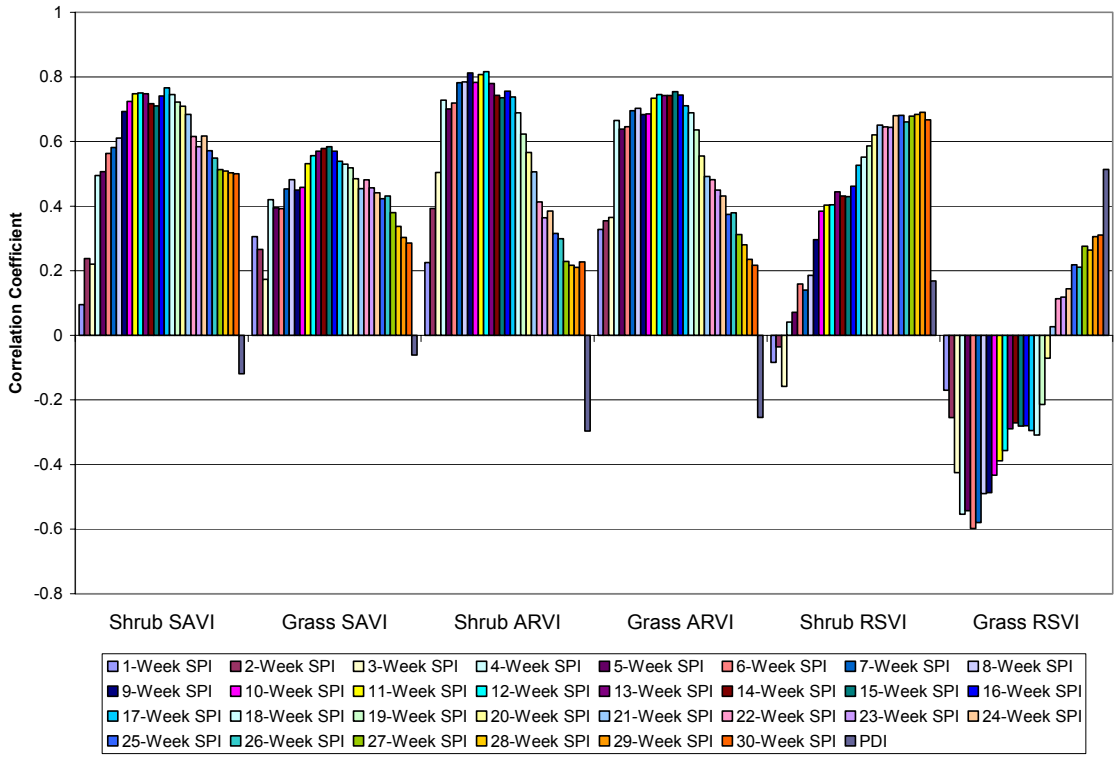

Figure 3-56: Linear Correlations between SPI scales and SAVI, ARVI and RSVI, two weeks lag.

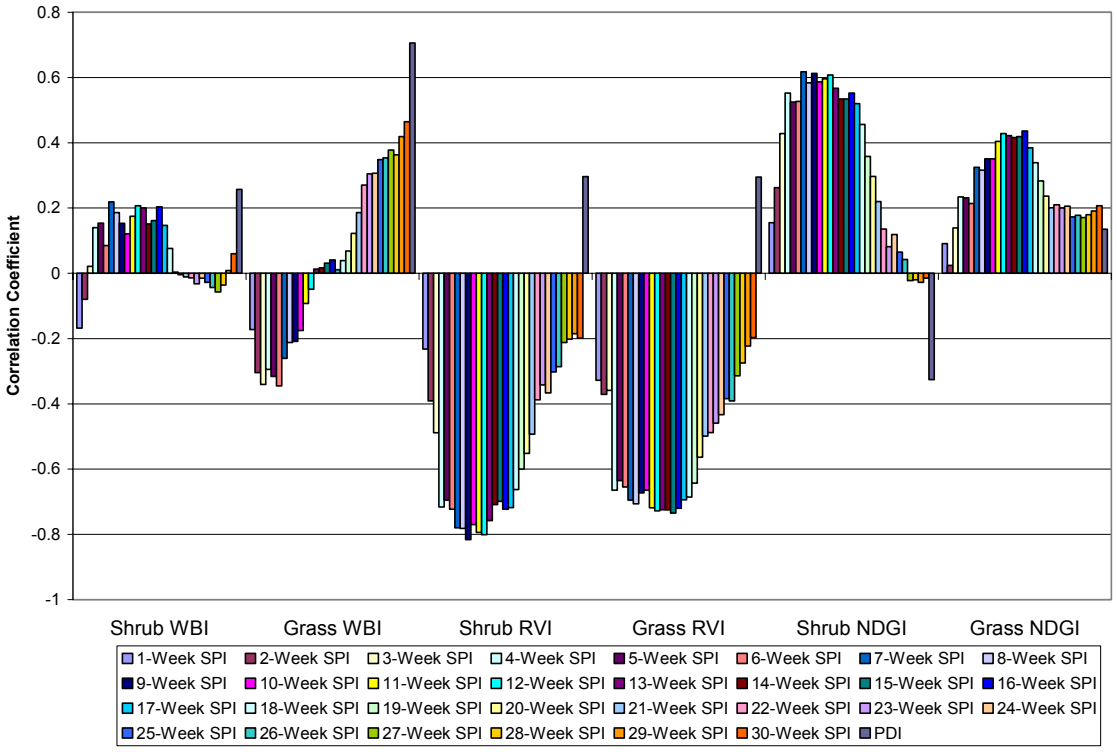

Figure 3-57: Linear Correlations between SPI scales and WBI, RVI and NDGI, two weeks lag.

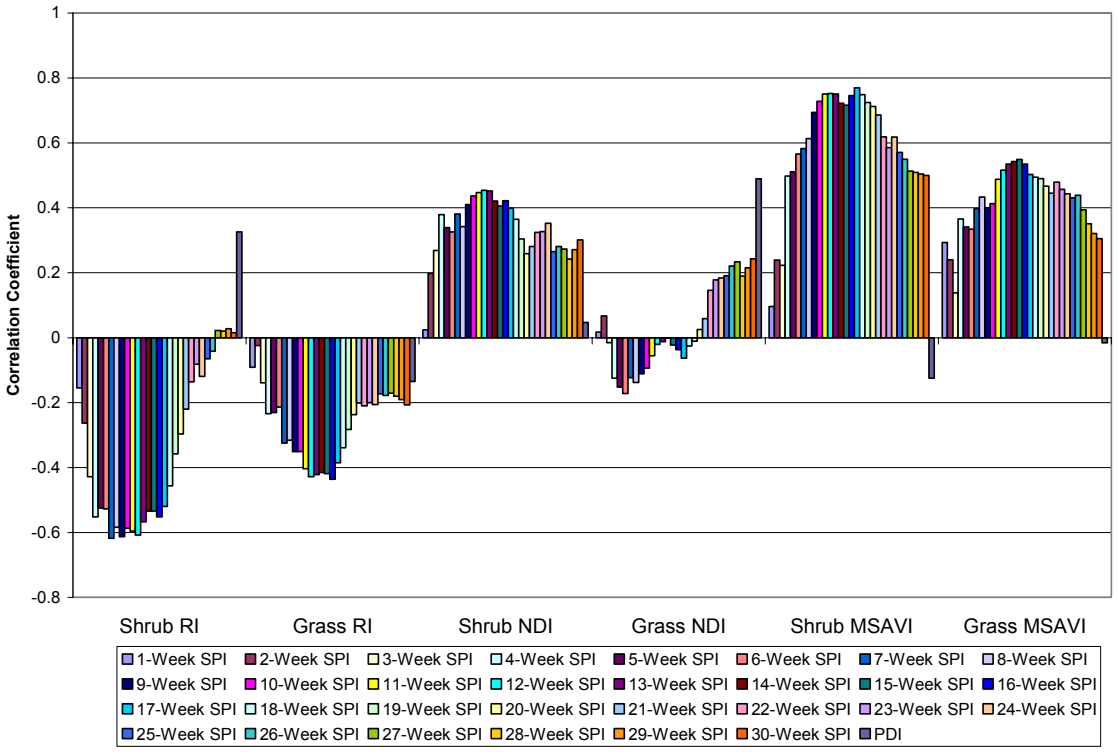

Figure 3-58: Linear Correlations between SPI scales and NDRI, NDI and MSAVI, two weeks lag.

3.3.4 Rain-sheltered Site Regression Analysis with Three Weeks Lag

Figures 3-59 to 3-62 show the correlation coefficients of SPI vs. all 12 vegetation indices assuming a three-week time lag between SPI and the rain-sheltered Site vegetation indices. The highest shrub correlations for the NDVI and ARVI are with the 8-week and 11-week scales, still showing a response to an increase in lag by shifting with a given lag-increase. In general, most of the bell-curve trends seen are now becoming more left-skewed in their distribution, while the RSVI is showing declines in the higher SPI scale values compared to its shape with no time lag. The grass data had a stronger correlation with the NDVI and similar indices at this lag interval, when compared to the other lag intervals.

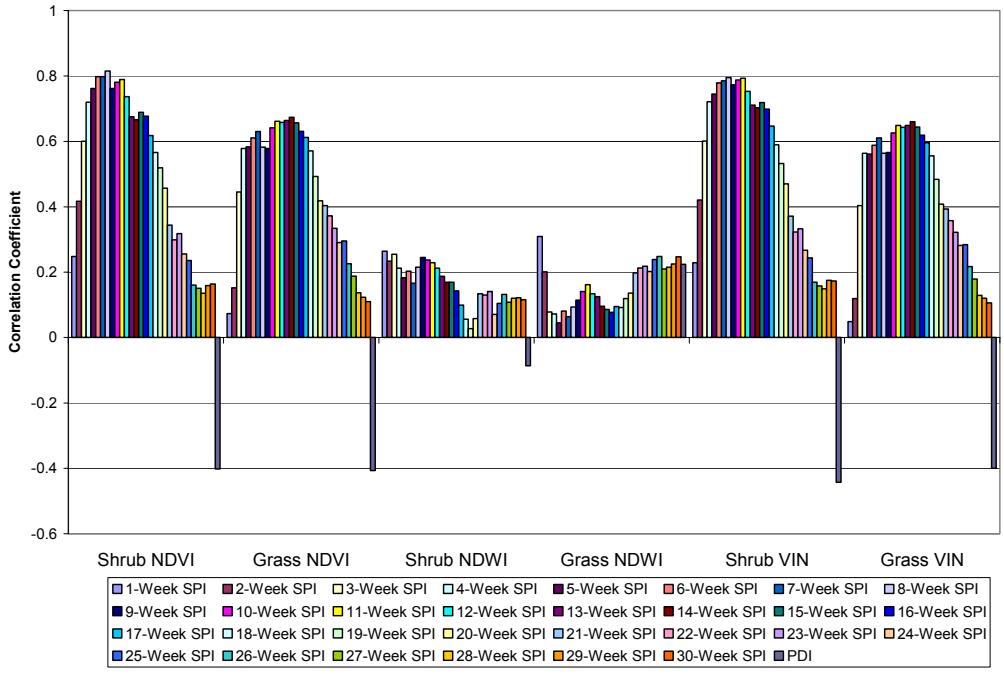

Figure 3-59: Linear Correlation coefficients between various SPI scales and NDVI, NDWI and VIN, three weeks lag.

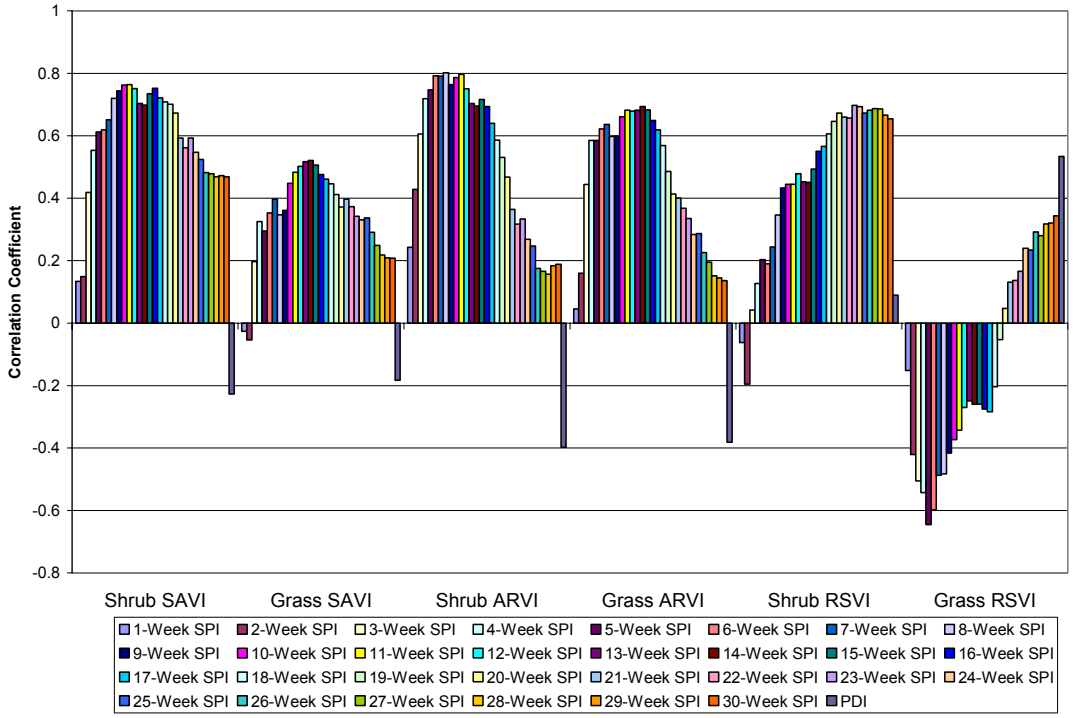

Figure 3-60: Linear correlation coefficients between various SPI scales and SAVI, ARVI and RSVI, three weeks lag.

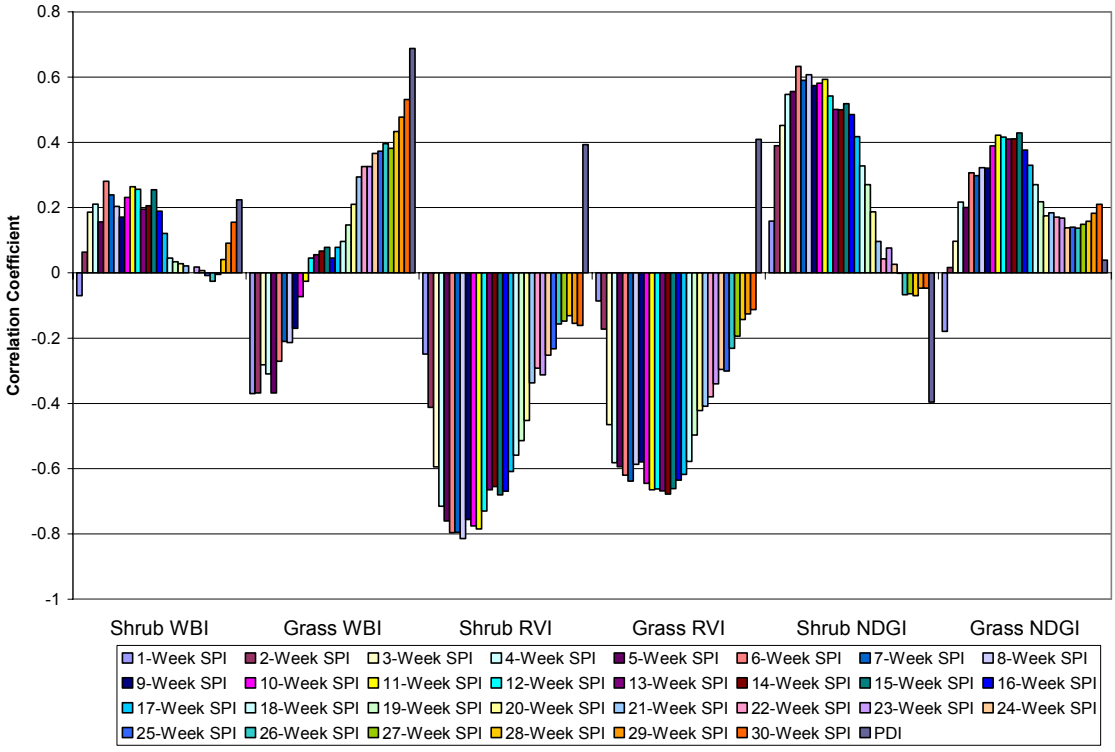

Figure 3-61: Linear correlation coefficients between various SPI scales and WBI, RVI and NDGI, three weeks lag.

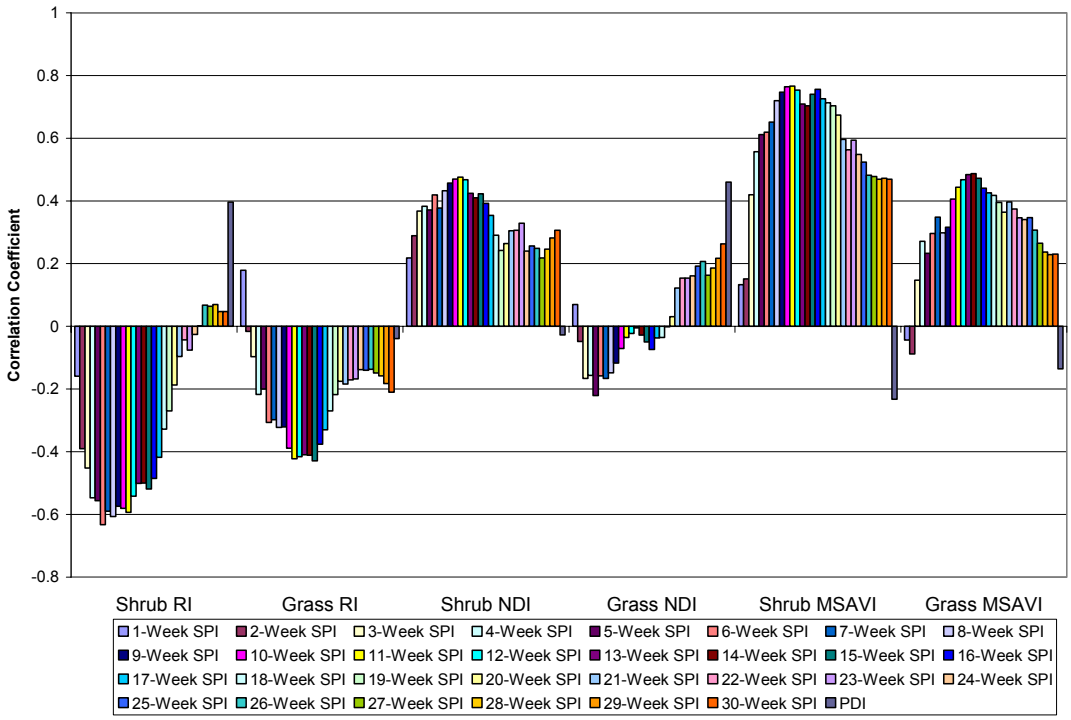

Figure 3-62: Linear correlation coefficients between various vegetation indices and NDRI, NDI and MSAVI, three weeks lag.

3.3.5 Rain-sheltered Site Regression Analysis with Four Weeks Lag

Figures 3-63 to 3-66 show the correlation coefficient of SPI vs. all 12 vegetation indices assuming a four-week time lag between SPI and the rain-sheltered Site vegetation indices. The most significant correlation occurs with the 5-week SPI for most shrub indices and the 13-week SPI for most grass indices. Also, the left-skew trend from the previous lag-time continues when examining the overall shape of the coefficient histograms.

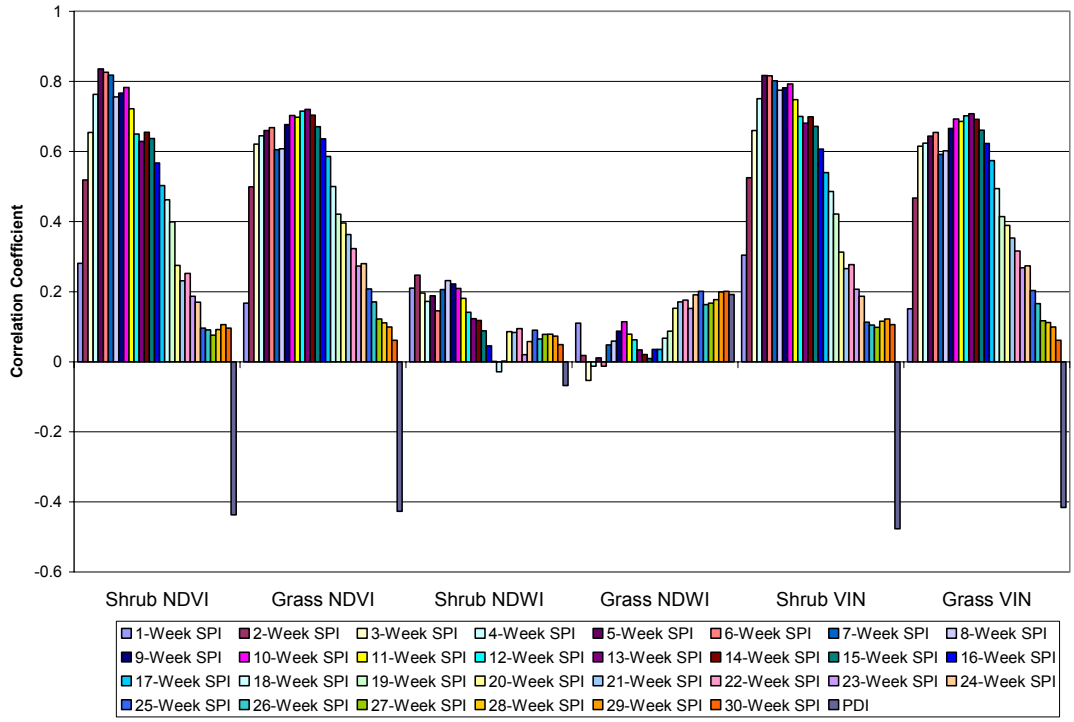

Figure 3-63: Linear correlation coefficients of SPI and NDVI, NDWI and VIN, four week lag.

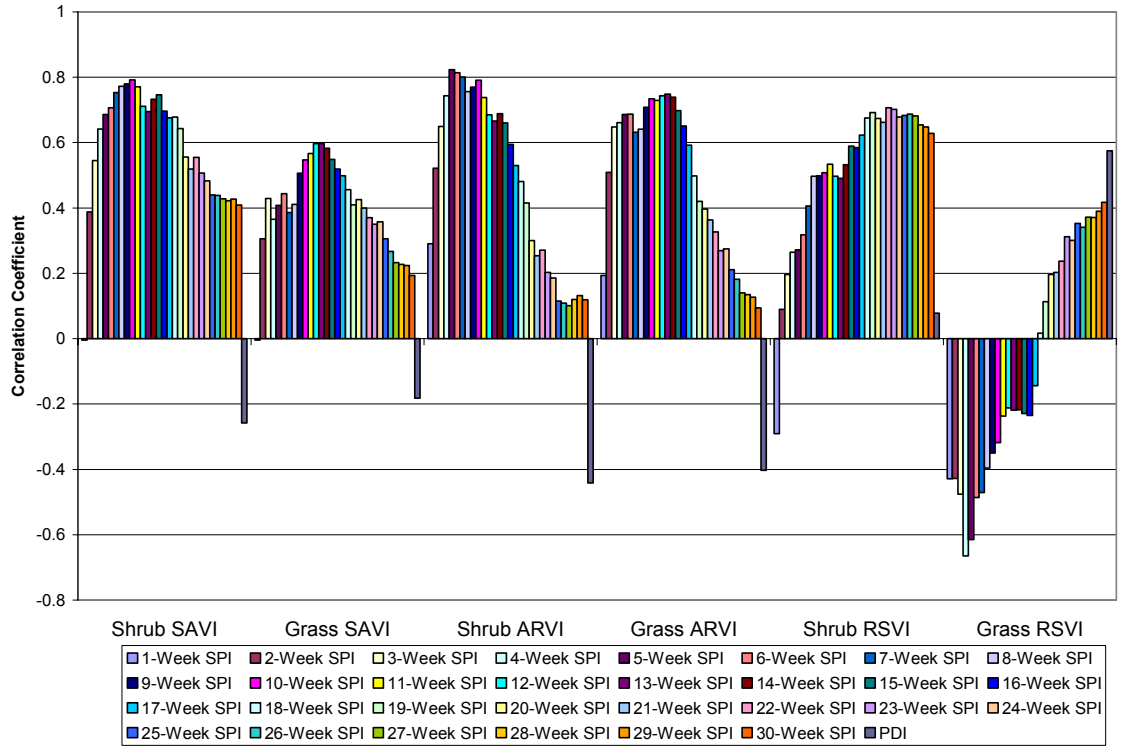

Figure 3-64: Linear correlation coefficients of SPI and SAVI, ARVI and RSVI, four week lag.

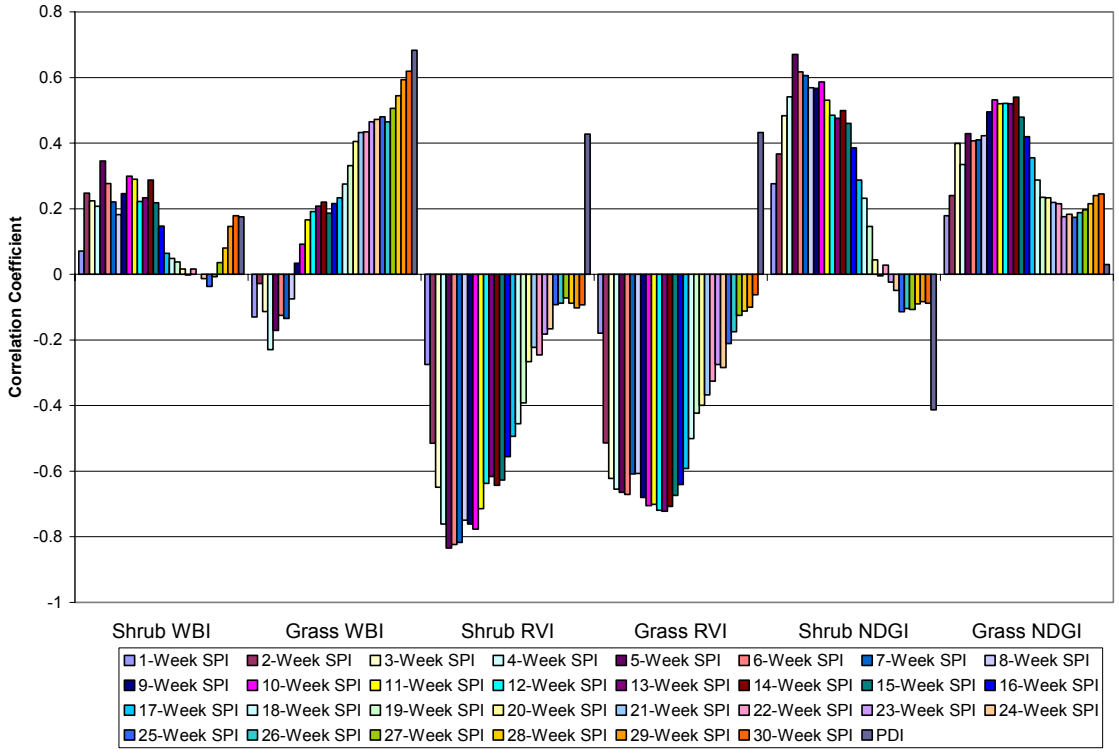

Figure 3-65: Linear correlation coefficients between SPI and WBI, RVI and NDGI, four week lag.

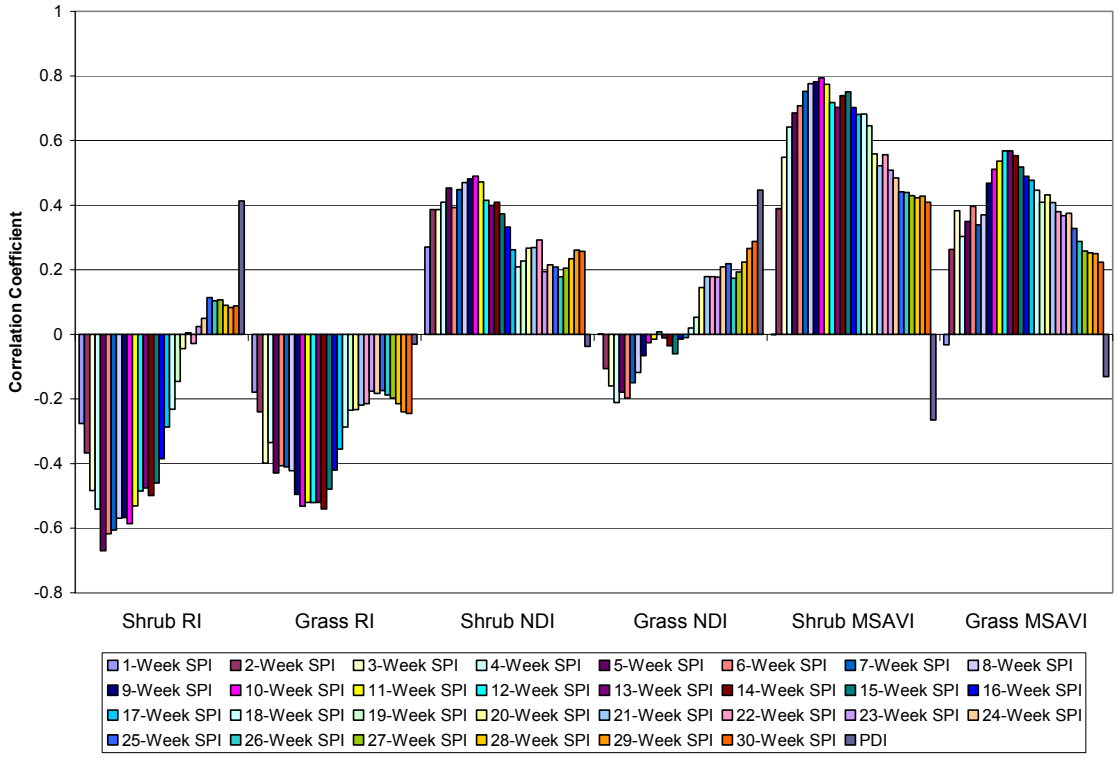

Figure 3-66: Linear correlation coefficients between SPI and NDRI, NDI and MSAVI, four week lag.

3.3.6 Rain-sheltered Site Regression Analysis with Five Weeks Lag

Figures 3-67 to 3-70 show the correlation coefficient of SPI vs. all 12 vegetation indices assuming a five-week time lag between SPI and the rain-sheltered Site vegetation indices. The most significant correlations for the NDVI and similar indices were with the 5-week SPI, and correlations began to decrease after about the 10-week period. For the previous lag periods, significant correlations did not begin appearing until the 4-week SPI time scale, so the SPI time scale correlation with vegetation indices has a significant response to lag time. However, this can be interpreted as a result of the amount of precipitation received by this region over the time considered, instead of just a function of the time lag. This can be seen more clearly when we investigate the watered Site data.

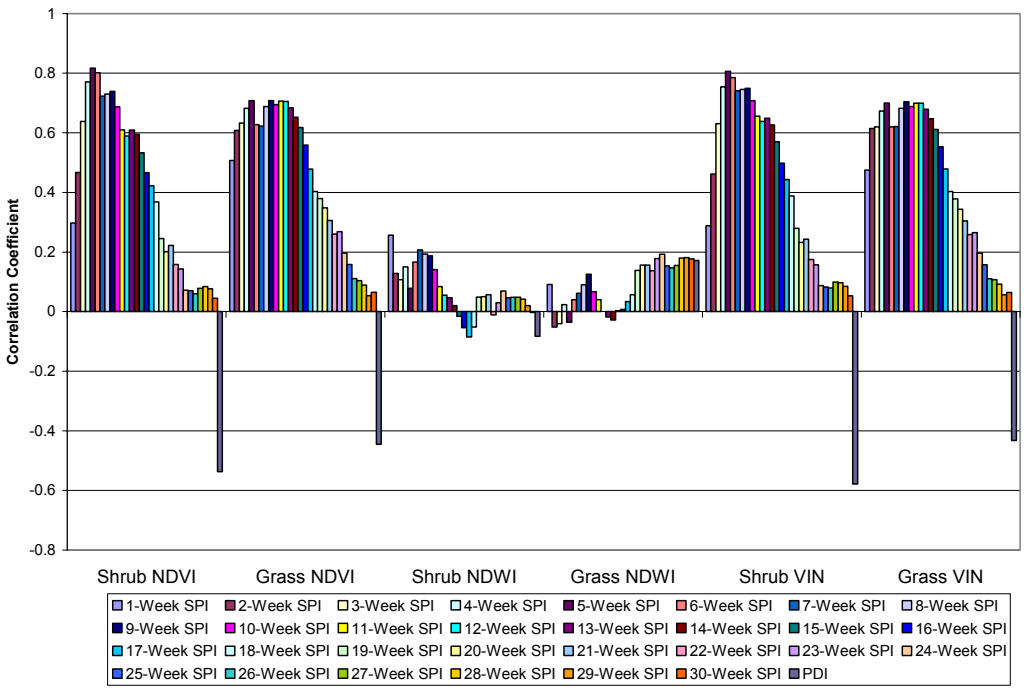

Figure 3-67: Linear correlation coefficients between SPI and NDVI, NDWI and VIN, five weeks lag.

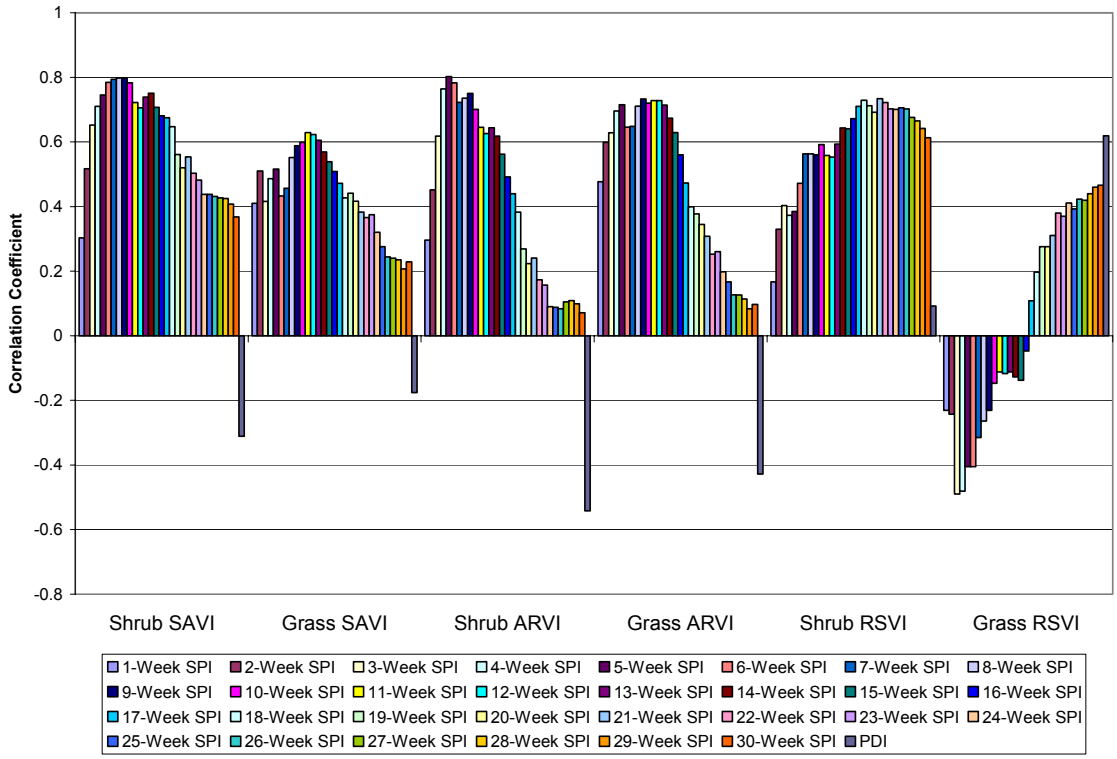

Figure 3-68: Linear correlation coefficients between SPI and SAVI, ARVI and RSVI, five weeks lag

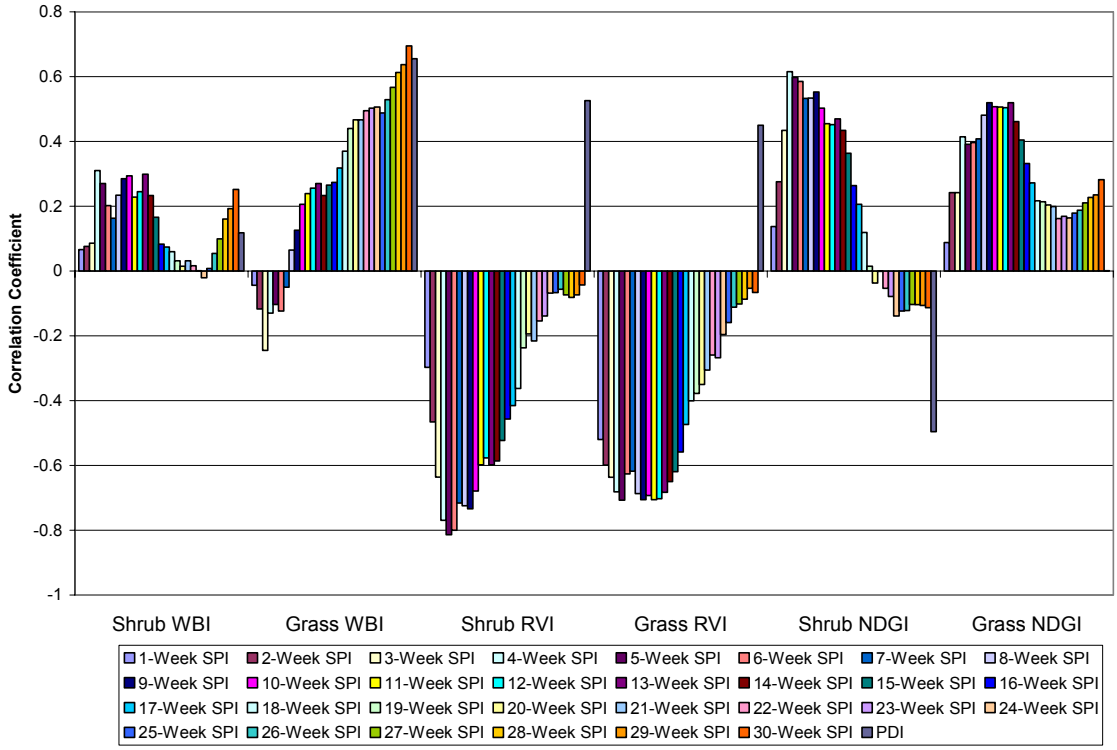

Figure 3-69: Linear correlation coefficients between SPI and WBI, RVI and NDGI, five weeks lag.

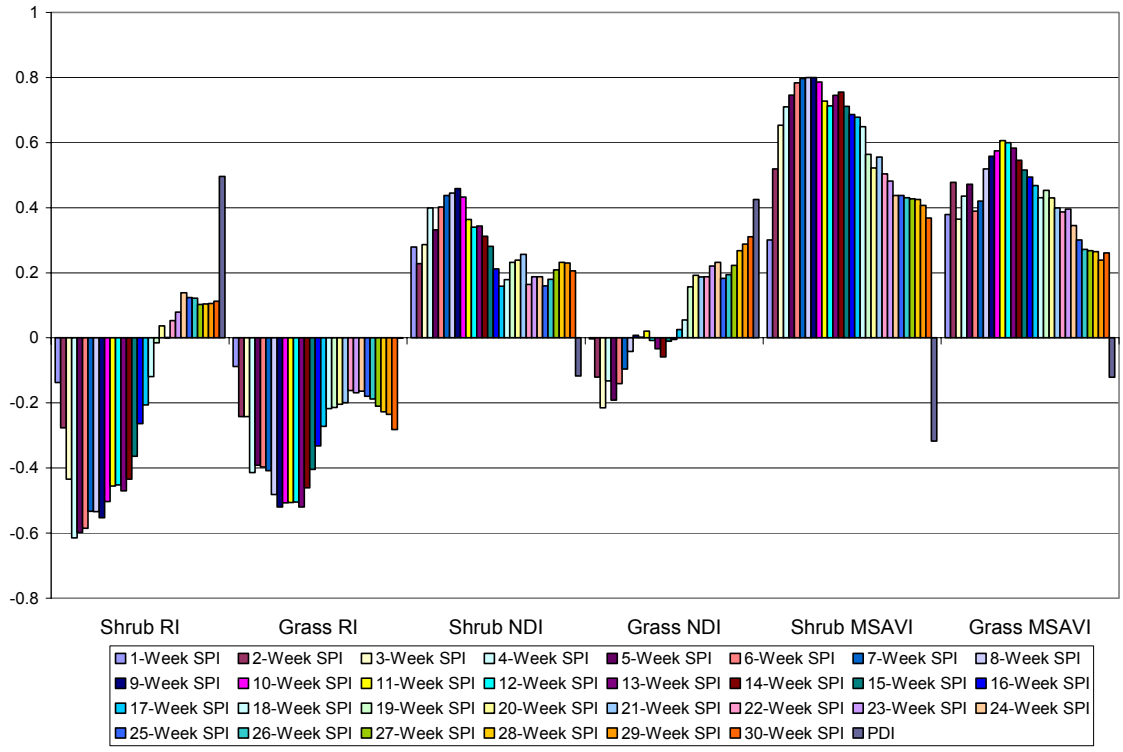

Figure 3-70: Linear correlation between SPI and NDRI, NDI and MSAVI, five weeks lag.

3.3.7 Irrigated Site Regression Analysis with no lag

The watered Site SPI was calculated by adding the simulated rainfall total as described in chapter 2 to the actual rainfall as recorded at the 5 Points weather station. Figures 3-71 and 3-72 show the correlation coefficient of SPI vs. all 12 vegetation indices assuming no time lag between SPI and the irrigated Site vegetation indices. Compared to the correlations shown at the control Site, the values here are highest in the shorter SPI time scales. The maximum correlation for the NDVI and most of the other indices occurs at the 4-week SPI mark and then decreases in significance from there, with negative correlations occurring after the 20-week period for most of the vegetation indices. The exception is the RSVI, which has mostly negative correlations after the 1-week SPI measurement. This is in stark contrast to the rain-sheltered Site no-lag results, where the highest correlations were at the mid-range SPI scales. None of the negative correlation

coefficients in Figures 3-110 and 3-111 are statistically significant, and the trend most likely does not have any real-world significance. Linear regressions of the most significant correlations are presented in Appendix C.

3.3.8 Irrigated Site Regression Analysis with one week lag

Figures 3-73 and 3-74 show the correlation coefficient of SPI vs. all 12 vegetation indices assuming a one-week time lag between SPI and the irrigated Site vegetation indices. The only significant correlations for most of the indices with a one-week lag occur in the two-week and three-week SPI timescales. The trend of decreasing and increasing correlations as the SPI timescale increases is also shown here, but as with the no-lag SPI the values are not statistically significant and most likely do not have any real-world significance.

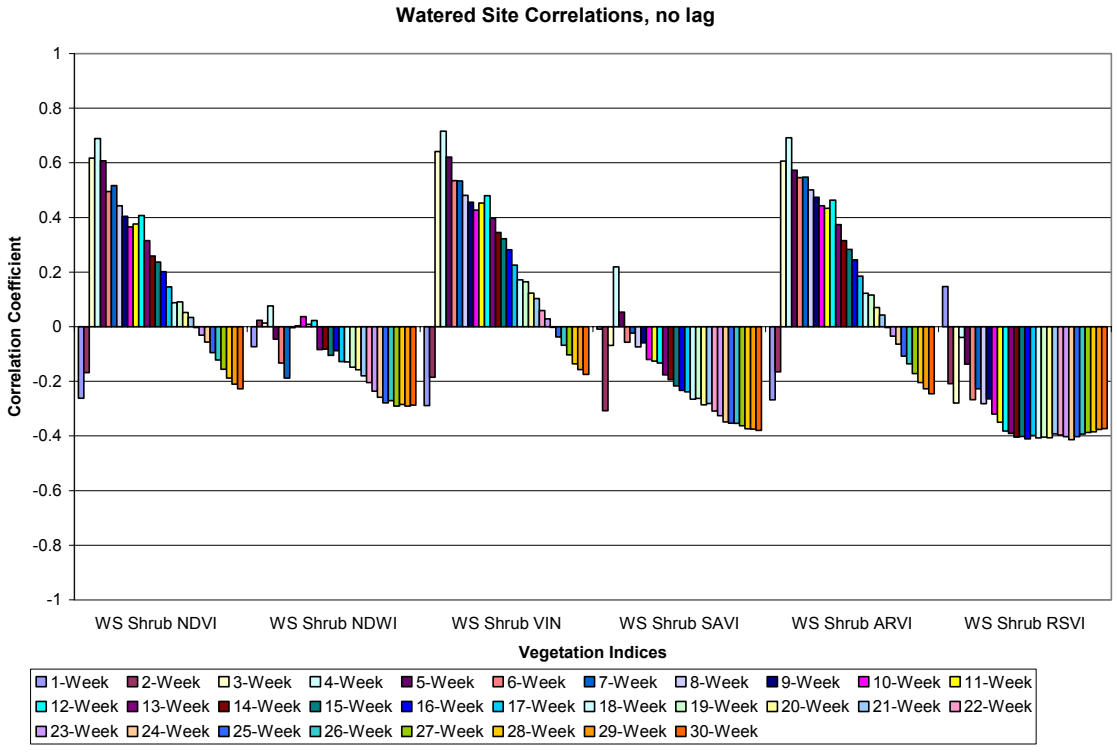

Figure 3-71: Linear Correlation graphs of various SPI scales vs. various vegetation index values for the irrigated Site, no lag.

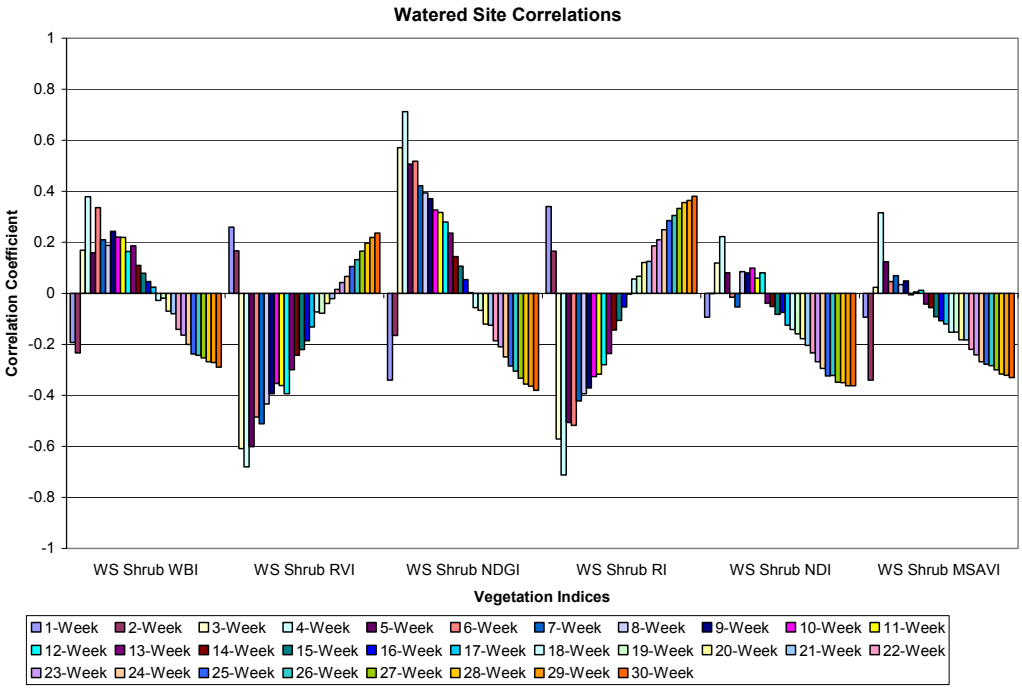

Figure 3-72: Linear Correlation graph of SPI vs. vegetation indices for the irrigated Site, no lag

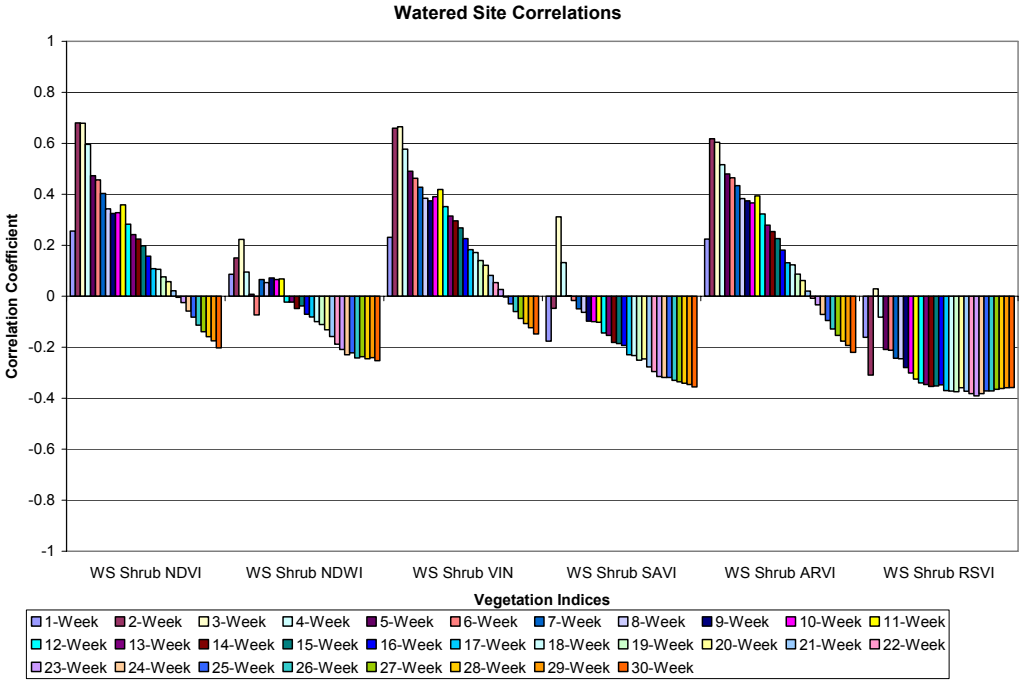

Figure 3-73: Linear Correlation coefficients between various SPI scales and vegetation indices, one week lag.

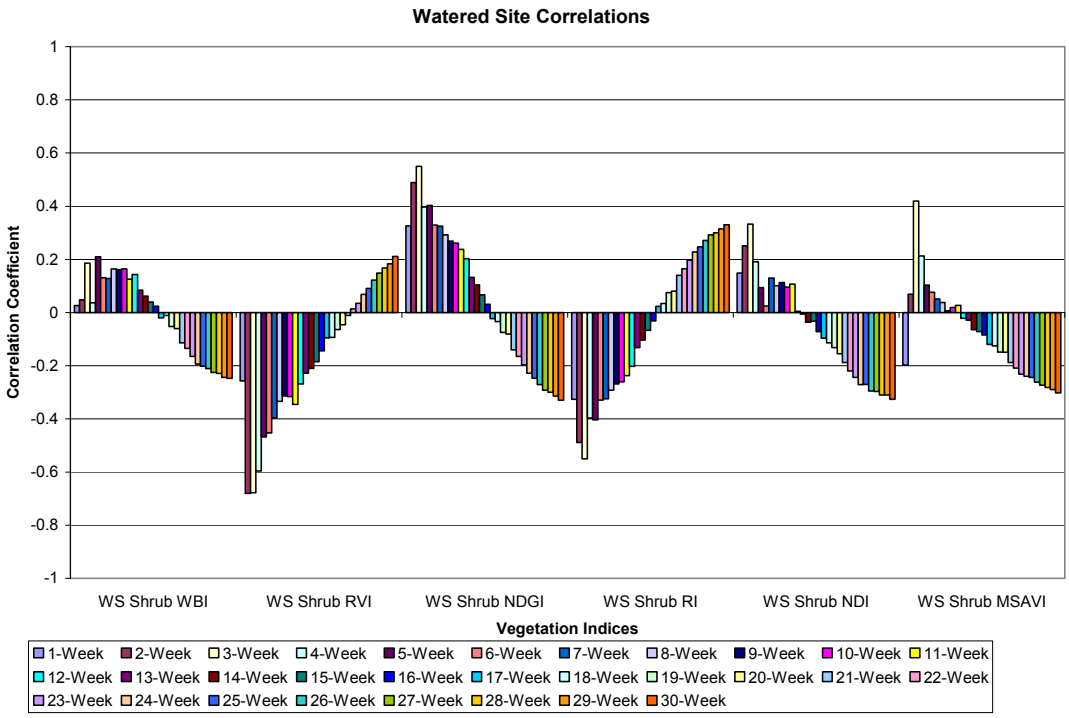

Figure 3-74: Linear Correlation coefficients between various SPI scales and vegetation indices, one week lag

3.3.9 Irrigated Site Regression Analysis with two week lag

Figures 3-75 and 3-76 show the correlation coefficient of SPI vs. all 12 vegetation indices assuming a two-week time lag between SPI and the irrigated Site vegetation indices. The values here are much lower than before for most of the indices, and no significant correlations occur after the 3-week SPI for any of the vegetation indices. The trend of steadily decreasing correlations with increasing SPI timescale continues as well (and steadily increasing for the RVI and NDRI).

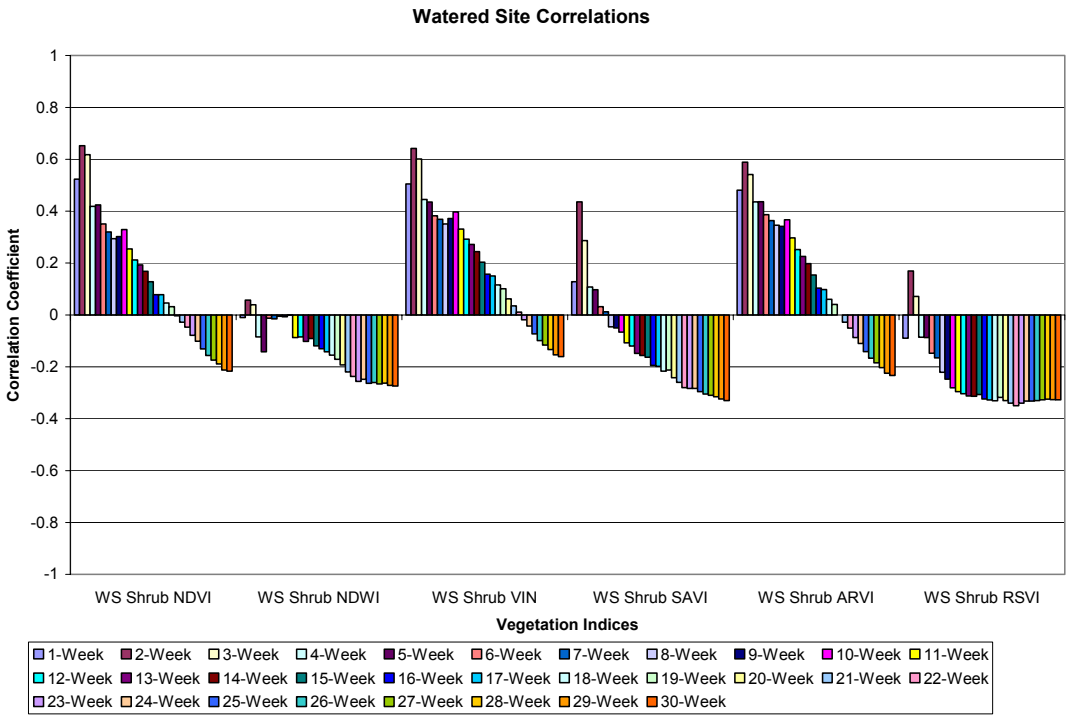

Figure 3-75: Linear correlations between SPI and NDVI, NDWI, VIN, SAVI, ARVI and RSVI, two weeks lag

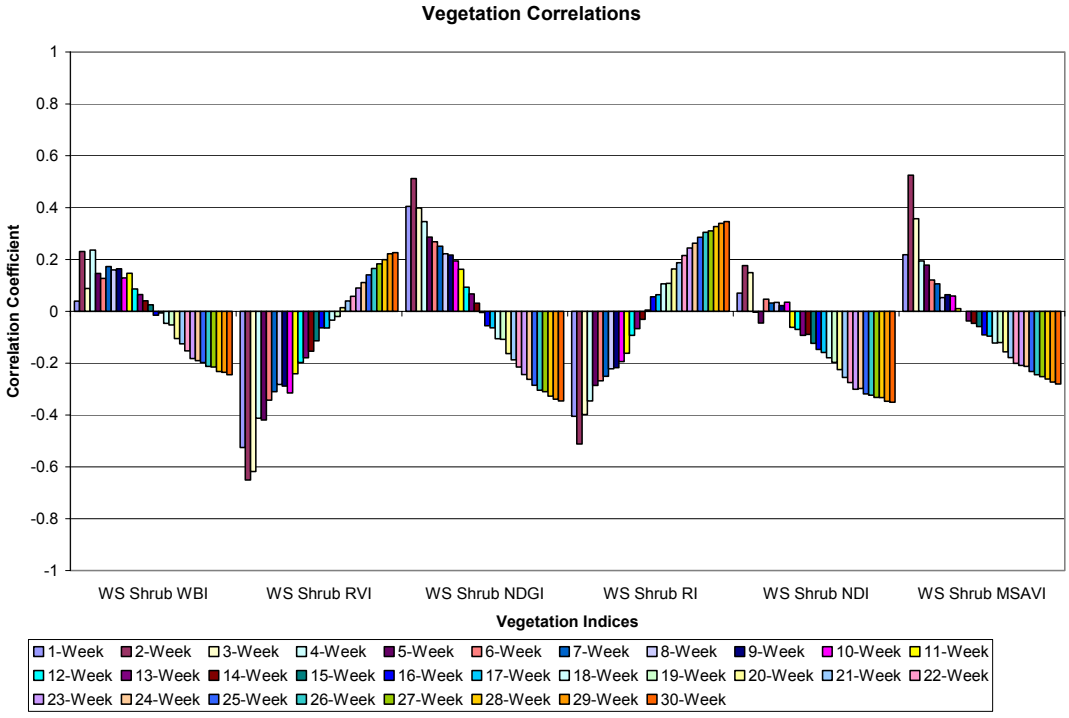

Figure 3-76: Linear correlations between SPI and WBI, RVI, NDGI, NDRI, NDI and MSAVI, two weeks lag.

3.3.10 Irrigated Site Regression Analysis with three week lag

Figures 3-77 and 3-78 show the correlation coefficient of SPI vs. all 12 vegetation indices assuming a three-week time lag between SPI and the irrigated Site vegetation indices. The main significant correlation for the NDVI and similar indices is with the one-week SPI; there is a huge drop after this measurement and most of the other correlations are negative and insignificant statistically. The NDGI is the main exception to this rule, as it steadily increases to a negative correlation of -0.4 which is barely within the statistical significance limit.

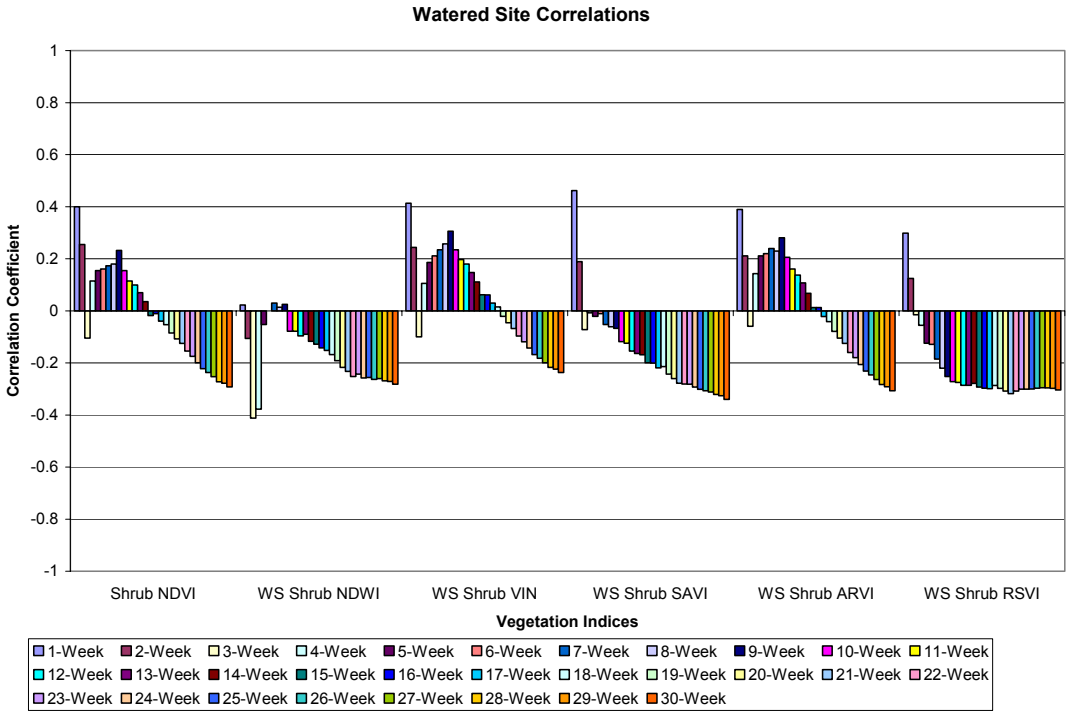

Figure 3-77: Linear correlation coefficients between SPI and NDVI, NDWI, VIN, SAVI, ARVI and RSVI, watered Site, three weeks lag.

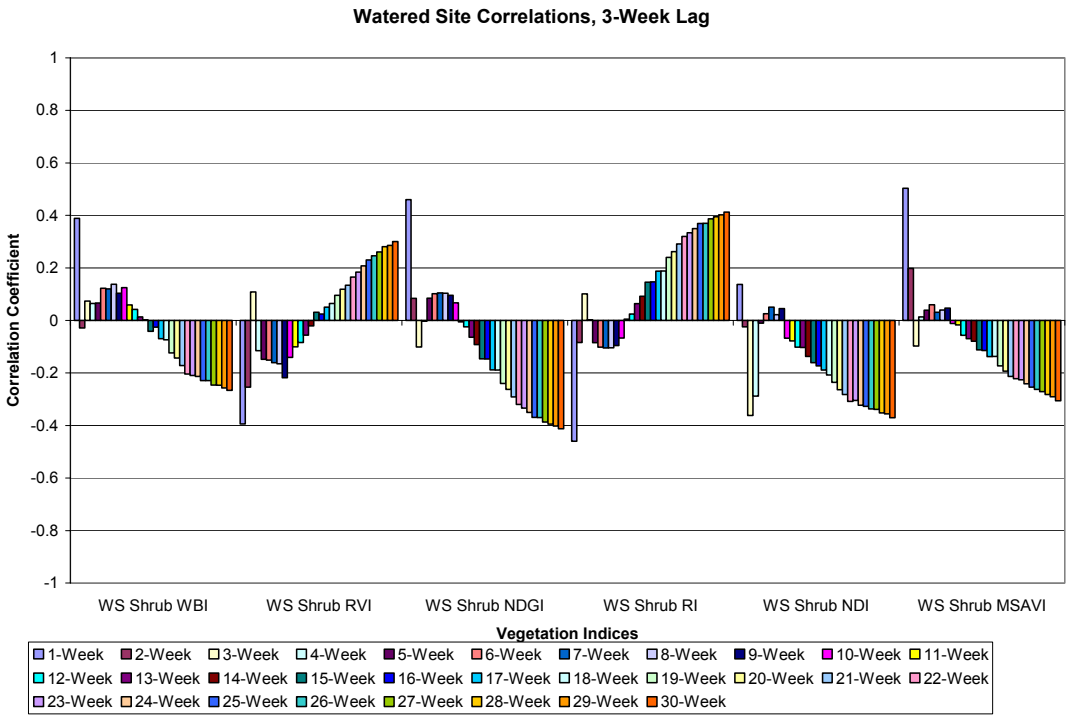

Figure 3-78: Linear correlation coefficients between SPI and WBI, RVI, NDGI, NDRI, NDI and MSAVI, watered Site, three weeks lag.

3.3.11 Irrigated Site Regression Analysis with four weeks lag

Figures 3-79 to 3-80 show the correlation coefficient of SPI vs. all 12 vegetation indices assuming a four-week time lag between SPI and the Irrigated Site vegetation indices. The significant correlations in the four week lag measurements are negative correlations, but this is most likely a statistical result rather than an actual response.

3.3.12 Irrigated Site Regression Analysis with five week lag

Figures 3-124 to 3-125 show the correlation coefficient of SPI vs. all 12 vegetation indices assuming a five-week time lag between SPI and the Irrigated Site vegetation indices. The results here are very similar to those stated in the four week lag results, with the only significant correlations being negative ones (except for the NDRI and RVI). These most likely have no significant real-world cause or explanation.

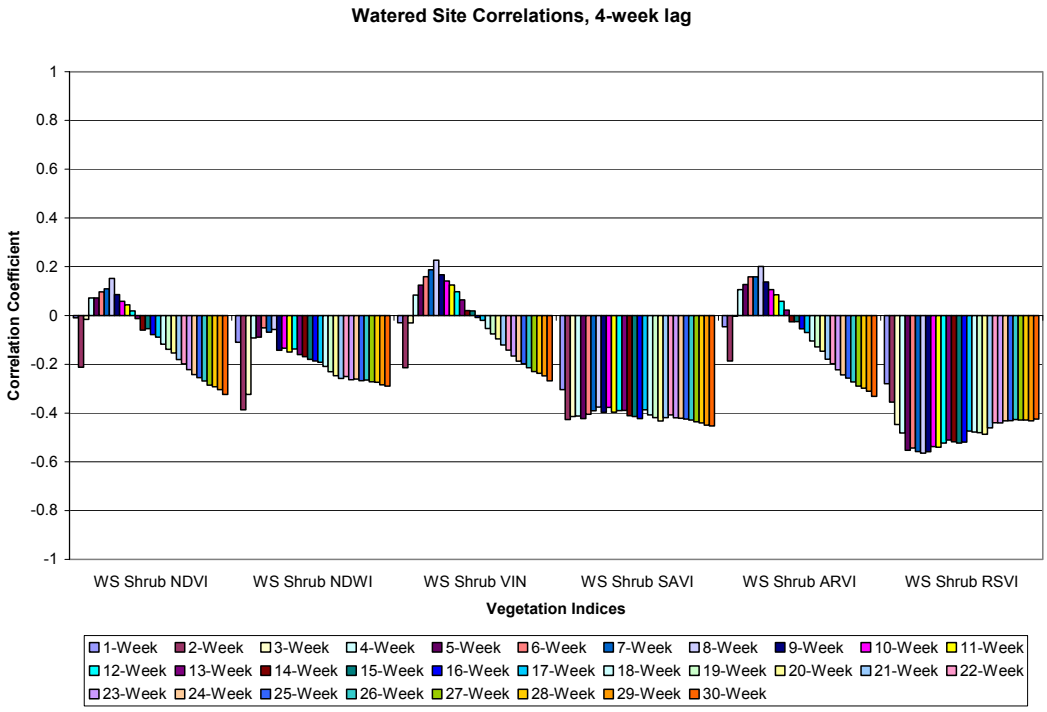

Figure 3-79: Linear correlation coefficients between SPI and NDVI, NDWI, VIN, SAVI, ARVI and RSVI, Irrigated Site, four weeks lag.

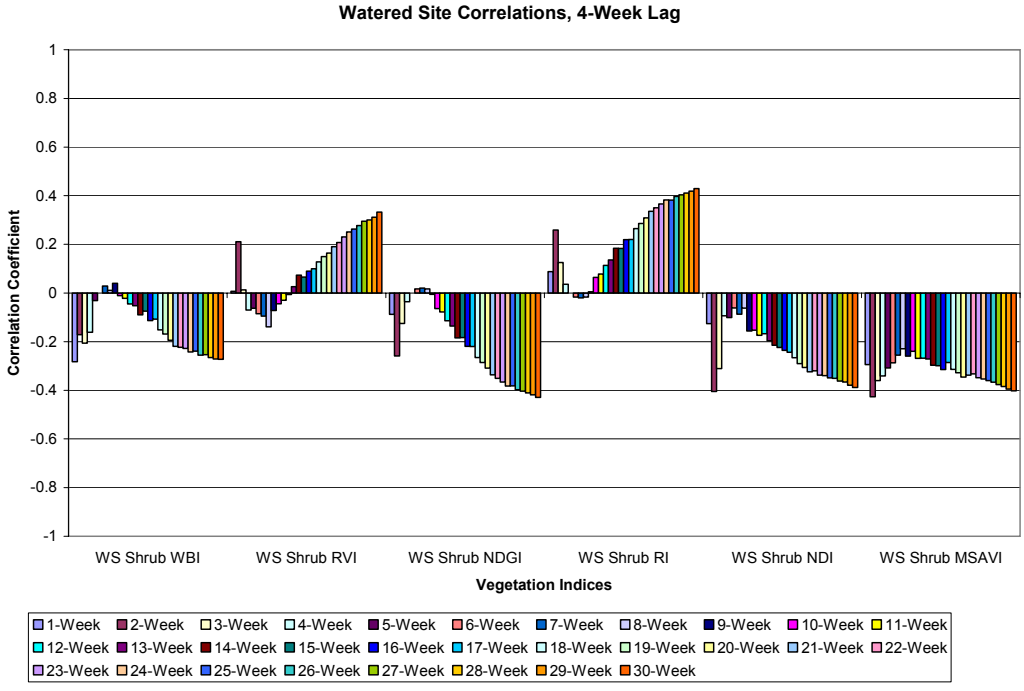

Figure 3-80: Linear correlation coefficients between SPI and WBI, RVI, NDGI, NDRI, NDI and MSAVI, Irrigated Site, four weeks lag.

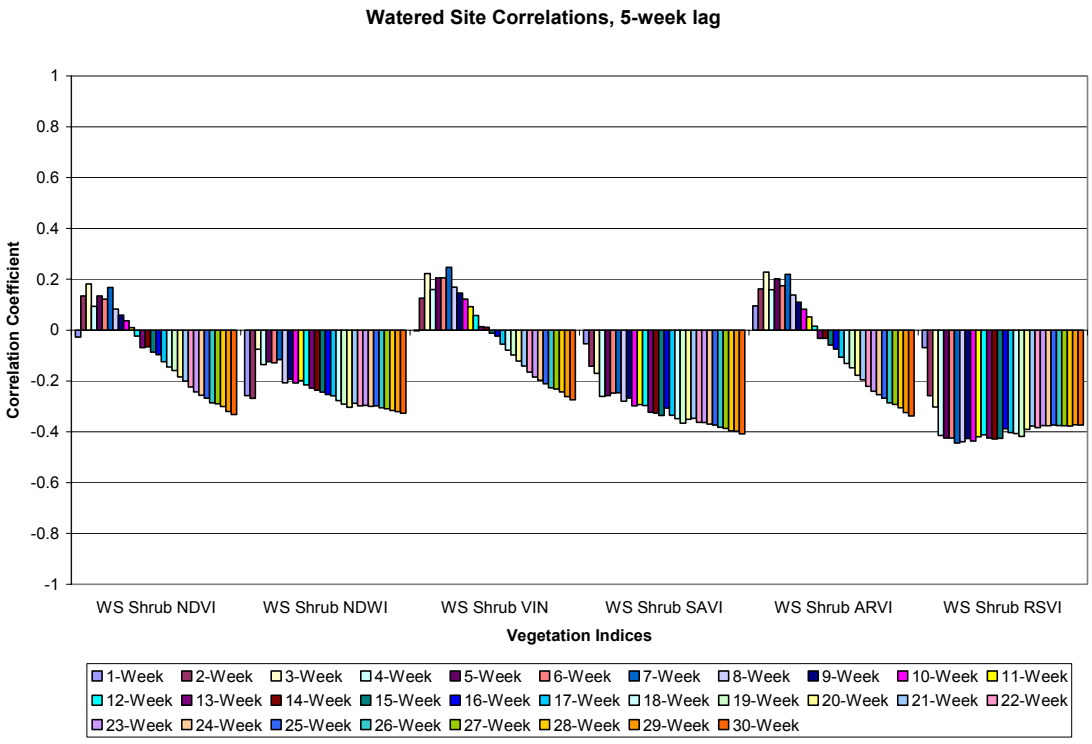

Figure 3-81: Linear correlation coefficients between SPI and NDVI, NDWI, VIN, SAVI, ARVI and RSVI, 5 weeks lag.

Figure 3-82: Linear correlation coefficients between SPI and WBI, RVI, NDGI, NDRI, NDI and MSAVI, Irrigated Site, 5 weeks lag.

4. SATELLITE IMAGE ANALYSIS OF DROUGHT STRESS

4.1 Application of Derived Algorithms

One of the goals of this research is to upscale the relationships derived from field measurements to wider regions using satellite images. Satellite images of the central New Mexico region were acquired from the Sevilleta National Wildlife Refuge data archives and NASA, and analyzed using the results developed from the previous chapters. The satellite images used were from the ASTER sensor, which has a higher resolution than the Landsat sensor does. While the field data was originally processed using Landsat 7 band specifications (described in chapter 2), the Landsat sensor has the same bandwidths as the ASTER sensor for red and green bands, while the ASTER near-infrared band wavelength is from 780 *nm* to 860 *nm*, compared to 760 to 900 *nm* for Landsat 7. The ASTER satellite data ordered for this study are atmospherically corrected surface reflectance preprocessed by the EOS. All images were processed using ERDAS Imagine 8.6 and ArcGIS 9, while spectral un-mixing results were processed using ENVI 4.0. Vegetation index images were then developed from the band reflectance images using algebraic calculations based on the formulae presented in Chapter 3. Finally, SPI maps were developed using formulae derived from the correlation equations with the vegetation indices presented in Chapter 3.

One of the better correlations discovered between vegetation indices and SPI was that between the 12-Week SPI and the Grass NDVI with no lag considered. The regression graph for this relationship is reproduced in Figure 4-1. This relationship was

not as strong as that between the 17-Week SPI and Grass NDVI, as seen in Figure 4-2. However, the 12-Week SPI was chosen as a comparison with other SPI maps from other agencies which used a 3-month SPI scale. It is hypothesized that at the 12-week/3-month scale, there is a greater seasonal effect on the part of the vegetation which may have an effect on the relationship to SPI, as suggested by Ji and Peters (2003).

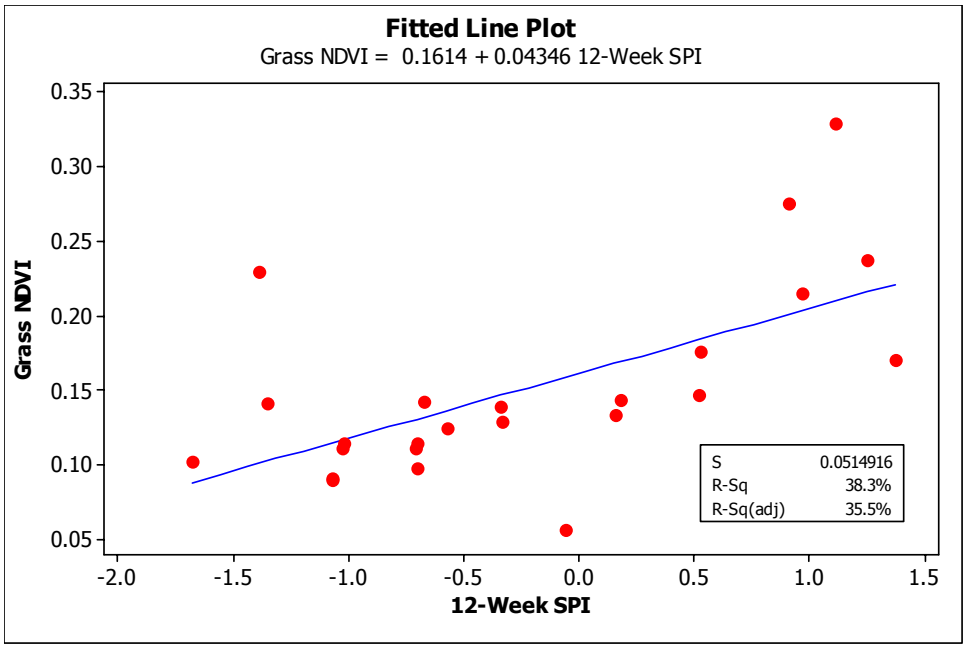

Figure 4-1: Linear Regression of Grass NDVI vs. 12 Week SPI, no lag

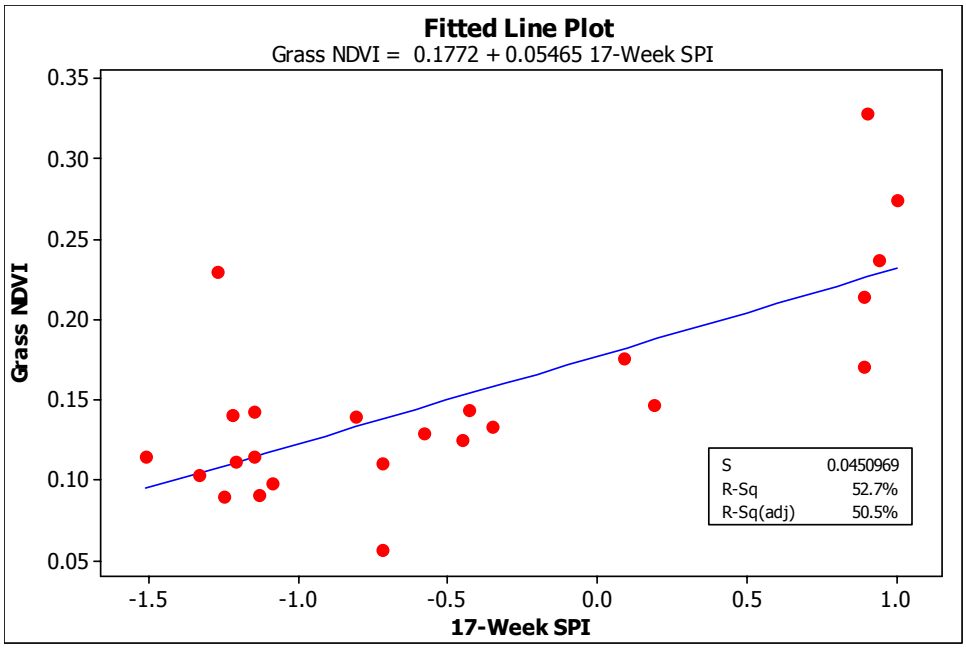

Figure 4-2: Linear Regression of Grass NDVI vs. 17 Week SPI, no lag

The linear regression equation for the Grass NDVI vs. the 12-Week SPI was:

$$\text{Grass NDVI} = 0.1614 + 0.04346 * \text{12-Week SPI} \qquad (66)$$

The theory behind this regression is that precipitation (represented by SPI in all scales) causes a response in vegetation (represented by the NDVI and other vegetation indices). Solving equation (66) for 12-Week SPI since we have values for NDVI, we get equation (67):

$$\text{12-Week SPI} = 23.00966 * \text{Grass NDVI} - 3.71376 \qquad (67)$$

This relationship was used in satellite data analysis. The shrub regression analysis was much stronger, as seen in Figure 4-3.

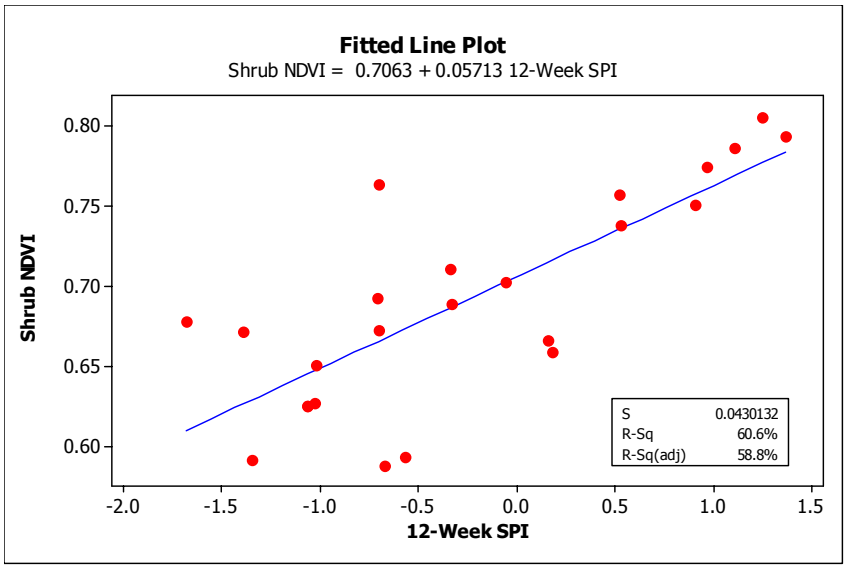

Figure 4-3: Linear Regression of Shrub NDVI vs. 12-Week SPI, no lag

Equation (68) presents the SPI-Shrub NDVI relationship:

$$\text{12-Week SPI} = 17.50393839 * \text{Shrub NDVI} - 12.36303168 \qquad (68)$$

4.2 Land Cover Classification and Linear Spectral Un-mixing

4.2.1 Previous Land Cover Classifications and Vegetation Index Classifications

One issue that presented itself in creating these maps was that of classification of the ground surface. While the measurements and correlations in this thesis are for creosote shrub and black gramma grass, the pixels with a satellite image will often have a mixture of soil, grass and shrub targets as well as additional components or vegetation species not considered in this research. Furthermore, soil is a main component in the satellite images, and while soil reflectance measurements were collected along with the shrub and grass measurements, they were not expected to have a significant relationship with SPI values. An examination of soil and SPI correlations is presented in Appendix C in Figures A-1 through A-12.

The first solution investigated to the pixel mixing and land cover classification issue was to use a previously defined land cover map as a basis for classification. The land cover map used was acquired from http://rgis.unm.edu and was a land-cover map of New Mexico produced in 2000 from a Landsat Mosaic. It was created by the USGS, and is reproduced in Figure 4-4 showing the Sevilleta National Wildlife Refuge land cover. This map states that the majority of the SNWR is covered in shrubland with a small amount of grassland and patches of evergreen forest in mountainous regions, as well as some outcrops of rocks and the Rio Grande. However, field observations were taken at the points indicated in the diagram, and photos of some of these observations are reproduced in Figures 4-5 through 4-7. These photos indicate that a great majority of the regions classified as shrubland by the land-cover map are in reality dominated by grasses. Even in the regions where shrub dominates, soil and grass would have a large effect on the pixel value at ASTER and LANDSAT resolutions. This can be seen in the NDVI images processed using ASTER data, seen in Figure 4-7. NDVI measurements of green vegetation are usually above the value 0.6, and most of the higher NDVI values in this region are found in the mountainous regions to the east of the refuge and the western tip, or near the Rio Grande which runs through the narrow section in the middle. This does not mean that creosote shrubs have a low NDVI, as the field measurements show that they have a regular NDVI value. It does indicate that shrubs are difficult to detect in satellite images of this scale because of the comparative small size of the shrubs, the lack of pure shrub pixels, and the strong background of soil and grass at this resolution.

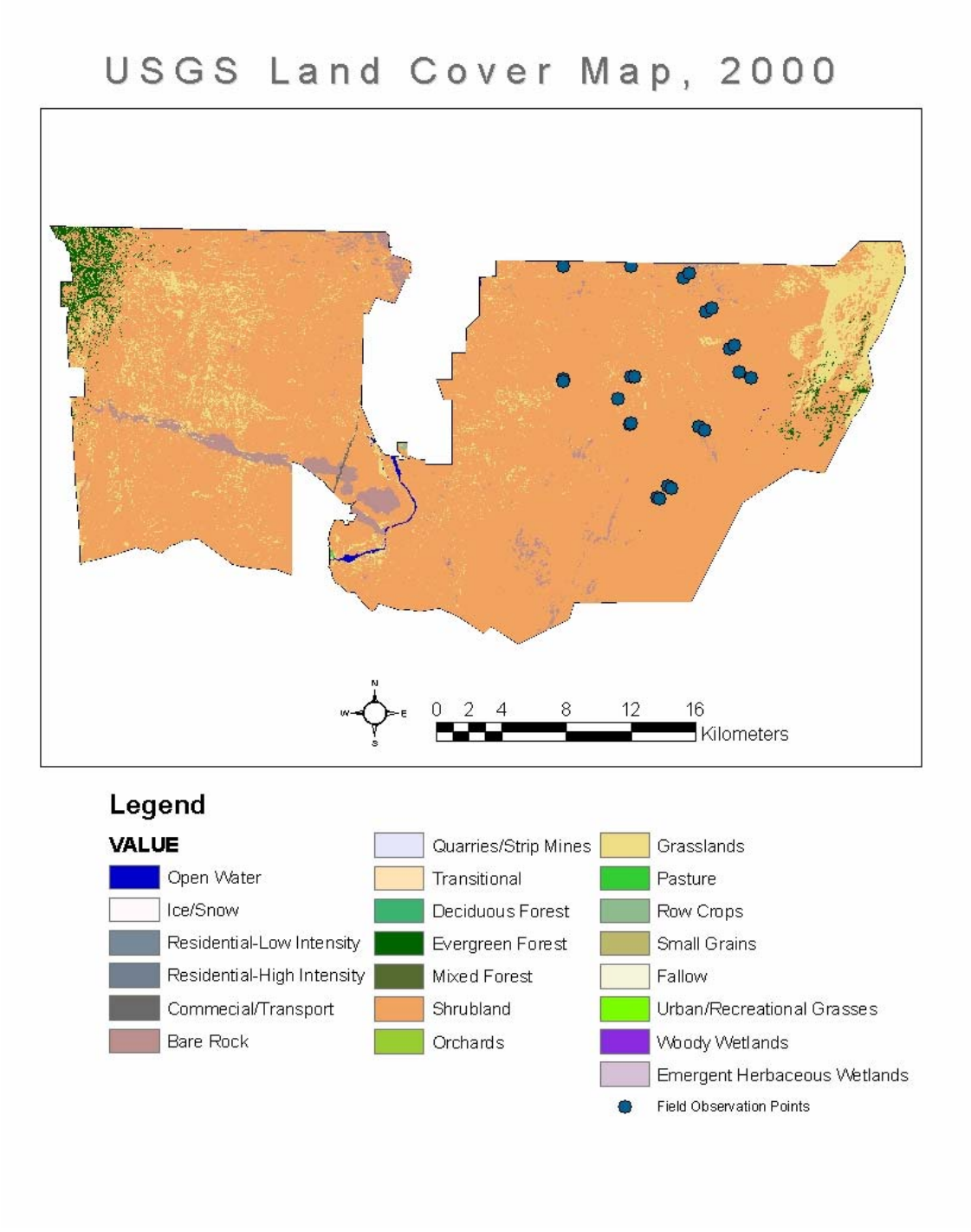

Figure 4-4: Predicted Land cover map of the Sevilleta National Wildlife Refuge.

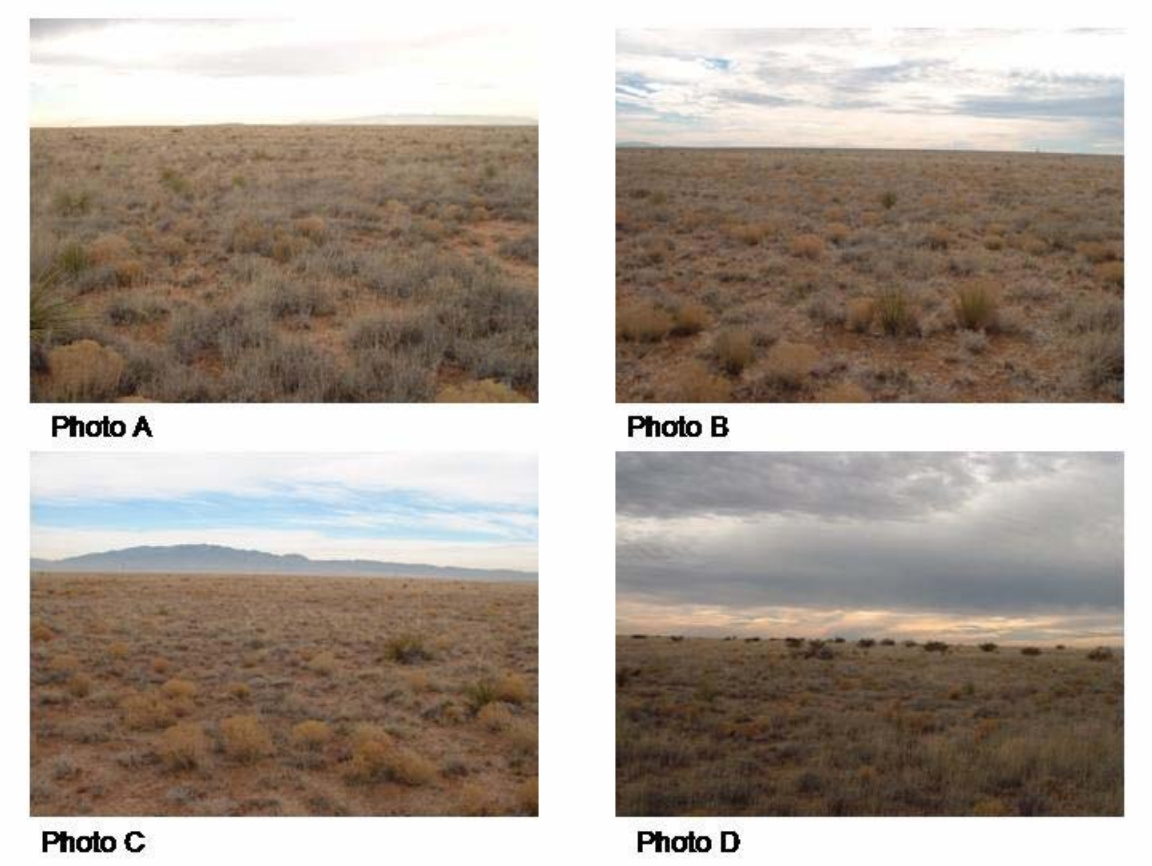

Figure 4-5: Photos of various regions of the Sevilleta Wildlife Refuge as represented in Figure 4-4. Photos A and B are from the northernmost measurement points. Photos C and D are from the eastern points. All of these points are defined as "shrubland" on the USGS land cover map.

Figure 4-6: Photo of the SNWR, in the shrub region. Canopy cover is about 40-50% and soil will have a strong impact on imagery taken at altitude

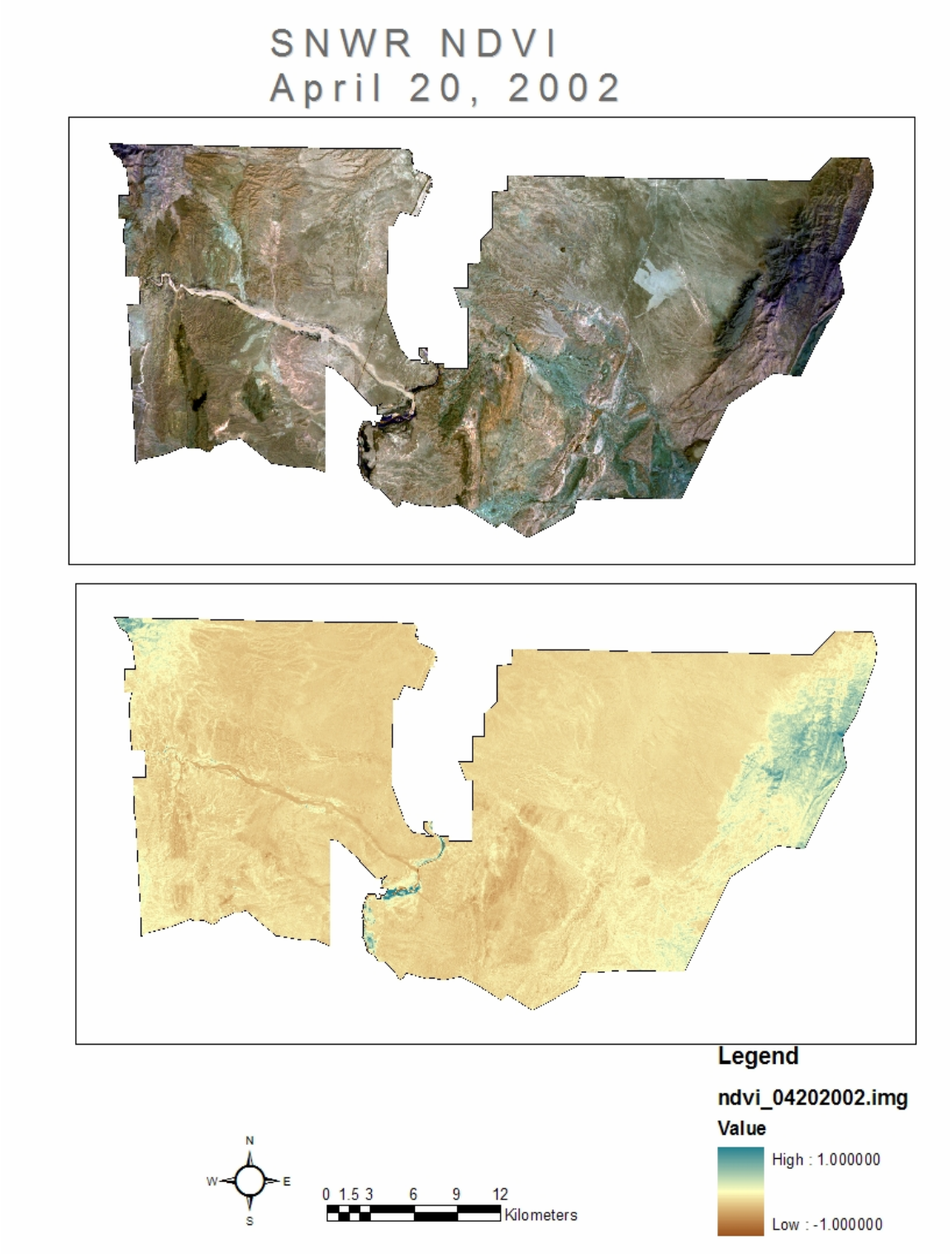

Figure 4-7: ASTER Surface Reflectance (upper image) and NDVI (lower image) at the SNWR for April 20, 2002.

One interesting observation made was the comparison of the NDGI values of soil, shrub and grass targets. As a reminder, the NDGI is the normalized difference between the red and green band reflectance (green –red/green + red). A graph of this comparison is shown in Figure 4-8.

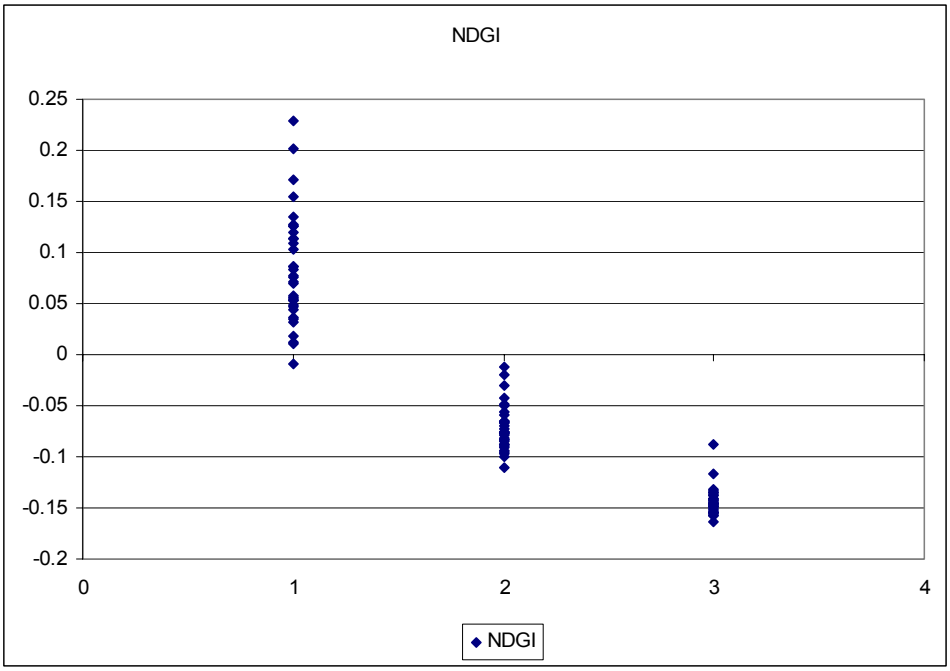

Figure 4-8: Comparison of measured NDGI values for shrub(1), grass(2) and soil(3) targets.

The graph indicates that shrub measurements tend to be greater than 0, grass measurements tend to be between -0.1 and 0, and soil measurements tend to be smaller than -0.1. This is not conclusive, and it must be taken into consideration that there are more components to pixels in the SNWR than these three components; but they are the three main components of the area and I thought it worthwhile to examine the NDGI variance over the region, shown in Figure 4-9. A general prediction that can be made is that all brown regions have soil/bare rock as the main ground component, while the greener regions are predominantly grass/shrub regions. However, these are just

predictions based upon personal knowledge of the region, and further study is needed to verify this.

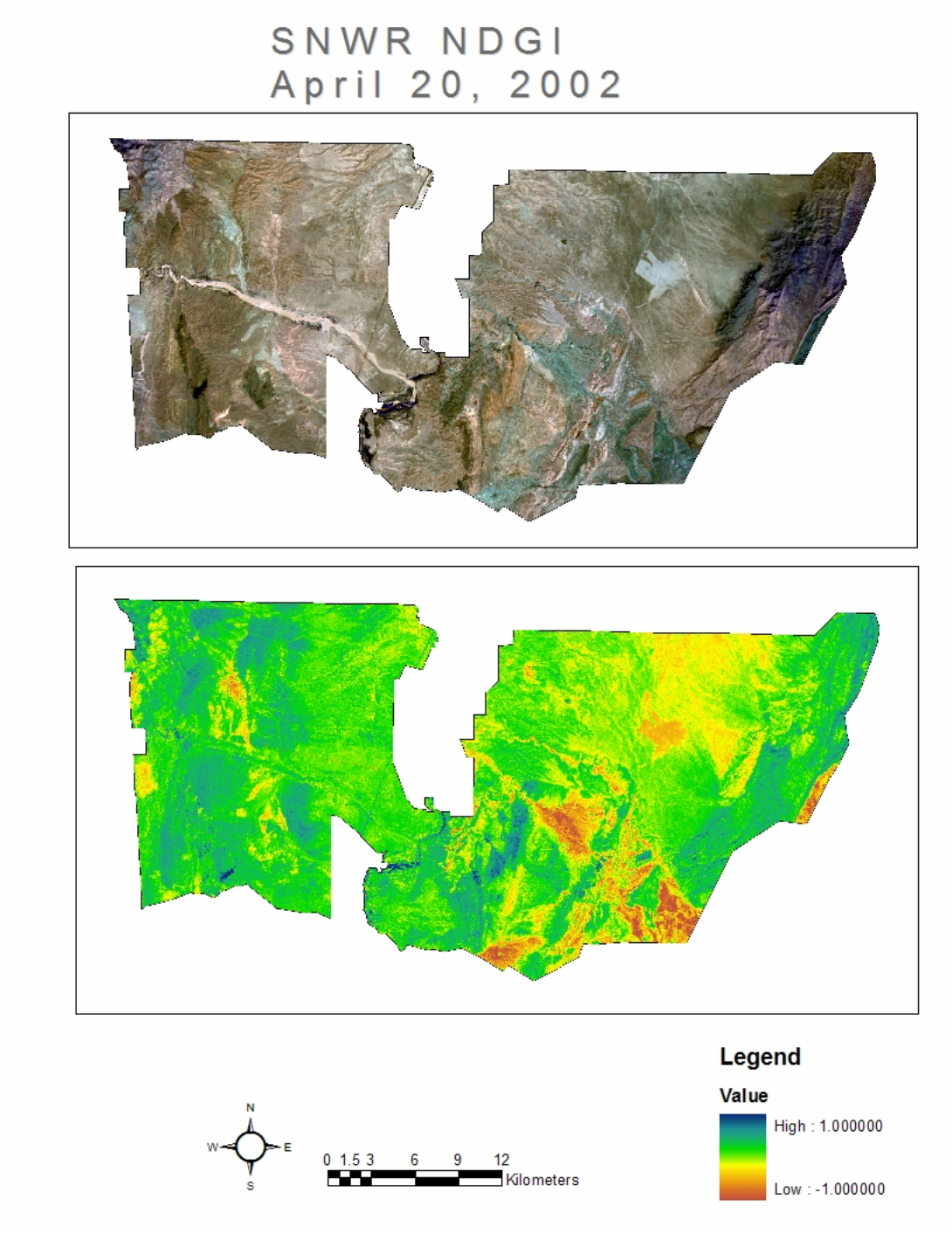

Figure 4-9: ASTER Surface Reflectance (upper image) and NDGI (lower image) at the SNWR for April 20, 2002.

4.2.2 Linear Spectral Un-mixing

Another approach that was applied was the use of linear spectral algorithms with the ENVI image analysis software to extract signal information from each pixel. Linear Spectral Un-mixing is based on the assumption that spectral mixing occurs when materials with different spectral properties are represented by a single pixel, and that "linear" indicates that there is no interaction between the materials. Pixels are unmixed using **endmembers** which are either known from field data collection/analysis of known pixel values, or are derived. The pixel reflectance is defined by equation (69):

$$\rho_{total} = \sum_{i=1}^{n} f_i \rho_i \qquad (69)$$

where ρ_{total} is the total reflectance of a pixel, f_i is the fraction of endmember *i* in the pixel, ρ_i is the reflectance of endmember *i* in the pixel, and *n* is the total number of endmembers in the pixel. The actual un-mixing is done using statistical analyses as is explained by the National Technical University of Athens, viewable at the following link: http://www.survey.ntua.gr/main/labs/rsens/DeCETI/SURREY/Page41.html:

> One can view a mixed pixel as an instantiation of the outcome of a random process. All pixels that come from the same mixed region then constitute an ensemble of outcomes of the same random process. In a similar way, the pixels that represent a single pure class are instantiations of the outcomes of the random process that creates the intra-class variability. In figure 10 then, the sets that represent the pure classes represent the distributions of three independent random variables, and the set that represents the mixed region represents the distribution of a linear combination of these variables. Bosdogianni, Petrou and Kittler used this idea to work out the proportions of the mixed region by trying to match the shapes of the distributions of the pure and the mixed pixels (*Mixture models with higher order moments, P Bosdogianni, M Petrou and J Kittler, IEEE Trans. Geoscience and Remote Sensing,vol 35, pp 341-353, 1997*). The shape of a distribution is expressed by the moments of the distribution: Its 1st moment (i.e. the mean), its 2nd moments (i.e. the elements of its covariance matrix), its 3rd moments etc. From the theory of random variables, we know the relationships

> between the moments of the independent variables and the corresponding moments of any linear combination of them. This way an augmented set of equations is created and it can be solved in terms of the unknown mixing proportions.

Linear Spectral Un-mixing is an active area of research in remote sensing. It has been investigated by Asner and Heidebrecht (2002) in the Jornada Experimental Range, New Mexico for comparison of multispectral and hyperspectral observations. Their research focused on using photosynthetic vegetation (PV), non-photosynthetic vegetation (NPV) and bare soil as endmembers, and they employed four different sensors: Airborne Visible/InfraRed Imaging Spectrometer (AVIRIS), Landsat 5 TM, MODIS, and ASTER imagery. For actual un-mixing, they developed a general probabilistic model called *AutoMCU* which uses a Monte Carlo approach to derive uncertainty estimates of the sub-pixel cover fraction values. *AutoMCU* uses three spectral endmembers from field measurements to decompose each pixel using equation (66) in this thesis. Their comparison results indicated that the full optical spectrum (400-2500 *nm*) grossly underestimate PV and overestimate bare soil, but provide some measure of NPV presence. Asner and Heidebrecht concluded by stating their belief that the shortwave infrared 2 region (SWIR2, 2000 *nm* to 2300 *nm*) is one of the best ways to estimate the fractional cover of PV, NPV and bare soil in arid regions, since their measurements in this spectrum showed distinct differences between all endmembers.

Qi *et al* (2002) has also investigated the use of the SWIR region of the spectrum, specifically using the Landsat sensor's bands 5 and 7 based on the theory that when vegetation becomes senescent (dries up), the spectral responses in these regions will increase due to loss of water in leaf tissues. They proposed the Normalized Difference Senescent Vegetation Index (NDSVI), defined in equatiton (70):

$$NDSVI = \frac{\rho_{SWIR} - \rho_{red}}{\rho_{SWIR} + \rho_{red}} \tag{70}$$

Qi used this index to estimate a fractional senescent vegetation cover from Landsat images. He compared the Landsat product to field-based fractional cover, and found that the satellite estimates were very close to the field observations, with a 0.95 correlation coefficient. However, he did not state how the field observations were made, nor did he present data for them. Furthermore, since Qi's research was based for rangeland studies, woody components such as shrubs were masked out of his biomass and forage cover estimates. For total accuracy, the application of equation (70) should include both shrub and rangeland, since the exclusion of shrubs automatically deprives the results of "total vegetation cover". Since this thesis focused mostly on drought quantification and less on land cover classification, and since the existence of this index was not known to me until late into the completion of this thesis, the use of the NDSVI was not examined in this research. However, the NDI as defined in equation (43) of this thesis is similar to the NDSVI, using the infrared band in place of the red band. The correlation results for NDI and SPI values were not very significant, but it may have some application for land cover classification. The results of Asner and Heidebrecht's work and Qi's research provide a glimpse at a promising new aspect of field data classification and upscaling. Qi's group, which is based at Michigan State University, has prepared a proposal to study this topic further which can be read at the following URL:

http://foliage.geo.msu.edu/research/projects/nasa_usda/Final_NASA_proposal.pdf .

It is believed that Qi's work and similar research in this area will be of great value for the research topic of this thesis, both for vegetation classification and further research of the index described in equation (72) as well as examining correlations between this index and

the SPI. In this thesis, linear spectral un-mixing was examined with two types of base image data; surface reflectance data and vegetation index data. The endmembers for each un-mixing analysis came from the mean field measurements of soil, shrub and grass. For the reflectance analysis, there were two methods examined. For the first method, the mean grass, soil and shrub reflectance were used directly as endmembers. For the second method, the grass mean was scaled by a factor of 0.7 and the shrub mean by a factor of 0.3 to simulate their predicted pixel composition percentage, while soil remained unchanged. The vegetation index un-mixing was performed by creating a vegetation index image comprising of NDGI, NDRI, and NDVI values, and performing a linear spectral un-mixing of this image based on the endmember's vegetation index values. The results of the surface reflectance un-mixing were moderately successful, and can be seen in Figures 4-11 through 4-13. It should be noted that the pixel components include more than those three targets. The results for the scaled un-mixing and vegetation index un-mixing are used in the research but are not presented as images in this thesis. Also, the results from the grass and soil comparison give misleading results on the Rio Salado, which is visible as white sand in the original image but appears as high grass content in the un-mixing. This is probably due to differences in mineral content between the Salado sand and the Sevilleta soils. As a comparison, an unsupervised classification was performed in ERDAS 8.6 over the region using 4 classes, the results of which are shown in Figure 4-13. These figures provide a general idea of land-cover classification in the SNWR.

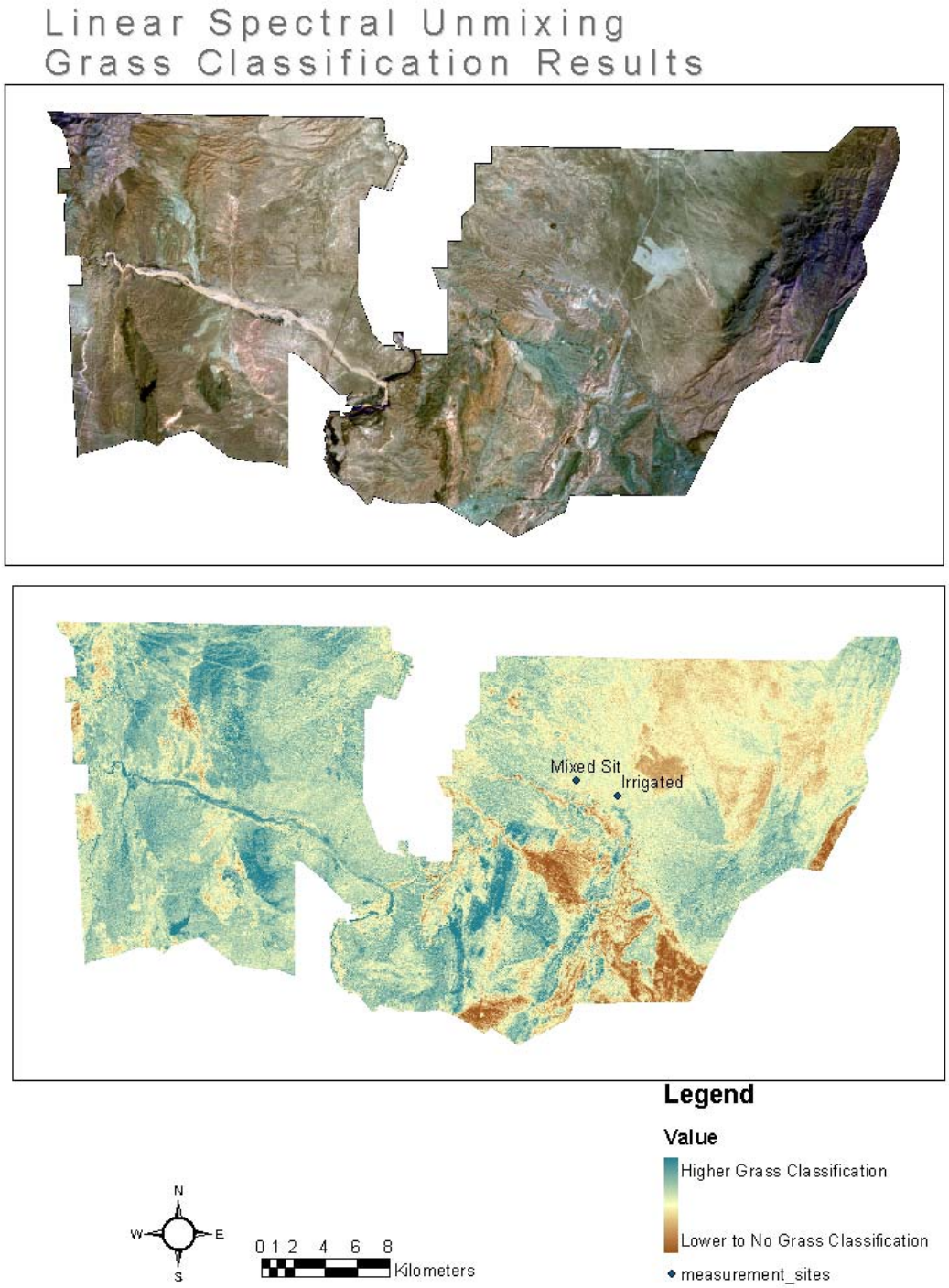

Figure 4-10: Linear Spectral Un-mixing Results from grass targets.

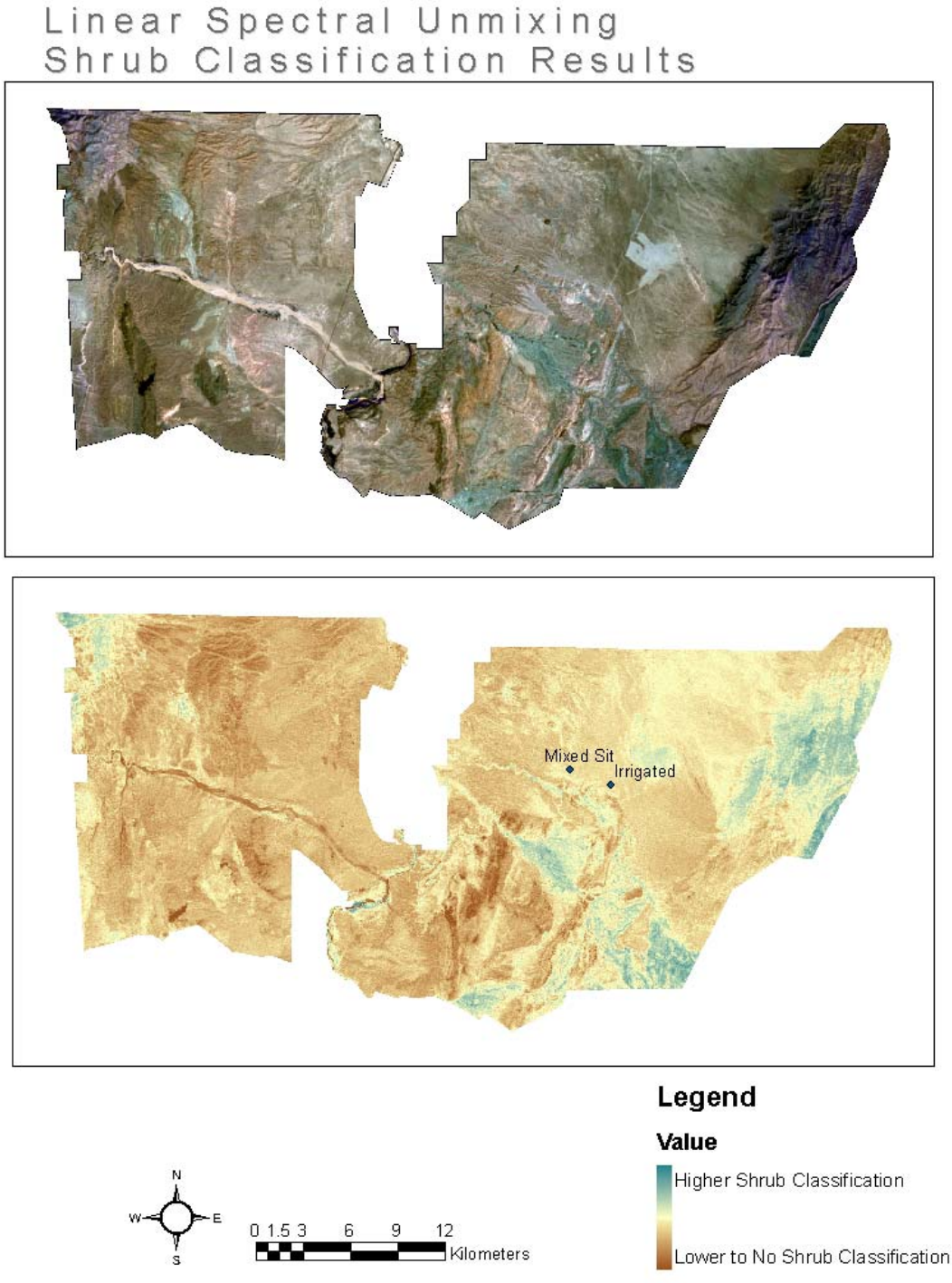

Figure 4-11: Linear Spectral Un-mixing from Shrub Target

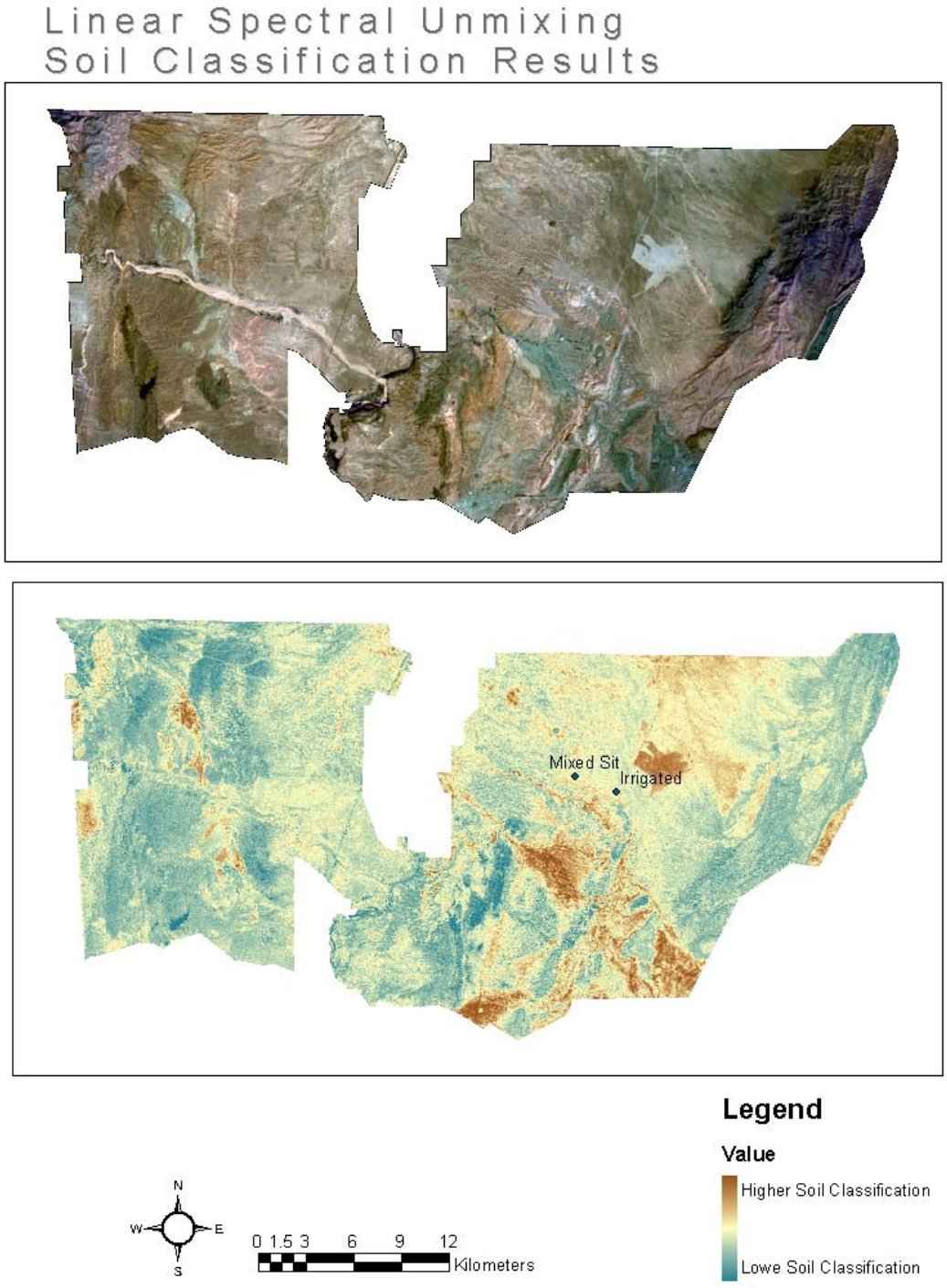

Figure 4-12: Linear Spectral Un-mixing Soil Classification results

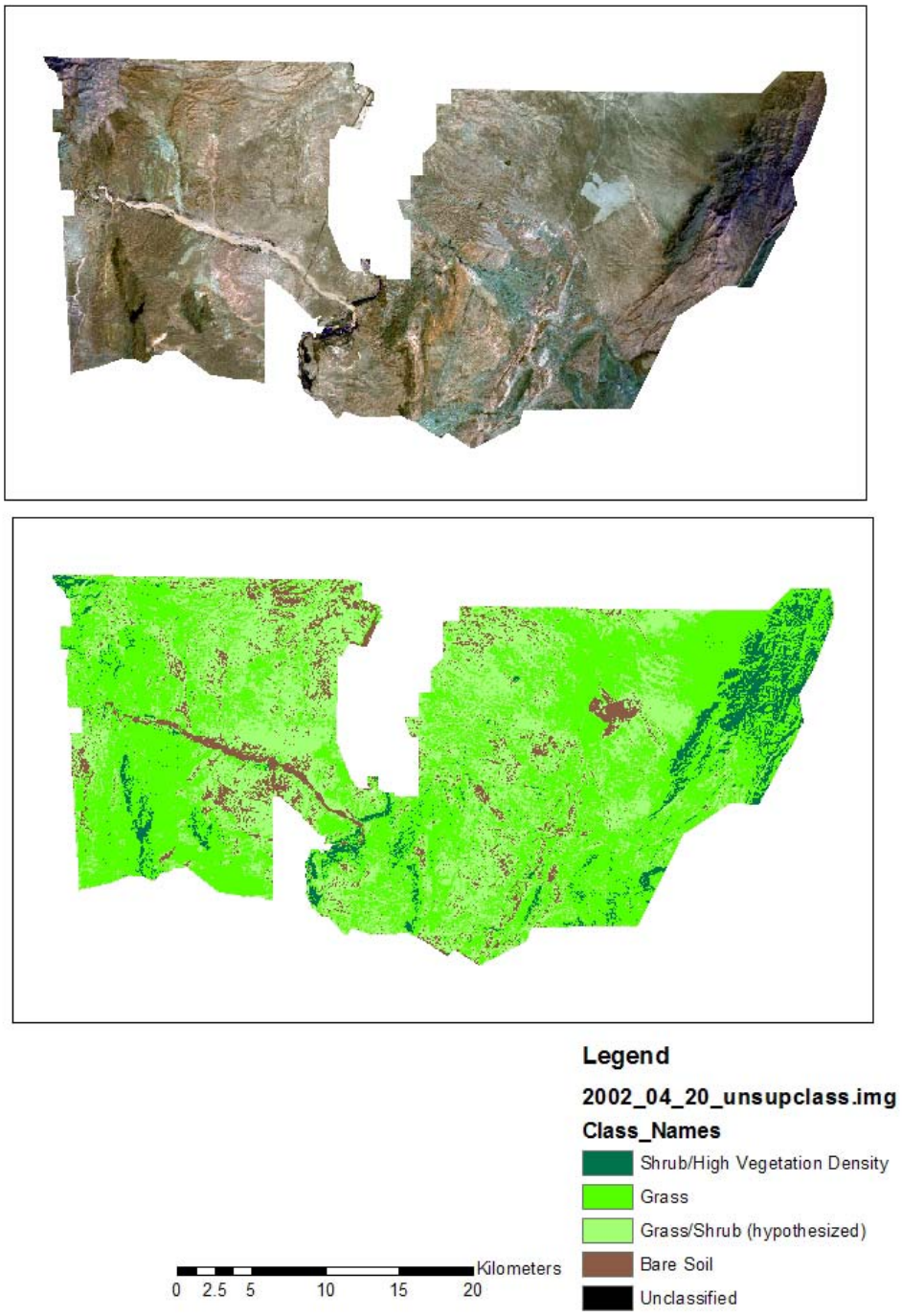

Figure 4-13: Unsupervised Classification results from ASTER image.

4.3 Drought Index Images

Figure 4-14 presents a map of New Mexico's climatic divisions, showing the locations of the SNWR and the Central Valley. Figures 4-15 through 4-18 show the predicted SPI from NDVI values, and compare them to the calculated SPI from the National Drought Mitigation Center (NDMC) as seen in the New Mexico Central Valley Climatic region. The NDMC's national 3-Month SPI for the dates under review is presented in Figures 4-19 through 4-23. The Surface NDVI-SPI results were calculated from taking surface NDVI data and applying the linear grass regression equation (equation 65) for the 12-Week SPI to all pixels, assuming that grass was the dominant endmember. The reflectance un-mixing and vegetation index un-mixing SPI results were processed using equation 70:

$$12-WeekSPI = f_{grass}\left(F\left(GrassNDVI \rightarrow SPI\right)\right) + f_{shrub}\left(F\left(ShrubNDVI \rightarrow SPI\right)\right) \quad (70)$$

where:

$F\left(GrassNDVI \rightarrow SPI\right)$ = equation (66)

$F\left(ShrubNDVI \rightarrow SPI\right)$ = equation (67)

f_{grass} = sub-pixel fraction designated as grass by un-mixing results

f_{shrub} = sub-pixel fraction designated as shrub by un-mixing results

Thus, the total SPI of a pixel is the sum of the SPI results predicted for each target.

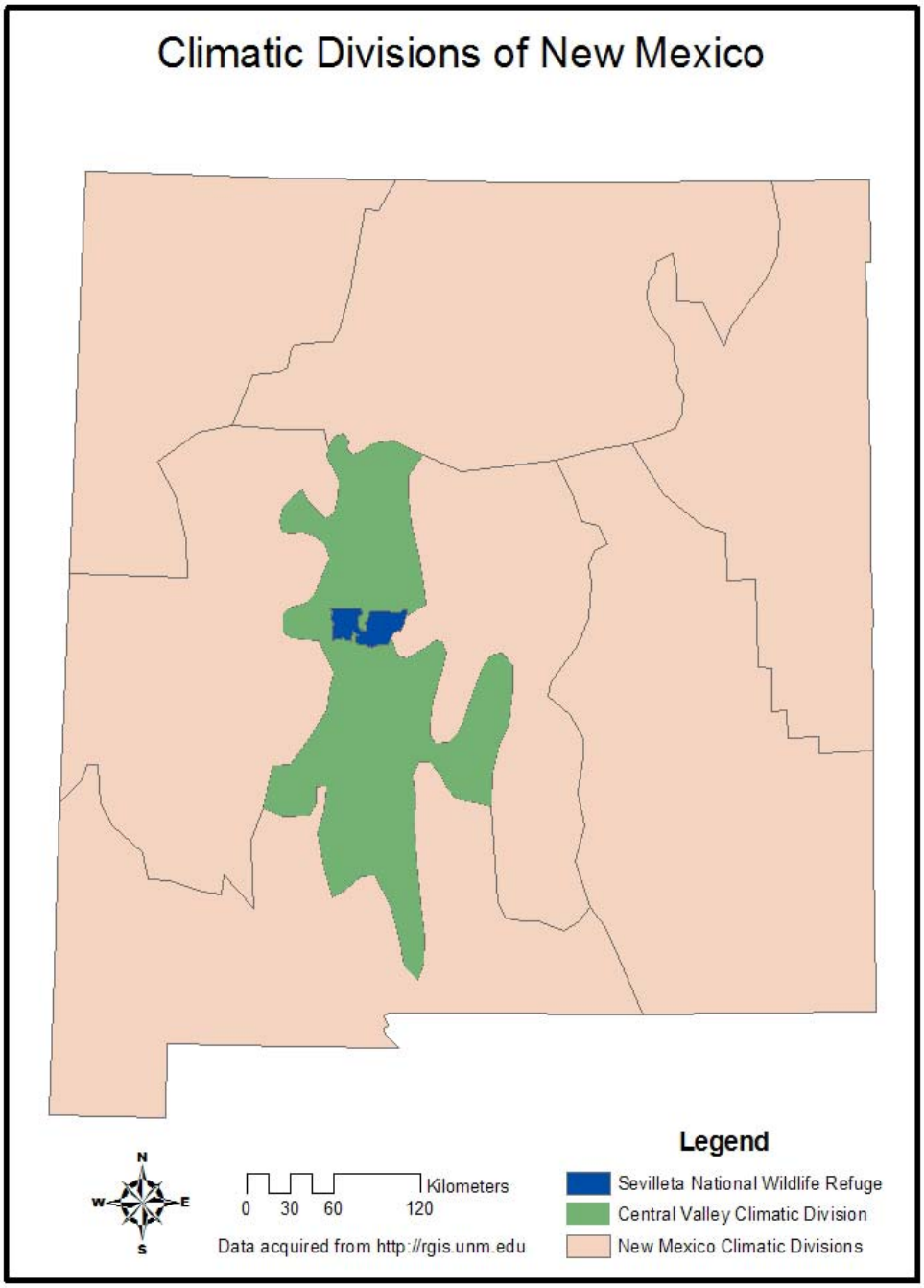

Figure 4-14: Climatic divisions of New Mexico.

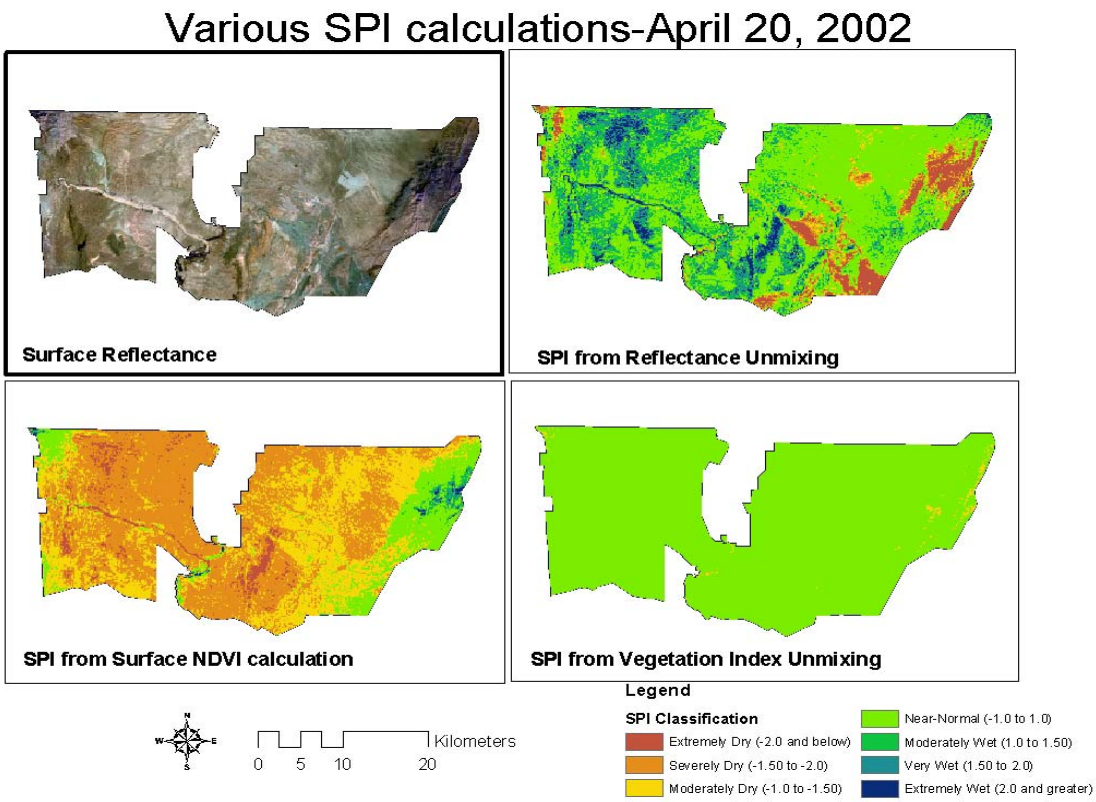

Figure 4-15: SPI Calculations for April 20, 2002

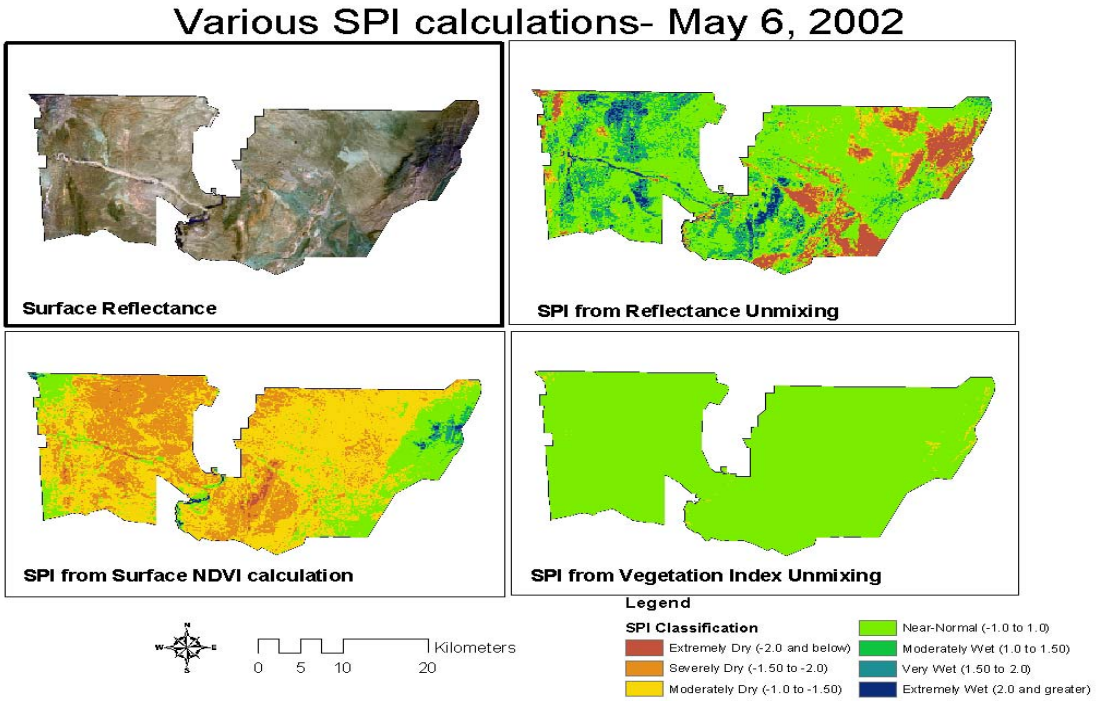

Figure 4-16: SPI Calculations for May 6, 2002

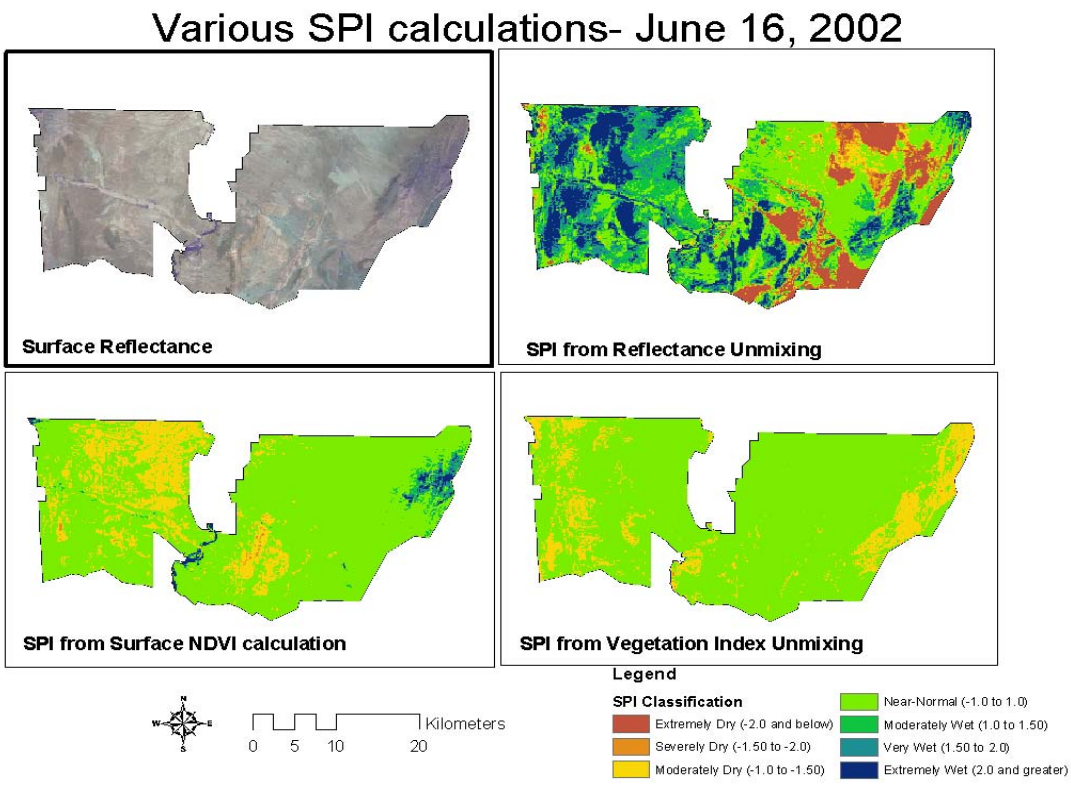

Figure 4-17: SPI Calculations, June 16, 2002

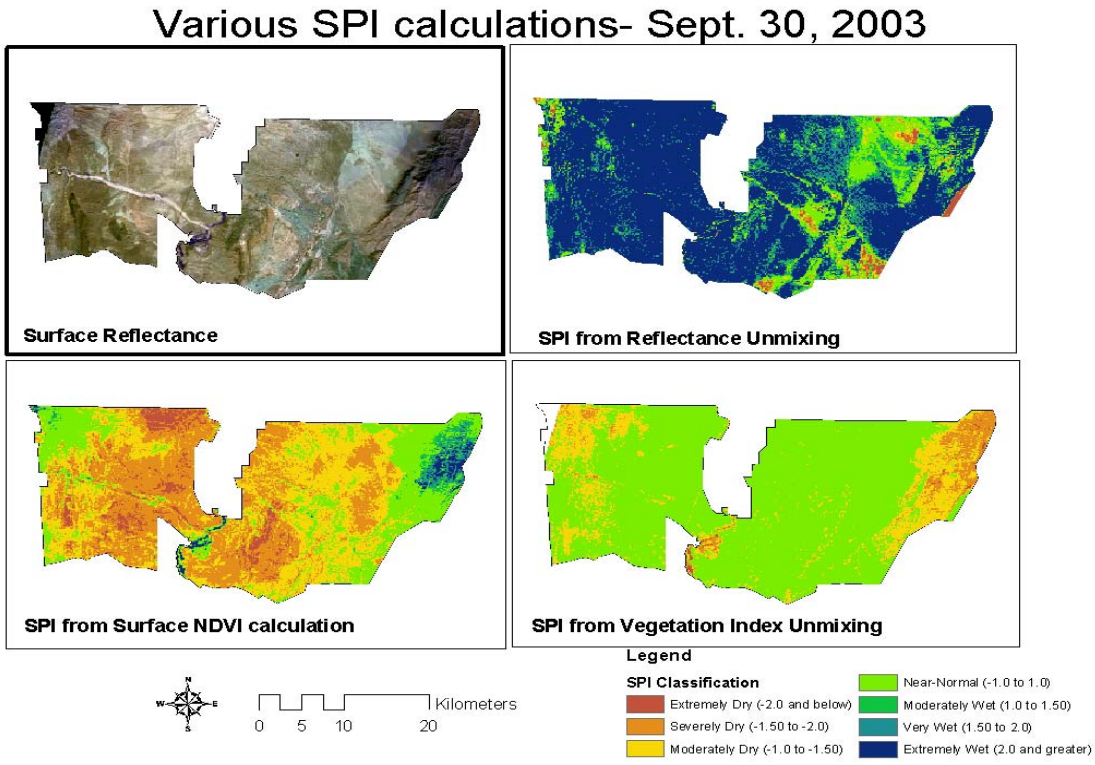

Figure 4-18: SPI classifications for September 30, 2003.

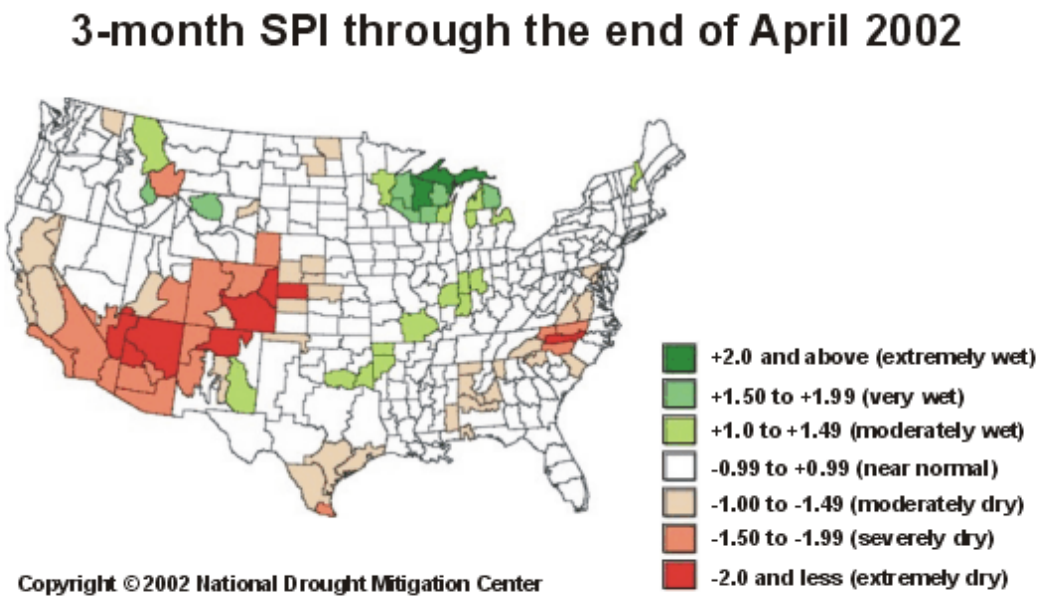

Figure 4-19: 3-Month SPI throughout the USA for April 2002.

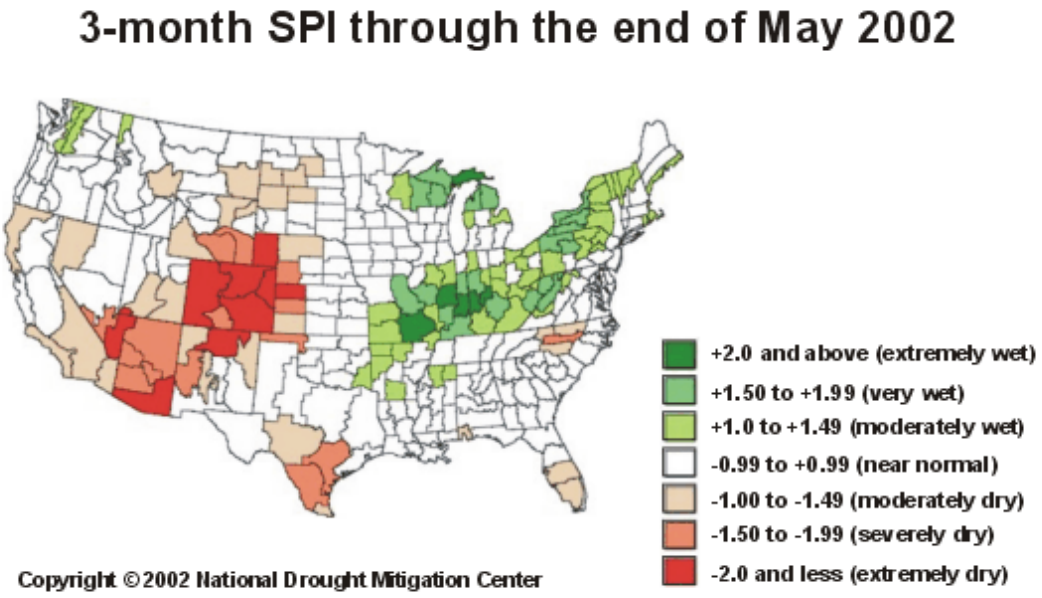

Figure 4-20: 3-Month SPI throughout the USA for May 2002

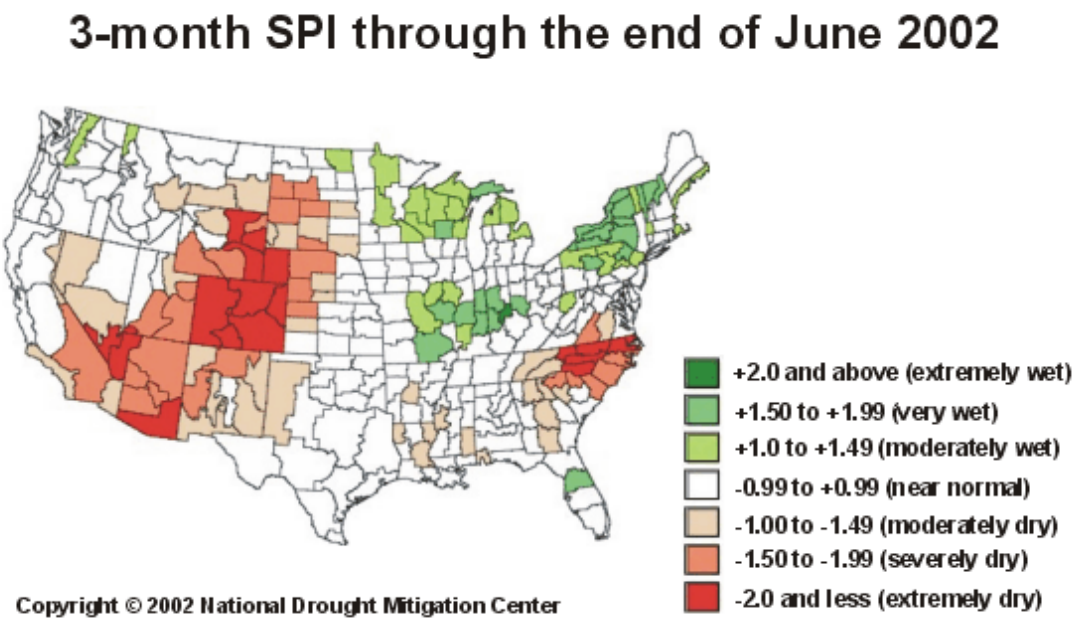

Figure 4-21: 3-Month SPI throughout the USA for June 2002

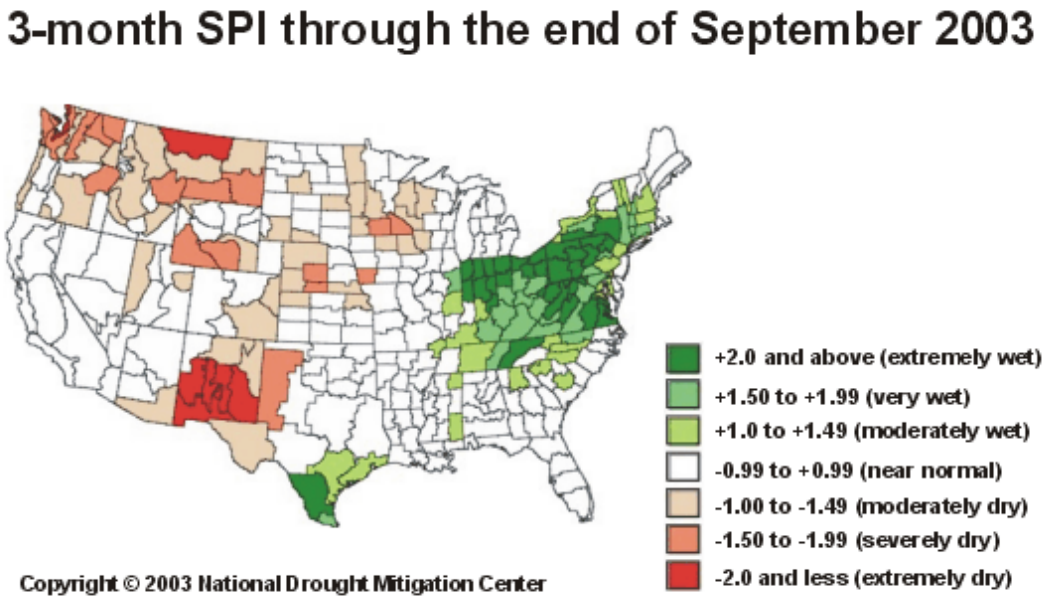

Figure 4-22: 3-Month SPI throughout the USA for September 2003.

4.4 Validation

The predicted values from Figures 4-15 to 4-18 for the SNWR 12-Week SPI using various classification methods gave diverse results depending on the method used. From the NDMC images, the Central New Mexico Valley climatic division had near-normal 3-Month SPI conditions in April 2002, moderately dry 3-month SPI conditions in May and June 2002, and severely dry conditions in September 2003. Table 4 presents a 25-pixel comparison of agreement with derived SPI results to the NDMC stated drought severity.

Table 4: Percent Agreement of Derived SPI images with stated NDMC drought severity.

Period of Interest	NDMC RESULTS	NDVI-to-SPI direct (using Grass Regression)	SPI from Linear Spectral Un-mixing	SPI from Adjusted Linear Spectral Un-mixing	SPI from Vegetation Index Linear Spectral Un-mixing
Apr-02	Near-Normal	8%	76%	52%	100%
May-02	Moderately Dry	6%	8%	12%	0%
Jun-02	Moderately Dry	8%	8%	4%	0%
Sep-03	Extremely Dry	0% (72% with other dry ranges)	4%(44% with other dry ranges)	0%	0%

These results are not very positive, and are quite diverse from each other. The differences can be explained from scale and SPI-calculations, in that the SPI from the NDMC is calculated from a much longer and more varied precipitation record than the SPI from the weather station. Also, the NDMC region is many times larger than the Sevilleta but may be incorporating much less weather stations to account for the region's area, as it is stated that the resolution of western state SPI calculation is hampered by the presence of too few weather stations. The results from the unmixed data did not include soil effects as soil reflectance is not expected to be a significant predictor of SPI (see

appendix C). However, soil reflectance would still have a strong effect on satellite NDVI images which might affect the results of using NDVI; results for SAVI or similar data may be more consistent. It must also be noted that the use of relationships obtained from field-based vegetation indices may relate to satellite vegetation indices in different ways. Jackson and Huete (1991) stated that care must be exercised in comparing ground-based data with satellite-based data, since the band-response functions are different for each instrument, the fields of view are usually different and the data used may be either raw or transformed data. Ideally, vegetation indices calculated for one sensor should be correlated with the exact indices calculated for other sensors, if a data record is available.

5. DISCUSSION

5.1 T-Test Discussion

It is expected that if the rain-sheltered vegetation experienced physical changes to plant leaf structure which did not occur in the control vegetation, then these physical changes should affect the spectral response of rain-sheltered plants, and thus differences between drought-stress and control plant reflectance values and vegetation index values may be observed. The T-tests for grass show that 11 of the 12 vegetation indices datasets were statistically different when comparing both the rain-sheltered grass to the control grass. The only index which did not show any statistical difference between the rain-sheltered and control grass was the RSVI. It was thus concluded that all of these vegetation indices except the RSVI can be used to distinguish and identify drought-stressed grass regions, if compared to index measurements of normal grass reflectance. The control grass did not have as much chlorophyll as the shrub did, which helped to lower the red spectrum absorption; but the rain-sheltered grass was usually dead or near-death and the cellular structure was also very degraded, thus providing very little reflectance in the infra-red spectrum. Table 5 summarizes the Rain-sheltered Site grass T-test results.

However, when investigating the T-test results comparing the rain-sheltered creosote shrubs to the control creosote shrubs, only 6 of the 12 indices show a statistical difference between datasets. The indices that showed a statistical difference were the

NDWI, WBI, ARVI, WBI, NDRI, NDGI and NDI, while the non-responsive indices were the NDVI, VIN, SAVI, MSAVI, RVSI and RVI. The responsive indices were the ones which either focused on water absorption such as the NDWI and WBI, or on chlorophyll absorption/reflectance such as the NDGI and NDRI, while the majority of non-responsive indices were those comprised infrared and red bands. However, the T-values for the some of the infrared/red band indices were significant to a lesser degree than the stated 95% probability; the NDVI difference was significant to within 90% with a p-value of 0.1. The precipitation for the control vegetation was quite low over the given time period and was similar to the drought vegetation precipitation, and an irrigated shrub may have more of a detectable difference when compared to control vegetation. The differences in the water-absorption indices are probably due to the long-term drought stress imposed, rather than the precipitation difference over the reflectance measurement period. Table 6 summarizes the Rain-sheltered Site shrub T-test results.

Since there is a distinct possibility that the control vegetation was also under a degree of drought-stress, the irrigated vegetation results should help to illustrate whether shrub reflectance data is affected for all indices by drought-stress/water availability. The t-tests on the irrigated plot showed that 11 of the 12 vegetation showed a statistical difference between the irrigated shrub and the control shrub, with the NDWI as the non-responsive vegetation index. The intuitive reason for this is that the regular abundant supply of water helped to increase the irrigated shrub vigor and health, and this increased vigor showed itself in the plant leaf structure and the plant reflectance. However, further research may be required to see if an excess of water may actually have a negative effect on creosote or if the amount of water added was enough to be an excess, though as

mentioned by Smith (1997) that may not be the case. Table 7 summarizes the Irrigated Site shrub T-test results.

These results indicate that rain-sheltered creosote bushes at this site are more resistant to the effects of stress than are rain-sheltered grasses at this site. It also shows which indices are better suited for examining drought-stress vs. normal conditions for both vegetation types. These results can be compared to similar research done by Everitt and Nixon (1986) on rangeland shrubs in Texas. Their study focused on two species of shrub: Texas persimmon (*Diospyros texana*) and lime pricklyash (*Zanthoxylum fagara*), and compared the reflectance of drought-stressed vs. non-stressed shrubs at five wavelengths: 550, 650, 850, 1650 and 2200 *nm*. These wavelengths are in the green, red, infrared and microwave (final two bands) respectively. Everitt and Nixon also compared leaf water content (LWC) and chlorophyll content at the time of reflectance measurement, and used the T-test with $p \leq 0.05$ indicating significance to test the differences between between canopy reflectances at the five wavelengths selected for study along with differences in LWC and chlorophyll content. Their non-stressed vegetation was located near Linn, TX, while the drought-stressed site was located near La Joya, TX. These sites are approximately 70 miles apart, but have similar native vegetation. The results from their study showed that there were significant differences at all five wavelengths between the drought-stressed and control shrubs. While these results do not corroborate well with the Rain-sheltered Site data, this may be because there was not that much difference between the drought-stressed and control vegetation due to creosote's drought resistance and the similarity of precipitation between both the control and rain-sheltered plots (Pockman, personal correspondence). Everitt's and Nixon's

results do fit with the Irrigated site data and Rain-sheltered Site grass data which showed a clear difference between all of the band-derived vegetation indices.

Table 5: T-Test results for Control Grass vs. Rain-Sheltered Grass, Rain-Sheltered site

	Control Grass	R.S. Grass	Control Grass S.D.	R.S. Grass S.D.	T-Values	P-Value
NDVI	0.1722	0.1216	0.0762	0.0281	3.9700	0.0000
NDWI	-0.1259	-0.1517	0.0443	0.0255	3.4200	0.0020
VIN	1.4378	1.2792	0.2451	0.0743	3.8900	0.0000
SAVI	0.0858	0.0593	0.0403	0.0171	3.7600	0.0010
ARVI	0.0450	-0.0079	0.0824	0.0305	4.3600	0.0000
RSVI	0.1313	0.1222	0.0331	0.0268	1.6300	0.1110
WBI	0.9555	0.9374	0.0123	0.0095	8.8600	0.0000
RVI	0.7130	0.7842	0.1069	0.0443	-3.9900	0.0000
NDGI	-0.0723	-0.0844	0.0245	0.0218	3.8700	0.0000
NDRI	0.0723	0.0844	0.0245	0.0218	-3.8700	0.0000
NDI	-0.2047	-0.2624	0.0756	0.0483	4.8700	0.0000
MSAVI	0.0709	0.0482	0.0349	0.0149	3.6900	0.0010

Table 6: T-Test results for Control Shrubs vs. Rain-Sheltered Shrubs, Rain-Sheltered site

	Control Shrub	R.S. Shrub	Control Shrub S.D.	R.S. Shrub S.D.	T-Values	P-Value
NDVI	0.6887	0.6719	0.0629	0.0737	1.4300	0.1620
NDWI	0.0145	-0.0120	0.0549	0.0275	2.5700	0.0150
VIN	5.7092	5.4238	1.4904	1.5614	1.0200	0.3150
SAVI	0.4688	0.4597	0.0686	0.0737	1.2300	0.2290
ARVI	0.5789	0.5537	0.0740	0.0906	1.8400	0.0750
RSVI	0.2448	0.2444	0.0429	0.0484	0.0700	0.9480
WBI	1.0130	0.9942	0.0124	0.0134	9.0300	0.0000
RVI	0.1859	0.1985	0.0440	0.0533	-1.5000	0.1430
NDGI	0.0807	0.0580	0.0493	0.0514	3.6800	0.0010
NDRI	-0.0807	-0.0580	0.0493	0.0514	-3.6800	0.0010
NDI	0.2913	0.2593	0.0643	0.0662	2.6300	0.0130
MSAVI	0.4631	0.4523	0.0839	0.0880	1.1900	0.2450

Table 7: T-Test results for Irrigated Shrub vs. Control Shrub, Irrigated Site

	Irrigated Shrub	Control Shrub	Irrigated Shrub S.D.	Control Shrub S.D.	T-Values	P-Value
NDVI	0.7015	0.6598	0.0586	0.0664	3.7200	0.0010
NDWI	0.0565	0.0229	0.1722	0.1534	1.9200	0.0670
VIN	5.9855	5.0954	1.5390	1.1665	3.7800	0.0010
SAVI	0.5041	0.4628	0.0984	0.0935	6.2300	0.0000
ARVI	0.5885	0.5437	0.0717	0.0702	4.0100	0.0000
RSVI	0.3115	0.2912	0.2807	0.2655	4.1400	0.0000
WBI	1.0091	0.9947	0.0089	0.0099	8.7600	0.0000
RVI	0.1768	0.2068	0.0402	0.0490	-3.6700	0.0010
NDGI	0.0879	0.0514	0.0561	0.0387	5.4200	0.0000
NDRI	-0.0879	-0.0514	0.0561	0.0387	-5.4200	0.0000
NDI	0.3379	0.2858	0.1445	0.1353	3.6100	0.0010
MSAVI	0.4980	0.4492	0.0908	0.0859	6.1700	0.0000

5.2 Vegetation Index-Drought Index Correlation Discussion

The correlation results showed a clear connection between drought severity and natural vegetation spectral responses, with the significant correlations between various SPI timescales and shrub/grass NDVI, ARVI, SAVI, MSAVI, RSVI, VIN, NDGI, NDRI and RVI. These correlations indicate that the accumulated effect of precipitation is most likely the key factor in plant vigor. Tables 4 through 9 present the most significant linear correlation coefficients for each index during each lag period. It is observed that generally, the most significant correlations decreased in drought time scale with increasing lag. This indicates that it is the total accumulation of precipitation that has an effect on vegetation vigor, and not just the amount of time that elapses. The apparent three-week gap between the maximum correlations for shrub and grassland may be due to the grass being more sensitive to seasonal changes. These results are similar to Ji and Peters' (2003) results, in that a correlation is seen between the vegetation indices and drought index for time series near the 3-month mark for shrubs and a few weeks after the three month mark for grass data for this data. Ji and Peters showed that the NDVI correlation was strongest for the 3-month SPI over his study regions, as described in the

literature review in chapter 1. It should be noted that while this thesis examined field-based data over a one-year period, Ji and Peters examined monthly correlations over a 12-year period, focusing on the months of May through October. For example, Ji and Peter's correlations for May incorporated all May NDVI values and their equivalent SPIs for each year from 1989 through 2000, and so forth. Also, the precipitation record for which the SPI was calculated was from 1895-2000, a much more robust record than in the Sevilleta. The regression equations derived by Ji and Peters for their model using dummy variables for each month as seen in equation (57) were significant with *p*-values <0.0001 and R^2=0.67. His grassland regression functions are presented in equation (71).

$$\begin{aligned}
&\text{May} && NDVI = 0.2772 + 0.0180(SPI)\\
&\text{June} && NDVI = 0.3588 + 0.0478(SPI)\\
&\text{July} && NDVI = 0.3462 + 0.1289(SPI)\\
&\text{August} && NDVI = 0.3282 + 0.0178(SPI)\\
&\text{September} && NDVI = 0.2772 + 0.0178(SPI)\\
&\text{October} && NDVI = 0.2054 + 0.0178(SPI)
\end{aligned} \qquad (71)$$

where *SPI* is the 3-Month SPI. In contrast, the best linear grass regression with no time lag in this thesis was with the 17-Week SPI, which was also significant with the *p*-value<0.0001 and R^2=0.52. The regression function here was:

$$NDVI = 0.1772 + 0.05465(SPI) \qquad (72)$$

where *SPI*=17-Week SPI. The normal NDVI (when SPI=0) of equation (72) is 86% of the smallest normal NDVI from equation (71), and 67% of the largest normal NDVI from equation (71). Also, the normal NDVI from equation (72) compares fairly well to the mean control grass NDVI calculated from the data record of this thesis over the period of record, which is 0.1587. However, the gradient of equation (72) is more than 5 times that

of all of the gradients in equation (71) except for July. The initial interpretation of this finding is that precipitation has a stronger effect on grasses in semi-arid regions than in the great plains region, but one must remember the different SPI scales in use, as well as the differences in scale and the fact that the field measurements in this thesis are over one year instead of a monthly series over a 12-year period. Even with these caveats, the results do not drastically contradict each other and are similar.

While the shrub and grass NDVI and other infrared/red band vegetation indices had their largest correlations around the 14-Week SPI (shrub) and 17-Week SPI (grass), the shrub RSVI values had their most significant correlation with the longer SPI time scales (30-week SPI with no lag, to 21-Week SPI with five weeks lag). This index uses the region of the spectrum between the red absorption and the infrared reflection, and may be representative of the long-term plant leaf structure. More research is needed to examine this index and possible uses of this long-term response. Tables 8 through 13 summarize the most significant correlations for each vegetation index at each lag period.

When the correlations for the irrigated shrub were investigated, the most significant correlations were much lower than for the control site, and were with shorter SPI timescales (with the 5-week SPI timescale for no lag consideration). As the lag increased, the correlation also decreased and by the 4-week lag time, there were no significant correlations between the irrigation-affected SPI and the vegetation indices. The most significant correlations are presented in tables 14 through 19. This indicates that the time-lag element is incorporated into the SPI calculations depending upon the timeline under consideration and that the total amount of precipitation that the vegetation receives within a given time period is the most significant influence on plant vigor. It is

also possible that the creosote vegetation may have a negative reaction to excess precipitation. However, it is not the only influence, seasonal changes and other weather elements may play a part in the response as well. Seasonal variation was not taken into account for this research, but most of the precipitation in this region is seasonal in nature, falling in the monsoon period (between June and October) as well as winter precipitation. Seasonal variation is expected to play a significant role in the grass results (Wang *et al*, 2001; Ji and Peters, 2003), but is not expected to have much effect on the creosote shrub data, as the grass is likely to be more active in summer than in winter. This is a topic that could be further studied and analyzed for this region, but much more data is required. Precipitation data was also quite short, and while the present data was utilized as best it could, a longer data set would have been much more useful and probably would have provided even more accurate results.

5.3 Satellite Image Analysis Discussion

The satellite interpretation of the correlation results were hampered by classification problems and upscaling issues. Although the direct NDVI-to-SPI conversion was based on the assumption of a majority of grass cover, the effect of soil would still be very strong and thus SPI values from this conversion would most likely be underestimated. While the general classification using linear spectral unmixing was moderately successful, the actual fractions derived are most likely underestimated for grass values, and overestimated for soil, similarly to Asner and Heidebrecht (20002). Further investigation can be done using vegetation index values calculated from a time series of satellite images, or by using smaller resolution images such as IKONOS and examining the classification results on those scales. Such a premise was initially explored

in this research, but was limited by the age of the available images (acquired in 2000) and by an apparent anomaly in the images which manifested itself during image processing. Asner and Heidebrecht's previously discussed results are similar to the un-mixing results in this thesis, where grass (NPV) was shown as the most prevalent cover while shrubs (PV) were not represented much. The fraction values derived in this thesis for shrub presence had a lot of negative values as well, and so while the results were adequate for a general classification, they were not well-suited for precise land-cover definitions.

Table 8: Most Significant Correlations for Vegetation Indices at Drought Plot, No Lag

Vegetation Index	Correlation Coefficient	Drought Index
Shrub NDVI	0.818	14-Week SPI
Grass NDVI	0.726	17-Week SPI
Shrub NDWI	0.19	12-Week SPI
Grass NDWI	-0.364	1-Week SPI
Shrub VIN	0.848	14-Week SPI
Grass VIN	0.715	17-Week SPI
Shrub SAVI	0.796	19-Week SPI
Grass SAVI	0.522	17-Week SPI
Shrub ARVI	0.826	14-Week SPI
Grass ARVI	0.734	17-Week SPI
Shrub RSVI	0.755	30-Week SPI
Grass RSVI	-0.577	9-Week SPI
Shrub WBI	0.37	PDI
Grass WBI	0.736	PDI
Shrub RVI	-0.808	14-Week SPI
Grass RVI	-0.727	17-Week SPI
Shrub NDGI	0.654	14-Week SPI
Grass NDGI	0.371	14-Week SPI
Shrub NDRI	-0.654	14-Week SPI
Grass NDRI	-0.371	14-Week SPI
Shrub NDI	0.411	14-Week SPI
Grass NDI	-0.458	2-Week SPI
Shrub MSAVI	0.801	19-Week SPI
Grass MSAVI	0.478	17-Week SPI

Table 9: Most Significant Correlations for Vegetation Indices at Drought Plot, one week lag

Vegetation Index	Correlation Coefficient	Drought Index
Shrub NDVI	0.817	13-Week SPI
Grass NDVI	0.737	16-Week SPI
Shrub NDWI	0.229	4-Week SPI
Grass NDWI	0.24	28-Week SPI
Shrub VIN	0.838	13-Week SPI
Grass VIN	0.735	16-Week SPI
Shrub SAVI	0.828	18-Week SPI
Grass SAVI	0.57	16-Week SPI
Shrub ARVI	0.829	13-Week SPI
Grass ARVI	0.747	16-Week SPI
Shrub RSVI	0.774	30-Week SPI
Grass RSVI	-0.546	8-Week SPI
Shrub WBI	0.318	PDI
Grass WBI	0.723	PDI
Shrub RVI	-0.809	13-Week SPI
Grass RVI	-0.733	16-Week SPI
Shrub NDGI	0.63	13-Week SPI
Grass NDGI	0.403	13-Week SPI
Shrub NDRI	-0.63	13-Week SPI
Grass NDRI	-0.403	13-Week SPI
Shrub NDI	0.457	14-Week SPI
Grass NDI	0.451	PDI
Shrub MSAVI	0.832	18-Week SPI
Grass MSAVI	0.532	15-Week SPI

Table 10: Most Significant Correlations for Vegetation Indices at Drought Plot, two weeks lag

Vegetation Index	Correlation Coefficient	Drought Index
Shrub NDVI	0.817	9-Week SPI
Grass NDVI	0.74	15-Week SPI
Shrub NDWI	0.219	10-Week SPI
Grass NDWI	0.271	27-Week SPI
Shrub VIN	0.808	12-Week SPI
Grass VIN	0.739	15-Week SPI
Shrub SAVI	0.766	17-Week SPI
Grass SAVI	0.584	15-Week SPI
Shrub ARVI	0.816	12-Week SPI
Grass ARVI	0.754	15-Week SPI
Shrub RSVI	0.69	29-Week SPI
Grass RSVI	-0.598	6-Week SPI
Shrub WBI	0.257	PDI
Grass WBI	0.706	PDI
Shrub RVI	-0.816	9-Week SPI
Grass RVI	-0.735	15-Week SPI
Shrub NDGI	0.618	7-Week SPI
Grass NDGI	0.436	16-Week SPI
Shrub NDRI	-0.618	7-Week SPI
Grass NDRI	-0.436	16-Week SPI
Shrub NDI	0.454	12-Week SPI
Grass NDI	0.489	PDI
Shrub MSAVI	0.77	17-Week SPI
Grass MSAVI	0.549	15-Week SPI

Table 11: Most Significant Correlations for Vegetation Indices at Drought Plot, three weeks lag

Vegetation Index	Correlation Coefficient	Drought Index
Shrub NDVI	0.815	8-Week SPI
Grass NDVI	0.674	14-Week SPI
Shrub NDWI	0.264	1-Week SPI
Grass NDWI	0.309	1-Week SPI
Shrub VIN	0.795	8-Week SPI
Grass VIN	0.66	14-Week SPI
Shrub SAVI	0.764	11-Week SPI
Grass SAVI	0.521	14-Week SPI
Shrub ARVI	0.802	8-Week SPI
Grass ARVI	0.694	14-Week SPI
Shrub RSVI	0.697	23-Week SPI
Grass RSVI	-0.645	5-Week SPI
Shrub WBI	0.281	6-Week SPI
Grass WBI	0.688	PDI
Shrub RVI	-0.814	8-Week SPI
Grass RVI	-0.678	14-Week SPI
Shrub NDGI	0.633	6-Week SPI
Grass NDGI	0.429	15-Week SPI
Shrub NDRI	-0.633	6-Week SPI
Grass NDRI	-0.429	15-Week SPI
Shrub NDI	0.476	11-Week SPI
Grass NDI	0.46	PDI
Shrub MSAVI	0.766	11-Week SPI
Grass MSAVI	0.487	14-Week SPI

Table 12: Most Significant Correlations for Vegetation Indices at Drought Plot, four weeks lag

Vegetation Index	Correlation Coefficient	Drought Index
Shrub NDVI	0.836	5-Week SPI
Grass NDVI	0.72	13-Week SPI
Shrub NDWI	0.247	2-Week SPI
Grass NDWI	0.201	25-Week SPI
Shrub VIN	0.817	5-Week SPI
Grass VIN	0.708	13-Week SPI
Shrub SAVI	0.792	10-Week SPI
Grass SAVI	0.597	12-Week SPI
Shrub ARVI	0.823	5-Week SPI
Grass ARVI	0.748	13-Week SPI
Shrub RSVI	0.707	22-Week SPI
Grass RSVI	-0.665	4-Week SPI
Shrub WBI	0.345	5-Week SPI
Grass WBI	0.683	PDI
Shrub RVI	-0.834	5-Week SPI
Grass RVI	-0.722	13-Week SPI
Shrub NDGI	0.67	5-Week SPI
Grass NDGI	0.54	14-Week SPI
Shrub NDRI	0.413	5-Week SPI
Grass NDRI	-0.03	14-Week SPI
Shrub NDI	0.49	10-Week SPI
Grass NDI	0.447	PDI
Shrub MSAVI	0.794	10-Week SPI
Grass MSAVI	0.568	12-Week SPI

Table 13: Most Significant Correlations for Vegetation Indices at Drought Plot, five weeks lag

Vegetation Index	Correlation Coefficient	Drought Index
Shrub NDVI	0.817	5-Week SPI
Grass NDVI	0.708	5- and 9-Week SPI
Shrub NDWI	0.256	1-Week SPI
Grass NDWI	0.192	24-Week SPI
Shrub VIN	0.806	5-Week SPI
Grass VIN	0.704	9-Week SPI
Shrub SAVI	0.798	8- and 9-Week SPI
Grass SAVI	0.629	11-Week SPI
Shrub ARVI	0.802	5-Week SPI
Grass ARVI	0.733	9-Week SPI
Shrub RSVI	0.734	21-Week SPI
Grass RSVI	0.619	PDI
Shrub WBI	0.31	4-Week SPI
Grass WBI	0.695	30-Week SPI
Shrub RVI	-0.814	5-Week SPI
Grass RVI	-0.707	5-Week SPI
Shrub NDGI	0.615	4-Week SPI
Grass NDGI	0.52	9-Week SPI
Shrub NDRI	-0.615	4-Week SPI
Grass NDRI	-0.52	9-Week SPI
Shrub NDI	0.459	9-Week SPI
Grass NDI	0.425	PDI
Shrub MSAVI	0.8	8- and 9-Week SPI
Grass MSAVI	0.606	11-Week SPI

Table 14: Most Significant Correlations for Vegetation Indices at Irrigated Plot, no lag

Vegetation Index	Most Significant Correlation	Drought Scale
WS Shrub NDVI	0.689	4-Week SPI
WS Shrub NDWI	-0.291	27-Week SPI
WS Shrub VIN	0.716	4-Week SPI
WS Shrub SAVI	-0.38	30-Week SPI
WS Shrub ARVI	0.692	4-Week SPI
WS Shrub RSVI	-0.414	24-Week SPI
WS Shrub WBI	0.379	4-Week SPI
WS Shrub RVI	-0.68	4-Week SPI
WS Shrub NDGI	0.712	4-Week SPI
WS Shrub NDRI	-0.712	4-Week SPI
WS Shrub NDI	-0.362	30-Week SPI
WS Shrub MSAVI	-0.34	4-Week SPI

Table 15: Most Significant Correlations for Vegetation Indices at Irrigated Plot, one-week lag

Vegetation Index	Most Significant Correlation	Drought Scale
WS Shrub NDVI	0.68	2-Week SPI
WS Shrub NDWI	-0.252	30-Week SPI
WS Shrub VIN	0.665	3-Week SPI
WS Shrub SAVI	-0.355	30-Week SPI
WS Shrub ARVI	0.618	2-Week SPI
WS Shrub RSVI	-0.391	23-Week SPI
WS Shrub WBI	-0.248	30-Week SPI
WS Shrub RVI	-0.68	2-Week SPI
WS Shrub NDGI	0.55	3-Week SPI
WS Shrub NDRI	-0.55	2-Week SPI
WS Shrub NDI	0.333	3-Week SPI
WS Shrub MSAVI	0.419	3-Week SPI

Table 16: Most Significant Correlations for Vegetation Indices at Irrigated Plot, two weeks lag

Vegetation Index	Most Significant Correlation	Drought Scale
WS Shrub NDVI	0.652	2-Week SPI
WS Shrub NDWI	-0.274	30-Week SPI
WS Shrub VIN	0.642	2-Week SPI
WS Shrub SAVI	0.436	2-Week SPI
WS Shrub ARVI	0.589	2-Week SPI
WS Shrub RSVI	-0.35	21-Week SPI
WS Shrub WBI	-0.245	30-Week SPI
WS Shrub RVI	-0.651	2-Week SPI
WS Shrub NDGI	0.512	2-Week SPI
WS Shrub NDRI	0.346	2-Week SPI
WS Shrub NDI	-0.351	30-Week SPI
WS Shrub MSAVI	0.525	2-Week SPI

Table 17: Most Significant Correlations for Vegetation Indices at Irrigated Plot, three weeks lag

Vegetation Index	Most Significant Correlation	Drought Scale
WS Shrub NDVI	0.4	1-Week SPI
WS Shrub NDWI	-0.412	3-Week SPI
WS Shrub VIN	0.414	1-Week SPI
WS Shrub SAVI	0.462	1-Week SPI
WS Shrub ARVI	0.389	1-Week SPI
WS Shrub RSVI	-0.318	21-Week SPI
WS Shrub WBI	0.389	1-Week SPI
WS Shrub RVI	-0.394	1-Week SPI
WS Shrub NDGI	0.46	1-Week SPI
WS Shrub NDRI	-0.46	1-Week SPI
WS Shrub NDI	-0.371	26-Week SPI
WS Shrub MSAVI	0.503	1-Week SPI

Table 18: Most Significant Correlations for Vegetation Indices at Irrigated Plot, four weeks lag

Vegetation Index	Most Significant Correlation	Drought Scale
WS Shrub NDVI	-0.324	30-Week SPI
WS Shrub NDWI	-0.387	2-Week SPI
WS Shrub VIN	-0.268	30-Week SPI
WS Shrub SAVI	-0.453	30-Week SPI
WS Shrub ARVI	-0.332	30-Week SPI
WS Shrub RSVI	-0.564	8-Week SPI
WS Shrub WBI	-0.283	1-Week SPI
WS Shrub RVI	0.332	30-Week SPI
WS Shrub NDGI	-0.429	30-Week SPI
WS Shrub NDRI	0.429	30-Week SPI
WS Shrub NDI	-0.405	2-Week SPI
WS Shrub MSAVI	-0.426	2-Week SPI

Table 19: Most Significant Correlations for Vegetation Indices at Irrigated Plot, five weeks lag

Vegetation Index	Most Significant Correlation	Drought Scale
WS Shrub NDVI	-0.332	30-Week SPI
WS Shrub NDWI	-0.327	30-Week SPI
WS Shrub VIN	-0.274	30-Week SPI
WS Shrub SAVI	-0.408	30-Week SPI
WS Shrub ARVI	-0.338	30-Week SPI
WS Shrub RSVI	-0.444	7-Week SPI
WS Shrub WBI	0.42	1-Week SPI
WS Shrub RVI	0.34	30-Week SPI
WS Shrub NDGI	-0.432	30-Week SPI
WS Shrub NDRI	0.432	30-Week SPI
WS Shrub NDI	-0.426	30-Week SPI
WS Shrub MSAVI	-0.364	30-Week SPI

6. CONCLUSIONS AND FUTURE WORK

This thesis has examined the statistical differences between vegetation spectral reflectance data collected from rain-sheltered, irrigated and control vegetation plots using T-Tests, as well as possible correlations between vegetation indices and drought stress as interpreted by the Standardized Precipitation Index and Palmer Drought Index. The vegetation under study was creosote shrubs and gramma grass located in a rain-sheltered plot and a control plot, as well as an irrigated creosote shrub and a control creosote shrub at a separate location. Reflectance data was collected from these plots from January 2003 to October 2004 on a bi-weekly basis (weekly during the month of August 2003) unless weather or instrument error intervened. The precipitation was obtained from the 5-Points weather station administered by the Sevilleta National Wildlife Refuge Long-term Ecological Research Center, from 1999-2004, and SPI data was calculated from this precipitation using a computer program downloaded from the National Drought Mitigation Center. PDI data was obtained from the National Climatic Data Center. The vegetation indices calculated were the NDVI, NDWI, VIN, SAVI, ARVI, RSVI, WBI, RVI, NDGI, NDRI, NDI and MSAVI.

It was concluded from the T-test statistical analysis that there was an 91% success rate from analysis of these vegetation indices to examine the difference between irrigated and control creosote vegetation, and rain-sheltered and control grass. However, the success rate was only 50% for the difference between rain-sheltered and control creosote

shrubs. It can be inferred from these conclusions that creosote is more drought-resistant than gramma grass, and that vegetation indices can be used to detect drought-stressed vegetation when compared to reference measurements of healthy vegetation.

It was also concluded that of the previously mentioned vegetation indices, the NDVI, VIN, SAVI, MSAVI and RVI, are good proxy indicators of weekly SPI drought severity as calculated from field reflectance data of shrubs and grasses collected at the Rain-sheltered Site and that time lags are incorporated in the SPI timescale. With no time lag, the most significant correlation for the shrub NDVI was 0.818 with the 14-Week SPI, and for the grass NDVI was 0.726 with the 17-Week SPI. The most significant correlation for the Shrub VIN with no time lag was 0.848 with the 14-Week SPI and 0.715 for the Grass VIN with the 17-Week SPI. The most significant correlation for the Shrub SAVI was 0.796 with the 19-Week SPI, and 0.522 for the Grass SAVI with the 17-Week SPI. The most significant correlation for the Shrub RVI was -0.808 with the 14-Week SPI and -0.727 for the Grass RVI with the 17-Week SPI. The most significant correlation for the Shrub MSAVI was 0.801 with the 19-Week SPI and 0.478 for the Grass MSAVI with the 17-Week SPI. It was also concluded that creosote shrub vegetation indices are more strongly correlated with precipitation and SPI values than gramma grass vegetation indices. However, this conclusion is based upon field-reflectance measurements, and it is more practical to use grass relationships for wider scale remote sensing measurements, until better methods of classification and spectral identity extraction are perfected and investigated due to the difficulty of identifying shrub regions with coarse resolution data. The PDI data is significantly correlated only with the grass WBI data with a correlation of 0.736, and in general is not very responsive or useful

for detection with most remote sensing measurements. Furthermore, it was concluded that the high correlation of the field data from the drought plot with longer drought time scales indicates that the total amount of precipitation is the most significant factor to semi-arid vegetation vigor, and not just the frequency of precipitation events. This is supported by the Irrigated Site data, which only had significant correlations with much shorter timescales. The most significant correlation for the Irrigated Shrub NDVI was 0.689 with the 4-Week SPI; for the Irrigated Shrub VIN was 0.716 with the 4-Week SPI; for the Irrigated Shrub ARVI was 0.692 with the 4-Week SPI; for the Irrigated Shrub NDGI was 0.712 with the 4-Week SPI; and for the Irrigated Shrub NDRI was -0.712 with the 4-Week SPI. This may be due to the extra moisture it received compared to the control shrub and grass plot at the Rain-sheltered site.

The results from the satellite up scaling were not very conclusive. Pixel analysis comparing results of NDMC SPI drought data and predicted drought data from linear regression of the 12-Week SPI and Shrub/Grass NDVI gave conflicting results, from 0% agreement to 72% agreement. This confliction is most likely due to the issues of land cover classification, spectral un-mixing, and synchronization of land-based spectral sensors and satellite-based spectral sensors. Some work has been done in this area (Maingi *et al* 2002; Skirvin *et al,* 2004, Asner and Heidebrecht, 2002, Qi *et al*, 2002) and should be reviewed for more insights on land cover classification and spectral un-mixing, particularly the use of the SWIR2 regions for un-mixing analysis. Also, the exact relationship between ground-based vegetation indices and satellite-based indices may need to be examined, in case there is a significant difference due to sensor construction or data acquisition methods. While the ground-based data in this thesis was corrected for

solar zenith angle and time of measurement, it is not always apparent whether or not satellite imagery is corrected in a similar manner. This data is for a one-year period, and the relationships may vary from year to year; so further data collection should be implemented to more fully document the temporal variance of vegetation spectral response.

There are significant areas of this research that can be explored more fully. One area is a continued/expanded collection of field data, both vegetation reflectance data and precipitation data to better identify long-term trends and clarify existing relationships between both. Also, seasonal effects should be considered to get more accurate results from existing relationships, and a longer-data collection period should more clearly discriminate between seasonal effects and random changes in value. Another possibility is the investigation of other vegetation indices for correlation with SPI drought values. The simplest method would be to use all possible differentiated ratios in available satellite bands, and investigate the responses of these ratios to time and precipitation, as well as to investigate any difference between rain-sheltered, irrigated and control vegetation. This would require investigation into the real-world causes of these responses and how the plant biology causes the changes in ratios. I limited this research to vegetation indices previously described by other scientists, but the potential for further statistical investigation is limitless.

Another area which has potential for future work is the use of satellite imagery and drought analysis. This has been done extensively as presented in the literature review, but I think that analysis of satellite imagery time series over semi-arid regions on the same level as that done over prairie grasslands like Ji (2003) and Peters (2001) will produce

more accurate results of seasonal NDVI and other vegetation index responses of regional land cover. As previously stated, an investigation into the exact correlation between field-measured vegetation indices and satellite-measured vegetation indices should better assist in creating SPI images along with better classification of remote sensing images. Finally, although it is not directly connected to this research, further study of image classification via vegetation indices and spectral un-mixing would be very beneficial in using field remote sensing results and is deserving of its own separate research, as can be seen in Qi *et al* (2002).

APPENDICES

The following appendices contain operation theory and instruction for the Analytical Spectral Devices Fieldspec Pro spectroradiometer, code for the Perlscript program used to process the radiance data measured in the field, correlations of soil vegetation indices with SPI measurements, and linear regression graphs of selected indices

Appendix A

The following is a description of the Analytical Spectral Devices Fieldspec Pro Spectroradiometer. This instrument was used to collect radiance data for this master's thesis. The Fieldspec Pro is a highly portable general-purpose spectroradiometer useful for recording the absolute or relative measurements of electromagnetic energy in either a field or lab setting. The instrument uses a fiber-optic bundle to collect light. Inside the instrument, light is protected from the fiber optics onto a holographic diffraction grating where the wavelength components are separated and reflected for independent measurements by the detectors. Each detector converts incident photons into electrons that are stored, or integrated, until the detector is "read out". At readout time, the photoelectric current for each detector is converted to a voltage and is digitized by a 16-bit analog to digital converter. The digital data is then transferred directly to the computer's main memory using the Enhanced Parallel Port on the controlling computer. The spectral data is then available for processing by the controlling software.

The Visible/Near Infrared (VNIR) portion of the spectrum, the 350-1050 nm wavelength domain, is most commonly measured by a 512-channel silicon photodiode array overlaid with an order separation filter. Each channel, an individual detector itself, is geometrically positioned to receive light within a narrow (1.4 nm) bandwidth. The VNIR spectrometer has a spectral resolution of approximately 3 nm at around 700 nm. The Shortwave Infrared (SWIR), also called the Near Infrared (NIR) portion of the

spectrum is acquired with two scanning spectrometers. These differ from the array used in the VNIR in that they measure wavelengths sequentially, rather than simultaneously. Each spectrometer consists of a concave holographic grating and a single thermoelectrically cooled indium gallium arsenide detector. The gratings are mounted about a common shaft which oscillates with a period of about 200 milliseconds. Unlike the VNIR, each SWIR spectrometer has only one detector, which is exposed to different wavelengths of light as the grating oscillates. The first spectrometer (SWIR1) measures light between about 900-1850 nm, while the second (SWIR2) measures light between about 1700-2500 nm. The controlling software automatically accounts for the overlap in wavelength intervals by using a preset wavelength within the common subset at which to place a "splice". The sampling interval for each SWIR region is about 2 nm and the spectral resolution varies between 10 nm and 12 nm, depending on the scan angle at that wavelength.

Light energy is collected through a bundle of specially formulated optical fibers which are precisely cut, polished and sealed. The fiber optic cable has a conical view subtending a full angle of about 25 degrees. The raw data (raw DN for "digital numbers") returned by the FieldSpec Pro are 16-bit numbers corresponding to the output of each element in the VNIR detector array and each 2 nm sample of the SWIR spectra. All other data types such as reflectance, radiance and irradiance are calculated by the software fro these raw digital numbers. Raw data is a function both of the characteristics of the light field being measured and of the instrument itself. Parameters such as the foreoptic transmission, fiberoptic transmission, grating efficiency and detector sensitivity all vary with wavelength. This results in a raw spectrum whose shape can be very different from

that of the radiance spectrum of the light field being measured. Because these parameters do not vary with time though, a linear relationship does exist between the raw spectra and the intensity of the light field being measured.

Recorded data is stored on the controlling computer's hard drive for processing with ViewSpec Pro (the processing software specifically for this instrument). The data can be viewed in graphical format, statistically analyzed or converted into ASCII format for use with Microsoft Excel or other data processing software.

Appendix B

Many computer programs were written or utilized to facilitate more rapid data processing for this thesis research. These included:

- A Perl script written by Matt Richmond (formerly of New Mexico Tech) and modified by Geoffrey Marshall, which was used to calculate a single radiance value for all radiance measurements taken per target, while corrected for solar zenith angle and Julian day.
- A C++ program from the National Drought Mitigation Center used to calculate SPI values over varying time scales.
- Various macros written by Geoffrey Marshall in Microsoft Excel to calculate and manipulate spreadsheet values during data analysis.
- Commercial software such as Minitab 14 for statistical analysis, Microsoft Excel for analysis and data manipulation, ViewSpec Pro for collecting radiance data from the spectroradiometer and converting said data to ASCII format, Microsoft Word, etc.

The Perl script is reproduced overleaf *verbatim*. The script shown was created for the Rain-sheltered Site data while taking into account daylight saving. Variations to this script included latitude and longitude differences for the Irrigated Site, and non-daylight saving time measurement periods. Microsoft Excel Macros can be found on the companion compact disks attached to this thesis containing the field data measurements.

```
--------------------------------------------------------------------------------

#!/usr/bin/perl -w

print "Enter the julian day for this measurement: ";
$jday = <STDIN>;
$wave_min = 350;
$wave_max = 2500;
$Pi = 3.14159265358979;
$Longitude = 106.733;                           #Approximate Longtitude
of Study Region, Positive west of Greenwich
$Latitude = 34.338;                             #Approximate Latitude
of Study Region, Positive in Northern Hemisphere
#$EPSILN = 0.016733;                            #Eccentricity of earth
orbit
$SINOB = 0.3978;                                #sine of obliquity of
ecliptic
$DPY = 365.242;                                 #Days per year
$DPH = 15;                                      #Degrees per hour
$RPD = $Pi/180;                                 #Radians to degrees
$DPR = 1/$RPD;                                  #Degrees to radians
$DANG = 2*$Pi*($jday-1)/$DPY;                         #Angle measured
from perihelion in radians which is taken as midnight Jan. 1

$HOMP = 12+0.12357*sin($DANG)-
0.004289*cos($DANG)+0.153809*sin(2*$DANG)+0.060783*cos(2*$DANG);
#HOMP = Hours of Meridian Passage or true solar noon
$ANG = 279.9348*$RPD+$DANG;                     #ANG = Reference -EQ
1.3A
$SIGMA = ($ANG*$DPR+0.4087*sin($ANG)+1.8724*cos($ANG)-
0.0182*sin(2*$ANG)+0.0083*cos(2*$ANG))*$RPD; #SIGMA = Reference - EQ
1.3B
$SINDLT = $SINOB*sin($SIGMA);                   #SINDLT = sine of
Declination angle (EQ 1.2)
$COSDLT = sqrt(1-$SINDLT*2);              #COSDLT = cosine of
declination angle
#-------------------------------------------------------------------------
--------------------------------------

#initialize our hash to store wavelength data in
for ($i = $wave_min; $i <= $wave_max; $i++) {
        $bighash{$i} = 0;
}


########################
#begin script execution

#OK, lets see what files exist in the current directory
# If you want to always use the same directory, do:
# chdir "whatever/directory";
```

```
# first

#now read the directory, and filter out anything that does not end in
.txt
#you may want to change the grep line to change the files it's looking
for
#you'll almost certainly want to do some filtering, as you probably
have
# "." and ".." entries in a directory

opendir (DIRH, ".") or die "Can't read the current directory: $!";
@datafiles = grep {/.txt/} readdir DIRH;
closedir DIRH;

$totalfiles = $#datafiles + 1;
print "reading $totalfiles files:\n";

foreach $file (@datafiles) {
        $state = 0;
        open (DATAFILE, "<$file") or die "Can't open datafile $file:
$!";

        #this is a syntactically strange construct, but you'll find it
        #in almost every perl script.  It reads one line from the file,
        #and sets the variable $_ equal to it.  It quits looping at end
of file
        while (<DATAFILE>) {

                if($_ =~ /Spectrum saved:.* (\d+):(\d+):(\d+)/) {
                        $hour = $1; $minute = $2; $second = $3;
                    #print "$hour $minute $second\n";
                    #convert to decimal
                    $dec_time = $hour + ($minute / 60) + ($second /
3600);
                    #print "$dec_time\n";
                        if($state != 0) {
                                print "this can't happen: got another
time line\n";
                                exit -1;
                        }
                        $state = 1;
                }

                elsif($_ =~ /^(\d+)\s+([0-9\.Ee-]+)/) {
                        $wavelength = $1;
                        $raw_magnitude = $2;
                        if ($state != 1) {
                                print "got to data without getting
time; aborting\n";
                                exit -1;
                        }
                        #print "wavelength: $1 magnitude: $2\n";

                        #at this point, you have $dec_time, so you can
do whatever
                        #processing you need to on the $raw_magnitude
here
```

```
                    #The SZA code was converted from a Fortran code for
finding the cosine of Solar Zenith Angle
                    #Comments are taken directly from the original
Fortran code comments
                    #Constants are defined globally in this code
                    #Reference for this code is from H.M. Woolf, NASA TM
"On The Computation of Solar Elevation Angles and the Determination of
Sunrise and Sunset Times"
                    #Add 7 hours to the time to convert it to GMT, or 6
hours depending on Daylight Saving Time.
                    #DST begins on April 6, 2003 and ends October 26,
2003
                    $Time = $dec_time + 6;                          #GMT at
local time
                    $HANG = $DPH * ($Time - $HOMP) - $Longitude;
#HANG = Hour Angle, a measure of the longitudinal distance to the sun
from the point calculated
                    $COSZENITH = $SINDLT * sin($RPD * $Latitude) +
$COSDLT * cos($RPD * $Latitude) * cos($RPD * $HANG);  #cosine of Zenith
Angle
                          $magnitude = $raw_magnitude/$COSZENITH;
                          #accumulate the magnitude data
                          $bighash{$wavelength} += $magnitude;
                }
        } #end of while loop
        close DATAFILE;
} #end of foreach loop

#output data here in tab separated variable format:
open(OUTFILE, ">output.xls") or die "can't open output file: $!";

for ($i = $wave_min; $i <= $wave_max; $i++) {
        print OUTFILE "$i\t";
        printf OUTFILE "%.14E\n",  $bighash{$i}/$totalfiles ;
}

close OUTFILE;

#all done!
```

Appendix C

This appendix contains correlation values from meteorological analyses, regression figures and other correlation graphs. Figures A-1 through A-12 represent linear correlations between soil vegetation indices (or ratio indices, since the soil is not vegetation) and SPI values. The only ratios that have significant correlations are the ARVI and WBI. The ARVI is probably responding to the soil reflectance in the blue spectrum, while the WBI is responding to the soil water content.

Table 20: Linear Correlation /between Rain-sheltered site control vegetation and various meteorological variables I

	Max Temp	p-value	Min Temp	p-value	Mean Temp	p-value
Shrub NDVI	-0.229	0.283	-0.310	0.140	-0.270	0.201
Grass NDVI	-0.277	0.190	-0.343	0.101	-0.313	0.137
Shrub NDWI	-0.093	0.665	-0.165	0.441	-0.128	0.551
Grass NDWI	-0.210	0.324	-0.275	0.193	-0.242	0.254
Shrub VIN	-0.241	0.257	-0.319	0.128	-0.281	0.183
Grass VIN	-0.295	0.161	-0.354	0.089	-0.328	0.118
Shrub SAVI	-0.488	0.016	-0.532	0.007	-0.515	0.010
Grass SAVI	-0.370	0.075	-0.419	0.042	-0.398	0.054
Shrub ARVI	-0.244	0.250	-0.333	0.112	-0.289	0.170
Grass ARVI	-0.294	0.163	-0.377	0.070	-0.338	0.107
Shrub RSVI	-0.610	0.002	-0.602	0.002	-0.613	0.001
Grass RSVI	-0.348	0.096	-0.238	0.262	-0.297	0.158
Shrub WBI	-0.108	0.615	-0.215	0.313	-0.159	0.457
Grass WBI	-0.498	0.013	-0.537	0.007	-0.521	0.009
Shrub RVI	0.224	0.292	0.307	0.145	0.267	0.208
Grass RVI	0.265	0.210	0.336	0.109	0.303	0.150
Shrub NDGI	-0.004	0.986	-0.107	0.619	-0.053	0.806
Grass NDGI	-0.251	0.236	-0.413	0.045	-0.331	0.115
Shrub RI	0.004	0.986	0.107	0.619	0.053	0.806
Grass RI	0.251	0.236	0.413	0.045	0.331	0.115
Shrub NDI	-0.281	0.183	-0.394	0.057	-0.337	0.107
Grass NDI	-0.248	0.243	-0.311	0.139	-0.279	0.187

Shrub MSAVI	-0.490	0.015	-0.532	0.007	-0.516	0.010
Grass MSAVI	-0.391	0.059	-0.433	0.035	-0.415	0.044

Table 21: Linear Correlation /between Rain-sheltered site control vegetation and various meteorological variables II

	Mean RH	**p-value**	**Mean Vapor**	**p-value**
Shrub NDVI	0.130	0.545	-0.131	0.542
Grass NDVI	0.187	0.383	-0.157	0.463
Shrub NDWI	0.194	0.363	0.023	0.916
Grass NDWI	0.001	0.995	-0.209	0.326
Shrub VIN	0.145	0.500	-0.146	0.497
Grass VIN	0.164	0.444	-0.185	0.386
Shrub SAVI	0.181	0.396	-0.385	0.063
Grass SAVI	0.125	0.562	-0.322	0.125
Shrub ARVI	0.134	0.533	-0.157	0.465
Grass ARVI	0.175	0.413	-0.194	0.365
Shrub RSVI	0.190	0.373	-0.526	0.008
Grass RSVI	-0.052	0.810	-0.418	0.042
Shrub WBI	-0.373	0.072	-0.410	0.047
Grass WBI	-0.180	0.401	-0.692	0.000
Shrub RVI	-0.124	0.564	0.129	0.548
Grass RVI	-0.203	0.342	0.138	0.521
Shrub NDGI	-0.022	0.919	-0.066	0.759
Grass NDGI	-0.062	0.773	-0.401	0.052
Shrub NDRI	0.022	0.919	0.066	0.759
Grass NDRI	0.062	0.773	0.401	0.052
Shrub NDI	0.139	0.517	-0.218	0.305
Grass NDI	-0.138	0.520	-0.373	0.073
Shrub MSAVI	0.183	0.391	-0.386	0.063
Grass MSAVI	0.119	0.580	-0.350	0.093

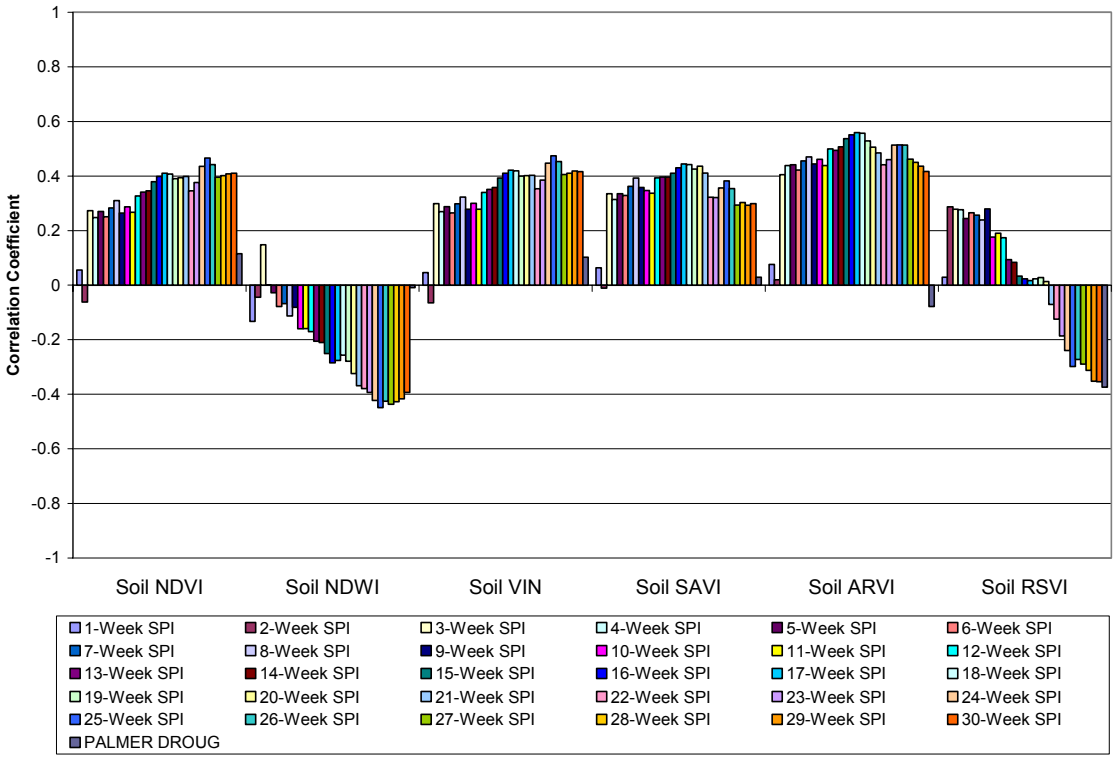

Figure A-1: Linear Correlations between measured Soil ratios and SPI time scales, no lag.

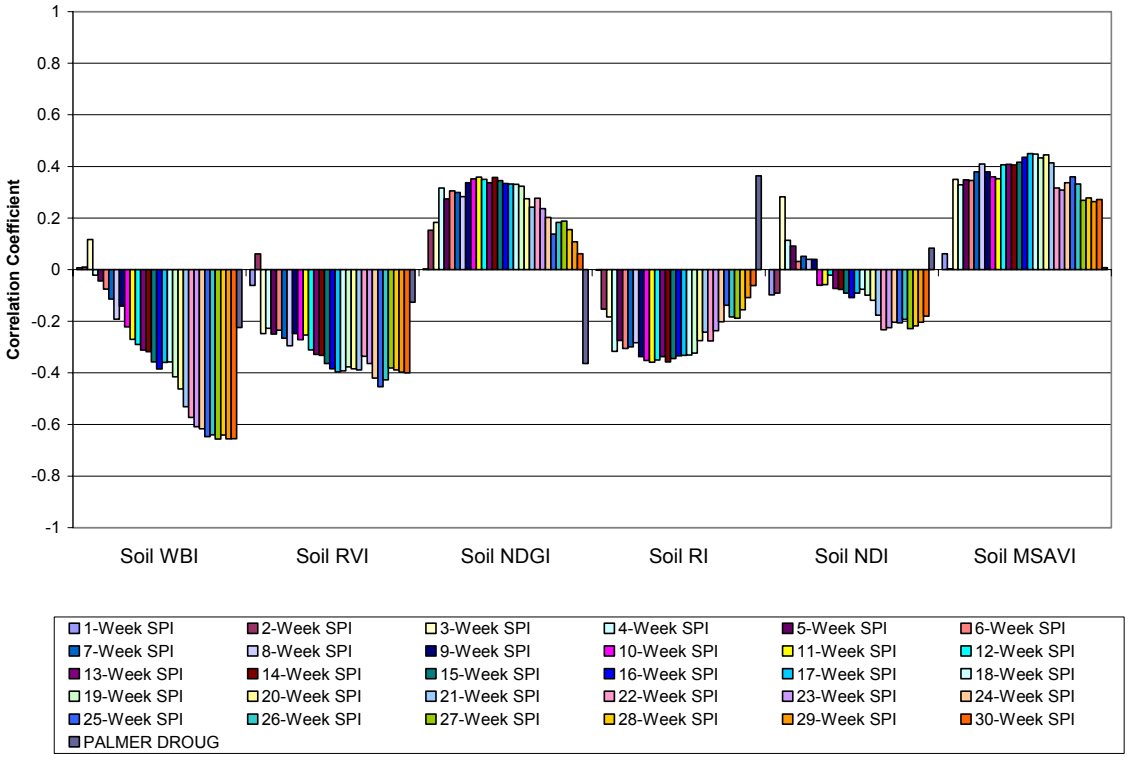

Figure A-2: Linear Correlations between measured Soil ratios and SPI time scales, no lag.

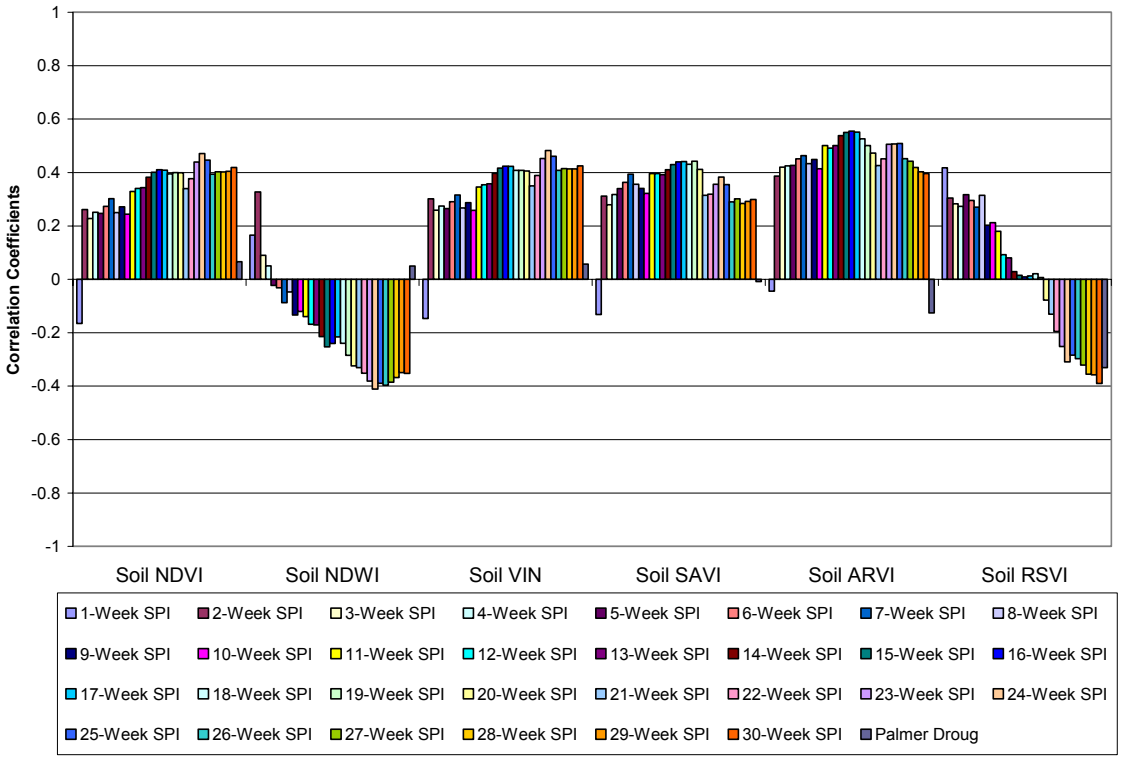

Figure A-3: Linear Correlations between measured Soil ratios and SPI time scales, one week lag.

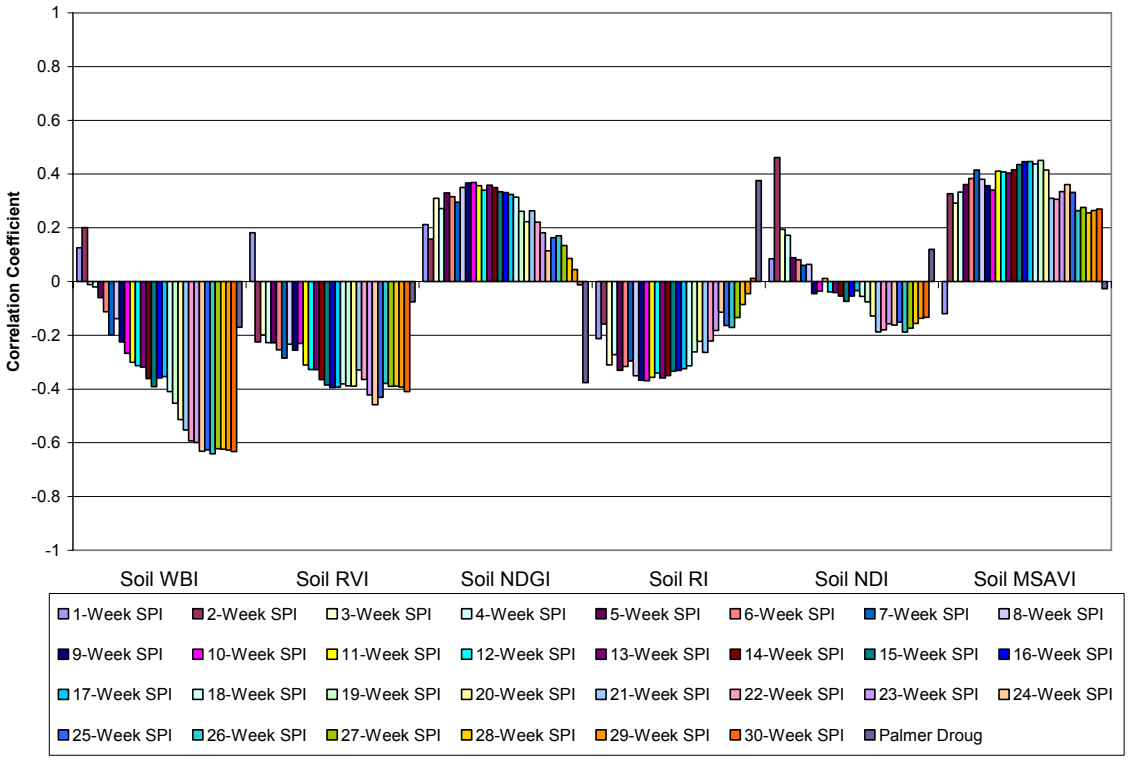

Figure A-4: Linear Correlations between measured Soil ratios and SPI time scales, one week lag.

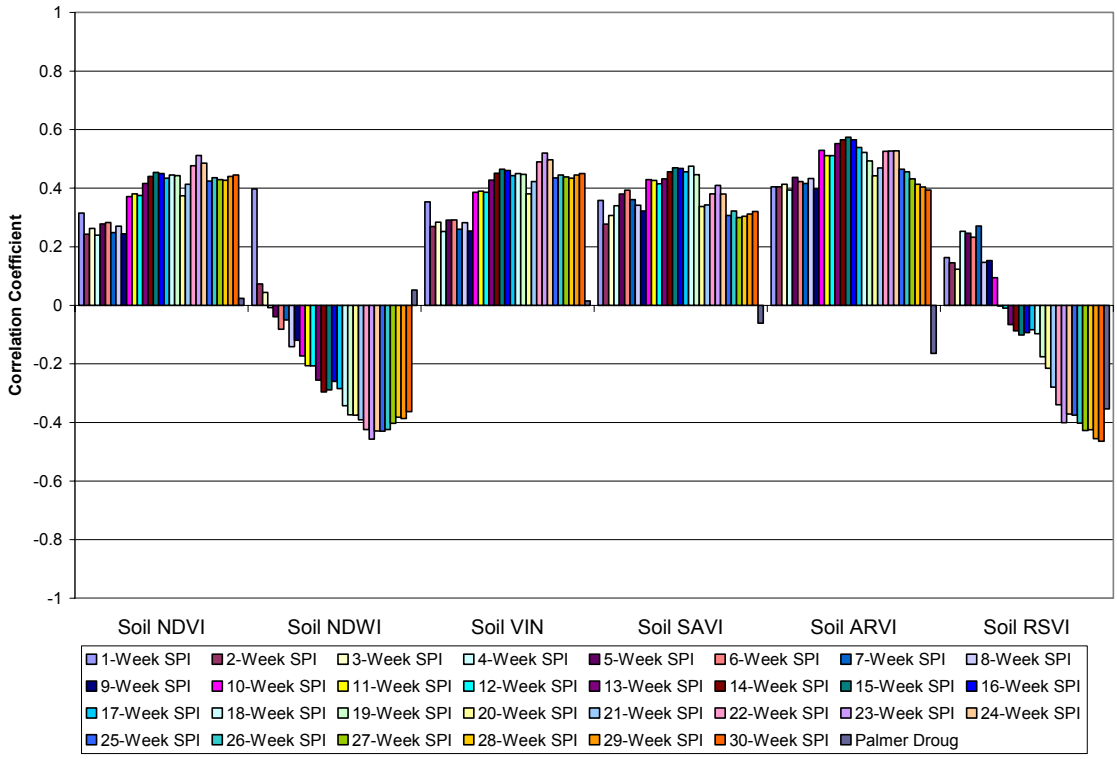

Figure A-5: Linear Correlations between measured Soil ratios and SPI time scales, two week lag.

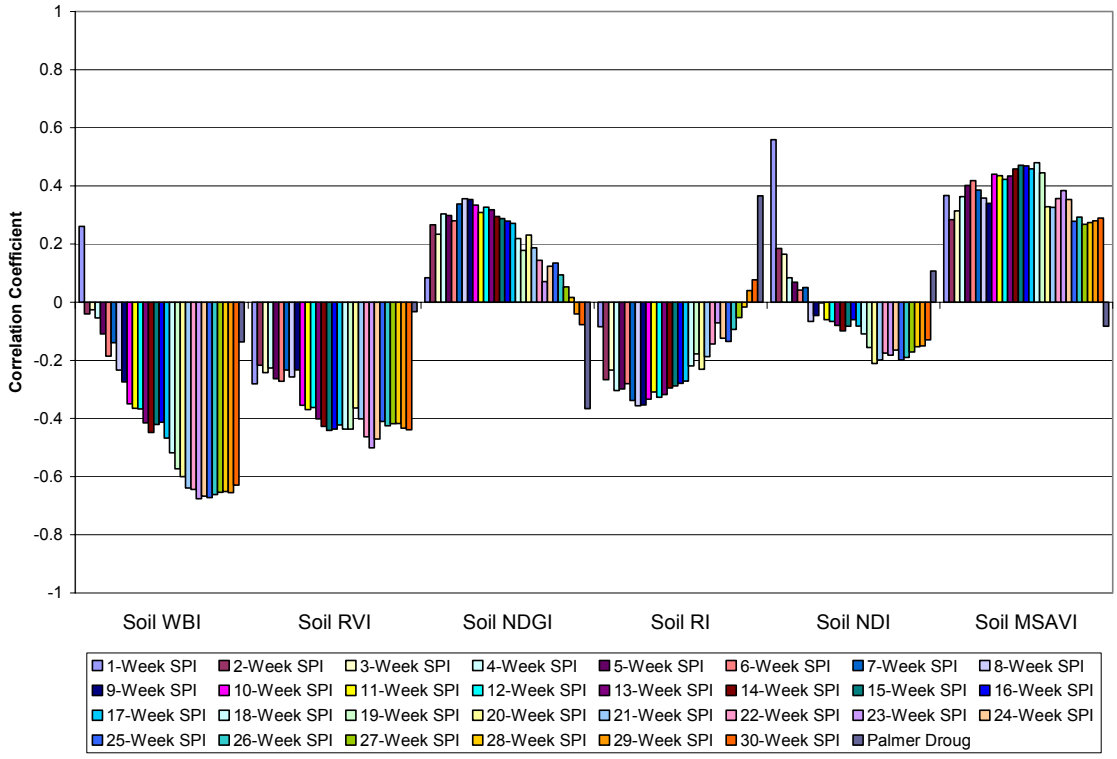

Figure A-6: Linear Correlations between measured Soil ratios and SPI time scales, two week lag.

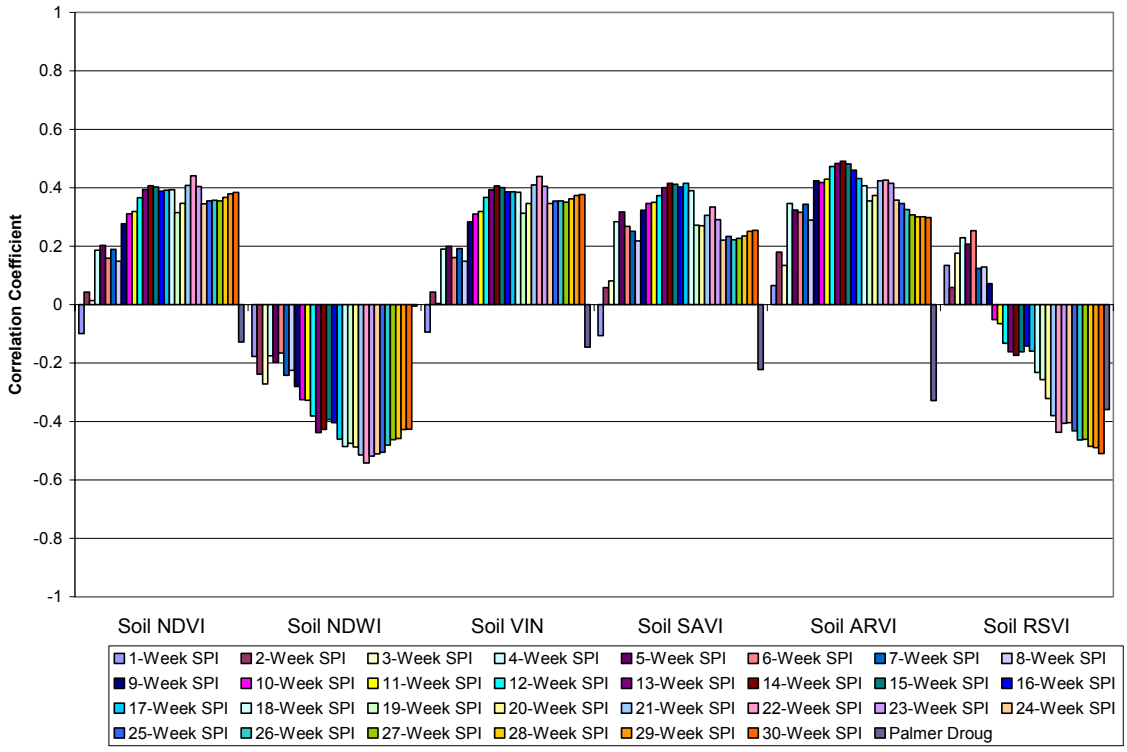

Figure A-7: Linear Correlations between measured Soil ratios and SPI time scales, three week lag.

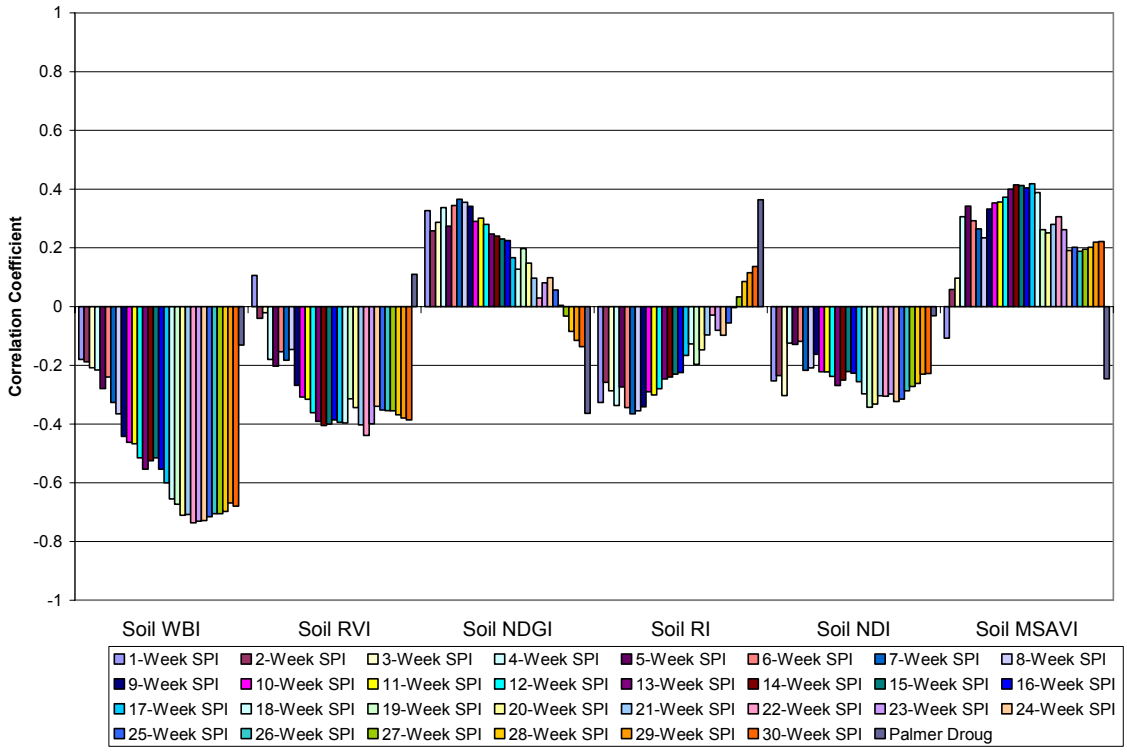

Figure A-8: Linear Correlations between measured Soil ratios and SPI time scales, three week lag.

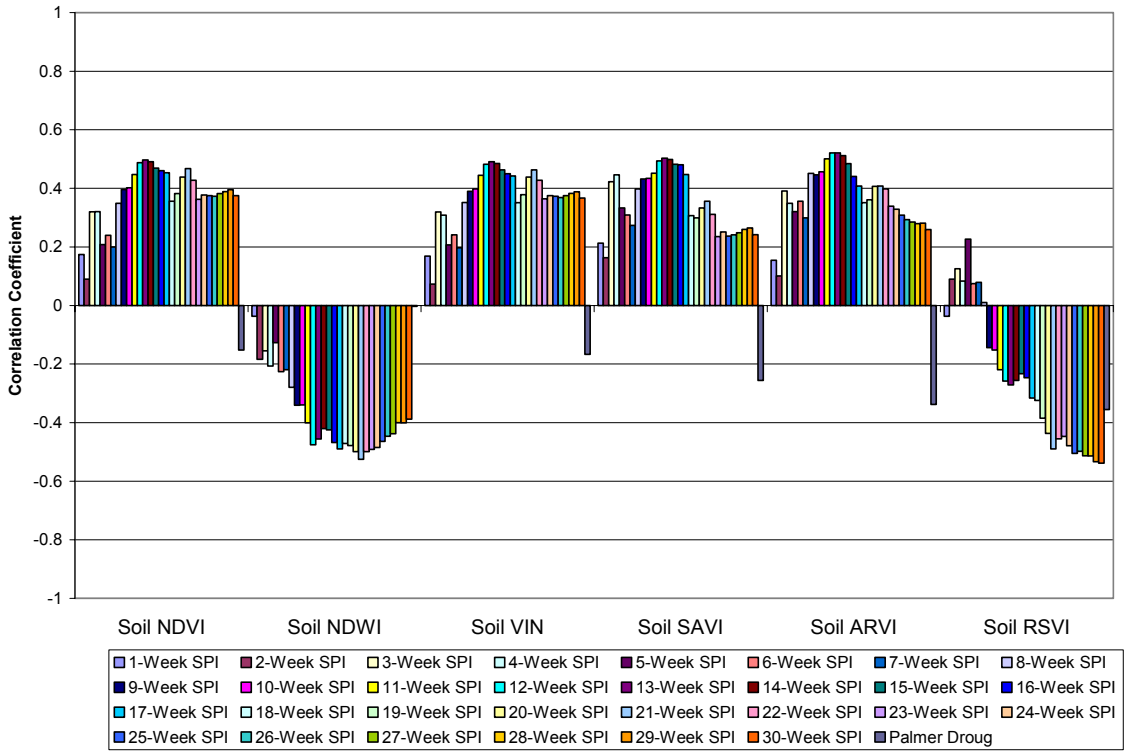

Figure A-9: Linear Correlations between measured Soil ratios and SPI time scales, four week lag.

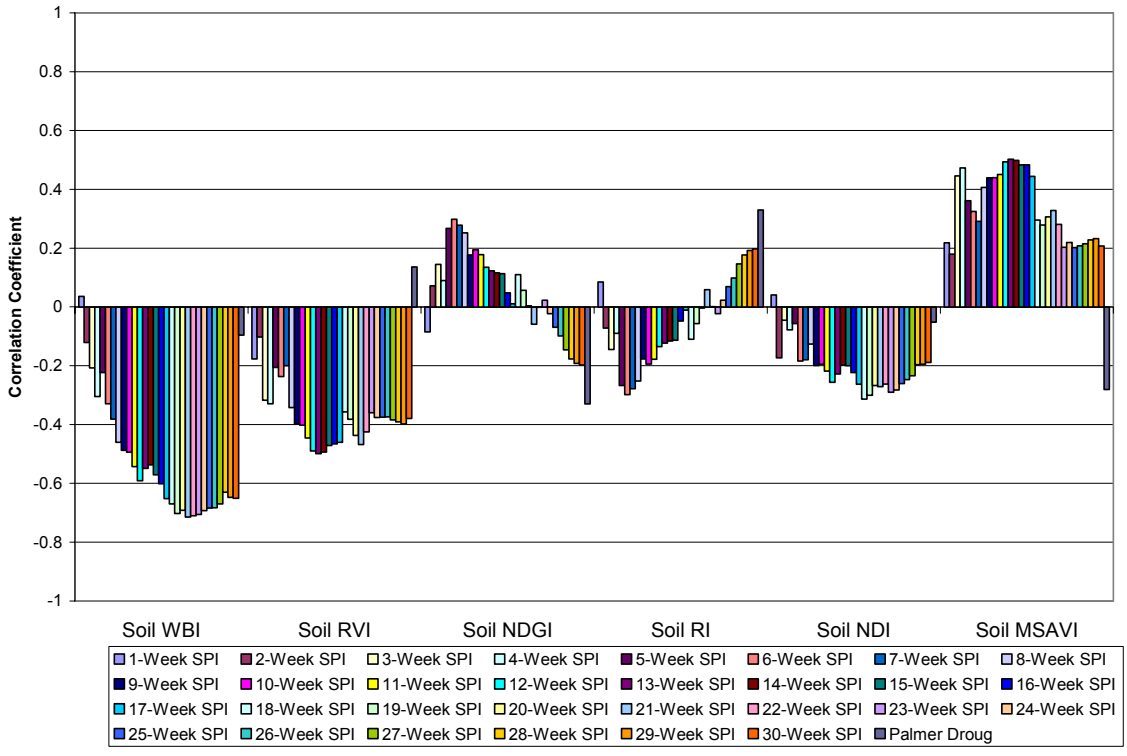

Figure A-10: Linear Correlations between measured Soil ratios and SPI time scales, four week lag.

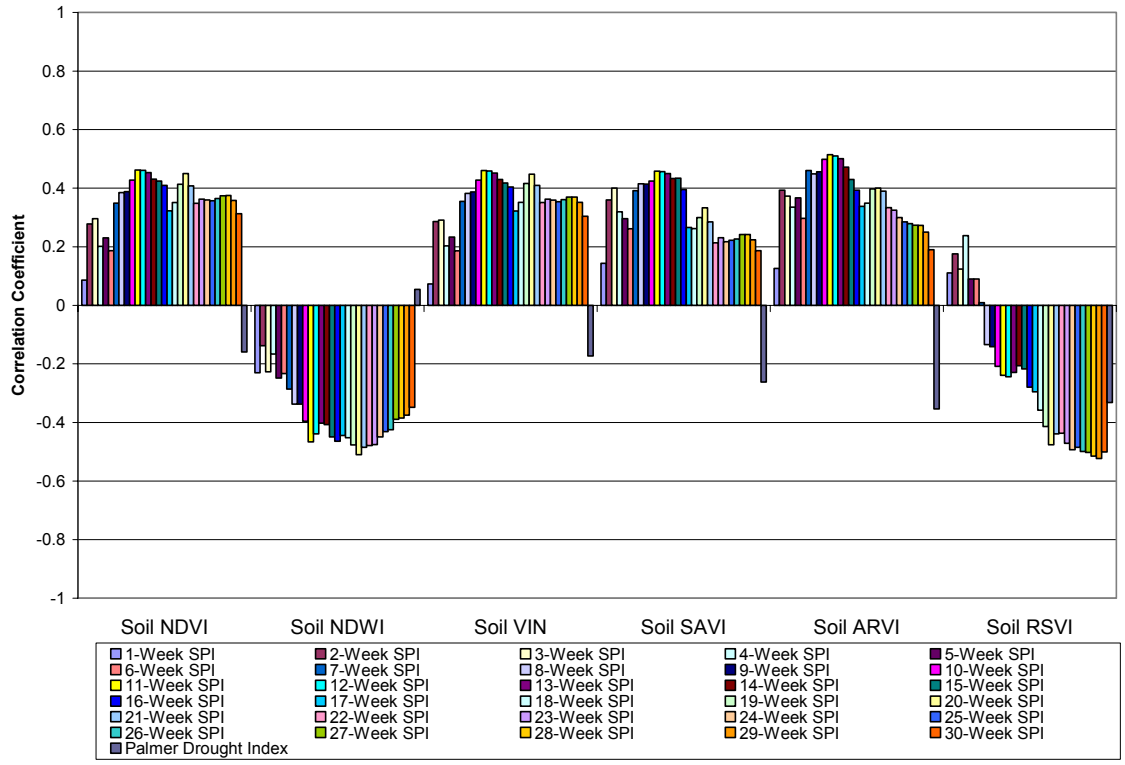

Figure A-11: Linear Correlations between measured Soil ratios and SPI time scales, five week lag.

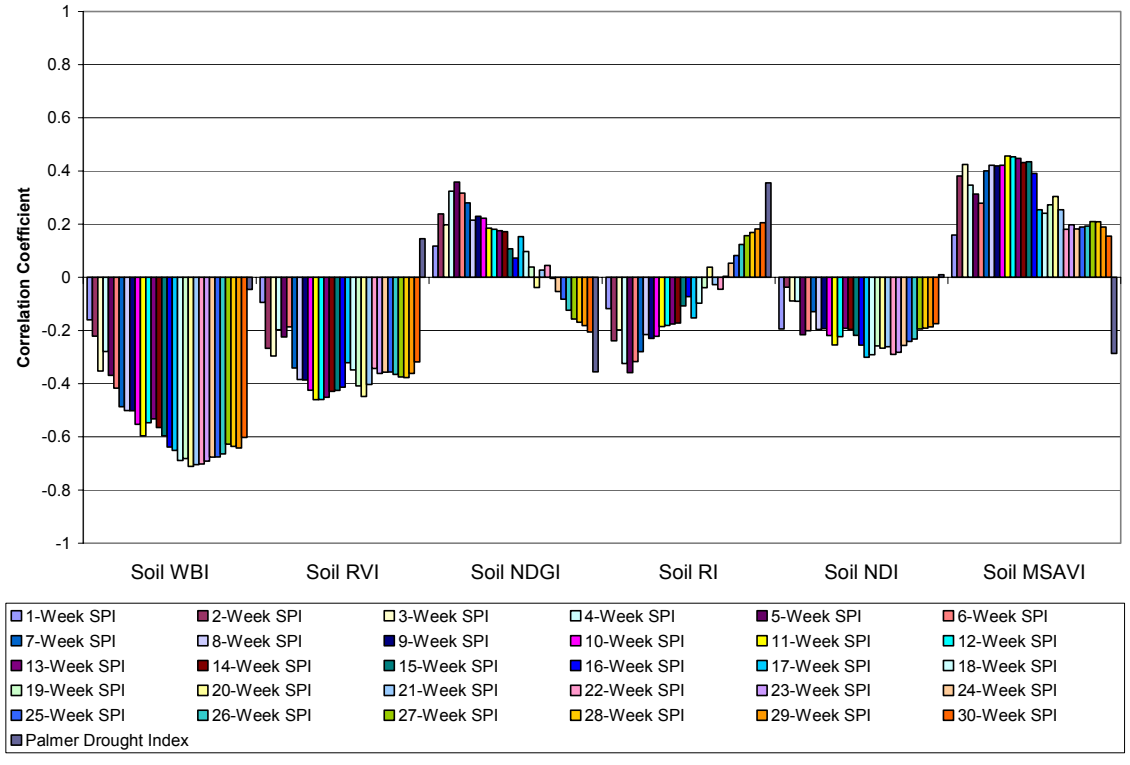

Figure A-12: Linear Correlations between measured Soil ratios and SPI time scales, five week lag.

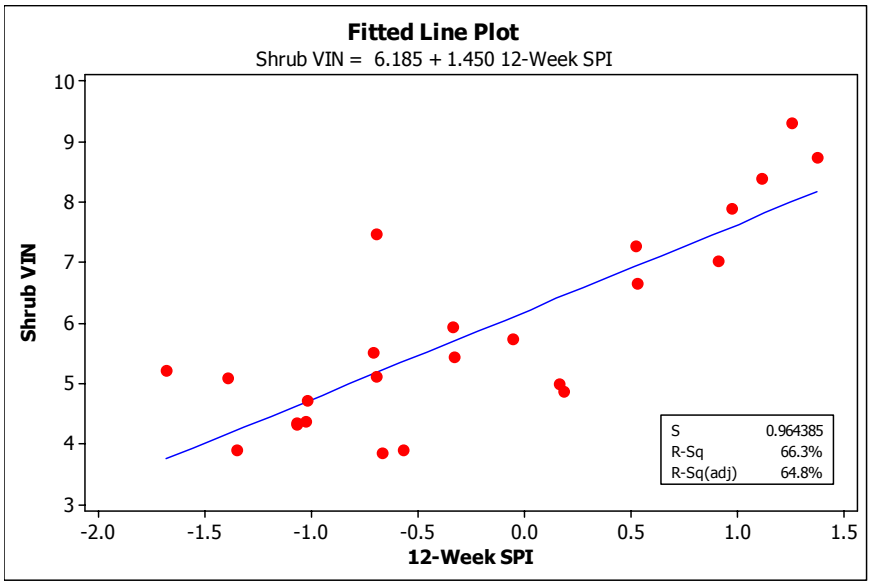

Figure A-13: Linear Regression between Shrub VIN and 12-week SPI, no lag

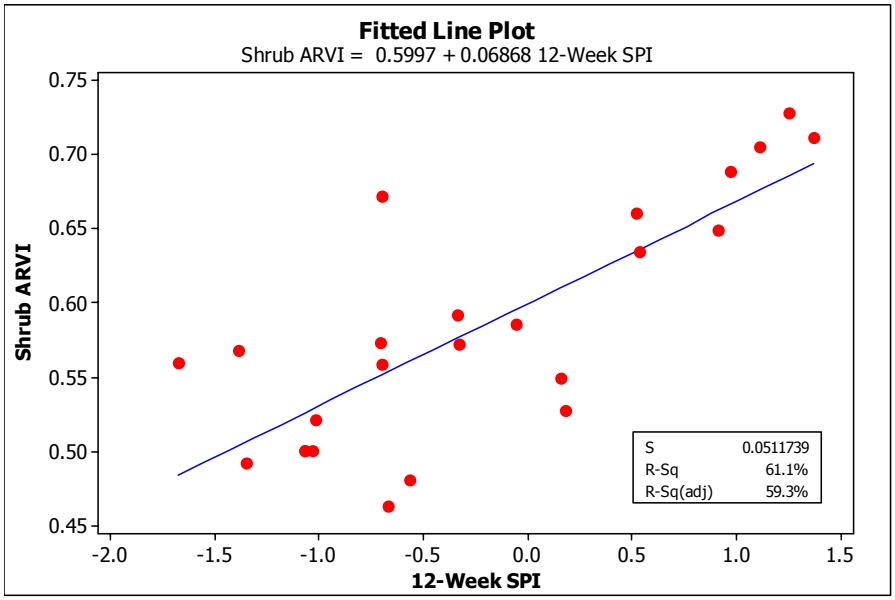

Figure A-14: Linear Regression between Shrub ARVI and 12-Week SPI

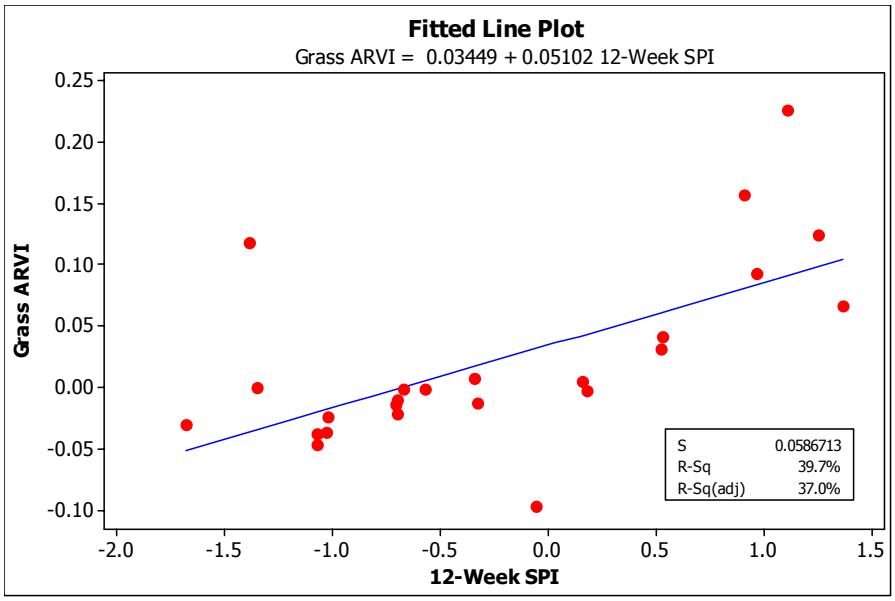

Figure A-15: Linear Regression between Grass ARVI and 12-Week SPI, no lag

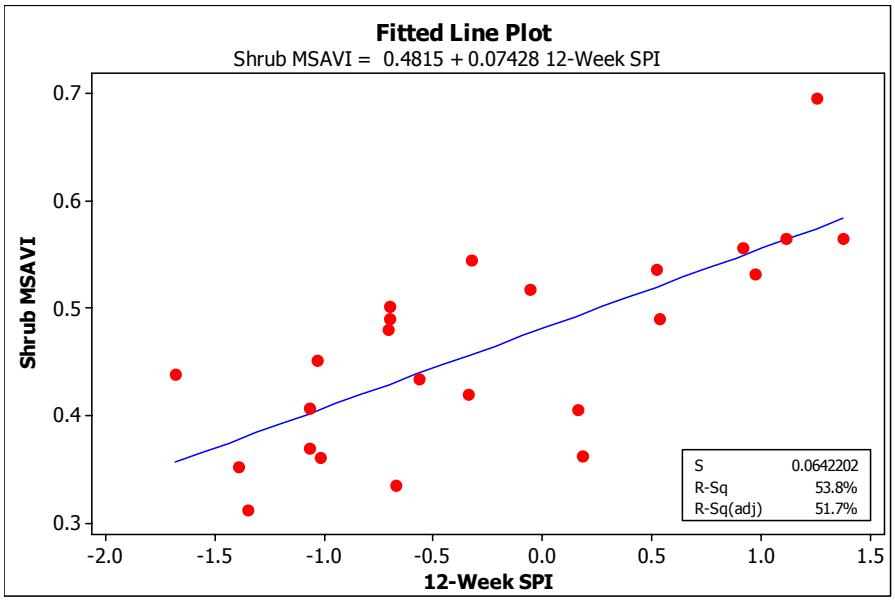

Figure A-16: Linear Regression between Shrub MSAVI and 12-Week SPI, no lag

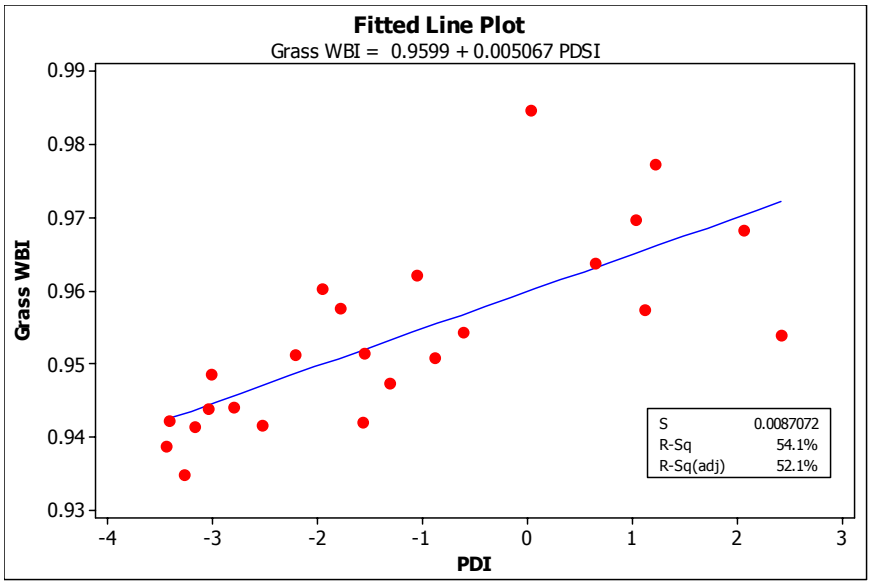

Figure A-17: Linear Regression between Grass WBI and Palmer Drought Index, no lag

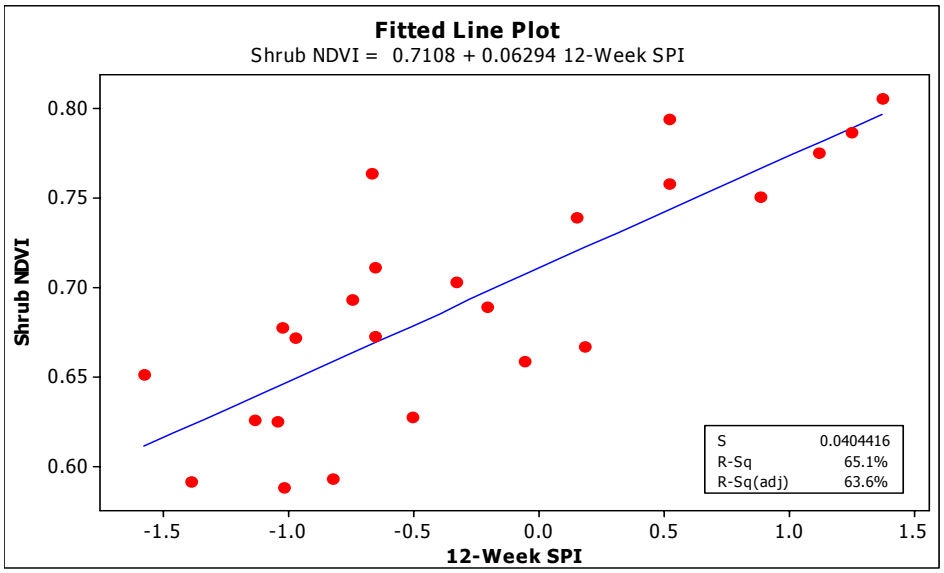

Figure A-18: Linear Regression of Shrub NDVI and 12-week SPI, one week lag

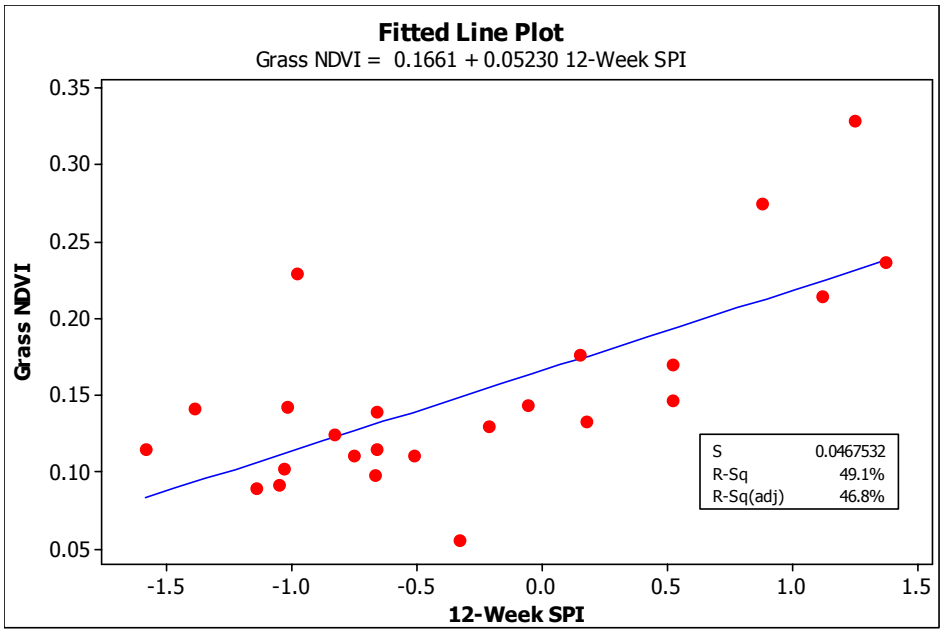

Figure A-19: Linear Regression of Grass NDVI and 12-Week SPI, one week lag

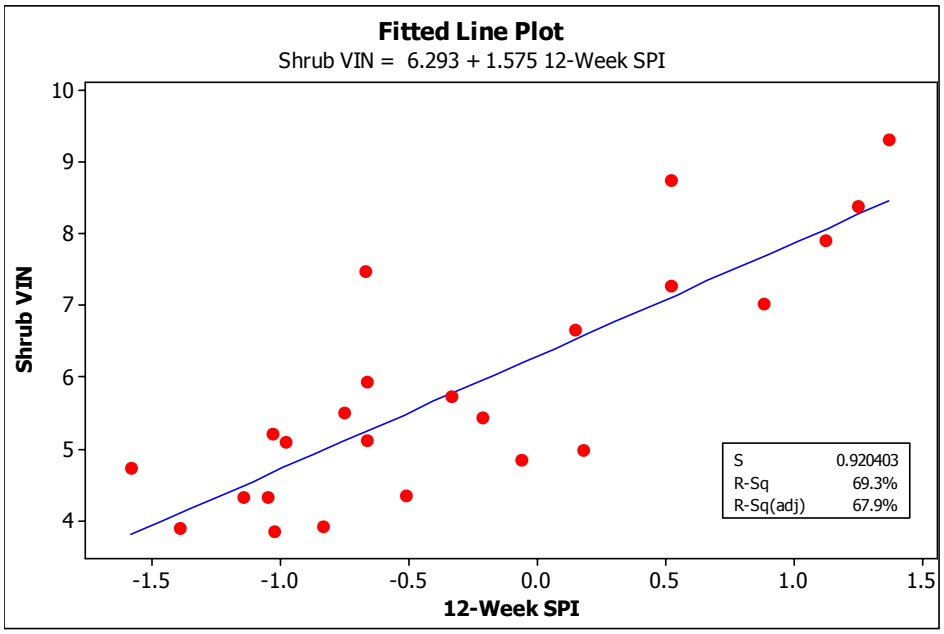

Figure A-20: Linear Regression of shrub VIN vs. 12-week SPI, one week lag

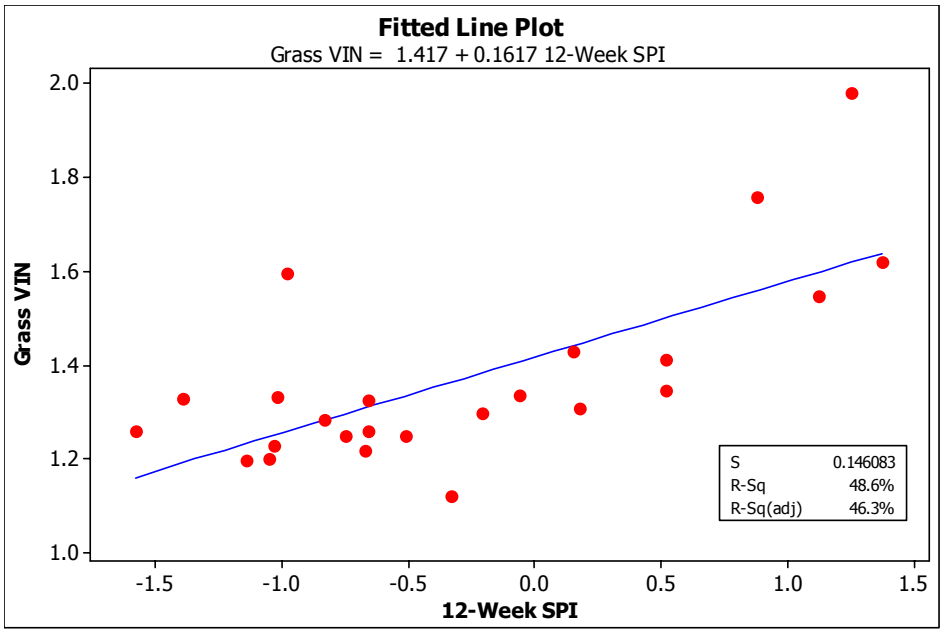

Figure A-21: Linear Regression of Grass VIN vs. 12-Week SPI, one week lag

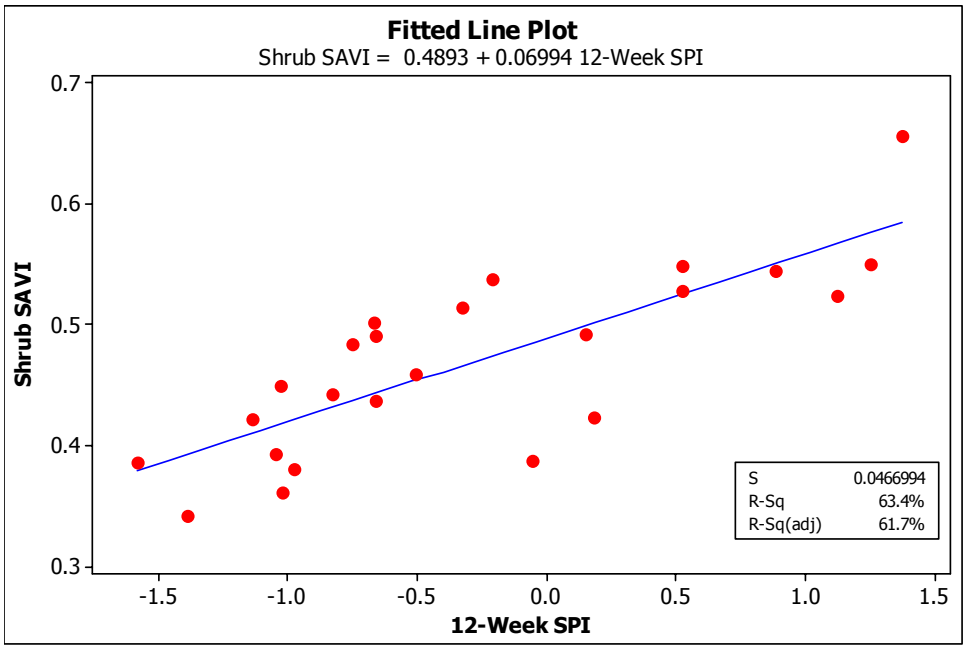

Figure A-22: Linear Regression of Shrub SAVI vs. 12-Week SPI, one week lag

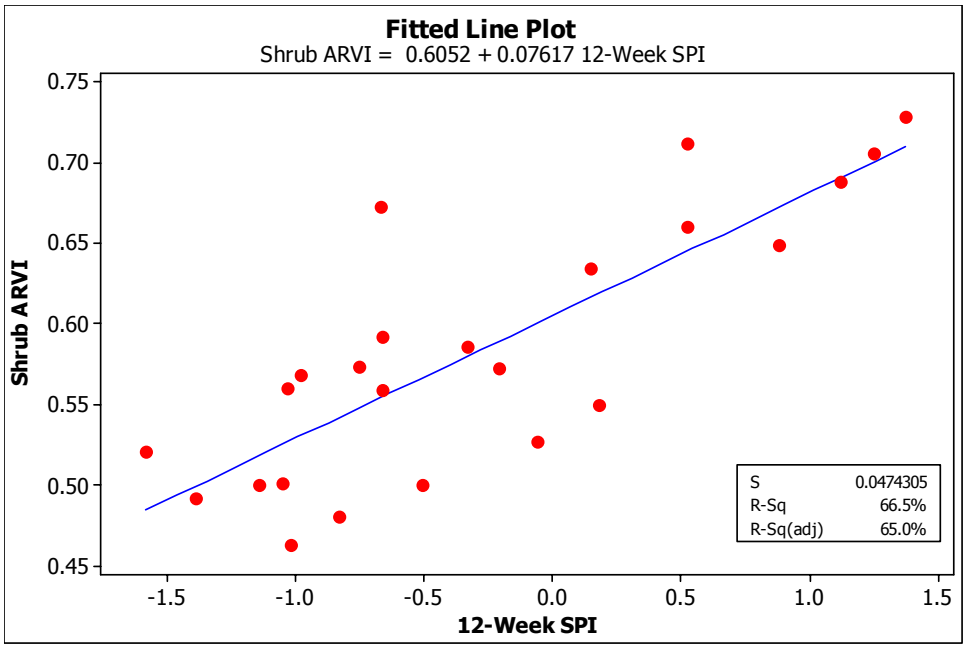

Figure A-23: Linear Regression of shrub ARVI vs. 12-Week SPI, one week lag

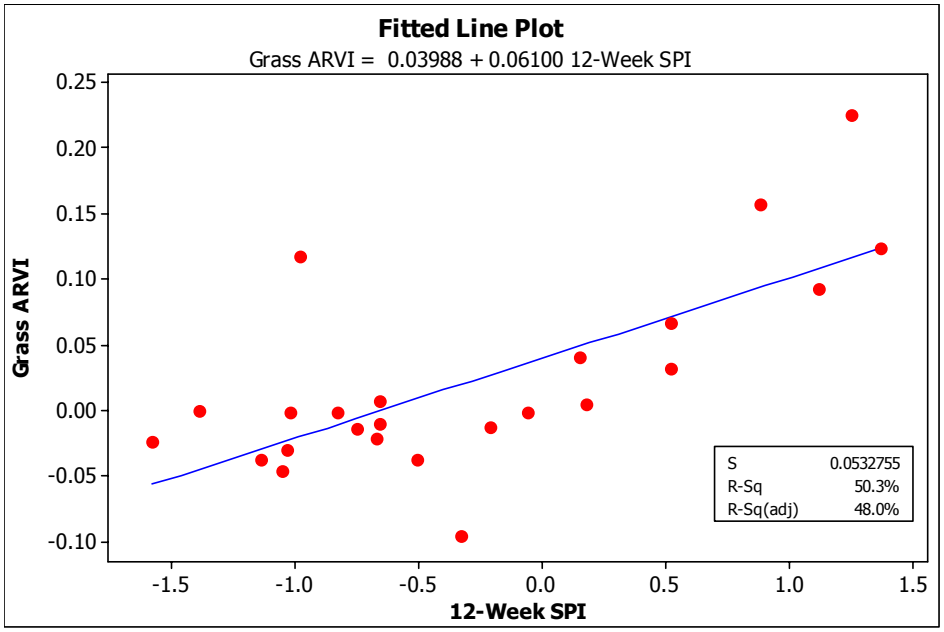

Figure A-24: Linear Regression of Grass ARVI vs. 12-Week SPI, one week lag

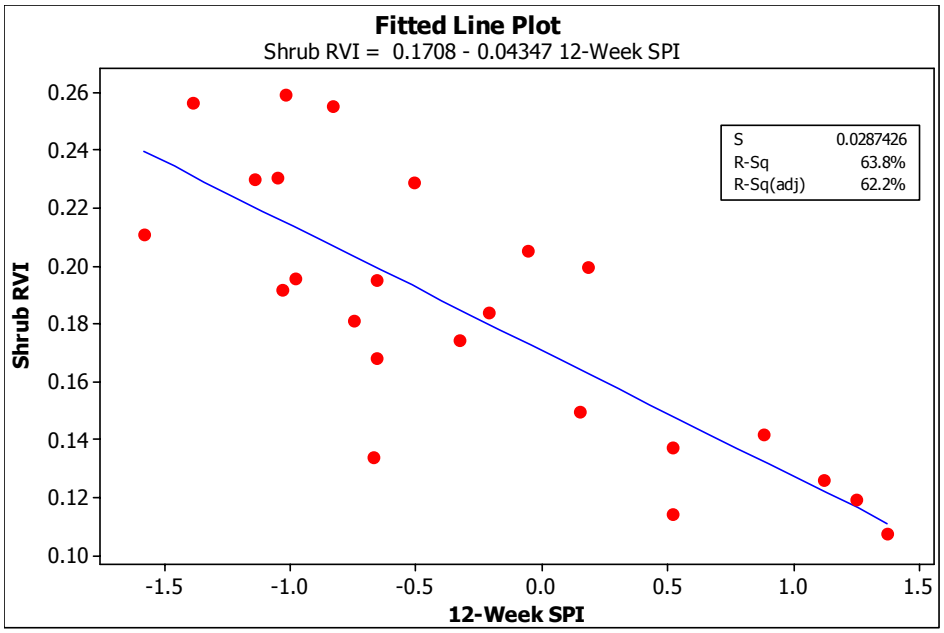

Figure A-25: Linear Regression of Shrub RVI vs. 12-Week SPI, no lag

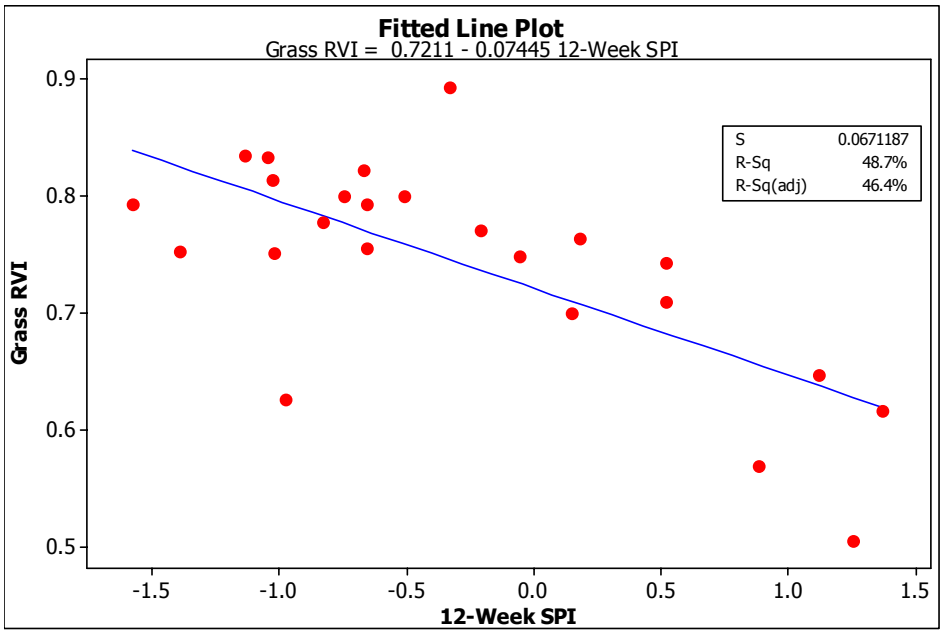

Figure A-26: Linear Regression of Grass RVI vs. 12-Week SPI, no time lag

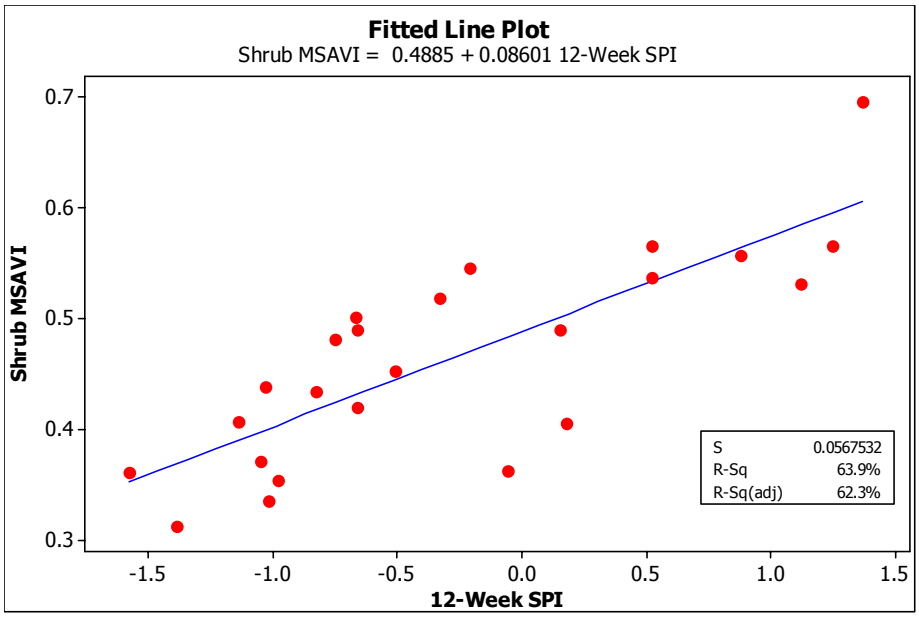

Figure A-27: Linear Regression of Shrub MSAVI vs. 12-Week SPI, one week lag

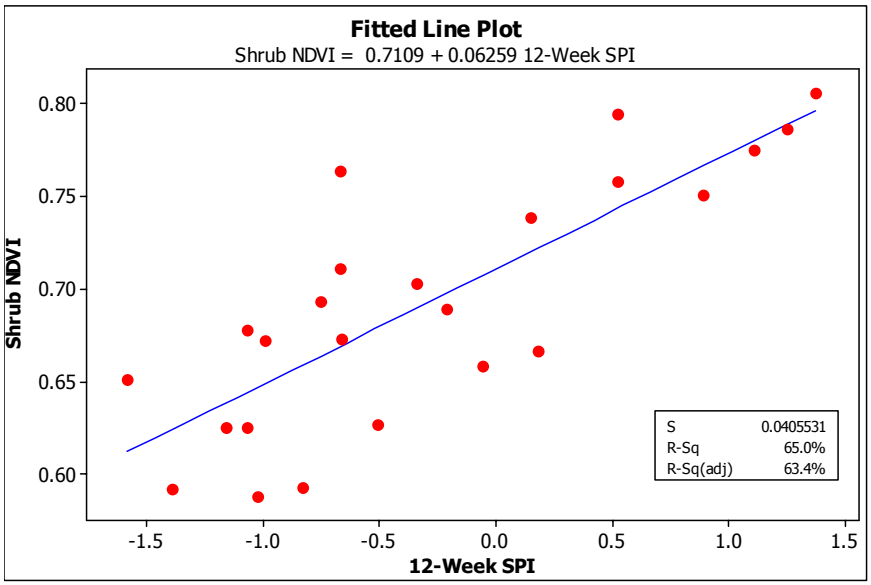

Figure A-28: Linear Regression of Shrub NDVI vs. 12-week SPI, two weeks time lag

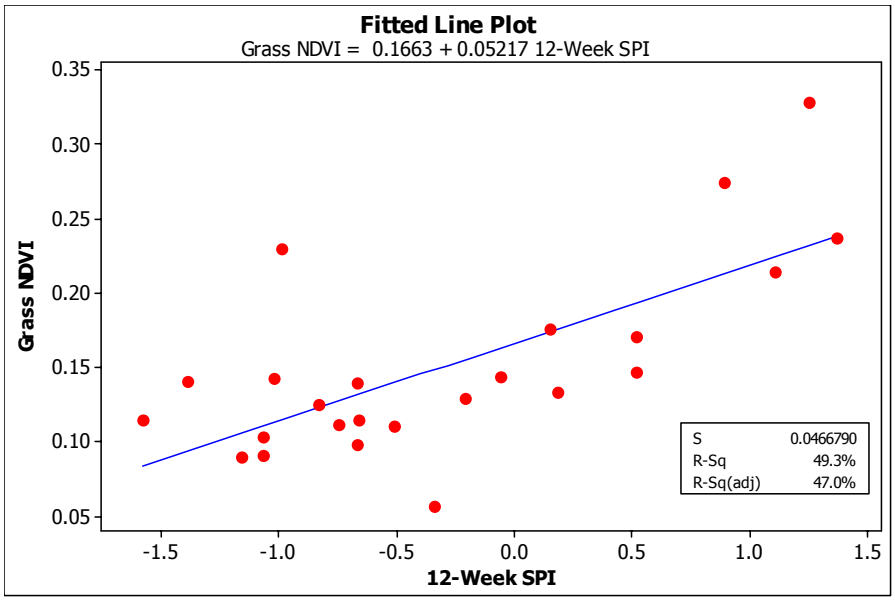

Figure A-29: Linear Regression of Grass NDVI vs. 12-Week SPI, two weeks lag

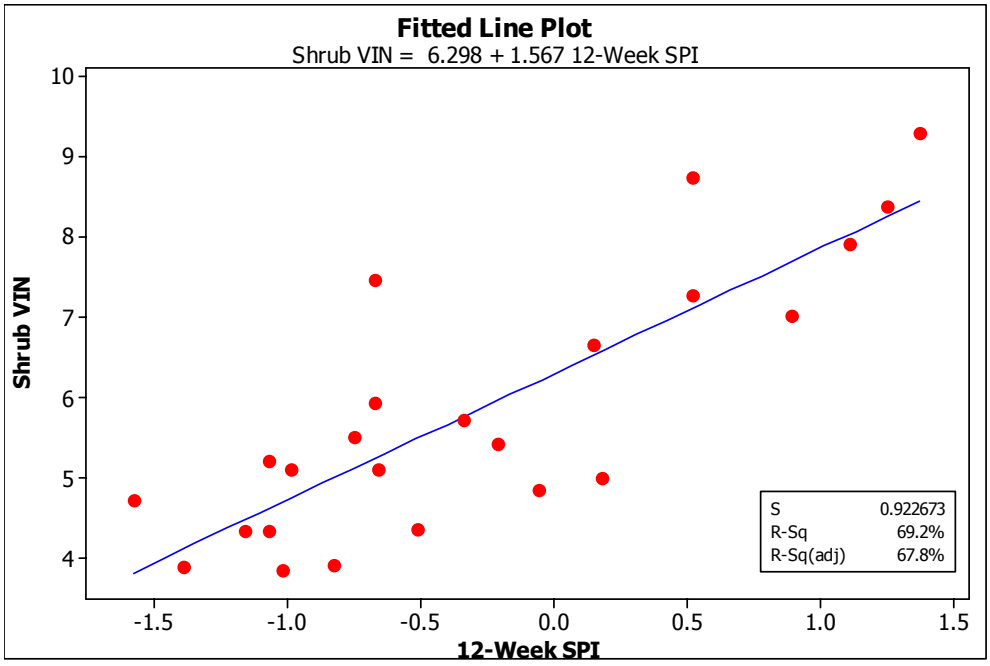

Figure A-30: Linear Regression of Shrub VIN vs. 12-Week SPI, two weeks lag

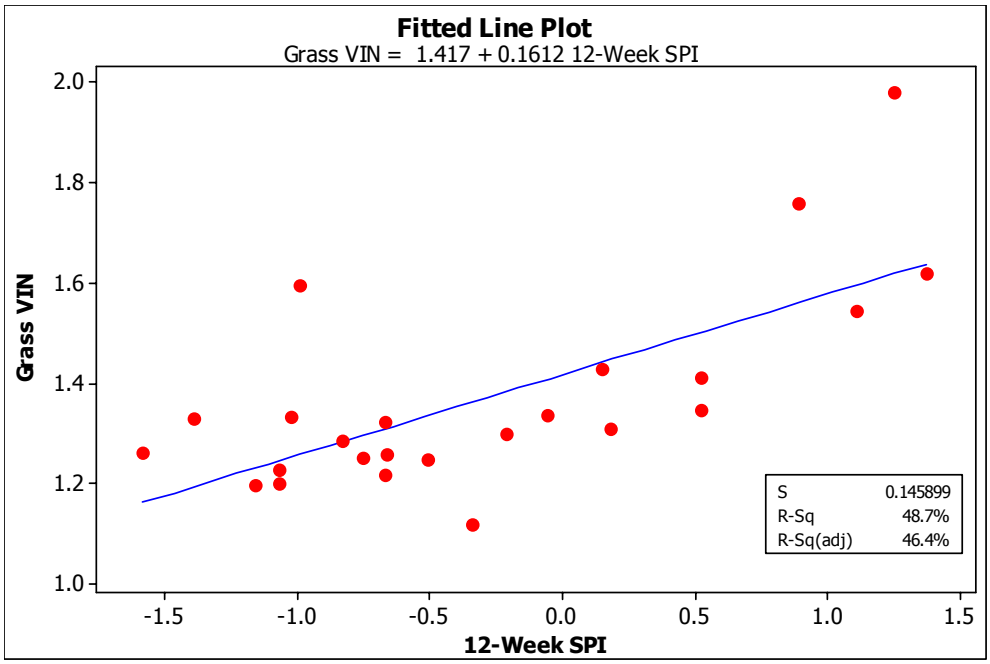

Figure A-31: Linear Regression of Grass VIN vs. 12-Week SPI, two weeks lag

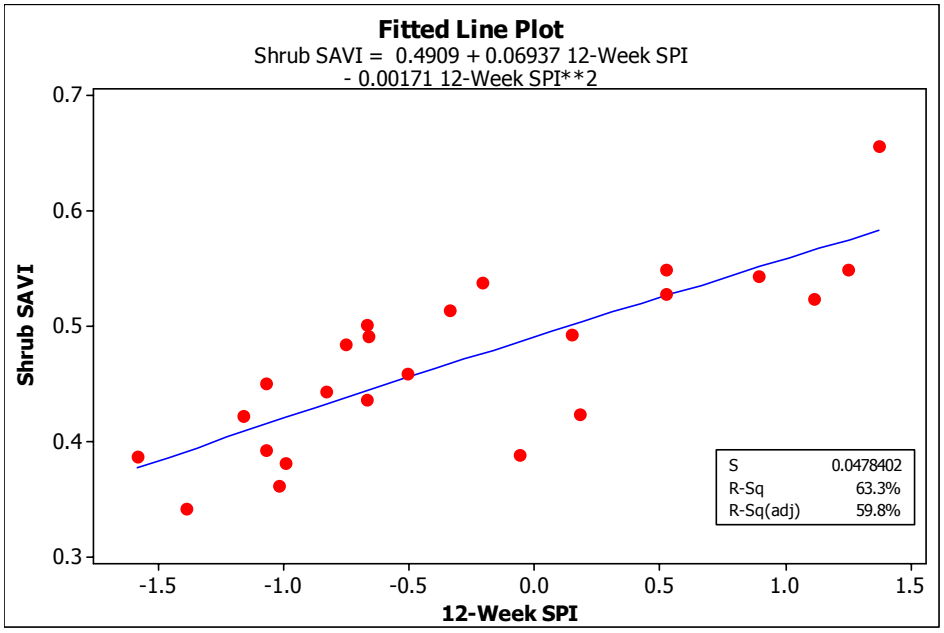

Figure A-32: Linear Regression of Shrub SAVI vs. 12-Week SPI, two weeks lag

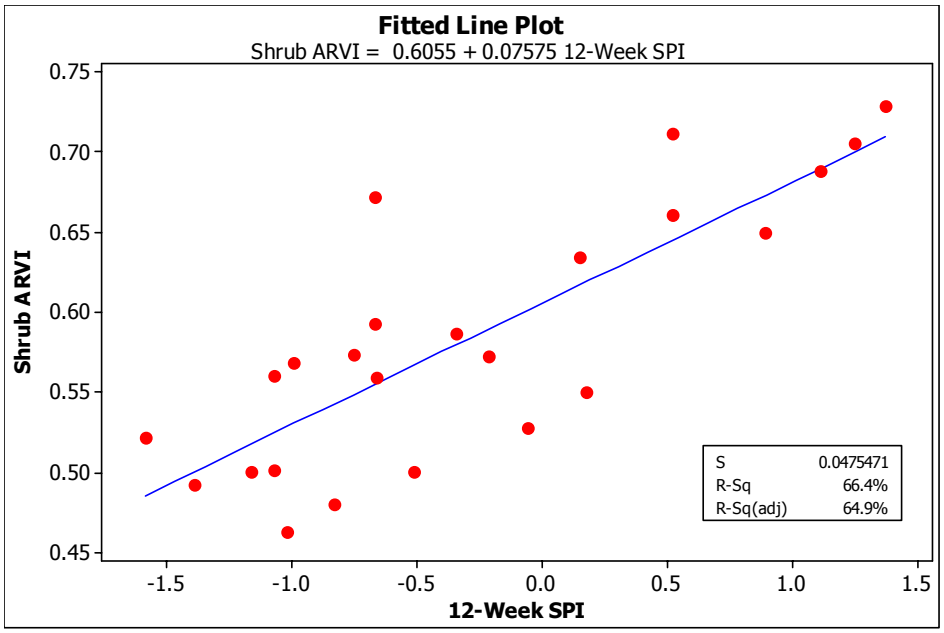

Figure A-33: Linear Regression of Shrub ARVI vs. 12-Week SPI, two weeks lag

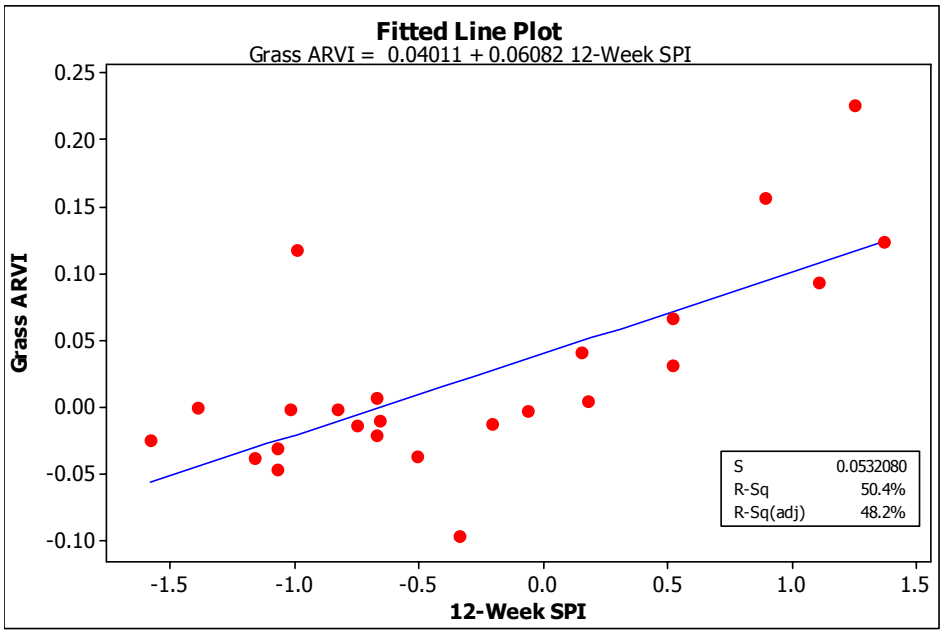

Figure A-34: Linear Regression of Grass ARVI vs. 12-Week SPI, two weeks lag

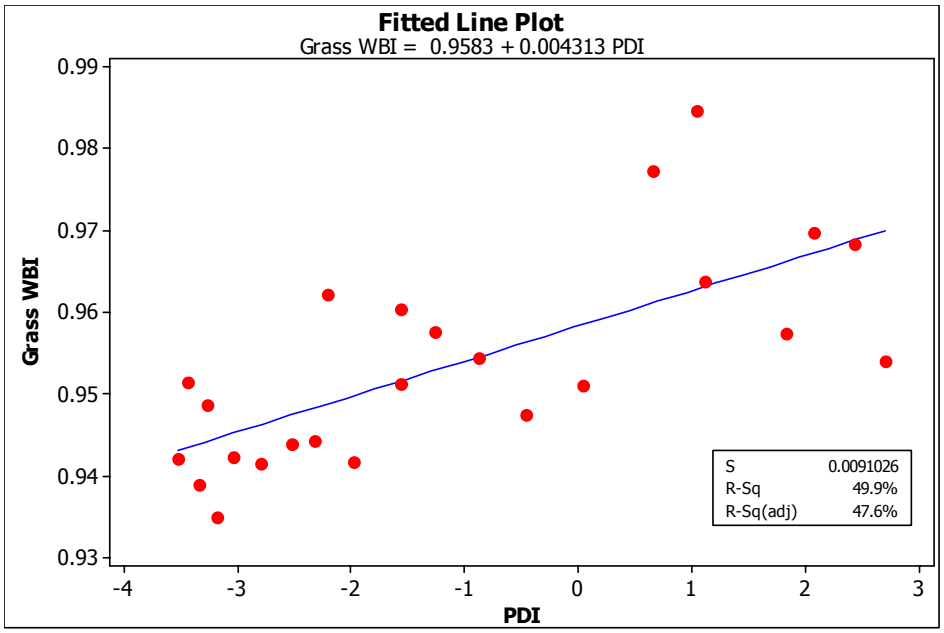

Figure A-35: Linear Regression of Grass WBI vs. PDI, two weeks lag

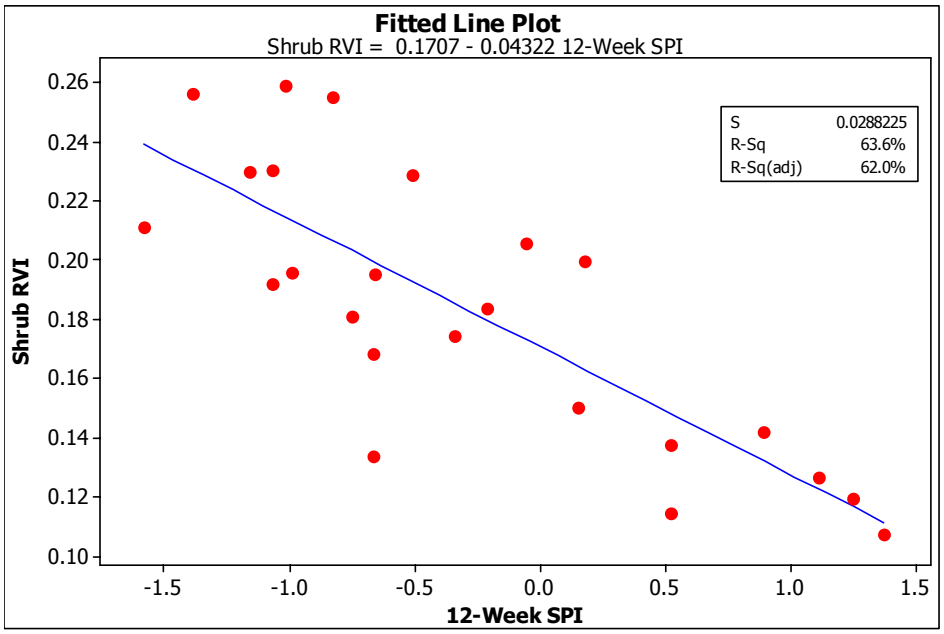

Figure A-36: Linear Regression of Shrub RVI vs. 12-week SPI, two weeks lag

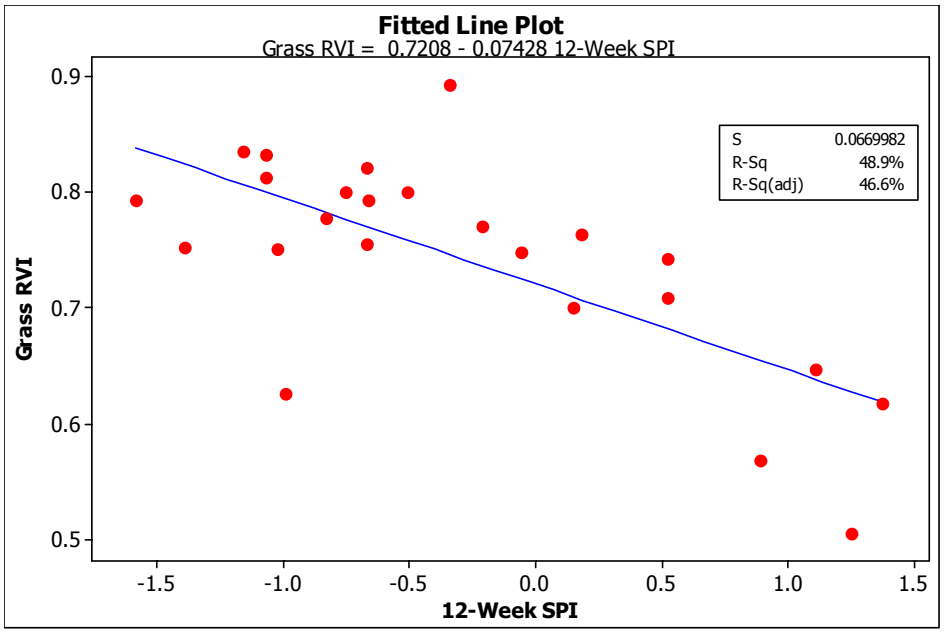

Figure A-37: Linear Regression of Grass RVI vs. 12-Week SPI, two weeks lag

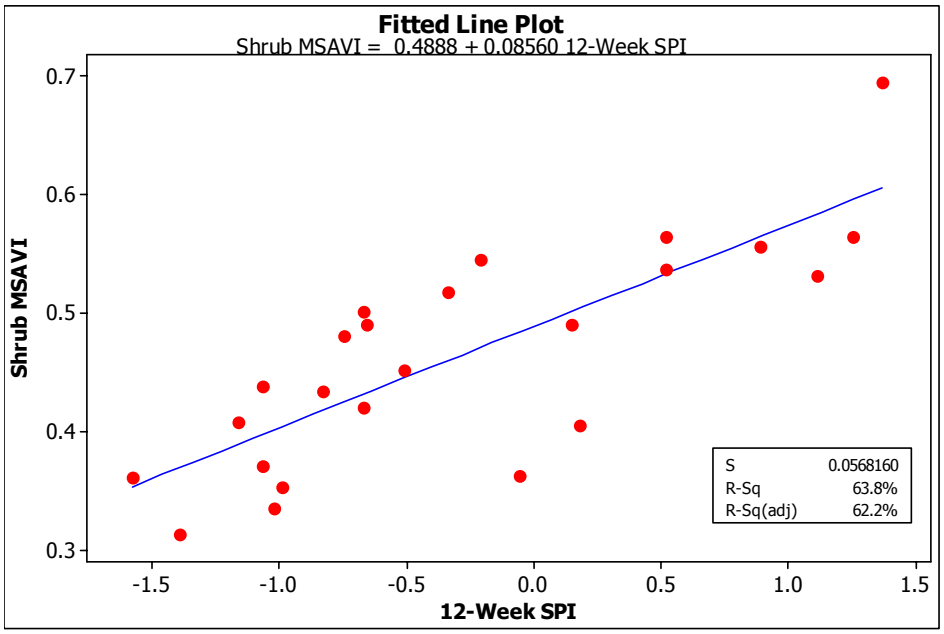

Figure A-38: Linear Regression of Shrub MSAVI vs. 12-Week SPI, two weeks lag

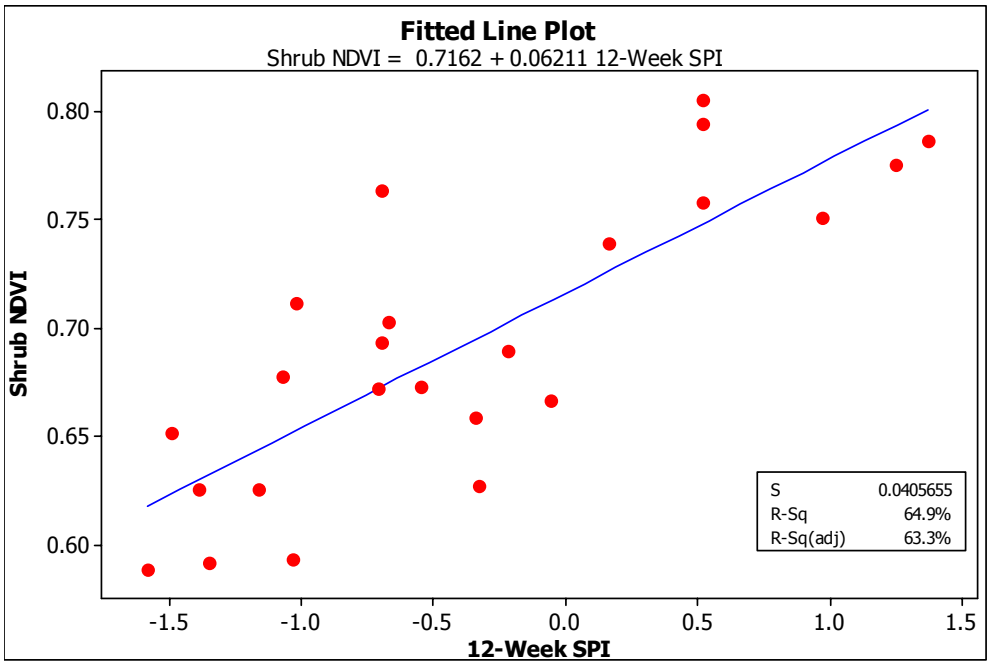

Figure A-39: Linear Regression of Shrub NDVI vs. 12-Week SPI, three weeks lag

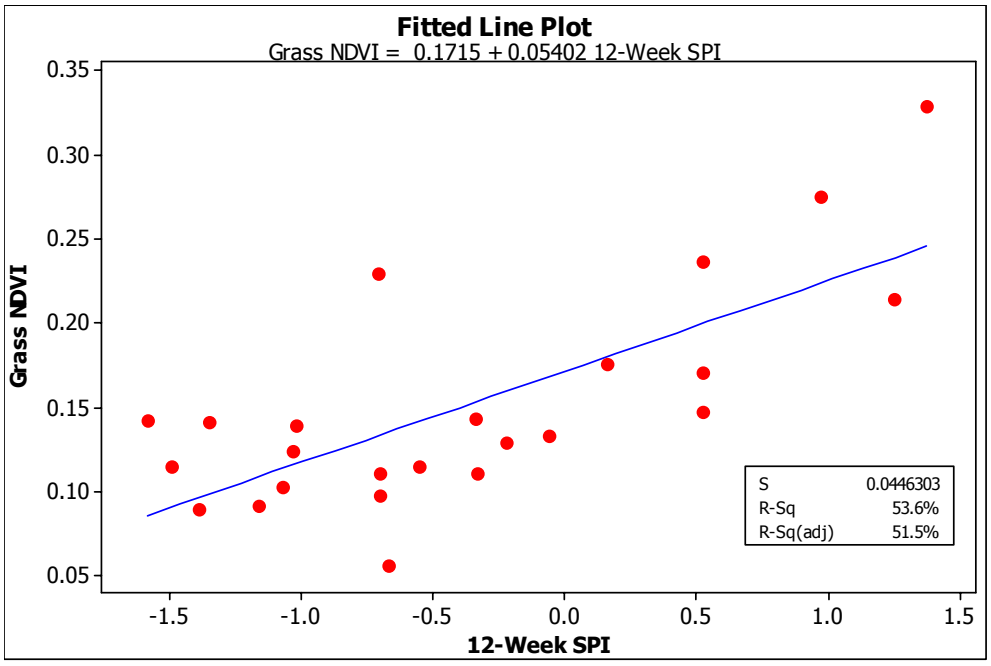

Figure A-40: Linear Regression of Grass NDVI vs. 12-Week SPI, three weeks lag

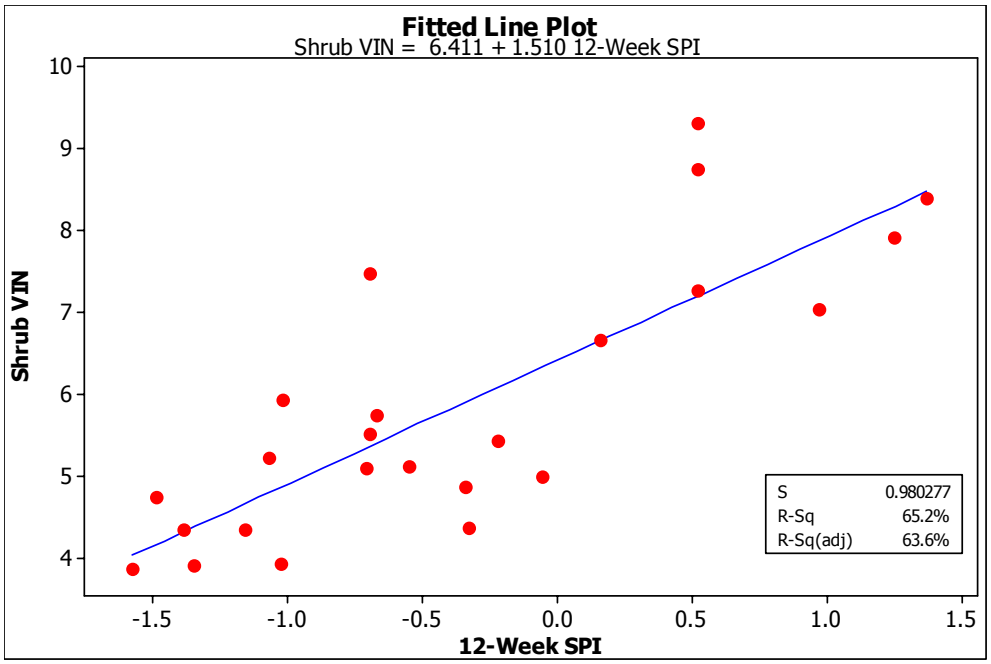

Figure A-41: Linear Regression of Shrub VIN vs. 12-Week SPI, three weeks lag

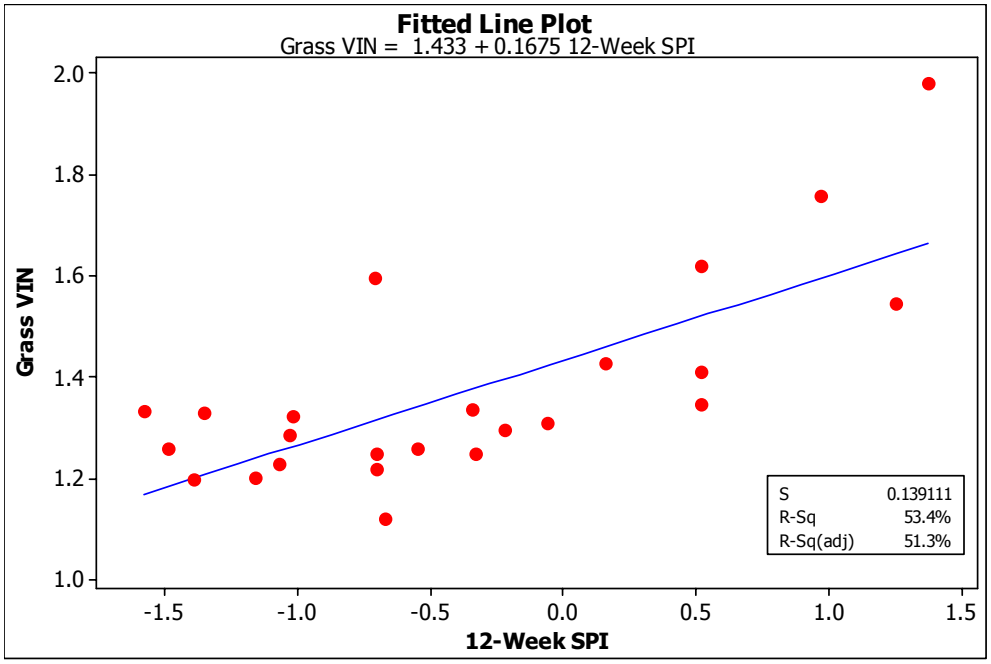

Figure A-42: Linear Regression of Grass VIN vs. 12-Week SPI, three week lag

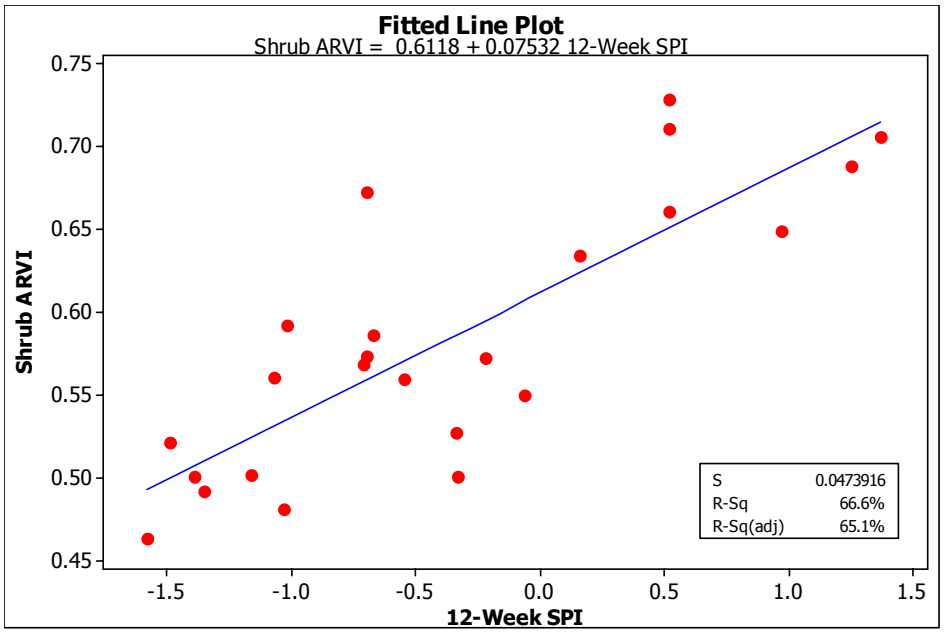

Figure A-43: Linear Regression of Shrub ARVI vs. 12-Week SPI, three weeks lag

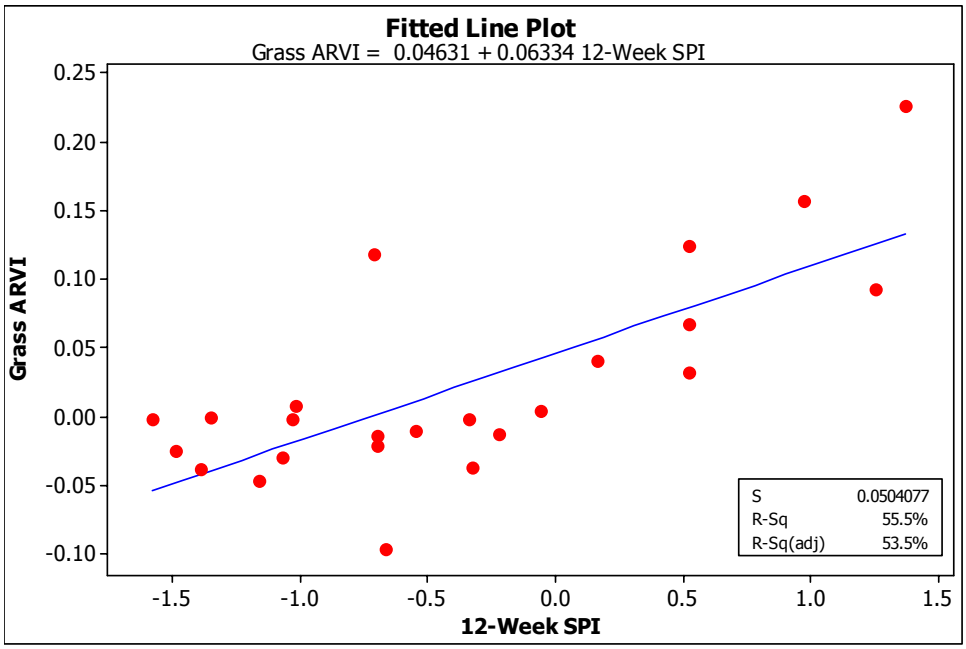

Figure A-44: Linear Regression of Grass ARVI vs. 12-Week SPI, three week lag

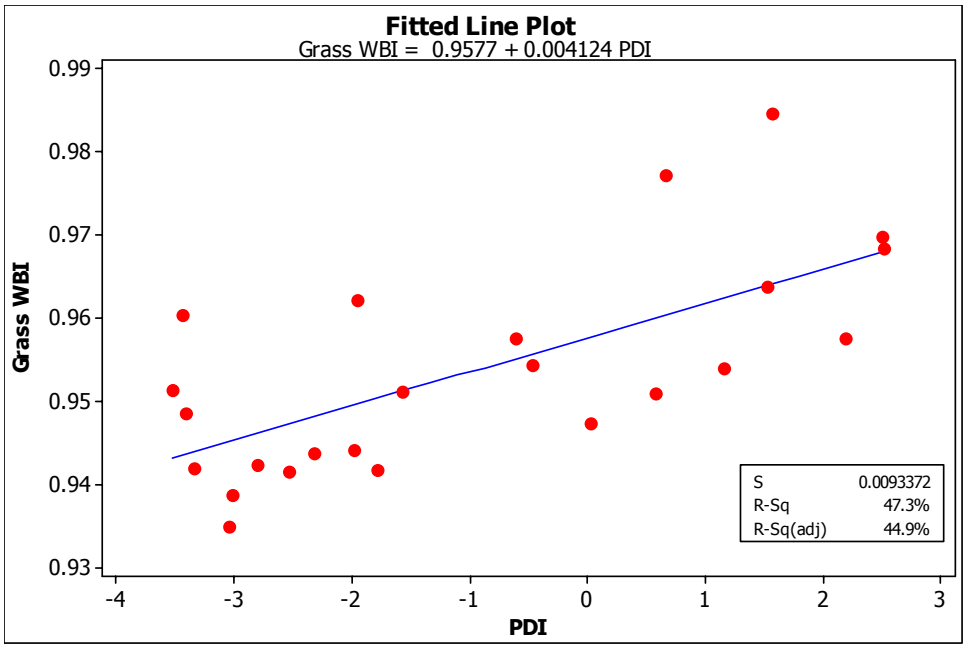

Figure A-45: Linear Regression of Grass WBI vs. PDI, three week lag

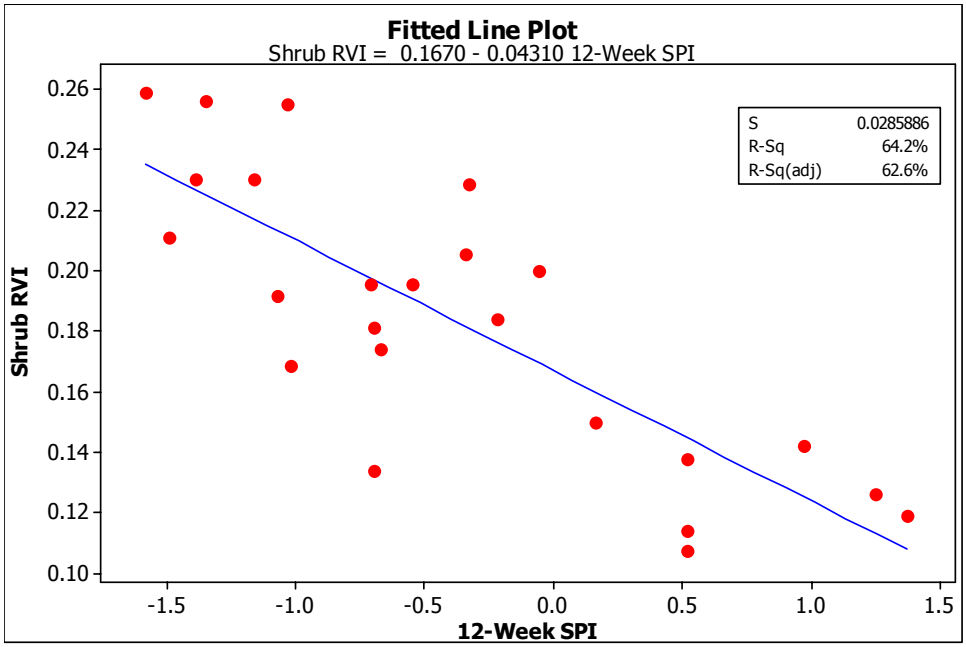

Figure A-46: Linear Regression of Shrub RVI vs. 12-Week SPI, three weeks lag

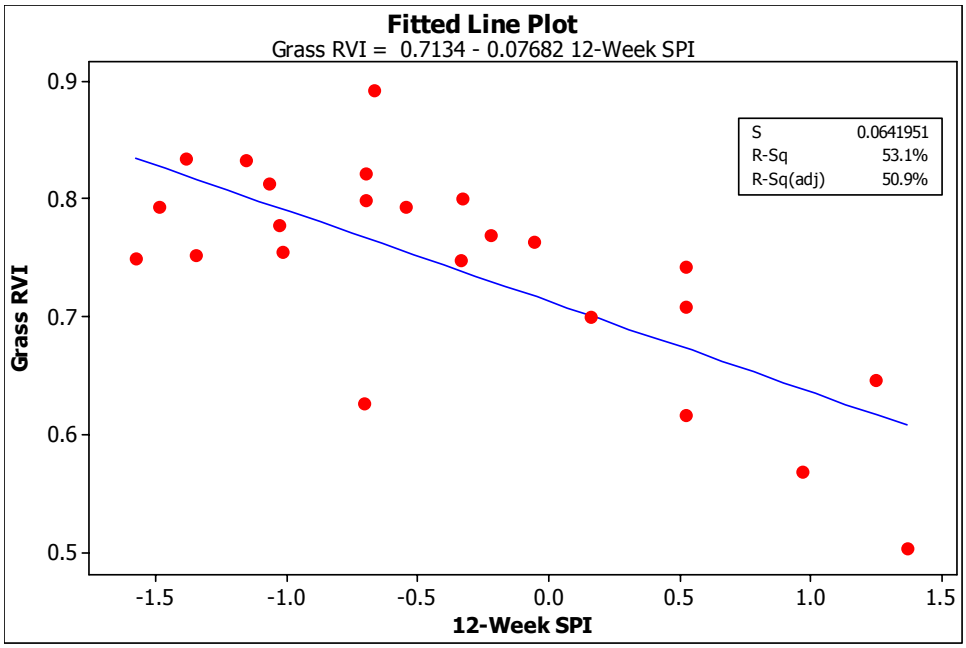

Figure A-47: Linear Regression of Grass RVI vs. 12-Week SPI

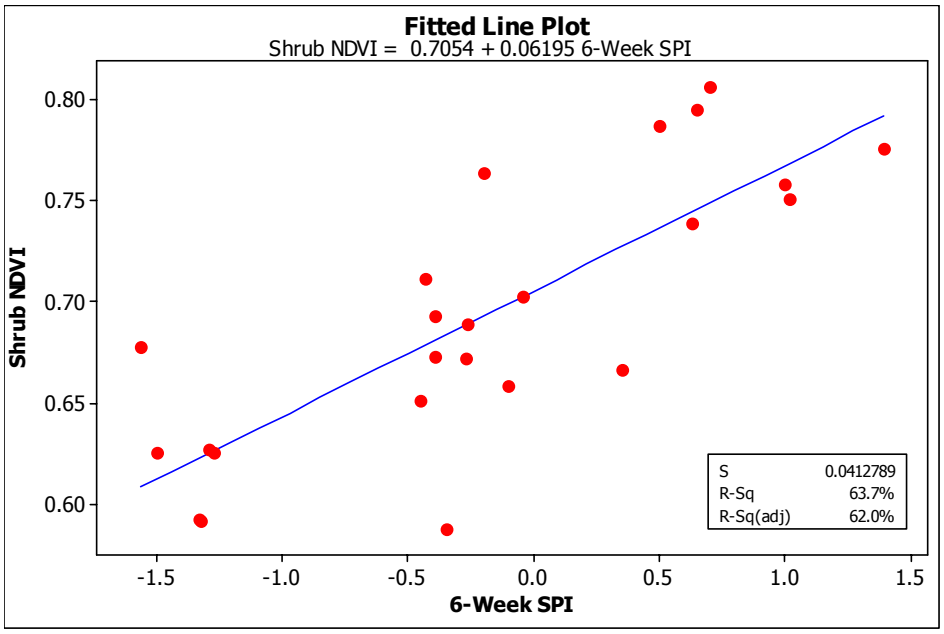

Figure A-48: Linear Regression of Shrub NDVI vs. 6-Week SPI, four week lag.

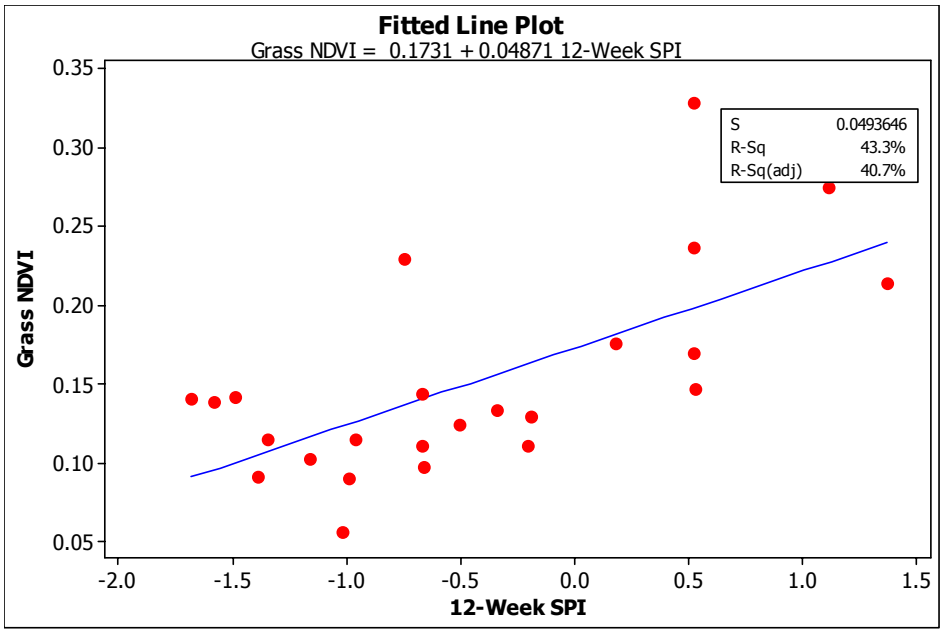

Figure A-49: Linear Regression of Grass NDVI vs. 12-Week SPI, four weeks lag

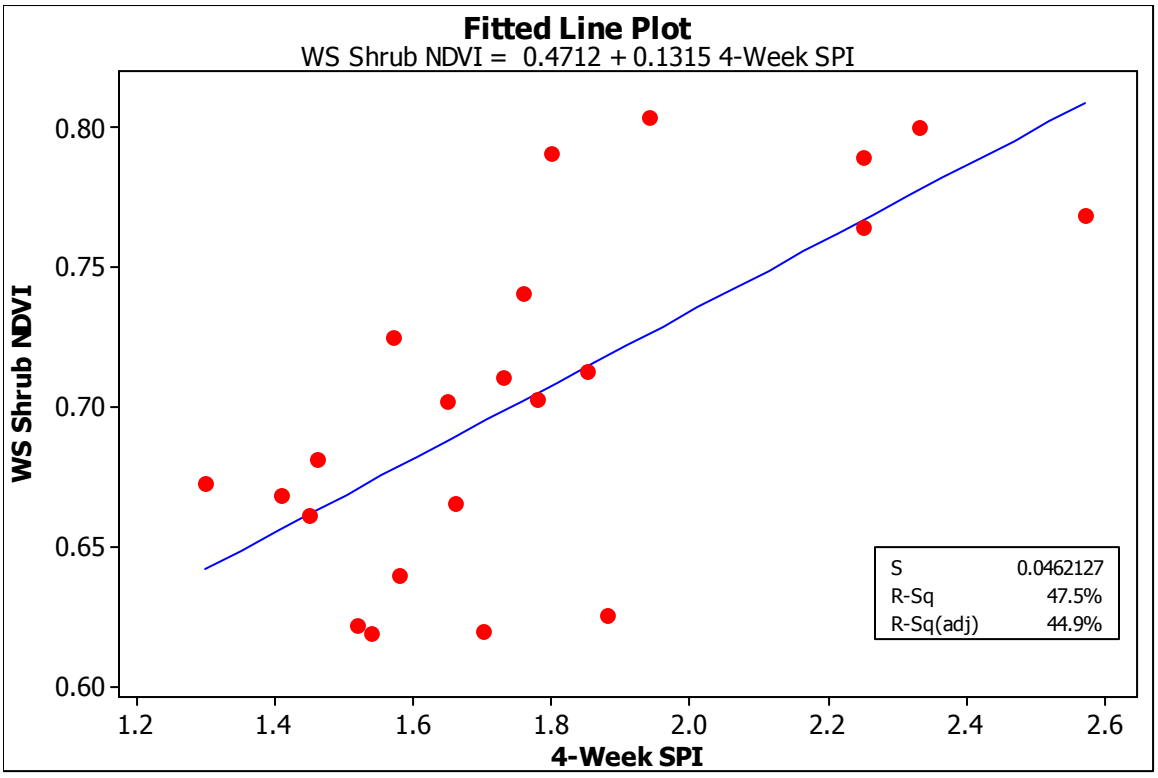

Figure A-50: Linear Correlation of 4-Week SPI and Shrub NDVI, no lag, Irrigated Site

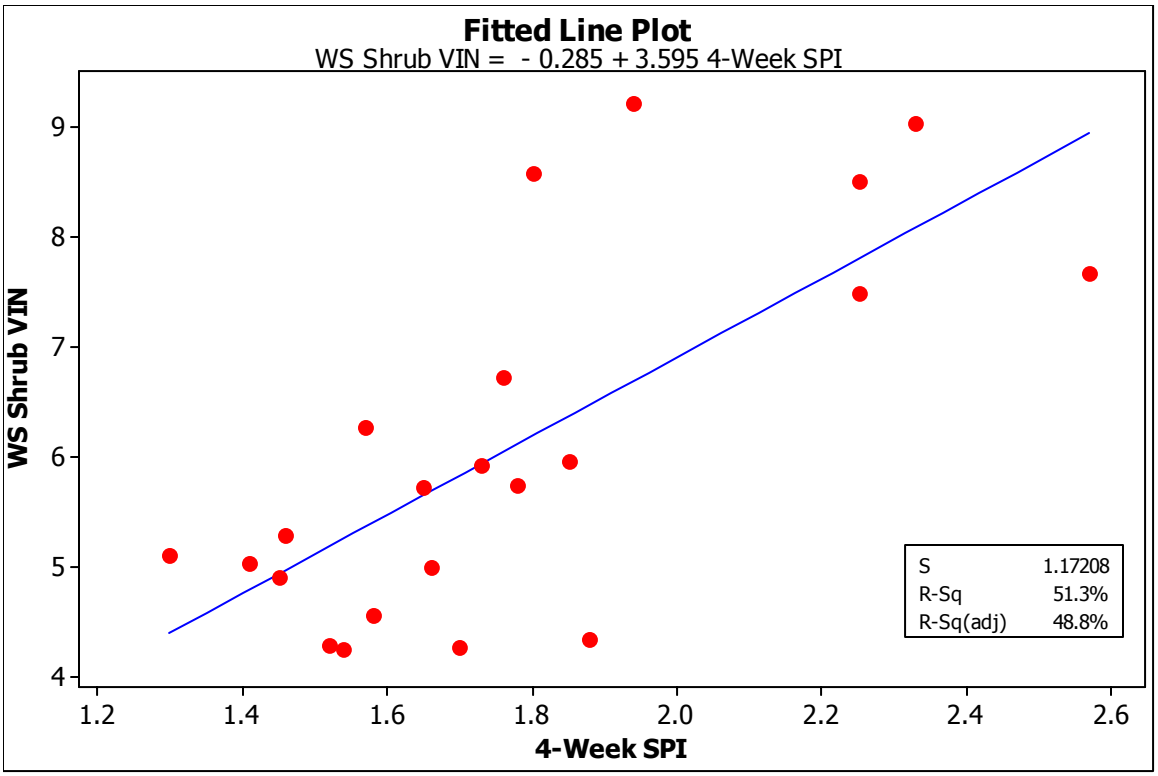

Figure A-51: Linear Correlation of 4-Week SPI and Shrub VIN, no lag, Irrigated Site.

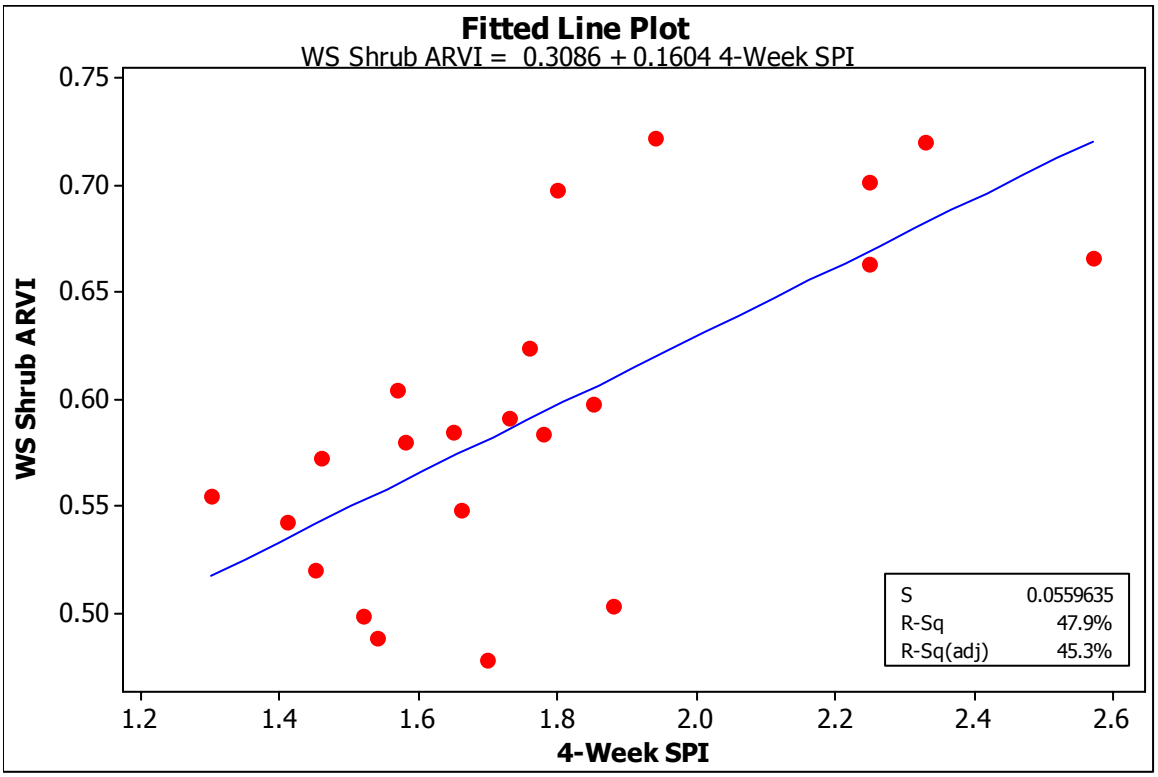

Figure A-52:Linear correlation plot between 4-Week SPI and Shrub ARVI, no lag, Irrigated Site

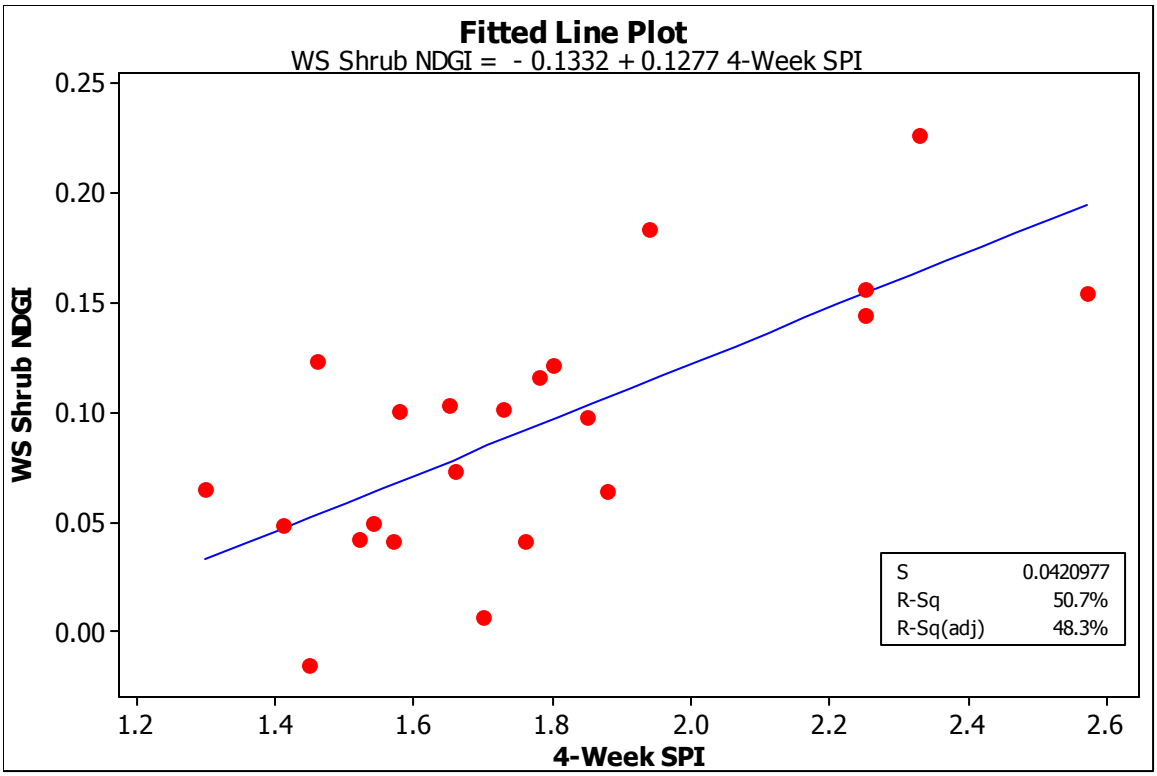

Figure A-53: Linear Regression of 4-Week SPI and Shrub NDGI, no lag, watered Site

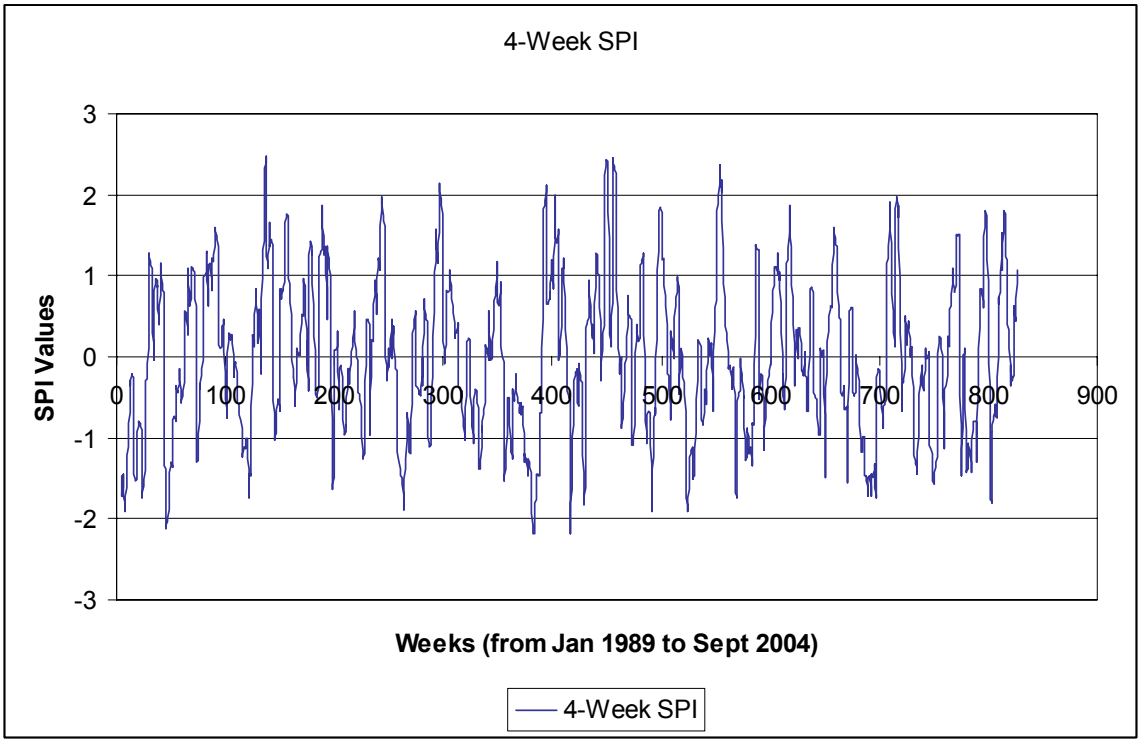

Figure A-54: SNWR 4-Week SPI from all operational rain gauges/weather stations

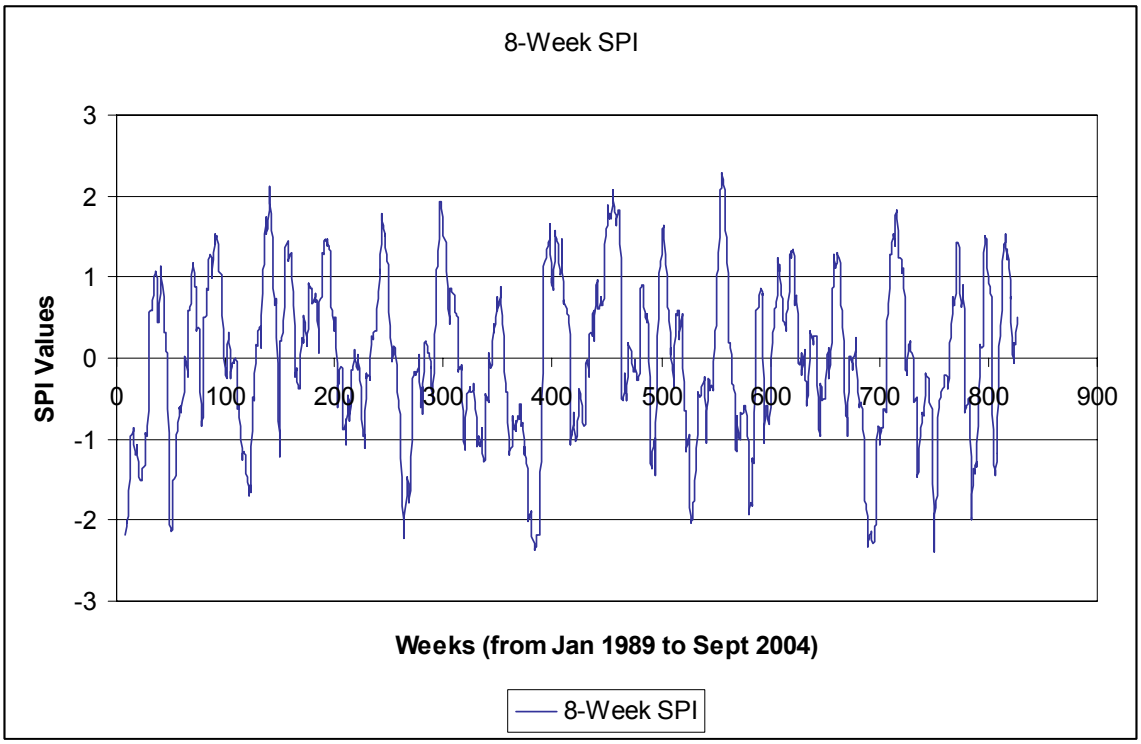

Figure A-55: SNWR 8-Week SPI from all operational rain gauges/weather stations

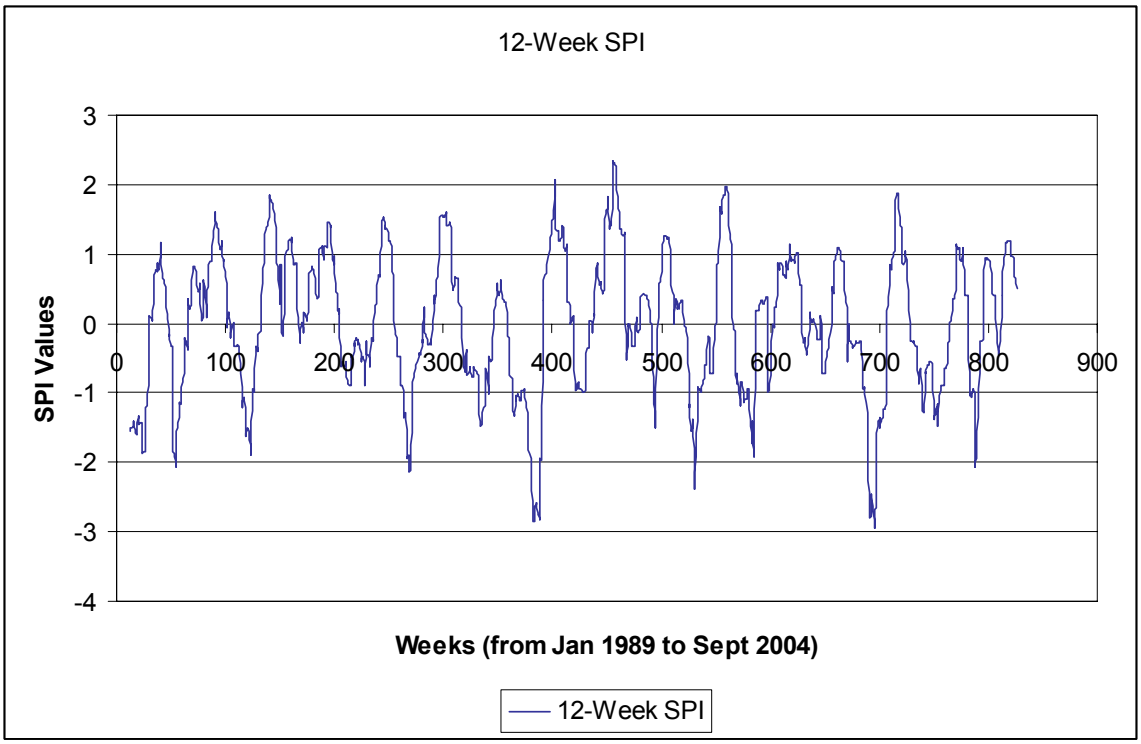

Figure A-56: SNWR 12-Week SPI from all operational rain gauges/weather stations

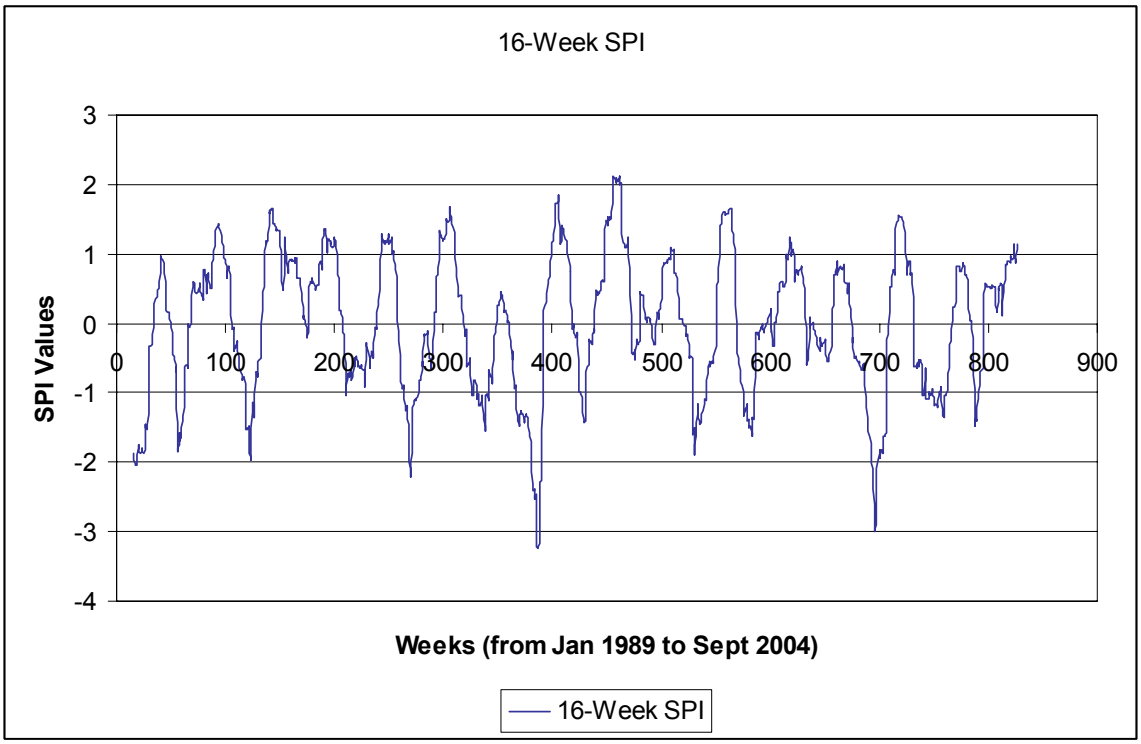

Figure A-57: SNWR 16-Week SPI from all operational rain gauges/weather stations

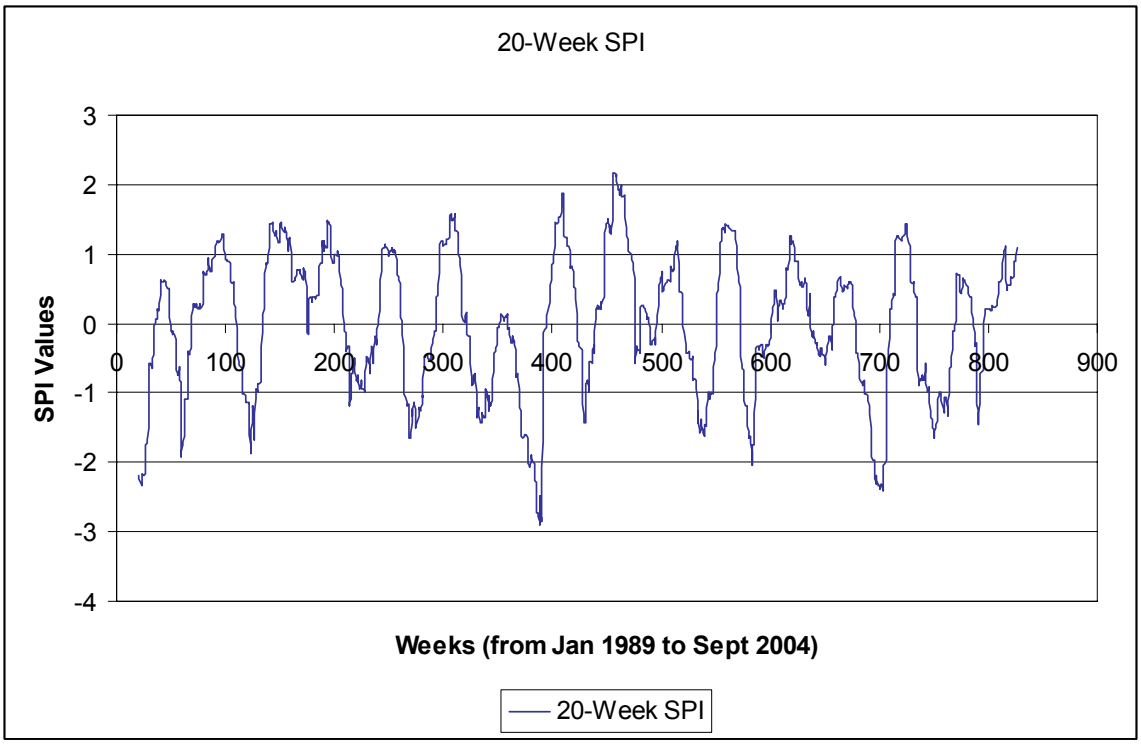

Figure A-58: SNWR 20-Week SPI from all operational rain gauges/weather stations

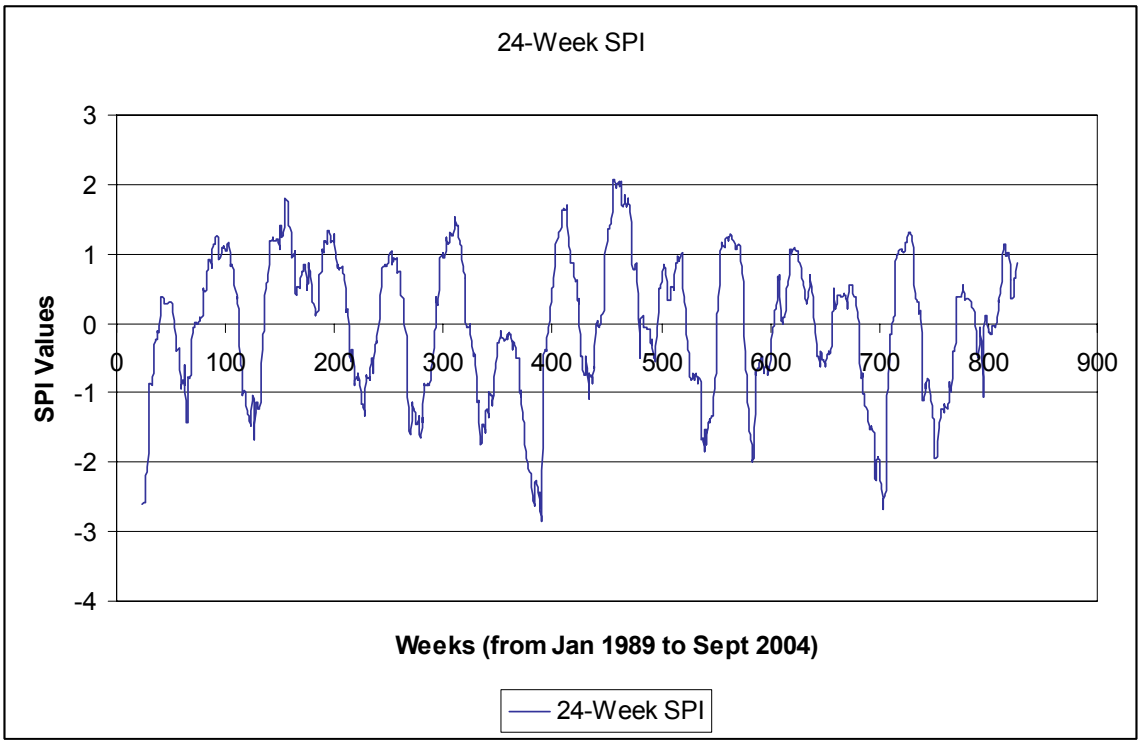

Figure A-59: SNWR 24-Week SPI from all operational rain gauges/weather stations

REFERENCES

Alley, W. M. (1984). "The Palmer Drought Severity Index: Limitations and Assumptions." Journal of Climate and Applied Meteorology **23**: 1100-1109.

Asner, G. P., Heidebrecht, K.B. (2002). "Spectral Un-mixing of vegetation, soil and dry carbon cover in arid regions: comparing multispectral and hyperspectral observations." International Journal of Remote Sensing **23**(19): 3939-3958.

Bahrun, A., Mogensen, V.O., Jensen, C.R. (2003). "Water Stress Detection in Field-Grown Maize by Using Spectral Vegetation Index." Communications in Soil Science and Plant Analysis **34**(1&2): 65-79.

Bannari, A., Morin, D., Bonn, F., Huete, A. (1995). "A Review of Vegetation Indices." Remote Sensing Reviews **13**: 95-120.

Baret, F., Guyot, G. (1991). "Potentials and Limits of Vegetation Indices for LAI and APAR Assesment." Remote Sensing of Environment **35**: 161-173.

Bowker, D. E., Davis, R.E., Myrick, D.L., Stacy, K., Jones, W.T. (1985). Spectral Reflectance of Natural Targets for Use in Remote Sensing Studies. Hampton, Langley Research Center, NASA Reference Publication 1139**:** 26 pp.

Boyd, D. S., Phipps, P.C., Foody, G.M., Walsh,R.P.D. (2002). "Exploring the utility of NOAA AVHRR middle infrared reflectance to monitor the impacts of ENSO-induced drought stress on Sabah rainforests." International Journal of Remote Sensing **23**(23): 5141-5147.

Buschmann, C., Nagel, E. (1993). "In Vivo spectroscopy and internal optics of leaves as basis for remote sensing of vegetation." International Journal of Remote Sensing **14**(4): 711-722.

Byun, H., Wilhite, D.A. (1999). "Objective Quantification of Drought Severity and Duration." Bulletin of the American Meteorolgical Society **12**: 2747-2756.

Carter, G. (1993). "Responses of Leaf Spectral Reflectance to Plant Stress." American Journal of Botany **80**(3): 239-243.

Chamard, P., Courel, Ducousso, M., Guenegou, M., le Rhun, J., Levasseur, J., Loisel, C., Togola, M. (1991). "Utilisation des bandes spectrales du vert et du rouge pour une meilleure evaluation des formations vegetales actives." Teledectection et cartographie: 203-209.

Di, L., Rundquist, D.C., Han, L. (1994). "Modeling Relationships between NDVI and Precipitation during vegetative growth cycles." International Journal of Remote Sensing **15**(10): 2121-2136.

Edwards, D. (1993). Characteristics of 20th Century Drought in the United States at multiple time scales. Atmospheric Science. Fort Collins, Colorado State University**:** 155 pp.

Everitt, J. H., Nixon, P.R. (1986). "Canopy Reflectance of Two Drought-Stressed Shrubs." Photogrammetric Engineering and Remote Sensing **52**(8): 1189-1192.

Fitzgerald, G. J. (2000). "Hyperspectral Remote Sensing Systems and Analysis." http://webpages.acs.ttu.edu/smaas/asa2000/fitzgerald.htm

Gao, B. (1996). "NDWI-A Normalized Difference Water Index for Remote Sensing of Vegetation Liquid Water from Space." Remote Sensing of Environment **58**: 257-266.

Gates, D. M., Keegan, H.J., Schleter, J.C., Weidner, V.R. (1965). "Spectral Properties of Plants." Applied Optics **4**(1): 11-20.

Gausman, H. W. (1985). Plant Leaf Optical Properties in Visible and Near-Infrared Light. Lubbock, Texas, Texas Tech University, 78 pp.

Ghosh, T. K. (1997). "Investigation of Drought Through Digital Analysis of Satellite Data and Geographical Informaion Systems." Theoretical and Applied Climatology **58**: 105-112.

Gibbs, W. J., Maher, J.V. (1967). Rainfall deciles as drought indicators, Bulletin No. 48, Bureau of Meteorology, Australia**:** 84 pp.

Guttman, N. B. (1998). "Comparing the Palmer Drought Index and the Standardized Precipitation Index." Journal of the American Water Resources Association **34**(1): 113-121.

Hale, M. G., Orcutt, D.M. (1987). The Physiology of Plants Under Stress. New York City, John Wiley and Sons Inc. 220 pp.

Haug, G. H., Gunther, D., Peterson, L.C., Sigman, D.M., Hughen, K.A., Aeschlimann, B. (2003). "Climate and the Collapse of Maya Civilization." Science **299**: 1731-1735.

Hayes, M. J., Svoboda, M.D., Wilhite, D.A., Vanyarkho, O.V. (1999). "Monitoring the 1996 Drought using the Standardized Precipitation Index." Bulletin of the American Meteorological Society **80**(3): 429-438.

Hayes, M. (2003). Drought Indices. Lincoln, NE., National Drought Mitigation Center http://www.drought.unl.edu/whatis/indices.htm

Heim Jr., R. R. (2002). "A Review of Twentieth-Century Drought Indices used in the United States." Bulletin of the American Meteorological Society **83**(8): 1149-1165.

Holben, B. N., Justice, C.O. (1981). "An Examination of Spectral Band Ratioing to Reduce the Topographic Effect on Remotely Sensed Data." International Journal of Remote Sensing **2**(3): 115-133.

Huete, A. R. (1988). "A Soil-Adjusted Vegetation Index." Remote Sensing of Environment **25**: 295-309.

Huete, A., Justice, C., Liu, H. (1994). "Development of Vegetation and Soil Indices for MODIS-EOS." Remote Sensing of Environment **49**: 224-234.

Jackson, R. D., Huete, A.R. (1991). "Interpreting Vegetation Indices." Preventitive Veterinary Medicine **11**: 185-200.

Jacobberger-Jellison, P. A. (1994). "Detection of post-drought environmental conditions in the Tombouctou region." International Journal of Remote Sensing **15**(16): 3183-3197.

Jacquemoud, S., Ustin, S.L. (2001). Leaf Optical Properties: A State of the Art. 8th Interntional Symposium Physical Measurements and Signatures in Remote Sensing, Aussois, France: 223-232

Jensen, M., Haise, H. (1963). "Estimating evapotranspiration from solar radiation." ASCE Journal of Irrigation and Drainage **89**: 15-41.

Ji, L., Peters, A.J (2003). "Assessing Vegetation Response to Drought in the Northern Great Plains using vegetation and drought indices." Remote Sensing of Environment **87**: 85-98.

Julian, P. R., Fritts, H.C. (1968). On The Possibility of Quantitatively Extending Climatic Records by Means of Dendroclimatological Analysis. 1st Statistical Meteorological Conference, American Meteorological Society, CL C TREE: 76-82.

Karnieli, A., Dall'Olmo, G. (2003). "Remote-sensing monitoring of desertification, phenology and droughts." Management of Environmental Quality **14**(1): 22-38.

Kaufman, Y. J., Tanre,D. (1992). "Atmospherically Resistant Vegetation Index (ARVI) for EOS-MODIS." IEEE Transactions on Geoscience and Remote Sensing **30**(2): 261-

270.

Keyantash, J., Dracup, J.A. (2002). The Quantification of Drought: An evaluation of Drought Indices. Bulletin of the American Meteorological Society. **83:** 1167-1179.

Kincer, J. (1919). "The Seasonal Distribution of Precipitation and its Frequency and Intensity in the United States." Monthly Weather Review **47**: 624-631.

Kogan, F. (1997). "Global Drought Watch from Space." Bulletin of the American Meterological Society **78**(4): 621-635.

Leprieur, C., Kerr, Y.H., Pichon, J.M. (1996). "Critical assessment of vegetation indices from AVHRR in a semi-arid environment." International Journal of Remote Sensing **17**(13): 2549-2563.

Liangming, L., Deren, L. (2001). Drought Analysis Based on Remote Sensing and Ancillary Data. Proceedings of SPIE Vol. 4548: 232-237

Liu, G., Liang, C.K., Kuo, T.H., Lin, T.H., Huang, S. (2004). "Comparison of the NDVI, ARVI and AFRI Vegetation Index, along with their Relations with the AOD using SPOT 4 Vegetation data." The Journal of Terrestrial, Atmospheric and Oceanic Sciences **15**(1): 15-31.

Maingi, J. K., Marsh, S.E., Keptner, W.G., Edmonds, C.M. (2002). An Accuracy Assessment of 1992 Landsat-MSS Derived Land Cover for the Upper San Pedro Watershed (U.S./Mexico). Washington DC, Environmental Protection Agency**:** 21 pp.

Markovitch, S. (1930). "The Measure of Droughtiness." Monthly Weather Review **58**(March): 113

McKee, T. B., Doesken, N.J., Kleist, J. (1993). Drought Monitoring with Multiple Time Scales. 9th Conference on Applied Climatology, Anaheim, CA, American Meteorological Society: 233-236

McKee, T. B., Doesken, N.J., Kleist, J. (1993). The Relationship of Drought Frequency and Duration to Time Scales. 8th Conference on Applied Climatology, Anaheim, CA: 179-184

McNairn, H., Protz. R. (1993). "Mapping Corn Residue Cover on Agricultural FIelds in Oxford County, Ontario, Using Thematic Mapper." Canadian Journal of Remote Sensing **10**(2): 152-159.

Merton, R., Huntington, J (2002). Early Simulation Results Of the ARIES-1 Satellite Sensor for Multi-Temporal Vegetation Research derived from AVIRIS, CSIRO Exploration and Minig, and ARIES Consortium**:** 10 pp.

Munger, T. (1916). "Graphic Method of Representing and Comparing Drought Intensities." Monthly Weather Review(November): 642-643.

Nicholson, S. E., Davenport, M.L., Malo, A.R. (1990). "A Comparison of the Vegetation Reponse to Rainfall in the Sahel and East Africa using Normalized Difference Vegetation Index from NOAA AVHRR." Climate Change **17**: 209-241.

Odening, W. R., Strain, B.R., Oechel, W.C. (1974). "The effect of decreasing water potential on net CO2 exchange of intact desert shrubs." Ecology **55**: 1086-1095.

Oechel, W. C., Strain, B.R., Odening, W.R. (1972). "Tissue Water potential, photosynthesis, 14-C-Labeled phoosynthate utilization, and growth in the desert shrub Larrea Divaricata." Ecological Monograms **42**: 127-141.

Okamoto, K., Kawashima, H. (2002). Role of satellite remote sensing in monitoring system for environmental disasters related to water resources. Risk Analysis III. C. A. Brebbia, WIT Press. **5:** 551-560.

Okin, G. S., Roberts, D.A. (2004). Remote Sensing in Arid Regions: Challenges and Opportunities. The Manual of Remote Sensing. S. Ustin, Wiley and Sons. **4:** 768 pp.

Palmer, W. C. (1965). "Meteorological Drought." U.S. Weather Bureau Research Paper **45**: 58 pp.

Panofsky, H. A., Brier G.W. (1958). Some Applications of Statistics to Meteorology. University Park, PA, Pennsylvania State University, 224 pp.

Pearson, R. L., Miller, L.D. (1972). Remote mapping of standing crop biomass for estimation of the productivity of the short-grass Prairie, Pawnee National Grasslands, Colorado. Proceedings of the 8th International Symposium on Remote Sensings of Environment, Ann Arbor, MI, ERIM: 1357-1381

Penuelas, J., Pinol, J., Ogaya, R. and Filella, I. (1997). "Estimation of plant water concentration by the reflectance Water Index WI (R900/R970)." International Journal of Remote Sensing **18**(13): 2869-2875.

Peters, A. J., Rundquist, D.C., Wilhite, D.A. (1991). "Satellite detection of the geographic core of the 1988 Nebraska drought." Agricultural and Forest Meteorology **57**: 35-47.

Peters, A. J., Reed, B.C., Eve, M.D., Havstad, K.M. (1993). "Satellite assessment of drought impact on native plant communities of southeastern New Mexico, USA." Journal of Arid Environment **24**: 305-319.

Peters, A., Walter-Shea, E., Ji, L., Vina, A., Hayes, M., Svoboda, M. (2002). "Drought Monitoring with NDVI-Based Standardized Vegetation Index." Photogrammetric Engineering and Remote Sensing **68**(1): 71-75.

Qi, J., Chehbouni, A., Huete, A.R., Kerr, Y.H., Sorooshian, S. (1994). "A Modified Soil Adjusted Vegetation Index." Remote Sensing of Environment **48**: 119-126.

Qi, J., Marsett, R., Heilman, P., Biedenbender, S., Moran, S., Goodrich, D., Weltz, M. (2002). "RANGES improves satellite-based information and land cover assessments in southwest United States." EOS **83**(51): 601-606.

Redmond, K. T. (2002). "The Depiction of Drought." Bulletin of the American Meteorological Society **83**(8): 1143-1147.

Rouse, J. W., Haas, R.H., Deering, D.W., Schell, J.A., Harlan, J.C. (1972). Monitoring the Vernal Advancement and Retrogradation of Natural Vegetation. College Station, Texas, Remote Sensing Center, Texas A&M University**:** 200 pp.

Sabins, F. (1997). Remote Sensing: Principles and Interpretation, WH Freeman: 494 pp.

Seiler, R. A., Kogan, F., Sullivan, J (1998). "AVHRR-Based Vegetation and Temperature Condition Indices for Drought Detection in Argentina." Advanced Space Res. **21**(3): 481-484.

Sellers, P. J. (1987). "Canopy reflectance, photosynthesis and transpiration II: The role of biophysics in the linearity of their interdependence." Remote Sensing of Environment **21**: 143-183.

Shafer, B. A., Dezman, L.E. (1982). Development of a Surface Water Supply Index (SWSI) to assess the severity of drought conditions in snowpack runoff areas. Proceedings of the Western Snow Conference, Fort Colins, Colorado, Colorado State University: 164-175

Skirvin, S. M., Kepner, W.G., Marsh, S.E., Drake, S.E., Maingi, J.K., Edmonds, C.M., Watts, C.J., Williams, D.R. (2004). "Assessing the Accuracy of Satellite-Derived Land-Cover Classification Using Historical Aerial Photography, Digital Orthophoto Quadrangles, and Airborne Video Data." Remote Sensing and GIS Accuracy Assessment. R. S. Lunetta, Lyon, J.G. Boca Raton London New York Washington D.C., CRC Press**:** 304 pp.

Small, E. E., Kurc, S.A. (2003). "Tight Coupling between soil moisture and the surface radiation budget in semiarid environments: Implications for land-atmosphere interations." Water Resources Research **39**(10): 1278, doi: 10.1029/2002WR001297

Smith, S. D., Monson, R.K., Anderson, J.E. (1997). Physiological ecology of North American desert plants, Springer: 286 pp.

Stegun, A. A., Ed. (1968). Handbook of Mathematical Functions with Formulas, Graphs and Mathematical Tables. Applied Mathematics Series, US Dept. of Commerce 1044 pp.

Svoboda, M., LeComte, D., Hayes, M., Heim, R., Gleason, K., Angel, J., Rippey, B., Tinker, R., Palecki, M., Stooksbury, D., Miskus, D., Stephens, S. (2002). "The Drought Monitor." Bulletin of the American Meteorological Society **83**(8): 1181-1190.

Szilagi, J., Rindquist, D.C., Gosselin, D.C., Parlange, M.B. (1998). "NDVI Relationship to Monthly Evaporation." Geophysical Research Letters **25**(10): 1753-1756.

Thom, H. C. S. (1966). Some Methods of Climatological Analysis. Geneva, Switzerland, WMO Technical Note Number 81, Secretariat of the World Meterological Association**:** 53 pp.

Thornwaite, C. (1931). "The Climates of North America according to a new classification." The Geographical Review **21**: 633-655.

Thornwaite, C. W., Mather, J.R., (1957). "Instructions and Tables for computing Potential Evapotranspiration and the Water Balance." Publications in Climatology **10**(3): 185-311.

Tucker, C. J., Sellers, P.J. (1986). "Satellite remote sensing of primary production." International Journal of Remote Sensing **7**: 1395-1416.

Viau, A., Vogt, J.V., Beaudin, I. (2000). "Comparison of a Satellite-Based and a Precipitation-Based Drought Index." Canadian Journal of Remote Sensing **26**(6): 580-583.

Vogt, J. V., Niemeyer, S., Somma, F., Beaudin, I., Viau, A.A. (2000). Drought Monitoring from Space. Drought and Drought Mitigation In Europe. J. V. Vogt, Somma, F., Kluwer Academic Publishers**:** 167-183.

Vorosmarty, C. J., Moore, B., Grace, A.L., Gildea, M.P., Melillo, J.M., Peterson, B.J., Rastetter, E.B., Steudler, P.A. (1989). "Continental-scale models of water balance and fluvial transport: An application to South America." Global Biochemistry Cycles **3**: 241-265.

Wan, Z., Wang, P., Li X. (2004). "Using MODIS Land Surface Temperature and Normalized Difference Vegetation Index products for monitoring drought in the Southern Great Plains, USA." International Journal of Remote Sensing **25**(1): 61-72.

Wang, J., Price, K.P., Rich, P.M. (2001). "Spatial patterns of NDVI in response to precipitation and temperature in the central Great Plains." International Journal of Remote Sensing **22**: 3827-3844.

Wang, J., Price, K.P., Rich, P.M. (2003). "Temporal responses of NDVI to precipitation and temperature in the Central Great Plains, USA." International Journal of Remote Sensing **24**(11): 2345-2364.

Washington-Allen, R. A., Ramsey, R.D., West, N.E. (2004). "Spatiotemporal mapping of the dry season vegetation response of sagebrush steppe." Community Ecology **5**(1): 69-79.

Wilhite, D. A., Hayes, M.J., Knutson, C., Smith, K.H. (1990). "The Basics of Drought Planning: A 10-Step Process." http://drought.unl.edu/plan/handbook/process.htm

Wilhite, D. A., Ed. (2001). Drought: a global assessment. National Hazards and Disasters. London, Routledge Publishers. 752 pp.

Woodhouse, C. A., Overpeck, J.T. (1998). "2000 Years of Drought Variability in the Central United States." Bulletin of the American Meteorological Society **79**(12): 2693-2714.